Tesi per il conseguimento del titolo

Precision tests of the Standard Model at the energy frontier

Clara Lavinia Del Pio

Università degli Studi di Pavia

Dipartimento di Fisica

DOTTORATO DI RICERCA IN FISICA - XXXVI CICLO

Precision tests of the Standard Model at the energy frontier

Clara Lavinia Del Pio

Submitted to the Graduate School of Physics in partial
fulfillment of the requirements for the degree of
DOTTORE DI RICERCA IN FISICA
DOCTOR OF PHILOSOPHY IN PHYSICS
at the
University of Pavia

Supervisor: Prof. Fulvio Piccinini

Contents

iii

Introduction and motivation

The Standard Model of Particle Physics (SM) is at present the most successful theory to describe the fundamental particles and their interactions. It comprises Quantum Chromodynamics (QCD), which treats the strong interaction, and the Electroweak (EW) sector, in which the electromagnetic and the weak forces are unified. At the present day, apart from few exceptions, the Standard Model has predicted results that are in excellent agreement with the experimental data. However, many open questions remain, connected for instance with the existence of dark matter, the nature of neutrinos, the Higgs hierarchy problem, and how to reconcile general relativity with quantum field theory. Moreover, some experimental results cannot be explained by the SM: the most significant one is the measurement of the anomalous magnetic dipole moment of the muon, whose value is at tension with the corresponding theoretical prediction at the level of 5σ [1–4]. Concerning the theoretical evaluation of the muon anomalous magnetic moment, however, the situation is puzzling, and different methods, which could lead to a better agreement between theoretical and experimental determinations, are currently under discussion.

All these facts support the general idea of the existence of physics beyond the Standard Model, which can be searched mainly in two ways: one approach consists in looking directly for new particles at the highest available energies; on the other hand, if the new particles are not kinematically accessible, another method is to search for indirect effects. Concerning direct new physics searches, new accelerators have been proposed, like, for example, the Future Circular Collider (FCC) and multi-TeV muon colliders. New physics indirect effects, on the other side, can be investigated with model independent analyses, for instance by means of the Standard Model Effective Field Theory (SMEFT), or within the SM by very precise measurements of some crucial parameters and distributions, in order to point out discrepancies in the comparison of these parameter determinations at different energies and machines. To cite an

example, the future High Luminosity Large Hadron Collider (HL-LHC) will allow to explore all these approaches.

The precise determination of SM parameters at hadronic machines plays a fundamental role in present and future physics programmes. In this context, the neutral-current Drell-Yan (NCDY) process, which has a large cross section and a clean experimental signature, is ideal to perform precision tests of the Standard Model electroweak parameters, like the W-boson mass and the weak mixing angle, at hadronic colliders. For example, the LHC Electroweak Working Group (EWWG) at CERN is dedicated to develop the theoretical and experimental setup for a high-precision determination of the effective weak mixing angle, $\sin^2 \theta_{eff}^\ell$, defined as the coupling of the Z boson with leptons at the Z peak, with the NCDY process.

On the theory side, precision means to evaluate the relevant observables at the best possible accuracy, by taking into account the radiative corrections of the strong and electroweak interactions, together with carefully quantify the theoretical uncertainty associated to a given prediction. In particular, a key observation for the determination of SM parameters is that one should have the parameter to be determined, i.e. the W mass or the weak mixing angle, among the inputs of the renormalization scheme, while keeping in mind that the choice of a particular scheme has an effect on the total theoretical uncertainty.

This thesis addresses these issues by presenting a critical comparison among different renormalization schemes in the electroweak sector of the Standard Model, in particular variants of the on-shell and of the $\overline{MS}$ schemes, at next-to-leading order (NLO) plus leading fermionic higher-order corrections, and with particular reference to the neutral-current Drell-Yan process. Beside a determination of the effective definition of the weak mixing angle, which will probe the energy scale at the Z resonance, one can conceive a high-energy test of the Standard Model, via the precise measurement of the $\overline{MS}$ weak mixing angle, $\sin^2 \theta_w^{\overline{MS}}(\mu)$: this can be achieved with the development of a new parameter scheme with $\sin^2 \theta_w^{\overline{MS}}(\mu)$ as input, as it is here discussed.

On top of this, several aspects have to be taken into account when calculating electroweak radiative corrections for the neutral-current Drell Yan, as the gauge-invariance properties of the treatment of the resonances. In fact, the correct description of unstable particles like the W and the Z boson, for energies close to their masses, require to include their decay width in the calculations, in such a way not to spoil the general properties of the theories, like gauge invariance. Different gauge-invariant options for the resonance treatment are here reviewed, and their numerical implementation is examined. Furthermore, some newly implemented alternatives for computing the hadronic contribution to the running of the electromagnetic coupling, as well as a detailed description of higher-order contributions, are discussed.

Finally, to be able to compare the theoretical predictions with experimental data, it is necessary to embed the computation of radiative corrections into a

simulation code. To this aim, an event generator is ideal, as it makes it possible to have a fully-differential description of the process. Electroweak corrections to the neutral-current Drell Yan at NLO+universal higher orders have thus been implemented within the `Z_ew-BMNNPV` package of the Monte Carlo event generator POWHEG-BOX-V2. Their effects on relevant differential distributions are studied in the energy region around the electroweak scale, as well as in the so-called Sudakov regime, at energies of the order of some TeVs.

The original results of this work allow, on one side, to quantify the theoretical uncertainties associated to a determination of $\sin^2 \theta_{eff}^\ell$, within the context of the LHC EWWG. On the other hand, having at disposal a new scheme with the $\overline{MS}$ weak mixing angle as input makes it possible to explore the sensitivity of LHC and HL-LHC to $\sin^2 \theta_w^{\overline{MS}}(\mu)$, opening the possibility to determine the running weak mixing angle, and eventually the $\overline{MS}$ electromagnetic coupling, at high scales. Both these determinations of the weak mixing angle − at the Z-peak and in the TeV region − will represent a fundamental test of the Standard Model.

The first four chapters of this work frame the theoretical aspects necessary to understand the code implementation and the numerical results. In Chap. 1, we review the building blocks of the Standard Model Lagrangian, while Chap. 2 examines the phenomenology of precision tests of some SM crucial parameters, like the W-boson mass and the weak mixing angle; moreover, the concept of running couplings is introduced.

In Chap. 3, the renormalization of the Standard Model in both the on-shell and the $\overline{MS}$ scheme is discussed, focusing on the neutral-current Drell-Yan process at NLO plus universal higher-order corrections. Special attention is devoted to the choice of the electroweak input parameter scheme, presenting the different options implemented in the `Z_ew-BMNNPV` package. The behaviour of electroweak corrections in the Sudakov regime is also examined.

Chap. 4 deals with the issue associated with the mathematical description of unstable particles while preserving gauge invariance. The different recipes to treat the resonance implemented in the `Z_ew-BMNNPV` code are described.

From Chap. 5 to Chap. 7, the original numerical results are presented: QED corrections to the neutral-current Drell-Yan are examined in Chap. 5, while the weak contributions are studied in Chap. 6, where predictions within several input schemes and with different resonance treatments are compared, to quantify the parametric and intrinsic uncertainties associated with the theoretical prediction of some relevant differential distributions. The effectiveness of the Sudakov approximation in the high energy regime, together with the possibility of quantifying the missing bosonic higher-order contributions, are also assessed. Finally, Chap. 7 presents some results on the sensitivity to the $\overline{MS}$ weak mixing angle in the Run 3 and High-Luminosity phases of the LHC, by studying the feasibility of a test of the Standard Model via a high-energy determination of $\sin^2 \theta_w^{\overline{MS}}(\mu)$.

1

The Standard Model

he Standard Model of Particle Physics is at present the most successful theory to explain how fundamental particles interact with each other, and comprises three of the four fundamental forces: the strong interaction is described in Quantum Chromodynamics, while the electromagnetic force, theorised in Quantum Electrodynamics (QED), can be treated in a unified way together with the weak one, to give the electroweak interaction. The gravitational force is not included in the theory.

The electroweak and strong sectors of the Standard Model are described in quantum field theory by non-abelian Yang-Mills gauge theories, characterized by the symmetry groups $SU(2)_L \times U(1)_Y$ and $SU(3)_c$, respectively. The theory of electroweak interactions is developed in the Glashow-Salam-Weinberg model, originally proposed by Glashow, Weinberg and Salam [5–7] for leptons and later extended to quarks by Glashow, Iliopoulos and Maiani [8]. The electroweak theory is characterised by two gauge coupling constants: g_2 for the weak isospin group $SU(2)_L$ and g_1 for the weak hypercharge group $U(1)_Y$. The hypercharge is defined from the relation:

$$T_3 + \frac{Y}{2} = Q \,, \tag{1.1}$$

where Q is the electric charge operator, and $T_3 = \tau_3/2$, with τ_3 the third of the generators of $SU(2)_L$, that are the Pauli matrices τ_1, τ_2 and τ_3. Quantum Chromodynamics has been theorised in the Seventies, as the result of different ideas coming from the description of interactions among nucleons in ordinary matter, together with experimental results [9–12]. The strong interaction is quantified by the coupling g_S and the $SU(3)_c$ group is generated, in its fundamental representation, by the Gell-Mann matrices, λ_A with $A = 1, \ldots, 8$.

The theory is completed with the spontaneous symmetry breaking provided by the Higgs mechanism, that is responsible to give mass to fermions and gauge bosons, while the photon and the gluon remain massless [13–15]. The most remarkable property of the Standard Model is that it is a consistent quantum field theory, meaning that it is renormalizable, as proven by 't Hooft [16], and

anomaly-free, thus making it possible, given a finite set of input parameters, to predict measurable quantities order by order in perturbation theory.

For future use throughout this work, we write here the Lagrangian of the Standard Model, and refer to [10, 17–21] for a complete dissertation on how the Lagrangian is built. The Lagrangian is gauge-invariant under $SU(2)_L \otimes U(1)_Y$ and $SU(3)_c$ transformations and reads:

$$
\begin{aligned}
\mathcal{L} =& -\frac{1}{4} W^a_{\mu\nu} W^{\mu\nu}_a - \frac{1}{4} B_{\mu\nu} B^{\mu\nu} - \frac{1}{4} G^A_{\mu\nu} G^{\mu\nu}_A \\
&+ \mathcal{L}_{SSB} \\
&+ \sum_i (\bar{L}'_i i \slashed{D} L'_i + \bar{Q}'_i i \slashed{D} Q'_i) + \sum_i (\bar{l}'^R_i i \slashed{D} l'^R_i + \bar{u}'^R_i i \slashed{D} u'^R_i + \bar{d}'^R_i i \slashed{D} d'^R_i) \\
&+ \sum_{i,j} (\bar{L}'_i i\, h^l_{ij}\, l'^R_j \Phi + \bar{Q}'_i i\, h^u_{ij}\, u'^R_j \Phi^c + \bar{Q}'_i i\, h^d_{ij}\, d'^R_j \Phi + \mathrm{h.\,c.}) \\
&+ \mathcal{L}_{fix} + \mathcal{L}_{ghost}\,,
\end{aligned}
\tag{1.2}
$$

where h.c. means hermitean conjugate. We now describe the content of this equation in detail.

$$-\frac{1}{4}W^a_{\mu\nu}W^{\mu\nu}_a - \frac{1}{4}B_{\mu\nu}B^{\mu\nu} - \frac{1}{4}G^A_{\mu\nu}G^{\mu\nu}_A$$

The first three terms represent the pure gauge-field Lagrangian of the electroweak and strong sectors: the gauge boson field strength tensors are denoted with $B^{\mu\nu}$ and $W^{\mu\nu}_a$, with $a = 1, 2, 3$, while $G^{\mu\nu}_A$ stands for the gluon strength tensor, that carries also a colour index $A = 1, \dots, 8$. They are defined as:

$$\begin{aligned}
B_{\mu\nu} &= \partial_\mu B_\nu - \partial_\nu B_\mu & (1.3)\\
W^a_{\mu\nu} &= \partial_\mu W^a_\nu - \partial_\nu W^a_\mu + g_2\,\epsilon^{abc}\,W^b_\mu W^c_\mu\,, \quad a = 1, 2, 3\\
G^A_{\mu\nu} &= \partial_\mu G^A_\nu - \partial_\nu G^A_\mu + g_S\,f^{ABC}\,G^B_\mu G^C_\mu\,, \quad A = 1, \dots, 8\,,
\end{aligned}$$

where ϵ^{abc} and f^{ABC} are the structure constants of $SU(2)_L$ and $SU(3)_c$, respectively. In Eq. 1.2 we are using the so-called interaction basis for the electroweak sector: it has the advantage of keeping the gauge symmetry manifest, but the fields W^a_μ, with $a = 1, 2, 3$, and B_μ are not the physical ones. They can be related to the physical gauge bosons by the relations $W^\pm_\mu = (W^1_\mu \mp iW^2_\mu)/\sqrt{2}$ and:

$$\begin{pmatrix} \cos\theta_w & \sin\theta_w \\ -\sin\theta_w & \cos\theta_w \end{pmatrix} \begin{pmatrix} W^3_\mu \\ B_\mu \end{pmatrix} = \begin{pmatrix} Z_\mu \\ A_\mu \end{pmatrix}\,, \quad (1.4)$$

where θ_w is the weak mixing angle, that enters also the electroweak unification relation:

$$g_2 \sin\theta_w = g_1 \cos\theta_w = e\,. \quad (1.5)$$

Eq. (1.4) and (1.5) state the unification of the electromagnetic and the weak forces.

$$\mathcal{L}^{SSB} = (D_\mu \Phi)^\dagger (D^\mu \Phi) - V(\Phi)$$

In the spontaneous symmetry breaking Lagrangian, one can recognise a first kinetic term, in which the symbol D_μ denotes the covariant derivative:

$$D_\mu = \partial_\mu - i g_s I^A G^A_\mu - i g_2 T^a W^a_\mu - i g_1 \frac{Y}{2} B_\mu \,, \qquad (1.6)$$

where $I^A = \lambda^A/2$ are the generators of $SU(3)_c$, T^a are the generators of $SU(2)_L$ and Y is the hypercharge. The second term is the scalar potential $V(\Phi)$, that must satisfy certain requirements. First, to guarantee the renormalizability of the theory, it must contain at most the fourth power of the field Φ, and has to be bounded from below, for the existence of a minimum in the Hamiltonian. Furthermore, it must have a stationary point at the origin. Under the hypothesis that only one Higgs doublet Φ exists, one writes the scalar potential as:

$$V(\Phi) = m^2 \Phi^\dagger \Phi + \frac{\lambda^2}{4} (\Phi^\dagger \Phi)^2 \,, \quad \lambda > 0 \,, \quad m^2 = -\lambda v^2 < 0 \,, \quad (1.7)$$

where the condition $\lambda > 0$ guarantees that the potential is bounded from below, i.e. it has minima in:

$$\phi_0(x) = e^{i\delta} \frac{v}{\sqrt{2}}, \qquad v = \sqrt{\frac{-4m^2}{\lambda}}, \qquad \delta \in [0, 2\pi) \,. \qquad (1.8)$$

The parameter v is called the non-vanishing vacuum expectation value (vev) and represents the order parameter of the system, i.e. the energy scale of spontaneous symmetry breaking. From the infinite set of local minima, we can choose the ground scale $\phi_0 = (0, \, v/\sqrt{2})$ and expand the Higgs doublet around this minimum:

$$\Phi(x) = \frac{1}{\sqrt{2}} \begin{pmatrix} 0 \\ v + H(x) \end{pmatrix} \exp\left(\frac{i\tau_i \chi_i(x)}{v} \right) = \frac{1}{\sqrt{2}} \begin{pmatrix} 0 \\ v + H(x) \end{pmatrix} \,, \quad (1.9)$$

where the last equivalence is valid in the unitary gauge, that allows us to eliminate the unphysical would-be Goldstone fields $\chi_i(x)$, $i = 1, 2, 3$. The Higgs scalar has been chosen not to carry electromagnetic and colour quantum numbers, in such a way that the generators τ_1, τ_2 and $T_3 - Y/2$ are broken, while the symmetries of $U(1)_{em}$ and $SU(3)_c$ are left unbroken, with the photon and the gluon massless. The final result are the masses of the $W^\pm$, Z and H bosons:

$$M_W = \frac{g_2 v}{2} \,, \qquad M_Z = \frac{\sqrt{g_1^2 + g_2^2}\, v}{2} \,, \qquad M_H = \sqrt{\frac{\lambda}{2}} v^2 \,. \qquad (1.10)$$

$$\sum_i (\bar{L}'_i i\slashed{D} L'_i \,+\, \bar{Q}'_i i\slashed{D} Q'_i) + \sum_i (\bar{l}'^{\,R}_i i\slashed{D} l'^{\,R}_i \,+\, \bar{u}'^{\,R}_i i\slashed{D} u'^{\,R}_i \,+\, \bar{d}'^{\,R}_i i\slashed{D} d'^{\,R}_i)$$
$$+ \sum_{i,j} (\bar{L}'_i i\, h^l_{ij}\, l'^{\,R}_j \Phi \,+\, \bar{Q}'_i i\, h^u_{ij}\, u'^{\,R}_j \Phi^c \,+\, \bar{Q}'_i i\, h^d_{ij}\, d'^{\,R}_j \Phi + \mathrm{h.\,c.})$$

In the following lines of Eq. (1.2) we have the kinetic terms of the fermions and their gauge interactions, and finally their Yukawa interactions with the scalar doublet. The fermion (i.e. lepton and quark) doublets and singlets read:

$$L'^{\,l}_i \;=\; \begin{pmatrix} \nu'_{L,i} \\ l'_{L,i} \end{pmatrix}, \quad Q'_i \;=\; \begin{pmatrix} u'_{L,i} \\ d'_{L,i} \end{pmatrix}, \quad l'_{R,i}, \quad u'_{R,i}, \quad d'_{R,i}, \quad i = 1, 2, 3 \,,$$
$$(1.11)$$

where the index i runs over the three lepton and the three quark families, with $l = e, \mu, \tau$. The colour index is suppressed here, but one should keep in mind that there are nine quark doublets, due to the colour quantum number. The labels u and d stand for up-type-quark and down-type-quark fields, respectively. The fermion fields are written here in the interaction basis, indicated by the apex, in which the covariant derivatives are diagonal with respect to the family indices, but fields are not mass eigenstates. We furthermore have the right-handed singlets $l'_{R,i}$, $u'_{R,i}$ and $d'_{R,i}$.

Finally, the couplings h^f, with $f = \nu, \ell, u, d$, denote Yukawa-coupling matrices, necessary for the generation of fermion masses. The field Φ^c, that couples to up-type right-handed fermions, is the charge-conjugate of the Higgs field:

$$\Phi^c \;=\; i\tau_2 \Phi^* \,. \tag{1.12}$$

The classical Lagrangian density needs then to be quantized, in order to obtain a complete description in quantum field theory. A convenient method to do so in a manifestly Lorentz-covariant way is via the path-integral formalism, that requires the specification of a gauge and the introduction of the Faddeev-Popov fields in order to eliminate from functional integrals the physically equivalent configurations due to gauge transformations [22, 23]. This has as a consequence the introduction of a gauge-fixing and a ghost Lagrangian.

$$\boxed{\mathcal{L}_{fix} = -\frac{1}{2\xi}C_a\{\mathbf{K}\}C^a\{\mathbf{K}\}}$$

In a general non-abelian gauge theory characterised by a gauge term of the kind:

$$\mathcal{L}_{gauge} = -\frac{1}{4}V^a_{\mu\nu}V_a^{\mu\nu}\,, \tag{1.13}$$

where $V^a_{\mu\nu} = \partial_\mu K^a_\nu - \partial_\nu K^a_\mu + g\epsilon^{abc}K^b_\mu K^c_\nu$ is the generic strength tensor of the field $\mathbf{K}$, the gauge-fixing Lagrangian takes the form reported in the grey rectangle above, where $\mathbf{C}$ is a set of local functionals of the gauge fields that allows us to fix the gauge condition, i.e. $C^a\{\mathbf{K}\} = 0$. For example, for the quantization of the electroweak sector, we have:

$$\mathcal{L}_{fix,\,EW} = -\frac{1}{2\xi_A}(C^A)^2 - \frac{1}{2\xi_Z}(C^Z)^2 - \frac{1}{\xi_W}C^+C^-\,, \tag{1.14}$$

with the gauge-fixing functionals expressed in a general renormalizable gauge:

$$C^\pm = \partial^\mu W^\pm_\mu \mp iM_W\xi'_W\chi^\pm \qquad C^Z = \partial^\mu Z_\mu - M_Z\xi'_Z\chi^3 \qquad C^A = \partial^\mu A_\mu\,, \tag{1.15}$$

where $\chi^\pm$, $i = 1,2$ are the would-be Goldstone fields and ξ_a with $a = A, Z, \pm$, and ξ'_b with $b = Z, \pm$, are independent gauge parameters. For the strong sector one has:

$$\mathcal{L}_{fix,\,QCD} = -\frac{1}{2\xi_G}(C^G)^2\,, \tag{1.16}$$

with:

$$C^G = \partial^\mu G^B_\mu\,, \tag{1.17}$$

where ξ_G appears as the gauge parameter and B denotes the colour index. Note that, from the gauge-fixing Lagrangian, a mass term of the kind $\sqrt{\xi}M$ corresponds to each would-be Goldstone boson. In the following we will work under the 't Hooft-Feynman gauge, where $\xi'_\pm = \xi_\pm$ and $\xi'_Z = \xi_Z$, and $\xi_a = 1$ for every $a = A, Z, \pm, G$.

$$\mathcal{L}_{ghost} = \bar{u}^a(x) \frac{\delta C^a(x)}{\delta \theta^b(y)} u^b(x)$$

The last term in Eq. (1.2) is the Faddeev-Popov ghost Lagrangian, resulting after the complete treatment of the path integral [17], where the derivative describes the variation of the gauge-fixing function C^a under infinitesimal gauge transformations characterised by the parameter θ^b. The Faddeev-Popov procedure is the formal way to remove the mathematical inconsistencies due to the presence of gauge-equivalent configurations in the path integral defining the generating functional of the theory. We have here introduced the unphysical anticommuting scalar fields, $u_a(x)$ and $\bar{u}_a(x)$, that are called Faddeev-Popov ghost fields and acquire the same mass as the would-be Goldstone boson fields, $\sqrt{\xi}M$.

2

Testing the electroweak Standard Model at high energies

fter its theoretical formulation was completed in the Seventies, the Standard Model has undergone a great number of precision experimental tests, emerging as the most successful theory in particle physics. Although the Standard Model can be considered a complete renormalizable quantum field theory, one should in fact prove its consistency against experimental data. In the last fifty years, a huge number of experimental results have confirmed the Standard Model predictions. As we will discuss, in some cases the theory led to the discovery of new particles, by correctly indicating the mass range in which they were expected.

However, many open questions cannot currently be solved by the SM: for example, experimental data indicate that neutrinos have a (small) mass, which is not foreseen in the Standard Model; yet, one can modify the theory to include neutrino masses, but it is not clear how to proceed: the main alternatives predict a Dirac or a Majorana nature for neutrinos. Moreover, mathematical difficulties arise when trying to express the theory of gravitation, i.e. general relativity, in terms of a quantum field theory, not to mention that the quantum effects of gravity would start to be visible at the Planck scale, making it impossible to discriminate among different quantum gravity theories with current technologies. Another problem is connected with the Higgs sector, and carries the name of hierarchy problem: it remains unclear the fundamental reason behind the different values of the fermion masses, or why the weak scale is so small with respect to the Planck scale. Finally, Standard Model particles are not able to account for the observed amount of cold dark matter and dark energy, and the matter-antimatter asymmetry in our universe is still without explanation.

On top of that, from a phenomenological point of view, a longstanding puzzle is due to the fact that the experimentally measured value of the anomalous magnetic dipole moment of the muon, usually referred to as the $(g-2)_\mu$, is

in tension with the Standard Model prediction, presently at the level of 5σ. This number is obtained by considering the theoretical evaluation which makes use of traditional dispersive techniques to compute the leading order hadronic contribution to $(g-2)_\mu$, the ingredient of the calculation affected by the highest uncertainty, due to the difficulties stemming from non-perturbative strong interaction effects. However, in recent years, lattice calculations have provided alternative evaluations of the leading order hadronic contribution, which differ from their dispersive counterparts by an amount from 2 to 2.5σ, depending on the reference value of the dispersive methods, and are in agreement with the experimental determinations. Moreover, a recent experimental result from the CMD3 collaboration in the pion channel, which plays the main part in the hadronic contribution to the $(g-2)_\mu$, would lead to a different dispersive value, closer to the experimental one [24]. The final picture is thus even more unclear.

Another experimental determination which has raised the attention of the community is the recent one on the W-boson mass from the CDF collaboration, based on the analysis of the full Run-2 dataset and characterised by the incredible precision of $1\cdot 10^{-4}$. This new determination should be considered to supersede the previous result, even if it is in disagreement with it, and stands 7σ from the Standard Model prediction [25], as it will be discussed.

On the basis of the scientific method, several consistency tests have been performed, to assess the validity of the theory and to explore the existence of possible New Physics (NP) beyond the Standard Model, that could provide some answers to these open issues. There are two complementary and intersecting approaches to look for beyond the Standard Model effects, usually identified with the exploration of the energy rather than the precision (or luminosity) frontier: on one side, we can search directly for new particles at the highest available energies; on the other hand, one can look for indirect effects. The latter can be searched with model independent analysis, for example by means of the SM Effective Field Theory: in the SMEFT approach, the SM is regarded as the low-energy limit of an unknown ultraviolet theory, and NP effects can be parametrised by a series of higher-dimensional non-renormalizable operators, built from the SM fields and symmetries, and weighted by inverse powers of the NP energy scale.

Another method to look for indirect effects it to obtain very precise measurements of some crucial parameters within the Standard Model, in order to point out discrepancies in the comparison of these parameter determinations at different energies and machines. In this work, we will discuss the test of the Standard Model in the high energy regime, focusing in particular on the precision measurement of electroweak observables, together with the determination of the coupling constants and their running.

From the historical point of view, electroweak precision physics started af-

ter the discovery of the $W^{\pm}$ and Z bosons, occurred in 1983 at the UA1 and UA2 experiments, at the Super Proton Synchrotron, CERN [26, 27]. The electroweak precision program was developed with the operation of two electron-positron accelerators, the Large Electron Positron collider (LEP) at CERN and the Stanford Linear Collider (SLC) at SLAC. A proton-antiproton collider, the Tevatron, was operating at Fermilab in the same years. The LEP1 phase (1989-1995) and SLC worked at centre-of-mass energies around the Z peak, about 91 GeV [28, 29], and studied two-fermion production from e^+e^- annihilation, mediated by a photon or a Z boson, i.e. $e^+e^- \to \gamma^*, Z^* \to f\bar{f}$, with $f = \nu, \ell, q$. The sample of Z bosons produced at the two machines was huge, amounting to about sixteen millions at LEP1 and thousands at SLC, and, together with a good control of systematic uncertainties, allowed for a very high precision, at the 0.1% or better, in the determination of observables such as the cross sections and the forward-backward asymmetries of the different channels. LEP1 provided the most precise determination of the Z boson mass up to now, by fitting the experimental cross sections to the relativistic Breit-Wigner distribution at different energies around the Z peak. The combined value, that takes into account the numbers quoted by each of the four experiments at LEP, is $M_Z = 91.1876 \pm 0.0021$ GeV [30]: after LEP1, the Z resonance is so well-known that is used today for the calibration of the detector response at hadronic colliders, that is essential for the determination of the W boson mass via the template fit approach.

In 1996, the LEP machine underwent an upgrade that took its centre-of-mass energy up to about 200 GeV, starting the LEP2 phase, and making it possible to explore the energy region beyond the WW production threshold, i.e. the four-fermion production through the processes $e^+e^- \to W^+W^- \to 4f$ and $e^+e^- \to ZZ \to 4f$, together with the search of the Higgs boson via the process $e^+e^- \to HZ \to b\bar{b}f\bar{f}$.

Meanwhile, the Tevatron Collider searched for the top quark, by studying the production of a $t\bar{t}$ pair from proton-antiproton collisions at a centre-of-mass energy of 2 TeV. The physics program at Tevatron included also the investigation of direct production of the Higgs boson and of new physics beyond the Standard Model. After the discovery of the top quark in 1995 [31, 32], the high luminosity of the machine, of the order of 10 fb^{-1}, made it possible to begin the first series of high precision determinations at a hadronic collider in history. The precision program of the Tevatron was continued at the Large Hadron Collider (LHC), at energies of $7 - 8$ TeV, and culminated with the discovery of the Higgs boson in 2012 [33, 34]. The centre-of-mass energy at LHC has then been upgraded to 13 TeV and very recently taken to 13.6 TeV with the start of Run 3; at the same time, the nominal luminosity have been doubled with respect to the design value [35], and is expected to reach a value five times larger than the present one in the High Luminosity phase, foreseen for the end of the decade [36]. With such luminosities, the LHC constitutes an ideal machine for precision physics, with the advantage of exploiting a large

number of processes and energy ranges, and will be even more crucial in the future for testing the Standard Model and physics beyond.

Precision physics in the Standard Model shows its full potential with the global electroweak fit: the idea is to exploit the contributions from quantum corrections to probe physics at energy scales that are much higher with respect to the masses of the particles directly entering the experimental reactions. In fact, the theoretical predictions of the observables depend on some unknown parameters, which can thus be indirectly determined via a best fitting procedure. To best constrain the unknown parameters, a high experimental precision is thus required, as well as a good control of the theoretical uncertainties which enter as systematics in the fit [37–39]. Global electroweak fit have been performed since LEP, and have demonstrated an impressive predictive power, making it possible to assess the value of the Higgs-boson and the top-quark mass before these particles were discovered, relying only on the impact that quantum loop corrections containing the Higgs or the top have on the predictions of other quantities.

The present work is framed in this context, since its main point is the developing of Monte Carlo tools that make it possible to perform precision determinations of Standard Model parameters, in particular the weak mixing angle, at hadronic colliders, and that allow to study the effect on the observables when varying the values or the choice of the input parameters.

The rest of this chapter is devoted to the two parameters currently used to perform electroweak precision tests, the W boson mass and the weak mixing angle. After introducing their definitions and the methods for their determinations, we briefly discuss the measurement of the running coupling constants in the Standard Model, a crucial concept in this work that will be fully developed in the next chapter.

2.1   The W boson mass

Since the particle discovery in 1983, the W boson mass has been measured with increasing precision, with both direct and indirect determinations at e^+e^- and hadron colliders. A starting point for the determination of M_W can be the tree-level relation with the Fermi coupling constant G_μ:

$$M_W = \sqrt{\frac{\alpha\pi}{\sqrt{2}\sin^2\theta_w G_\mu}} = \frac{M_Z}{\sqrt{2}}\sqrt{1 + \sqrt{1 - \frac{\sqrt{8}\pi\alpha}{G_\mu M_Z^2}}}. \qquad (2.1)$$

By knowing the values for α, G_μ and M_Z, the latter measured with very high precision, from Eq. (2.1) the LEP1 Collaboration obtained the leading order determination of the W-boson mass: $M_W \simeq 80.94$ GeV. This is a significantly different value from the current experimental average, $M_W \simeq 80.38$ GeV [30] [1],

---

[1]This number does not include the recent determination by the CDF collaboration based on their full Run-2 dataset [25].

2.1. The W boson mass

because it misses higher-order effects, absent in the tree-level relation. Beyond the leading order one gets [40]:

$$M_W = \frac{M_Z}{\sqrt{2}} \sqrt{1 + \sqrt{1 - \frac{\sqrt{8}\pi\alpha(1 + \Delta r)}{G_\mu M_Z^2}}}, \qquad (2.2)$$

The term Δr contains the radiative corrections to the muon decay [41, 42], after the factorization of QED corrections in the Fermi theory, and can be written as (cfr. Chap. 3):

$$\Delta r = \Delta\alpha - \frac{\cos^2\theta_w}{\sin^2\theta_w}\Delta\rho + \Delta r_{rem}, \qquad (2.3)$$

where $\Delta\alpha$ represents the running of α, $\Delta\rho = \rho - 1$ describes the deviation from 1 of the parameter $\rho = M_W^2/(M_Z^2 \cos^2\theta_w)$, and Δr_{rem} collects the remaining radiative corrections. The value of the W boson mass depends quadratically on the top-quark mass via $\Delta\rho$ and logarithmically on the Higgs-boson mass and on the fermion masses present in $\Delta\alpha$, as:

$$\Delta\rho \sim \frac{\alpha}{4\pi}\frac{3}{4s_w^2}\frac{m_t^2}{M_W^2} \quad \Delta\alpha(q^2) \sim \frac{\alpha}{3\pi}\sum_p N_p^c Q_p^2 \ln\frac{q^2}{m_p^2} \quad p \in \{\text{SM particles}\},$$

$$(2.4)$$

with q^2 the momentum flowing in the photon propagator. If one takes into account also mixed electroweak-QCD corrections, M_W acquire a dependence also on the running of the strong coupling constant, $\Delta\alpha_S$. The present state of the art on the calculation of radiative corrections leads to the theoretical prediction $M_W = 80.364 \pm 0.009$ GeV [43].

Experimentally, a precise determination of the W boson mass has been achieved at LEP2 both at the WW threshold, by deriving it from the cross section measurement, and below threshold from the distribution of the decay products, by defining M_W as the mass parameter in a Breit-Wigner distribution with mass-dependent width. The final LEP2 combination yields the value $M_W = 80.392 \pm 0.027\,(\text{stat}) \pm 0.028\,(\text{syst})$ GeV [44], an incredible precision if compared with the initial uncertainty of 5 GeV at the UA1 and UA2 experiments.

At hadronic colliders, the precision measurement of M_W is performed via a template fit approach: the value of M_W corresponds to the best fit to the data, obtained by comparing the final state distributions (called templates), predicted by Monte Carlo simulations, to the observed kinematic distributions. The Tevatron collider published the combined value of $M_W = 80.387 \pm 0.016$ GeV from the CDF (Collider Detector at Fermilab) and D0 collaborations [46]. Very recently, the CDF collaboration published a new result on the W mass, based on the analysis of the full Run-2 dataset of 8.8 fb^{-1}, with a precision greater than the one of all other experimental determinations of M_W combined: $M_W = 80.4335 \pm 0.0094$ GeV [25]. This new CDF determination includes data of the previous result, but is in significant disagreement

2. Testing the electroweak Standard Model at high energies
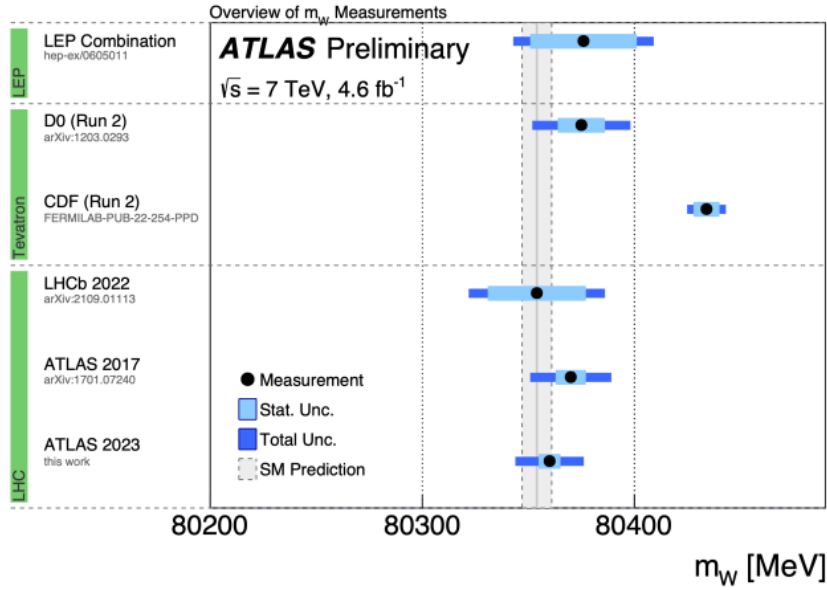
Figure 2.1: Overview of M_W measurements with the Tevatron results, the LEP experiments, ATLAS and LHCb, with total (dark blue band) and statistical (light-blue) uncertainties. The Standard Model prediction is shown by the gray band [45].

with it and stands 7σ from the Standard Model prediction, as it can be seen from Fig. 2.1.

The ATLAS experiment at the LHC obtained the value $M_W = 80.370 \pm 0.019$ GeV [47], based on data of proton-proton collisions collected at a centre-of-mass energy of 7 TeV. Recently, this measurement has been updated by reanalysing the 4.6 fb^{-1} sample of data used in the previous result with improved fitting methods, yielding $M_W = 80.360 \pm 0.016$, in agreement with the SM prediction [45].

Fig. 2.1 shows the described measurements, together with the LHCb determination [48]. The most recent combination, that does not include the latest CDF and ATLAS results, is $M_W = 80.377 \pm 0.012$ GeV [30]. It has furthermore to be reported the study in [49], which explores the compatibility of the discussed W-boson mass measurements at ATLAS, LHCb, CDF, and D0 by using a coherent framework with theory uncertainty correlations. The probability of compatibility among the different determinations is 91% when removing the CDF measurement, while dropping at 0.5% if including all experimental values.

2.2 The weak mixing angle as a test of the Standard Model

As already seen, the weak mixing angle θ_w is a fundamental parameter to describe the gauge structure of the electroweak interaction: in fact, it controls the mixing of the unphysical B_μ and W_μ^3 fields to give the photon and Z boson fields, A_μ and Z_μ, and appears in the unification relation of the weak and electromagnetic forces.

At tree level, we can define it via the relation:

$$\sin^2\theta_w = \frac{g_1^2}{g_1^2 + g_2^2} = 1 - \frac{M_W^2}{M_Z^2}, \tag{2.5}$$

as can be verified using Eq. (1.10). In on-shell schemes that include M_W and M_Z as lagrangian parameters (see Chap. 3), one can promote the last equality to an all-order on-shell definition of $\sin\theta_w$, called $\sin\theta_w^{OS}$ [40]. On the other hand, at the Z-boson mass scale, one has another, conceptually different but equivalent at tree level, definition of the parameter, the effective weak mixing angle, $\sin^2\theta_{eff}^f$, that is related to the couplings of the Z boson with fermions:

$$\sin^2\theta_{eff}^f = \frac{1}{4|Q^f|}\left(1 - \operatorname{Re}\frac{g_V^f}{g_A^f}\right), \tag{2.6}$$

where Q_f is the electric charge of the fermion f in units of the positron charge, while g_V^f and g_A^f are the effective vector and axial-vector couplings to the Z boson. A third definition of the weak mixing angle is possible if one performs the Standard Model renormalization within the $\overline{MS}$ scheme, that will be discussed at length in Chap. 3. This scheme makes apparent the energy dependence of the couplings, and since in Eq. (2.5) the weak mixing angle has been introduced as a ratio of couplings, it also acquire a dependence on the renormalization scale squared μ^2: we will label it $\sin\theta_w^{\overline{MS}}(\mu^2)$. The three definitions can be related to one another by appropriately taking into account the relevant radiative corrections:

$$\sin^2\theta_{eff}^f = \kappa_Z^f \sin^2\theta_w^{OS} = \kappa_Z^f(\mu^2)\sin\theta_w^{\overline{MS}}(\mu^2), \tag{2.7}$$

where the factor κ_Z^f and $\kappa_Z^f(\mu^2)$ includes the corrections to the $Zf\bar{f}$ vertex, calculated in the on-shell and $\overline{MS}$ scheme, respectively. The dominant contributions to these kind of corrections involve the same factors already discussed for the W-boson mass, $\Delta\alpha$ and $\Delta\rho$.

2.2.1 Determinations of the effective weak mixing angle

The effective weak mixing angle can be determined by probing the ratio of the vector and axial-vector couplings, defined at the Z pole, with observables like

2. Testing the electroweak Standard Model at high energies

the forward-backward asymmetries at leptonic and hadronic colliders. In fact, the unpolarized cross section of the $e^+e^- \to f\bar{f}$ annihilation process at lowest order can schematically be written as:

$$\frac{d\sigma}{d\cos\theta} = A(1 + \cos^2\theta) + B\cos\theta \,, \tag{2.8}$$

where θ is the angle between the incoming and outgoing fermions, and the coefficients A and B are functions of the electroweak vector and axial-vector couplings. The $(1 + \cos^2\theta)$ term is due to the pure QED diagram, mediated only by the photon, while the additional $\cos\theta$ dependence is due to the presence of the vector and axial-vector couplings in the Z-boson exchange. As a result, the number of events in the forward direction is not equal to the one of the backward production. This effect can be quantified by introducing the forward-backward asymmetry:

$$A_{\text{FB}} = \frac{\sigma_F - \sigma_B}{\sigma_F + \sigma_B}, \quad \sigma_F = \int_0^1 d\cos\theta \frac{d\sigma}{d\cos\theta}, \quad \sigma_B = \int_{-1}^0 d\cos\theta \frac{d\sigma}{d\cos\theta}. \tag{2.9}$$

At the Z-boson resonance, we can write the forward-backward asymmetry of the process $e^+e^- \to f\bar{f}$ at tree level, disregarding the photon exchange diagram and the $Z - \gamma$ interference (which is negligible):

$$A_{\text{FB}}^f = 3 \frac{(1 - 4|Q_e|\sin^2\theta_{eff}^e)}{1 + (1 - 4|Q_e|\sin^2\theta_{eff}^e)^2} \frac{(1 - 4|Q_f|\sin^2\theta_{eff}^f)}{1 + (1 - 4|Q_f|\sin^2\theta_{eff}^f)^2} \,. \tag{2.10}$$

Introducing the asymmetry parameter, defined by:

$$A_f \equiv \frac{2g_v^f g_a^f}{g_a^{f2} + g_v^{f2}} = \frac{1 - 4|Q_f|\sin^2\theta_{eff}^f}{1 - 4|Q_f|\sin^2\theta_{eff}^f + 8|Q_f|^2\sin^4\theta_{eff}^f} \,, \tag{2.11}$$

the forward-backward asymmetry at the Z peak takes the form:

$$A_{\text{FB}}^f = \frac{3}{4} A_e A_f \,, \tag{2.12}$$

where A_e is the asymmetry parameter corresponding to the production $e^+e^- \to Z$, while A_f is the one of the final $Z \to f\bar{f}$ vertex. Measurements of A_{FB}^f near the Z peak have been performed at both leptonic and at hadronic machines, leading to relative precisions below 0.1% and 0.2% on $\sin^2\theta_{eff}^f$, respectively. The advantage of using the asymmetry instead of other observables is that most systematic effects cancel in the ratio of cross sections. At LEP, $\sin^2\theta_{eff}^f$ was measured by counting the number of events to derive the forward and the backward cross section, then computing the forward-backward asymmetries and extracting $\sin^2\theta_{eff}^f$ from Eq. (2.10). SLC exploited the high polarization of the initial electron beam to measure instead the left-right asymmetry A_{LR}, defined as:

$$A_{\text{LR}} = \frac{\sigma_L - \sigma_R}{\sigma_L + \sigma_R} \,. \tag{2.13}$$

16

2.2. The weak mixing angle as a test of the Standard Model

By making use of the relation $A_{LR} = A_e P_e$, this asymmetry can be translated directly to the parameter A_e and then to the effective weak mixing angle, if one knows the average polarization of the initial electron beam, P_e [50, 51].

At hadron colliders, it is not possible to use the LEP/SLD approach based on the parameterization of the resonance in terms of pseudo-observables, because of the combined contribution of several partonic processes, characterised by different couplings to the Z bosons and different weights given by the partonic distribution functions. It is thus necessary to study differential distributions via the template fit method.

To this aim, the neutral current Drell-Yan process, i.e. $pp \to \gamma^*/Z^* + X \to \ell^+\ell^- + X$, is the best one to extract information on the forward-backward asymmetry, by virtue of its large cross section and clear experimental signature. Because of different contributing partonic subprocesses, however, these kind of measurements are affected by more uncertainties with respect to those at electronic machines: the reconstruction of the angle θ is more difficult because the direction of the incoming quark is not precisely known. Another problem is that QCD initial-state radiation leads to the fact that the directions of the incoming partons are not collinear in the laboratory frame, and as a consequence the vector boson acquires a non-negligible transverse momentum. Finally, the flavour of the quarks cannot be determined, making it necessary to take into account the parton density functions, as well as to average over all initial-state flavours.

These problems can be partially overcome if one chooses to measure the angular distributions of the decay leptons in a reference frame where the $\ell^+\ell^-$ pair is at rest. The common choice is the Collins-Soper (CS) frame [52], in which the x-axis is oriented to bisect the angle between the protons within the hadron plane, the y-axis is the normal vector to the hadron plane, and the z-axis is chosen to obtain a right-handed Cartesian coordinate system, as shown in Fig. 2.2. In the CS frame, the scattering angle θ_{CS} is expressed as:

$$\cos\theta_{CS} = \frac{p_z(\ell\ell)}{|p_z(\ell\ell)|} \frac{2(p_1^+ p_2^- - p_1^- p_2^+)}{m_{\ell\ell}\sqrt{m_{\ell\ell}^2 + p_T(\ell\ell)^2}}, \qquad (2.14)$$

with $p_i^\pm = (E_i \pm p_{z,i})/\sqrt{2}$, where E_i and $p_{z,i}$ are the energy and the z component of the momentum of lepton i. In this equation one can recognise two factors: the first one identifies the direction of the incoming quark, while the second one represents an average angle between the decay leptons and the quarks. Note that, since we are dealing with partons inside hadrons, one can correctly perform the assignment of the quark direction only on a statistical basis. In the following the CS subscript will be dropped, given it understood that when discussing measurements at hadronic colliders the angle θ is defined in the Collins-Soper frame.

To be more precise, we write the differential cross section of the Drell-Yan

2. Testing the electroweak Standard Model at high energies
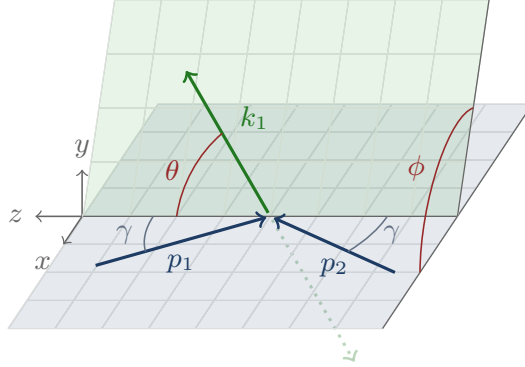
Figure 2.2: The Collins-Soper frame.

process in a general way:

$$
\frac{d\sigma}{dp_T^2 dy d\cos\theta d\phi} = \frac{d\sigma_{\text{unpol}}}{dp_T^2 dy}\left[(1+\cos^2\theta) + \frac{A_0}{2}(1-3\cos^2\theta)\right.
$$
$$
\left. + A_1\sin 2\theta\cos\phi + \frac{A_2}{2}\sin^2\theta\cos 2\phi + A_3\sin\theta\cos\phi + A_4\cos\theta+\right.
$$
$$
\left. + A_5\sin^2\theta\sin 2\phi + A_6\sin 2\theta\sin\phi + A_7\sin\theta\sin\phi\right],
$$

(2.15)

where we have made explicit the cross-section dependence on θ and ϕ, that are the polar and azimuthal angles in the CS frame. The A_i coefficients contain the dependence on the boson kinematics and indirectly depend on the parton distribution functions (PDFs) of the proton. By integrating Eq. (2.15) over the azimuthal angle, it is found that A_{FB} is proportional to A_4, and thus a measurement of A_4 can be used to determine the leptonic effective weak mixing angle.

After measuring the forward-backward asymmetry A_{FB} or the A_4 coefficient, the weak mixing angle is extracted by a template fit approach on the predicted observable set obtained by varying the value of $\sin^2\theta^\ell_{eff}$ in the MC generator program. This procedure requires the amplitude of the process to be written in terms of $\sin^2\theta^\ell_{eff}$, by choosing a suitable input parameter scheme, as we will discuss in Chap. 3. However, all analyses performed so far at hadronic machines rely on LO electroweak event generators: the determined parameter is $\sin^2\theta_w^{OS}$, rather than $\sin^2\theta^\ell_{eff}$, and then a conversion is performed by means of Eq. (2.7).

This procedure is perfectly fine at LO, but if one wants more precise determinations that take into account also NLO effects, more care has to be devoted to some interpretation issues. In fact, the forward-backward asymmetry can be written in terms of vector and axial-vector couplings only at the Z peak, where only the Z contributes to the amplitude and the overall factor of the Z

2.2. The weak mixing angle as a test of the Standard Model
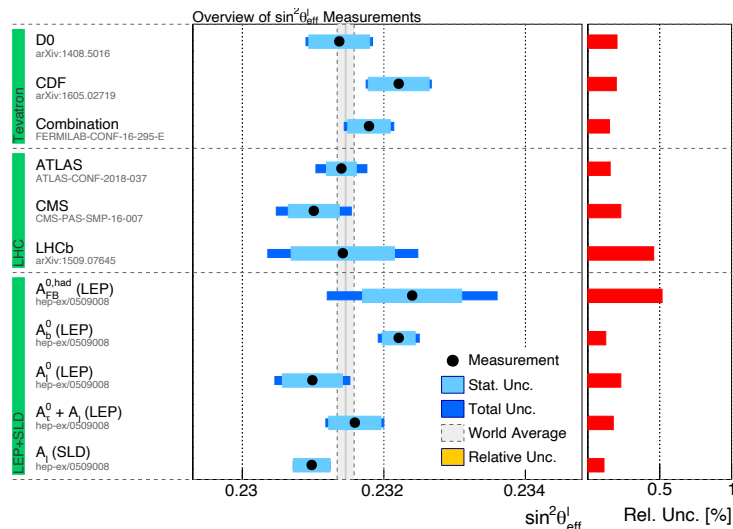
Figure 2.3: Precision measurements of $\sin^2 \theta_{eff}^{\ell}$ from the LEP and SLD experiments, from the D0 and CDF collaborations (Tevatron) and from ATLAS, CMS and LHCb (LHC) [56].

coupling, that in the templates used so far by the experimental collaborations depends on $\sin^2 \theta_w^{OS}$, cancels in the ratio. If one considers a kinematical distribution over an invariant-mass range, the presence of the photon-exchange and interference contributions prevents the cancellation of the overall $\sin^2 \theta_w^{OS}$ in the Z coupling, which at NLO does not coincide with $\sin^2 \theta_{eff}^{\ell}$ anymore, making it questionable to use the same parameter in the overall and in the vector couplings.

Another problem is due to the fact that at hadronic colliders the parameter fitted from A_{FB} is a non-trivial combination of different effective mixing angles, corresponding to the different parton flavours within the (anti)proton, from which one should extract the leptonic effective weak mixing angle.

The way out, within the SM, is to directly take $\sin^2 \theta_{eff}^{\ell}$ as an input parameter of the electroweak renormalization scheme [53], without relying on the combination fo M_Z and M_W that defines $\sin^2 \theta_w^{OS}$, as it will be discussed in Chap. 3.

At the Tevatron, $\sin^2 \theta_{eff}^{\ell}$ was determined by the D0 [54] and CDF [55] Collaborations, yielding a combined value of 0.23148 ± 0.00033 [56], which falls in between the LEP and SLD measurements, with a similar precision.

At the LHC, the most precise determination of $\sin^2 \theta_{eff}^{\ell}$ has been performed by the ATLAS collaboration [57], by fitting the angular coefficient A_4 in electronic and muonic decay channels from the full 2012 data sample. Determinations of $\sin^2 \theta_{eff}^{\ell}$ have been provided also by CMS [58] and LHCb [59], with similar statistical and PDF uncertainties. These measurements, that already reached a precision competitive with the one at the Tevatron, can improve further in the future with the large statistics already collected at a centre-of-

mass energy of 13 TeV during Run 2, with the on-going Run 3 and especially in view of the upgrade of High-Luminosity. Meanwhile, a further reduction of PDF uncertainties will be possible as new PDF constraining methods become available.

The combined value which stems from the results obtained at hadronic colliders (Tevatron and LHC) is $\sin^2\theta^\ell_{eff} = 0.23140 \pm 0.00023$ [56]. If one makes the assumption that this value is not correlated with the measurements at LEP and SLC, it is possible to get a global combination, that yields $\sin^2\theta^\ell_{eff} = 0.23151 \pm 0.00014$ [56]. All discussed experimental determinations are shown in Fig. 2.3.

2.2.2 Low energy experiments

It is possible to determine the weak mixing angle also at energies lower than the Z peak, by using different definitions with respect to the effective one. The low-energy measurements have usually less precision, but they can test the energy dependence, i.e. the running, of the parameter. They are usually performed by studying parity violation in atoms or neutrino and polarized electron scatterings on fixed targets.

The first of these methods exploits the fact that parity violation in atoms is related to the vector couplings of the proton, g_V^p, and the axial-vector couplings of the electrons around the nucleus, g_A^e, which can be combined in the parameter g_{AV}^{ep}. This can be directly seen in the definition of the atomic weak charge $Q_W^{Z,N}$:

$$Q_W^{Z,N} \approx -2\left(Zg_{AV}^{ep} + Ng_{AV}^{en}\right)\left(1 - \frac{\alpha}{2\pi}\right), \tag{2.16}$$

$$g_{AV}^{ep} = 2g_{AV}^{eu} + g_{AV}^{ed} \approx -\frac{1}{2} + 2\sin^2\theta_w, \tag{2.17}$$

$$g_{AV}^{en} = g_{AV}^{eu} + 2g_{AV}^{ed}, \tag{2.18}$$

where Z is the atomic number and N represents the number of neutrons in the atom. These measurements have been performed for several atoms such as cesium and isotope ratios [60–64].

Another approach is based on the study of the process $e_{L,R}N \rightarrow eX$, that is the scattering of a left- or right-handed polarized electron beam on a nuclear target such as deuteron. The left-right asymmetry in the cross section of these processes is a good observable to extract the electroweak mixing angle. This method has been adopted by several groups at different centre-of-mass energies, for example through deep inelastic scattering (DIS) at SLAC [65] and with an electron beam up to 6 GeV at the CEBAF accelerator facility at JLab [66]. Another determination was published by the Qweak Collaboration, which measured the left-right asymmetry by using a beam of longitudinally polarized electrons impinging at 1.16 GeV on a liquid-hydrogen target [67], with a precision of 5% on the weak mixing angle. The left-right asymmetry

2.2. The weak mixing angle as a test of the Standard Model
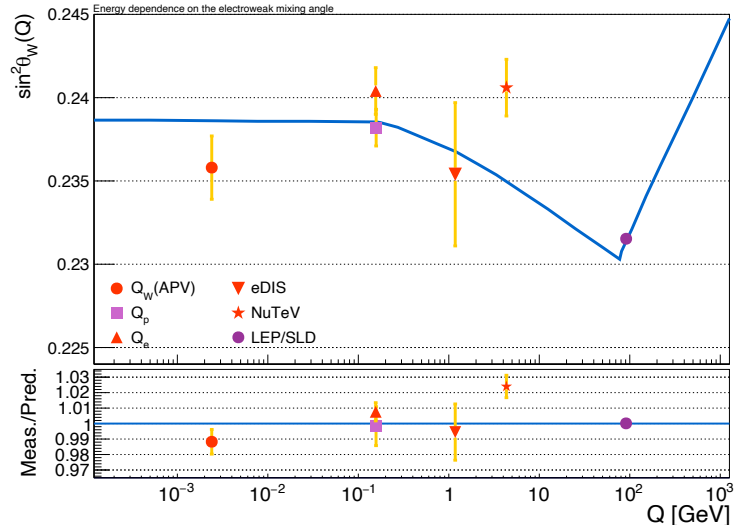
Figure 2.4: Running of $\sin^2 \theta_w$ in the $\overline{MS}$ renormalization scheme, and measurements from low energy experiments including atomic parity violation, parity violating electron scattering, e-DIS, and ν-DIS [56].

has also been studied in the reaction $e^- e^- \rightarrow e^- e^-$ using the electron beam of the SLC directed to liquid hydrogen [68].

Several results are expected for the future to test the low-energy running of the weak mixing angle with higher precision. After the CEBAF upgrade to 12 GeV, a new detector, SoLID, will operate to reduce the experimental uncertainty to the 0.5% level. The P2 experiment at the new Mainz Energy-Recovery Superconducting Accelerator (MESA) will study the forward-backward asymmetry in the elastic electron-proton scattering, by using a high-intensity and highly-polarized beam at 155 MeV. The relative precision is expected to be 0.13%, comparable to the Z pole measurements at LEP and the SLC. Moreover, the MOLLER collaboration at JLab will determine the asymmetry in Møller scattering with a fivefold greater precision as compared to SLAC. Finally, a scanning of the region from 10 to 90 GeV will be possible with the weak DIS data at the future Electron Ion Collider (EIC) [69].

To conclude this section, we turn our attention to neutrino scattering experiments, which are typically performed using the processes $\nu_\mu e \rightarrow \nu_\mu e$ and $\bar{\nu}_\mu e \rightarrow \bar{\nu}_\mu e$. In this case, the ratio of the cross sections of neutrino and anti-neutrino scattering constitutes the most precise available observable:

$$R = \frac{\sigma_{\nu_\mu e}}{\sigma_{\bar{\nu}_\mu e}} \ , \tag{2.19}$$

which is sensitive to the couplings g_V and g_A. Another possible observable is given by the ratio between neutral-current (NC) and charged-current (CC) cross sections in the DIS of neutrinos on isoscalar nuclear targets (N):

$$R_\nu = \frac{\sigma_{\nu N}^{\mathrm{NC}}}{\sigma_{\nu N}^{\mathrm{CC}}} \ . \tag{2.20}$$

21

The CDHS, CHARM and CCFR collaborations at CERN reached an experimental precision of 1% on the weak mixing angle by making use of this approach [70–72]. In 2002, a measurement by the NuTeV collaboration drew the international attention, by providing a value for the on-shell mixing angle that is 3σ larger than the expectation of the Standard Model [73]. Since then, many studies have been published, but a complete explanation of this feature is still subject of discussion. For these reasons, several neutrino experiments have the determination of the weak mixing angle on the agenda, hoping to shed light on the NuTeV puzzling result (cf. [74] and related references).

Fig. 2.4 shows the energy dependence of the weak mixing angle, as predicted by the Renormalization Group Evolution (RGE) equation, given by the blue line. The discussed low-energy experimental results and the most precise determination of the parameter at LEP/SLC are reported as points. In order to make a consistent comparison with the evolution predicted by the RGE equation, in this plot the measurements are interpreted by converting them to a common $\overline{MS}$ definition of the weak mixing angle, $\sin^2\theta_w^{\overline{MS}}(\mu)$, that we will discuss in the following section and in Chap. 3. Different points thus correspond to determinations of $\sin^2\theta_w^{\overline{MS}}(\mu)$ at different values of the renormalization scale μ.

2.2.3   The running weak mixing angle

As it can be seen from Fig. 2.4, low-energy determinations of the weak mixing angle can be translated into the $\overline{MS}$ definition of the parameter, thus allowing a test of the Standard Model running at low scales. In fact, in the $\overline{MS}$ scheme (cf. Chap. 3), the $U(1)_Y$ and $SU(2)_L$ couplings g_1 and g_2 acquire a dependence on the renormalisation scale μ, i.e. they become running quantities, thus making it possible to introduce the weak mixing angle as:

$$\sin^2\theta_w^{\overline{MS}}(\mu^2) \;=\; \frac{e^2_{\overline{MS}}(\mu^2)}{g^2_{2,\overline{MS}}(\mu^2)} \;=\; \frac{4\pi\,\alpha^{\overline{MS}}(\mu^2)}{g^2_{2,\overline{MS}}(\mu^2)}\,, \tag{2.21}$$

where we have used the relation $\alpha^{\overline{MS}}(\mu^2) = e^2_{\overline{MS}}(\mu^2)/4\pi$, where $e_{\overline{MS}}(\mu^2)$ and $g^2_{2,\overline{MS}}(\mu^2)$ are the positron charge and the $SU(2)_L$ coupling, respectively, renormalized in the $\overline{MS}$ scheme. In the following, we will drop the $\overline{MS}$ super- or subscript for all quantities but $\sin^2\theta_w^{\overline{MS}}(\mu^2)$, keeping explicit only the dependence on μ^2.

Together with the low-energy test of the running of the weak mixing angle, some results for larger space-like scales, of the order of a few hundreds of GeV, have been obtained from deep inelastic scattering data at the electron-proton collider HERA [75, 76]. The high-energy regime is particularly interesting: in fact, as it will be discussed in detail in the following chapters, the Renormalisation Group Equation, which governs the energy evolution of the weak mixing angle, predicts a running with a steep positive slope at high scales, because of the inclusion of the W-boson contribution above the W mass [77]. However,

the running at time-like scales above the Z-boson mass has not been experimentally explored. A preliminary analysis on the potential of a determination at the TeV scale, by using proton-proton collisions at $\sqrt{s} = 13.6$ TeV in the Run-3 and High-Luminosity phases of the LHC, can be found in [78], which represents one first important result of the work discussed here.

It should be noted that with this data at high energies it is also possible to probe new particles, beyond the Standard Model physics, provided that they carry electroweak quantum numbers: in fact, the effect of these new states would be a modification of the running of the electroweak gauge couplings [79–81]. These kinds of analysis are particularly interesting because they allow to see new physics particles in a way that is independent of their specific decay channels.

2.3 Running of the electromagnetic and strong coupling constants

To conclude the chapter, some words should be spent on the determinations of the strong and the electromagnetic coupling constants, that represent *per se* a fundamental test of the Standard Model, and cannot be omitted in a dissertation on running couplings. The electromagnetic coupling constant is defined as $\alpha = e^2/4\pi$, which in the on-shell renormalization scheme is required to coincide with the fine structure constant at all orders in perturbation theory, i.e. it is set to $\alpha \simeq 1/137$.

In the $\overline{MS}$ scheme, on the other hand, as a consequence of the renormalization procedure when considering the radiative corrections in the calculations of vacuum polarization diagrams, the electromagnetic coupling constant acquires a dependence on the renormalization scale μ, assimilated to the energy scale of the process under study. The evolution of this parameter from a scale μ_0 to the scale μ is described by the RGE equation, which has the solution:

$$\alpha(\mu^2) = \frac{\alpha(\mu_0^2)}{1 - \Delta\alpha\left(\mu^2, \mu_0^2\right)}, \tag{2.22}$$

where the term $\Delta\alpha\left(\mu^2, \mu_0^2\right)$ includes the resummed gauge-invariant subset of fermionic corrections to vacuum polarization diagrams, at a given order in perturbation theory. It is possible to express the energy dependence of α also in the on-shell scheme:

$$\alpha(s) = \frac{\alpha(0)}{1 - \Delta\alpha(s)}, \tag{2.23}$$

where again $\Delta\alpha(s)$ includes the fermionic corrections calculated in the on-shell scheme, that can be resummed at a certain perturbative order, with s a typical energy scale for the process under consideration. The term $\Delta\alpha$ can be decomposed as:

$$\Delta\alpha(s) = \Delta\alpha_{\text{lep}}(s) + \Delta\alpha_{\text{had}}^{(5)}(s) + \Delta\alpha_{\text{top}}(s), \tag{2.24}$$
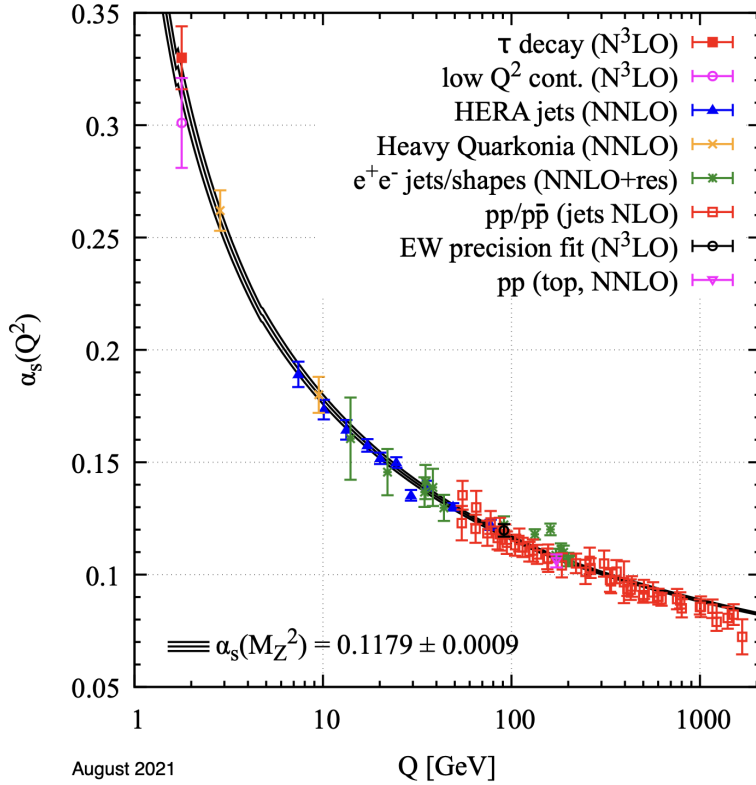
Figure 2.5: Measurements of α_S as a function of the energy scale Q. Between brackets one can see the order of the QCD calculation for the determination of α_S (NLO: next-to-leading order; NNLO: next-to-NLO; res. NNLO: NNLO matched to a resummed calculation; N^{3}LO: next-to-NNLO) [30].

where $\Delta\alpha_{\text{lep}}(s)$ is the leptonic contribution, $\Delta\alpha_{\text{top}}(s)$ is the contribution of top-quark loop, and $\Delta\alpha_{\text{had}}^{(5)}(s)$ represents the one from the five lighter quarks.

The determination of the fine structure constant can be obtained with different methods. One example is the extraction from the electron anomalous magnetic moment, which gives the value $\alpha^{-1} = 137.035999150(33)$ [82]. Another determination comes from the combination of measurements of the Rydberg constant and atomic masses with interferometry of atomic recoil kinematics, applied to rubidium and cesium, yielding $\alpha^{-1} = 137.035999183(10)$ [30]. These two approaches together provide the current world average of $\alpha^{-1} = 137.035999180(10)$ [30]. At $\sqrt{s} = M_Z$ the electromagnetic coupling constant is known with a precision level of few per mille or better, from LEP data or the electroweak precision fit, where the dominant uncertainty is from the five light-quark contributions in $\Delta\alpha(s)$, that is calculated using perturbative QCD for energies sufficiently larger than the strong interaction scale Λ_{QCD} (above about 2 GeV) and away from the $b\bar{b}$ resonance system at around 10 GeV. For energies below Λ_{QCD}, the evaluation of $\Delta\alpha_{\text{had}}^{(5)}(s)$ relies on the evaluation

24

2.3. Running of the electromagnetic and strong coupling constants

of dispersion relations, using a combination of experimental data from e^+e^- annihilation into hadrons [3, 29, 30, 83].

Also in the case of the strong coupling constant α_S, one needs to compute its Renormalization Group Evolution between two different energy scales μ, which can be currently calculated up to five-loop order in QCD and that we report here in the approximation where the five lighter quarks are taken as massless [56, 84]:

$$\frac{d}{d\ln\mu^2}\left(\frac{\alpha_S}{\pi}\right) = -\left[\frac{23}{12}\frac{\alpha_S^2}{\pi^2} + \frac{29}{12}\frac{\alpha_S^3}{\pi^3} + 2.827\frac{\alpha_S^4}{\pi^4} + 18.85\frac{\alpha_S^5}{\pi^5} + 15.1\frac{\alpha_S^6}{\pi^6} + \mathcal{O}\left(\frac{\alpha_S^7}{\pi^7}\right)\right].$$
(2.25)

As it can be seen from Fig. 2.5, the strong coupling constant can be considered sufficiently small at the Z pole, where its value is $\alpha_S(M_Z) = 0.1179 \pm 0.0009$ [30], but it rises greatly at small energy scales near the GeV region. The value of α_S can be determined with a wide range of approaches: some examples are the studies of e^+e^- annihilations, deep-inelastic lepton-nucleon scattering, τ decays, hadron collisions, and Z-pole observables such as Γ_Z and σ_0^h (σ_0^h is the hadronic cross section at the Z pole, which depends on α_S through final state QCD corrections), from which the strong coupling constant is determined as a free parameter in electroweak fits. At the LHC, recent measurements exploit the correlation parameters and the angular distributions of particle jets, while the determinations of α_S with the smallest quoted uncertainties currently come from lattice QCD calculations [30].

3

Electroweak virtual corrections to the neutral-current Drell Yan

n this Chapter, we introduce the building blocks for implementing electroweak virtual corrections at NLO, plus universal higher-order corrections, in a process like the neutral-current Drell Yan. In the literature, the first calculations for electroweak corrections to Drell-Yan processes can be found in the papers at the basis of the numerical codes RADY [85, 86] and Wgrad/Zgrad [87–90]. EW fixed-order corrections to the Drell-Yan processes are computed also in Horace-3.1 [91–93], WINHAC/ZINHAC [94, 95], SANC [96–98], KKMC-hh [99], Dizet [100], as well as in POWHEG-BOX-V2 [101, 102] or in implementations within the POWHEG framework (see e.g. [103]). A review of several studies concerning the Drell Yan and a comparison between different Monte Carlo codes can be found in [104].

We start by reviewing how the electroweak sector of the Standard Model is renormalized, by considering both the on-shell and $\overline{MS}$ scheme. Particular attention is devoted to the choice of the electroweak input parameter scheme: we present the different options implemented in the `Z_ew-BMNNPV` package of the event generator POWHEG-BOX-V2 [102, 105]. A brief description of the POWHEG-BOX framework will be postponed to Chap. 6, in which the numerical results will be discussed. The Chapter ends with some considerations on electroweak corrections at energy scales much greater than the electroweak one.

3.1 Renormalization of the Standard Model: general remarks

In the Standard Model Lagrangian (1.2), it appears a certain number of free parameters, that are not calculable from first principle and have to be determined experimentally. The usual way to proceed is to establish a relation,

3. Electroweak virtual corrections to the neutral-current Drell Yan

which depends on the perturbative order, between these lagrangian parameters and some experimental quantities, i.e. to put them in correspondence with physical masses and couplings.

Beyond the leading-order approximation of the theory, however, infinite (or better, not defined) momentum-loop integrations appear, as a consequence of the continuum structure of four-dimensional space-time; thus, the so-called bare parameters of the original Lagrangian differ from the corresponding physical quantities by divergent contributions. To consistently remove these singularities when evaluating relations between physical quantities and to restore meaningful predictions, one can proceed in two steps: first, one has to introduce a regularization scheme in terms of some parameter, to be able to carry out the calculations, and then proceed with the renormalization, that allows to obtain finite physical predictions.

First of all, the physical quantities are expressed in terms of the bare parameters, and then the resulting relations are used to establish a link between the bare parameters and a set of observables. The prediction of these observables depends on other physical quantities, which have to be determined from experiments. The starting point of any renormalization procedure is thus the choice of a set of independent lagrangian parameters and an input scheme of experimentally known quantities, as we will further discuss in Sec. 3.2. Together with the renormalization conditions, the set of chosen independent parameters defines a *renormalization scheme*. In principle, all renormalization schemes are equivalent to each other, but, when making calculations at some finite order of perturbation theory, the predictions obtained from different choices of input parameters differ by higher-order contributions.

As a non-abelian gauge theory with spontaneous symmetry breaking, the Standard Model has been proven to be renormalizable, which means that the renormalization constants, generated by the renormalization of the independent lagrangian parameters and of the fields, reabsorb all divergences occurring at high-momentum values, called ultraviolet (UV) singularities.

As we mentioned, the first step of this procedure consists in the choice of a regularization prescription, that usually corresponds to *dimensional* regularization, motivated by the fact that the divergent integrals would be finite if the n dimensions of space-time were less than four. One can introduce a parameter to measure how different n is with respect to four:

$$\epsilon = \frac{4 - n}{2} \, . \tag{3.1}$$

The infinite integrals in n dimensions are thus expressed in terms of the combination:

$$\Delta_{UV} = \frac{1}{\epsilon} - \gamma_E + \ln 4\pi \, , \tag{3.2}$$

where γ_E is the Eulero-Mascheroni constant. The $1/\epsilon$ part in the expression of Δ_{UV} becomes divergent in the limit $\epsilon \to 0$, when the original theory is restored, while the terms $-\gamma_E + \ln 4\pi$ are finite. Note that, since the number

of dimensions have changed, one needs to introduce a dimensional parameter μ_{dim}, to assure that dimensionless quantities in natural units, like the electric charge, remain so. Being an unphysical parameter, μ_{dim} cancels out in the calculation of physical quantities.

Beside UV singularities, infrared (IR) divergences can manifest in theories with a massless quantum field, like the photon in QED and the gluon in QCD. This kind of singularities can have a *soft* or *collinear* origin: the first ones are due to the null mass of the (real or virtual) photon or gluon, that is a divergent limit when integrating over the small-energy region; collinear divergences, on the other hand, are related to the emission of photons or gluons in the limit of vanishig angle with respect to the emitting particle and arise when one disregards the masses of the external particles in QED, while they are always present in QCD, where the parton masses are set to zero.

Infrared singularities arise when soft or collinear massless particles are present in the loop integrals, or when integrating over the phase space of emitted real soft/collinear particles. Also in the case of IR divergences a regularization scheme is required to carry on the calculations. In QED, the regularization is traditionally performed by associating a small mass to the photon field. In QCD, on the other side, such a scheme leads to gauge-invariance violations, and the dimensional regularization, sometimes employed also in QED, is preferred. However, both in QED and QCD infrared singularities cancel when evaluating together the contributions of real and virtual corrections.

After the regularization, one proceeds with the renormalization of the UV-singularities, usually performed in the countertem approach: all lagrangian (bare) parameters appearing in Eq. (1.2) are expressed as a combination of finite renormalized parameters and singular renormalization constants, called counterterms, that reabsorb the divergence Δ_{UV} in Eq. (3.2). The counterterms consist of a singular part, fixed in such a way that the resulting physical quantities are UV-finite, and a finite part, which is not constrained by the renormalization requirements. The choice of the finite part determines the renormalization conditions, that allow us to distinguish the two most common classes of renormalization schemes: the on-shell (OS) renormalization schemes, in which the renormalized parameters are usually chosen so to have a manifest physical meaning, and the $\overline{MS}$ renormalization schemes, obtained by setting the finite parts of the counterterms to zero. In each class, a particular scheme can then be specified by the selection of a set of independent input parameters.

3.2   Input-parameter schemes

The selection of an input scheme identifies the specific renormalization scheme adopted within one of the two main classes of on-shell and $\overline{MS}$ schemes: it consists in the specification of some lagrangian parameters, that should be independent from each other; we will refer to this set as *input parameters*. These bare parameters are then expressed in terms of their renormalized counterparts

3. Electroweak virtual corrections to the neutral-current Drell Yan

plus the counterterms as described in Sec. 3.1. In the electroweak sector of the Standard Model, the set of inputs usually comprises the fermionic and Higgs masses, plus three other independent lagrangian parameters, that can be chosen with some freedom, to define the couplings and the gauge-boson masses. All other masses and couplings not taken as inputs, as well as the observable predictions, are expressed as functions of this set.

At the end of the renormalization procedure, in order to have numerical evaluations that can be compared with experimental results, the corresponding renormalized parameters are linked with some measured quantities, that from this point on we will call *input data*, by means of the renormalization conditions. This is true in the on-shell scheme, while in the $\overline{MS}$ scheme the finite parts of the counterterms are simply set to zero. The $\overline{MS}$ scheme has the additional complication that the input renormalized parameters are running, and it can be more difficult to find their natural association to some measured values. The common strategy is to find a relation between $\overline{MS}$ renormalized parameters and physical quantities at a given scale.

The input data is usually chosen in a phenomenology-oriented way, and is relevant for many reasons. From a theoretical perspective, since the predicted observables within a chosen renormalization scheme depend parametrically on the input data, one should try to minimize the parametric uncertainty due to the measured values of the inputs. For this reason, the best known measured constants, such as for example α, G_μ and M_Z, are usually preferred as inputs. The convergence of the perturbative series expansion represents another important criterium for the choice of the input scheme. The idea is to select input quantities, by using which the description of a given process is good already at tree level, as they reabsorb in their definition large radiative corrections. For example, the scheme with G_μ, M_Z and M_W is particularly suitable to describe processes at the electroweak and higher scales, as the coupling contains already in its definition the logarithmic corrections connected with the running from 0 to the energy scale of the process.

In the literature, the usual on-shell scheme is identified by the set of reference measured quantities (α_0, M_W, M_Z), where α_0 denotes the value of the fine structure constant, i.e. the on-shell electromagnetic coupling evaluated at vanishing momenta. A variant of this scheme is $(\alpha(M_Z^2), M_W, M_Z)$, that makes it possible to reabsorb the logarithmic contributions related to the running of the electromagnetic coupling from the scale 0 to M_Z. Finally, the G_μ scheme is defined by the choice (G_μ, M_W, M_Z) and is particularly suited to describe Drell-Yan processes at hadron colliders, since it features a good convergence of the perturbative series.

From a phenomenological point of view, the crucial remark is that the predicted observable within a given scheme can be used in the determination of a parameter of the theory via the template method. When fitting the theoretical predictions onto experimental data, the fundamental constant to be determined must be a free parameter of the model, that can be varied in

the fit in a consistent way, order by order in perturbation theory, without spoiling the accuracy of the calculations. This approach can be applied to the direct determination of parameters defined in both the on-shell and the $\overline{MS}$ scheme. For instance, the measurements of M_Z at LEP1 and of M_W at LEP2, Tevatron and LHC were performed in this way, by having M_Z and M_W, respectively, as input parameters of the Monte Carlo simulation, while, for the determination of the leptonic effective weak mixing angle, schemes such as (α, M_Z, $\sin^2 \theta_{eff}^\ell$) and the (G_μ, M_Z, $\sin^2 \theta_{eff}^\ell$) are being discussed [53].

3.3 Renormalization in the EW Standard Model

In the following sections, we discuss how NLO calculations featuring different renormalization schemes in the electroweak sector can be developed for practical purposes, by referring in particular to their numerical implementation in the neutral-current Drell-Yan package of POWHEG-BOX-V2, `Z_ew-BMNNPV`.

3.3.1 EW renormalization with Lagrangian parameters e, M_W, M_Z

We here treat with some detail the classic on-shell renormalization scheme for the electroweak Standard Model at NLO accuracy, by choosing e, M_W and M_Z as independent parameters. For what concerns the input physical quantities, we present the three possible selections available in the `Z_ew-BMNNPV` package of POWHEG-BOX-V2, namely (α_0, M_W, M_Z), $(\alpha(M_Z^2), M_W, M_Z)$ and (G_μ, M_W, M_Z). The input data for e can be α_0, $\alpha(M_Z^2)$ or G_μ, while we choose the measured value for M_W discussed in Sec. 2.1 and M_Z measured at LEP for the Z-boson mass. This first subsection will serve as an example, to which we will refer in the following when discussing other renormalization scheme options. For this reason we will first give the reader an idea on how to start the calculations when renormalizing both the fermionic and bosonic sectors of the electroweak Standard Model. Then we will focus on the gauge sector, and on the possible choices of input parameters and data. We refer to [17, 106, 107] for the complete treatment of the renormalization procedure and to [103, 105] for the implementation in POWHEG-BOX-V2.

First of all, we start by taking α_0, M_W, and M_Z as input physical quantities. We denote bare quantities by an index B and express them in terms of renormalized quantities and renormalization constants, as follows:

$$
\begin{aligned}
e_B &= (1 + \delta Z_e)\, e\,, & (3.3) \\
M_{W,B}^2 &= M_W^2 + \delta M_W^2\,, & (3.4) \\
M_{Z,B}^2 &= M_Z^2 + \delta M_Z^2\,, & (3.5) \\
M_{H,B}^2 &= M_H^2 + \delta M_H^2\,, & (3.6) \\
m_{f,i,B}^2 &= m_{f,i}^2 + \delta m_{f,i}^2\,, & (3.7)
\end{aligned}
$$

where we have chosen the quark-mixing matrix V_{ij} as unitary.

Since radiative corrections have the effect to shift the minimum of the Higgs potential, one has to introduce an additional counterterm for the vacuum expectation value of the Higgs field, that is usually denoted as δt and is fixed in such a way that it cancels all tadpole diagrams. Besides the counterterms defined above, in order to have finite Green functions one needs also the renormalization of fields, so that renormalized fields are mass eigenstates:

$$
\begin{aligned}
W_B^\pm &= \left(1 + \frac{1}{2}\delta Z_W\right) W^\pm\,, \\
\begin{pmatrix} Z_B \\ A_B \end{pmatrix} &= \begin{pmatrix} 1 + \delta Z_{ZZ}/2 & \delta Z_{ZA}/2 \\ \delta Z_{AZ}/2 & 1 + \delta Z_{AA}/2 \end{pmatrix} \begin{pmatrix} Z \\ A \end{pmatrix}\,, \\
H_B &= \left(1 + \frac{1}{2}\delta Z_H\right) H\,, \quad\quad\quad\quad (3.8) \\
f_{i,B}^L &= \left(\delta_{ij} + \frac{1}{2}\delta Z_{ij}^{f,L}\right) f_j^L\,, \\
f_{i,B}^R &= \left(\delta_{ij} + \frac{1}{2}\delta Z_{ij}^{f,R}\right) f_j^R\,.
\end{aligned}
$$

$$(3.9)$$

The renormalization constants are fixed by imposing renormalization conditions. The first one determines the Higgs vev counterterm by using the Higgs one-point amputated renormalized Green function, or tadpole, T:

$$
T = \quad \overset{H}{\text{-----}}\bigcirc
$$

and by requiring:

$$T + \delta t = 0\,. \quad\quad\quad (3.10)$$

The field and mass renormalization constants are fixed by making use of the one-particle irreducible (1PI) two-point functions, that in the 't Hooft-Feynman gauge are defined as:
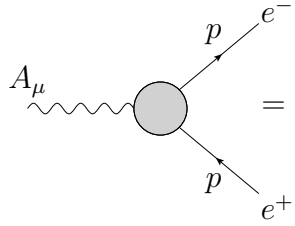
$$
\mu \overset{W}{\underset{k}{\text{wwww}}}\bigcirc \overset{W}{\underset{k}{\text{wwww}}}\nu \quad = \Gamma_{\mu\nu}^W(k)
$$

$$
= -ig_{\mu\nu}(k^2 - M_W^2) - i\left(g_{\mu\nu} - \frac{k_\mu k_\nu}{k^2}\right)\hat\Sigma_T^W(k^2) - i\frac{k_\mu k_\nu}{k^2}\hat\Sigma_L^W(k^2)\,,
$$

$$
\mu \overset{a}{\underset{k}{\text{wwww}}}\bigcirc \overset{b}{\underset{k}{\text{wwww}}}\nu \quad = \Gamma_{\mu\nu}^{ab}(k)
$$

$$
= -ig_{\mu\nu}(k^2 - M_a^2)\delta_{ab} - i\left(g_{\mu\nu} - \frac{k_\mu k_\nu}{k^2}\right)\hat\Sigma_T^{ab}(k^2) - i\frac{k_\mu k_\nu}{k^2}\hat\Sigma_L^{ab}(k^2)\,,
$$

3.3. Renormalization in the EW Standard Model

where $a, b = A, Z$ and $M_A = 0$, and:

$$\begin{array}{c}\overset{H}{\underset{k}{\text{-----}}} \bigcirc \overset{H}{\text{-----}}\end{array} = \Gamma^H(k) = i(k^2 - M_H^2) - i\hat{\Sigma}^H(k^2)\,,$$

$$\begin{array}{c}\overset{f_i}{\underset{p}{\longrightarrow}} \bigcirc \overset{f_j}{\longrightarrow}\end{array} = \Gamma_{ij}^f(k)$$

$$= i\delta_{ij}(\slashed{p} - m_i) + i\left[\slashed{p}\omega_- \hat{\Sigma}_{f,L}^{ij}(p^2) + \slashed{p}\omega_+ \hat{\Sigma}_{f,R}^{ij}(p^2) + (m_{f,i}\omega_- + m_{f,i}\omega_+)\hat{\Sigma}_{f,S}^{ij}(p^2)\right]\,,$$

with $\omega_\pm = (1 \pm \gamma_5)/2$. Following the usual convention, we denote with a caret the renormalized self-energies and suppress the index B from the bare ones. The particle propagators correspond to the inverse of the two-point functions. The renormalized masses are fixed by fulfilling the request that they must be equal to the corresponding physical masses, i.e. to the real parts of the poles of the corresponding propagators, or equivalently to the zeros of the 1PI two-point functions. The field renormalization matrices are taken in such a way that the renormalized 1PI two-point functions are diagonal if the external lines are on-shell. In this way, one determines the non-diagonal elements of the field renormalization matrices, while the diagonal is fixed so that the residues of the renormalized propagators equal one. In terms of two-point functions, the renormalization conditions for on-shell external fields are:

$$\text{Re}\,\Gamma_{\mu\nu}^W(k)\epsilon^\nu(k)|_{k^2=M_W^2} = 0\,, \qquad \lim_{k^2 \to M_W^2} \frac{1}{k^2 - M_W^2}\text{Re}\,\Gamma_{\mu\nu}^W(k)\epsilon^\nu(k) = -i\epsilon_\mu(k)\,,$$

$$\text{Re}\,\Gamma_{\mu\nu}^{ZZ}(k)\epsilon^\nu(k)|_{k^2=M_Z^2} = 0\,, \qquad \lim_{k^2 \to M_Z^2} \frac{1}{k^2 - M_Z^2}\text{Re}\,\Gamma_{\mu\nu}^{ZZ}(k)\epsilon^\nu(k) = -i\epsilon_\mu(k)\,,$$

$$\text{Re}\,\Gamma_{\mu\nu}^{AZ}(k)\epsilon^\nu(k)|_{k^2=M_Z^2} = 0\,, \qquad \lim_{k^2 \to 0} \frac{1}{k^2}\text{Re}\,\Gamma_{\mu\nu}^{AA}(k)\epsilon^\nu(k) = -i\epsilon_\mu(k)\,,$$

$$\text{Re}\,\Gamma_{\mu\nu}^{AZ}(k)\epsilon^\nu(k)|_{k^2=0} = 0\,, \qquad \text{Re}\,\Gamma_{\mu\nu}^{AA}(k)\epsilon^\nu(k)|_{k^2=0} = 0\,,$$

$$\text{Re}\,\Gamma^H(k)|_{k^2=M_H^2} = 0\,, \qquad \lim_{k^2 \to M_H^2} \frac{1}{k^2 - M_H^2}\text{Re}\,\Gamma^H(k) = i\,,$$

$$\widetilde{\text{Re}}\,\Gamma_{ij}^f(p)u_j(p)|_{p^2=m_{f,j}^2} = 0\,, \qquad \lim_{p^2 \to m_{f,i}^2} \frac{\slashed{p} + m_{f,i}}{p^2 - m_{f,i}^2}\widetilde{\text{Re}}\,\Gamma_{ii}^f(p)u_i(p) = iu_i(p)\,,$$

$$\widetilde{\text{Re}}\,\bar{u}_i(p')\Gamma_{ij}^f(p')|_{p'^2=m_{f,j}^2} = 0\,, \qquad \lim_{p'^2 \to m_{f,i}^2} \bar{u}_i(p')\widetilde{\text{Re}}\,\Gamma_{ii}^f(p')\frac{\slashed{p}' + m_{f,i}}{p'^2 - m_{f,i}^2} = i\bar{u}_i(p')\,,$$

$$(3.11)$$

where $\epsilon(k)$ is the polarization vector and $u(p)$ and $\bar{u}(p)$ are the spinors of the external fields. The operator $\widetilde{\text{Re}}$ takes the real part of the loop integrals but not of the quark-mixing matrix elements appearing in the self energies, and it

3. Electroweak virtual corrections to the neutral-current Drell Yan

coincides with the usual real part Re if one takes the quark-mixing matrix as real, as we do here, since we take it to be the identity. From Eqs. (3.11) we can derive the conditions on the renormalized self-energies that are reported in [107].

For the charge renormalization one needs the $ee\gamma$-vertex three-point function: one defines the electric charge as the $ee\gamma$-coupling for on-shell external particles in the Thomson limit, that corresponds to the following condition for the amputated three-point function:

$$\left. = \bar{u}(p)\Gamma_\mu(p,p)^{ee\gamma}u(p)\right|_{p^2=m_e^2} = ie\bar{u}(p)\gamma_\mu u(p)$$

By means of the renormalization conditions, one can express the counterterms as functions of the unrenormalized self-energies evaluated at special external momenta. For the complete expressions of the counterterms, we refer to [17, 107], while here we report only the ones concerning the gauge sector, that will be the most relevant when discussing the different options implemented in POWHEG-BOX-V2:

$$\delta M_W^2 = \operatorname{Re}\Sigma_T^W(M_W^2) \qquad \delta Z_W = -\operatorname{Re}\left.\frac{\partial\Sigma_T^W(k^2)}{\partial k^2}\right|_{k^2=M_W^2},$$

$$\delta M_Z^2 = \operatorname{Re}\Sigma_T^{ZZ}(M_Z^2) \qquad \delta Z_{ZZ} = -\operatorname{Re}\left.\frac{\partial\Sigma_T^{ZZ}(k^2)}{\partial k^2}\right|_{k^2=M_Z^2},$$

$$\delta Z_{AZ} = -2\operatorname{Re}\frac{\Sigma_T^{AZ}(M_Z^2)}{M_Z^2} \qquad \delta Z_{ZA} = 2\frac{\Sigma_T^{AZ}(0)}{M_Z^2}, \qquad \delta Z_{AA} = -\left.\frac{\partial\Sigma_T^{AA}(k^2)}{\partial k^2}\right|_{k^2=0}.$$

$$(3.12)$$

By virtue of the Ward identity, the charge renormalization can be written as:

$$\delta Z_e = -\frac{1}{2}\delta Z_{AA} = \frac{1}{2}\left.\frac{\partial\Sigma_T^{AA}(k^2)}{\partial k^2}\right|_{k^2=0}. \tag{3.13}$$

In the schemes where we choose the gauge-boson masses as independent lagrangian parameters, the weak mixing angle is a derived quantity and the counterterms of its sine and cosine, s_w and c_w, at one-loop order are expressed as:

$$\frac{\delta c_w}{c_w} = \frac{1}{2}\left(\frac{\delta M_W^2}{M_W^2} - \frac{\delta M_Z^2}{M_Z^2}\right) = \frac{1}{2}\operatorname{Re}\left(\frac{\Sigma_T^W(M_W^2)}{M_W^2} - \frac{\Sigma_T^{ZZ}(M_Z^2)}{M_Z^2}\right),$$

$$\frac{\delta s_w}{s_w} = -\frac{c_w^2}{s_w^2}\frac{\delta c_w}{c_w} = -\frac{1}{2}\frac{c_w^2}{s_w^2}\operatorname{Re}\left(\frac{\Sigma_T^W(M_W^2)}{M_W^2} - \frac{\Sigma_T^{ZZ}(M_Z^2)}{M_Z^2}\right). \tag{3.14}$$

3.3. Renormalization in the EW Standard Model

The unrenormalized self-energies can thus be calculated from the Feynman rules by making use of loop integral techniques discussed in [17, 107]. For example, in [108] it is computed the explicit expression of $\Sigma_T^{AA}(k^2)$ and the counterterm δZ_e.

From a practical point of view, when $\alpha(M_Z^2)$ or G_μ are used as input parameters, the calculation of the NLO corrections is formally the same one as in the (α_0, M_W, M_Z) scheme, provided that one makes the replacements:

$$\delta Z_e \;\to\; \delta Z_e - \frac{\Delta\alpha(M_Z^2)}{2}\,,$$
$$\delta Z_e \;\to\; \delta Z_e - \frac{\Delta r}{2}\,, \tag{3.15}$$

respectively for the $(\alpha(M_Z^2), M_W, M_Z)$ and the (G_μ, M_W, M_Z) scheme. The terms $\Delta\alpha(M_Z^2)$ and Δr remove the logarithmically enhanced fermionic corrections coming from the on-shell running of $\alpha(q^2)$ from $q = 0$ to the weak scale, which are already absorbed in the LO couplings $\alpha(M_Z^2)$ or G_μ. In particular, $\Delta\alpha(M_Z^2)$ represents the fermionic running of the electromagnetic coupling constant from 0 to M_Z, which will be discussed in Sec. 3.4.1, while Δr is the full one-loop electroweak corrections to the muon decay in the on-shell scheme (α_0, M_W, M_Z) after the subtraction of the QED effects in the Fermi theory. In this scheme, the factor Δr reads:

$$\Delta r = \Delta\alpha - \frac{c_w^2}{s_w^2}\Delta\rho + \Delta r_{rem}, \tag{3.16}$$

with

$$\Delta\rho = \frac{\Sigma_T^{ZZ}(0)}{M_Z^2} - \frac{\Sigma_T^W(0)}{M_W^2} = \frac{\alpha}{4\pi}\frac{3}{4s_w^2}\frac{m_t^2}{M_W^2} + \cdots = \Delta\rho^{1-\text{loop}} + \ldots\,, \tag{3.17}$$

and

$$
\begin{aligned}
\Delta r_{rem} \;=\;& \frac{\text{Re}\Sigma_T^{AA}(s)}{s} - \frac{c_w^2}{s_w^2}\left(\frac{\delta M_Z^2}{M_Z^2} - \frac{\Sigma_T^{ZZ}(0)}{M_Z^2}\right) \\
& + \frac{c_w^2 - s_w^2}{s_w^2}\left(\frac{\delta M_W^2}{M_W^2} - \frac{\Sigma_T^{WW}(0)}{M_W^2}\right) + 2\frac{c_w}{s_w}\frac{\Sigma_T^{AZ}(0)}{M_Z^2} \\
& + \frac{\alpha}{4\pi s_w^2}\left(6 + \frac{7 - 4s_w^2}{2s_w^2}\log(c_w^2)\right).
\end{aligned}
\tag{3.18}
$$

We make here an important remark about the functioning of the code. In the package `Z_ew-BMNNPV`, a flag called `a2a0-for-QED-only` has been implemented: when active, the same numerical value of the LO couplings (that can be α_0, $\alpha(M_Z^2)$ or α_{G_μ}, that is the value of α computed from G_μ) is also used for the overall weak loop factors. Otherwise, regardless of the scheme used, the additional loop factor coming from the virtual weak corrections is set by default to α_0; on the other hand, the additional α factor from QED corrections

is always equal to α_0, to assure the cancellation of IR divergences between the virtual and the real corrections. In fact, in the real emissions, photons are emitted on-shell, with momentum $q^2 = 0$, and the correct choice of the scale in the vertex coupling is thus 0. As a consequence, the right coupling to cancel the IR singularities is α_0, which has to be used also for the virtual corrections.

Given that in the NCDY it is possible to separate the pure weak corrections from the QED ones, as they are separately gauge invariant, for weak corrections one has some freedom to choose the loop coupling. In fact, if one aims at one-loop accuracy, the choice of the coupling that enters the virtual corrections is completely arbitrary, because spurious terms are beyond the nominal accuracy and thus out of control. When performing perturbative calculations, one can make the decision to use α_0 in all weak and QED loops to treat QED and weak corrections in the same manner, or choose to express α in terms of the corresponding combination of input quantities, according to the adopted scheme, as it has been done for the analysis presented in this work: the latter option highlights the differences among renormalization schemes.

3.3.2   Implementation of leading universal higher orders

In this section we address some features of the latest version of the package `Z_ew-BMNNPV` of POWHEG-BOX-V2, where the neutral-current Drell-Yan process is implemented at an accuracy that is NLO+leading universal higher-order (h.o.) contributions. We think it is useful to introduce the topic here, to discuss how these higher-order terms can be included in the $(\alpha_0/\alpha(M_Z^2)/G_\mu, M_W, M_Z)$ schemes. In the following sections, we will see how they are implemented in different renormalization schemes.

At collider energies of the order of $10 - 100$ GeV, the leading corrections to the neutral-current Drell-Yan production are related to the logarithms of the light fermion masses and to terms proportional to the top-quark mass squared. These contributions are connected to the counterterms for the process under consideration and arise from the running of $\alpha(q^2)$ (i.e. from $\Delta\alpha$) and from the term $\Delta\rho$.

Since the full two-loop calculation is not yet available for a $2 \to 2$ process like the Drell Yan, one possible way to evaluate the impact of these effects is taking the square of the part of the counterterm amplitude proportional to $\Delta\alpha$ and $\Delta\rho$ [86, 107, 109, 110] and combining it to the full NLO calculation, after having subtracted the linear terms in $\Delta\alpha$ and $\Delta\rho$ that are already present at one loop, to avoid double-counting. Furthermore, one could think of improving the one-loop accuracy by also including the dominant next-to-next-to-leading (NNLO) effects, coming from the fermionic corrections included in $\Delta\alpha$ and $\Delta\rho$, of course under the hypothesis that the bosonic contributions are suppressed. These terms are fermionic in the sense that they are related to closed fermion loops, and constitute a gauge-invariant set: thus, their inclusion does not spoil the gauge independence of the calculation and the validity of theoretical predictions, to be compared with experimental results.

3.3. Renormalization in the EW Standard Model

In the `Z_ew-BMNNPV` package the two-loop leptonic corrections related to $\Delta\alpha$ can be activated with the flag `dalpha_lep_2loop`. The results in Chap. 6 are however presented by using the one-loop expression for $\Delta\alpha$. Concerning $\Delta\rho$, in the code the leading Yukawa-enhanced corrections are included up to $\mathcal{O}(\alpha_S^2)$, $\mathcal{O}(\alpha_S x_t^2)$, and $\mathcal{O}(x_t^3)$, with $x_t = \sqrt{2}G_\mu m_{top}^2/16\pi^2$. To be more precise, $\Delta\rho$ is expressed as:

$$
\begin{aligned}
\Delta\rho \;=\;& 3x_t(\Delta\rho^{(1)} + x_t\Delta\rho^{(2)})\left(1 + \frac{\alpha_S}{\pi}\delta_{QCD}^{(2)} + \frac{\alpha_S^2}{\pi^2}\delta_{QCD}^{(3)}\right) \\
& + x_t^3\Delta\rho^{x_t^3} + \frac{\alpha_S}{\pi}x_t^2\Delta\rho^{x_t^2\alpha_S} - 3x_t^2\Delta\rho^{(2)}\frac{\alpha_S^2}{\pi^2}\delta_{QCD}^{(2)},
\end{aligned}
\tag{3.19}
$$

where $\Delta\rho^{(1)}$ and $\Delta\rho^{(2)}$ are the one and two-loop heavy-top corrections to the ρ parameter calculated in [111–113], $\delta_{QCD}^{(2)}$ and $\delta_{QCD}^{(3)}$ are the two and three-loop QCD corrections [114–117], and $\Delta\rho^{x_t^3}$ and $\Delta\rho^{x_t^2\alpha_S}$ are three-loop contributions where also the top mass squared is present [118]. The role of the last term in Eq. (3.19) is to avoid the double counting of the $\mathcal{O}(x_t^2\alpha_S^2)$ contribution, which is already present in a factorized form when performing the product in the first line of the equation. The four-loop QCD corrections to the ρ parameter [119] are not included in the code, but their impact is expected to be negligible at the energies available at the LHC, as it can be seen from the numerical results at three-loop in QCD presented in Chap. 6. Note that in Eq. (3.19) one should choose a renormalization scale for the strong coupling constant, that is renormalized in the $\overline{MS}$ scheme: for the numerical results in Chap. 6 we choose to set it to the invariant mass of the dilepton pair.

In the $(\alpha_0/\alpha(M_Z^2)/G_\mu, M_W, M_Z)$ schemes, by taking the expression of the counterterms one can notice that the leading fermionic corrections at NLO EW accuracy are related to:

$$
\delta Z_e \sim \frac{\Delta\alpha}{2}, \quad \frac{\delta s_W}{s_W} \sim \frac{1}{2}\frac{c_W^2}{s_W^2}\Delta\rho, \quad \Delta r \sim \Delta\alpha - \frac{c_W^2}{s_W^2}\Delta\rho.
\tag{3.20}
$$

In the `Z_ew-BMNNPV` package, the leading fermionic corrections to neutral-current Drell-Yan up to $\mathcal{O}(\alpha^2)$ have been implemented as in Eqs. (3.45)-(3.49) of Ref. [86], modified to be valid also in the complex-mass scheme [105] (cf. Sec. 4.1).

The calculation in this class of schemes is performed as follows. In the linear terms of the fermionic corrections, one has to apply the replacement:

$$
\Delta\rho \to (\Delta\rho - \Delta\rho^{1-\text{loop}}),
\tag{3.21}
$$

while the terms proportional to $\Delta\alpha$ are left untouched, since we are not including two-loop contributions to this factor. Note that, as already stated, it is necessary to subtract the effects already included in the one-loop calculation to avoid double counting, a procedure that requires some care concerning the treatment of the overall coupling constant in front of the weak corrections. In

fact, if the flag `a2a0-for-QED-only` is active, $\Delta\rho^{1-\mathrm{loop}}$ is computed as a function of α_0, $\alpha(M_Z^2)$, or G_μ for the (α_0, M_W, M_Z), $(\alpha(M_Z^2), M_W, M_Z)$, and (G_μ, M_W, M_Z) schemes, respectively. If instead α_0 is used for the overall weak-loop factors, one subtracts the quantity $\Delta\rho^{1-\mathrm{loop}}|_{\alpha_0}$ computed in the α_0 scheme, independently from the numerical value of α used as independent parameter.

3.3.3 EW renormalization with Lagrangian parameters e, $\sin^2\theta^\ell_{eff}$, M_Z

As it has already been discussed, the weak mixing angle is a fundamental parameter of the theory of the electroweak interaction. Its leptonic effective definition $\sin^2\theta^\ell_{eff}$, that is introduced at the Z peak, can be a quantity sensitive to new physics, and as such has been measured at LEP/SLD and then at the Tevatron and at the LHC with very high precision. The direct determination of $\sin^2\theta^\ell_{eff}$ can be made by following either a model independent approach or within the pure Standard Model, thus allowing for an internal self-consistency check of the theory. This latter approach proceeds through the template method: the theoretical kinematical distributions, obtained by varying the value of the input parameter $\sin^2\theta^\ell_{eff}$, are compared with the experimental data, and the best value for $\sin^2\theta^\ell_{eff}$ is extracted with a fit. In order to be consistently treated in the evaluation of perturbative corrections at any given fixed order, the leptonic effective weak mixing angle has to be an input parameter of the renormalization procedure, i.e. a free parameter in the model that can be varied during the fit, as already seen in Sec. 3.2.

We discuss here the formulation of a renormalization scheme which includes the leptonic effective weak mixing angle. Any code featuring such a scheme, like the package `Z_ew-BMNNPV` of POWHEG-BOX-V2, can be employed for a direct determination of $\sin^2\theta^\ell_{eff}$ with the Standard Model.

We start by choosing the lagrangian independent parameters to be e, $\sin^2\theta^\ell_{eff}$ and M_Z. The experimental reference data for e can be α_0, $\alpha(M_Z^2)$ or G_μ, while we take the values of $\sin^2\theta^\ell_{eff}$ and M_Z measured at LEP for the leptonic effective weak mixing angle and the Z-boson mass, respectively. We will collectively refer to these three possible schemes as the $(\alpha_i, \sin^2\theta^\ell_{eff}, M_Z)$ schemes, with $\alpha_i = \alpha_0, \alpha(M_Z^2), G_\mu$. The main references used for this discussion are [53, 105].

The leptonic effective weak mixing angle is defined in terms of the vector and axial-vector couplings of the Z boson to leptons, g_V^ℓ and g_A^ℓ, or, equivalently, in terms of the chiral couplings g_L^ℓ and g_R^ℓ, as measured at the Z peak:

$$\sin^2\theta^\ell_{eff} \;\equiv\; \frac{I_3^\ell}{Q_\ell}\,\mathrm{Re}\left(\frac{-g_R^\ell(M_Z^2)}{g_L^\ell(M_Z^2) - g_R^\ell(M_Z^2)}\right)\,, \tag{3.22}$$

where Q_ℓ and I_3^ℓ are the electromagnetic charge and the third component of the weak isospin for left-handed leptons, respectively.

In the $(\alpha_i, \sin^2\theta^\ell_{eff}, M_Z)$ schemes, the counterterms corresponding to the

3.3. Renormalization in the EW Standard Model

input parameters are defined as:

$$
\begin{aligned}
M_{Z,B} &= M_Z + \delta M_Z && (3.23) \\
\sin^2\theta_{w,B} &= \sin^2\theta^\ell_{eff} + \delta\sin^2\theta^\ell_{eff} && (3.24) \\
e_B &= e\,(1 + \delta Z_e)\,. && (3.25)
\end{aligned}
$$

We fix the expressions of δZ_e and δM_Z as discussed in Sect. 3.3.1, while the renormalization constant $\delta\sin^2\theta^\ell_{eff}$ is determined by requiring that the definition in Eq. (3.22) holds up to the order at which we are performing the calculation. More precisely, Eq. (3.22) can be written at one loop as:

$$
\begin{aligned}
\sin^2\theta^\ell_{eff} &\equiv \frac{I^\ell_3}{Q_\ell}\,\mathrm{Re}\left(\frac{-\mathcal{G}^\ell_R(M^2_Z)}{\mathcal{G}^\ell_L(M^2_Z) - \mathcal{G}^\ell_R(M^2_Z)}\right) && (3.26) \\
&= \frac{1}{2}\mathrm{Re}\,\frac{-g_R}{g_L - g_R} + \frac{1}{2}\mathrm{Re}\,\frac{g_L g_R}{(g_L - g_R)^2}\left(\frac{\delta g^\ell_L}{g^\ell_L} - \frac{\delta g^\ell_R}{g^\ell_R}\right),
\end{aligned}
$$

where $\mathcal{G}_{L/R}(M^2_Z) = g_{L/R} + \delta g_{L/R}(M^2_Z)$ are the NLO form factors for the vertices $Z\ell^L\ell^L$ and $Z\ell^R\ell^R$, respectively. Thus, the following condition must hold:

$$
\mathrm{Re}\left(\frac{-\mathcal{G}^\ell_R(M^2_Z)}{\mathcal{G}^\ell_L(M^2_Z) - \mathcal{G}^\ell_R(M^2_Z)}\right) = \mathrm{Re}\left(\frac{-g^\ell_R}{g^\ell_L - g^\ell_R}\right), \tag{3.27}
$$

which implies:

$$
\mathrm{Re}\left(\frac{\delta g^\ell_L}{g^\ell_L} - \frac{\delta g^\ell_R}{g^\ell_R}\right) = 0\,. \tag{3.28}
$$

Note that, if one uses the complex-mass scheme to treat the unstable particles, M_Z becomes complex, but $\sin^2\theta^\ell_{eff}$ and $g_{L/R}$ are kept real, and Eq. (3.28) remains unchanged. The factors $\delta g_{L/R}$ are functions of $\delta\sin^2\theta^\ell_{eff}$ and contain both bare vertices and counterterms. Thus, starting from the expressions of $\delta g_{L/R}$, one can use Eq. (3.28) to compute:

$$
\begin{aligned}
\frac{\delta\sin^2\theta^\ell_{eff}}{\sin^2\theta^\ell_{eff}} = \mathrm{Re}\Bigg\{ &-\frac{1}{2}\frac{\cos\theta^\ell_{eff}}{\sin\theta^\ell_{eff}}\delta Z_{AZ} \\
&+ \left(1 - \frac{Q_\ell}{I^\ell_3}\sin^2\theta^\ell_{eff}\right)\left[\delta Z^\ell_L + \delta V^L - \delta Z^\ell_R - \delta V^R\right]\Bigg\},
\end{aligned} \tag{3.29}
$$

where the first line includes the fermionic corrections, which are separately gauge invariant together with the bosonic ones, that appear in the second line. The renormalization constants $\delta Z^\ell_{L/R}$ represent the pure weak parts of the leptonic wave function renormalization counterterms, while $\delta V^{L/R}$ are the

3. Electroweak virtual corrections to the neutral-current Drell Yan

NLO weak corrections to the left/right $Z\ell\ell$ vertices and are defined as:

$$
\begin{aligned}
\delta V^L &= \left(g_L^\ell\right)^2 \frac{\alpha}{4\pi} \mathcal{V}_a \left(0, M_Z^2, 0, M_Z, 0, 0\right) \\
&+ \frac{1}{2s_{eff}^2} \frac{g_L^\nu}{g_L^\ell} \frac{\alpha}{4\pi} \mathcal{V}_a \left(0, M_Z^2, 0, M_W, 0, 0\right) \\
&- \frac{c_{eff}}{s_{eff}} \frac{1}{2s_{eff}^2} \frac{1}{g_L^\ell} \frac{\alpha}{4\pi} \mathcal{V}_b \left(0, M_Z^2, 0, 0, M_W, M_W\right) \\
\delta V^R &= \left(g_R^\ell\right)^2 \frac{\alpha}{4\pi} \mathcal{V}_a \left(0, M_Z^2, 0, M_Z, 0, 0\right) .
\end{aligned}
\tag{3.30}
$$

Note that the short-hand notation $s_{eff} = \sin\theta_{eff}^\ell$ and $c_{eff} = \cos\theta_{eff}^\ell$ has been used. The definitions of the vertex functions $\mathcal{V}_a$ and $\mathcal{V}_b$ can be found in Eqs. (C.1) and (C.2) of Ref. [107], respectively. An important remark is that Eq. (3.29) does not include any QED correction, since the QED contributions to the $Z\ell\ell$ vertex are the same for left or right-handed fermions and cancel in Eq. (3.28). Eq. (3.29) is valid also if the complex-mass scheme is employed to treat the Z resonance, provided that one takes the complex-mass expressions for $\delta Z_{L/R}^\ell$ and δZ_{AZ} [53], and paying attention to use a real $q^2 = M_Z^2$ value when this comes from the process kinematics.

As already discussed in Sect. 3.3.1, one can obtain the counterterms in the $(\alpha(M_Z^2), \sin^2\theta_{eff}^\ell, M_Z)$ and $(G_\mu, \sin^2\theta_{eff}^\ell, M_Z)$ schemes from the ones in the $(\alpha_0, \sin^2\theta_{eff}^\ell, M_Z)$ scheme by simply applying the replacements:

$$
\begin{aligned}
\delta Z_e &\rightarrow \delta Z_e - \frac{\Delta\alpha(M_Z^2)}{2} \\
\delta Z_e &\rightarrow \delta Z_e - \frac{\Delta\tilde{r}}{2},
\end{aligned}
\tag{3.31}
$$

respectively. The term $\Delta\tilde{r}$ embodies the one-loop electroweak corrections to the muon decay after the subtraction of QED effects in the Fermi theory, in the scheme $(\alpha_0, \sin^2\theta_{eff}^\ell, M_Z)$:

$$
\Delta\tilde{r} = \Delta\alpha - \Delta\rho + \Delta\tilde{r}_{rem},
\tag{3.32}
$$

with

$$
\begin{aligned}
\Delta\tilde{r}_{rem} &= \frac{\text{Re}\Sigma_T^{AA}(s)}{s} - \left(\frac{\delta M_Z^2}{M_Z^2} - \frac{\Sigma_T^{ZZ}(0)}{M_Z^2}\right) \\
&+ \frac{s_w^2 - c_w^2}{c_w^2} \frac{\delta s_{eff}^2}{s_w^2} + 2\frac{c_w}{s_w} \frac{\Sigma_T^{AZ}(0)}{M_Z^2} \\
&+ \frac{\alpha_0}{4\pi s_w^2} \left(6 + \frac{7 - 4s_w^2}{2s_w^2}\log(c_w^2)\right) .
\end{aligned}
\tag{3.33}
$$

For what concerns the higher-order contributions included in the numerical code, by inspecting Eqs. (3.29)-(3.32) one can immediately understand that the

3.3. Renormalization in the EW Standard Model

leading fermionic corrections in the schemes with $\sin^2\theta^\ell_{eff}$ in input are only related to:

$$\delta Z_e \sim \frac{\Delta\alpha}{2}\,, \qquad \Delta\tilde{r} \sim \Delta\alpha - \Delta\rho\,. \tag{3.34}$$

Thus, keeping in mind to avoid the double counting of the $\mathcal{O}(\alpha)$ terms, we are left with overall factors of the Born amplitude which incorporates all higher-order corrections in the $(\alpha_i,\ \sin^2\theta^\ell_{eff},\ M_Z)$ schemes. They are:

$$|M_{\mathrm{LO}}|^2\Big(\frac{1}{\left(1 - \Delta\alpha(M_Z^2)\right)^2} - 1 - 2\Delta\alpha(M_Z^2)\Big), \tag{3.35}$$

and

$$|M_{\mathrm{LO}}|^2\Big(\frac{1}{\left(1 - \Delta\rho\right)^2} - 1 - 2\Delta\rho^{1-\mathrm{loop}}\Big), \tag{3.36}$$

for the schemes with α_0 and G_μ as input parameters, respectively, while they vanish when $\alpha(M_Z^2)$ is used as independent parameter. Note that in Eq. (3.35) we have resummed the logarithms of the light-fermion masses, while in Eq. (3.36) the overall factor can be obtained from the relation between α and G_μ at NLO+h.o., namely:

$$\alpha = \frac{\sqrt{2}}{\pi}G_\mu s_w^2 c_w^2 M_Z^2(1 + \Delta\tilde{r} - \Delta\alpha)\,. \tag{3.37}$$

3.3.4 The $(\alpha_0,\ G_\mu,\ M_Z)$ scheme

This scheme has the couplings α_0 and G_μ and the Z-boson mass as input parameters: these three quantities are known with great experimental accuracy, with the consequence that parametric uncertainties are small. Moreover, having as inputs two couplings related to different energy scales makes it possible to write the LO amplitude of the neutral-current Drell-Yan process as the sum of the photon-exchange contribution, which is proportional to α, plus the Z-exchange amplitude, which has $G_\mu M_Z^2$ as the overall $Zf\bar{f}$ interaction computed at the weak scale. In particular, we can write:

$$\mathcal{M}^{\sigma,\tau} = A^{\sigma,\tau}_{spinor}\Big[-\frac{4\pi\alpha}{s}Q_q Q_\ell - \frac{4\sqrt{2}G_\mu M_Z^2}{s}G_q^\sigma G_\ell^\tau \chi_Z(s)\Big]\,, \tag{3.38}$$

where the factor $A^{\sigma,\tau}_{spinor}$ contains the γ matrices and the external fermions spinors ($\sigma, \tau = L, R$ represent the fermion helicities) and

$$G^\sigma_{q(\ell)} = I^{\sigma\, q(\ell)}_{w,3} - s_W^2 Q_{q(\ell)}\,, \quad \chi_Z(s) = \frac{s}{s - M_Z^2 + i\Gamma_Z M_Z}\,, \tag{3.39}$$

with $Q_{q(\ell)}$ and $I^{\sigma\, q(\ell)}_{w,3}$ that are the quark (lepton) charge and third component of the weak isospin, for a given σ. Note that in the complex-mass scheme the

3. Electroweak virtual corrections to the neutral-current Drell Yan

Z-boson propagator reads χ_Z is $s/(s - \mu_Z^2)$, with the complex mass μ_Z defined in Chap. 4.

In the code, it is possible to select two different realisations of this scheme, by means of the flag `azinscheme4`. If the flag is absent or negative, the coupling used is $\alpha = \alpha_0$, i.e. it corresponds to the $\gamma f \bar{f}$ coupling evaluated at low energies, while if `azinscheme4` is positive, $\alpha = \alpha_0/(1 - \Delta\alpha(M_Z^2))$, and thus also the phton-exchange part of the amplitude is evaluated with a coupling at the weak scale. In Chap. 6, if not otherwise stated, the numerical results are presented with the option `azinscheme4 1`.

We proceed by introducing the counterterms for the independent quantities:

$$M_{Z,B}^2 = M_Z^2 + \delta M_Z^2 \tag{3.40}$$

$$G_{\mu,B} = G_\mu + \delta G_\mu \tag{3.41}$$

$$e_B = e(1 + \delta Z_e). \tag{3.42}$$

where δZ_e and δM_Z^2 are determined as described in Sect. 3.3.1, while δG_μ is fixed by the requirement that in this scheme the muon decay does not receive any weak correction at NLO:

$$\frac{\delta G_\mu}{G_\mu} = -\frac{2}{s_w c_w}\frac{\Sigma_T^{AZ}(0)}{M_Z^2} - \frac{\Sigma_T^W(0)}{M_W^2} - \frac{\alpha}{4\pi s_w^2}\left[6 + \frac{7 - 4s_w^2}{2s_w^2}\log c_w^2\right]. \tag{3.43}$$

The derived quantities in this scheme are the weak mixing angle and the W-boson mass, which can be computed by:

$$(1 - s_w^2)s_w^2 = \frac{\pi\alpha}{\sqrt{2}G_\mu M_Z^2}, \tag{3.44}$$

$$c_w^2 = 1 - s_w^2, \qquad c_w^2 = \frac{M_W^2}{M_Z^2}, \tag{3.45}$$

$$M_W^2 = \frac{\pi\alpha}{\sqrt{2}G_\mu s_w^2}. \tag{3.46}$$

These parameters can be exploited as auxiliary quantities in the calculation of the leading fermionic corrections at higher orders. For this reason, we introduce also the corresponding counterterms:

$$\frac{\delta M_W^2}{M_W^2} = \frac{s_w^2}{c_w^2 - s_w^2}\left(-2\delta\tilde{Z}_e + \frac{\delta G_\mu}{G_\mu} + \frac{c_w^2}{s_w^2}\frac{\delta M_Z^2}{M_Z^2}\right), \tag{3.47}$$

$$\frac{\delta s_w}{s_w} = \frac{1}{2}\frac{c_w^2}{c_w^2 - s_w^2}\left(2\delta\tilde{Z}_e - \frac{\delta G_\mu}{G_\mu} - \frac{\delta M_Z^2}{M_Z^2}\right). \tag{3.48}$$

with

$$\delta\tilde{Z}_e = \delta Z_e - \frac{1}{2}\delta_{\rm opt}\Delta\alpha(M_Z^2) \quad \delta_{\rm opt} = \begin{cases} 1 & \text{if \texttt{azinscheme4} is active} \\ 0 & \text{otherwise} \end{cases}. \tag{3.49}$$

3.3. Renormalization in the EW Standard Model

For what concerns the implementation of the higher orders, from Eqs. (3.40)-(3.42) and (3.48), one can identify the leading fermionic corrections to the photon-exchange contribution, which come from δZ_e, and the ones to the Z-exchange amplitude, which are related to the counterterms of the overall coupling $G_\mu M_Z^2$ and to $\delta s_w / s_w$:

$$\delta \tilde{Z}_e \sim (1 - \delta_{\text{opt}}) \frac{\Delta \alpha}{2}, \qquad \frac{\delta G_\mu}{G_\mu} + \frac{\delta M_Z^2}{M_Z^2} \sim \Delta \rho,$$

$$\delta s_w^2 \sim \frac{s_w^2 c_w^2}{c_w^2 - s_w^2} \left((1 - \delta_{\text{opt}}) \Delta \alpha - \Delta \rho \right). \tag{3.50}$$

To include the leading fermionic contributions at higher orders, we employ s_w as an auxiliary parameter, i.e. we use two effective couplings by performing the substitutions:

$$\alpha_0 \to \frac{\alpha_0}{1 - \Delta \alpha}, \qquad s_w^2 \to \frac{1}{2} - \frac{1}{2} \sqrt{1 - \frac{\sqrt{8}\pi}{G_\mu M_Z^2} \frac{\alpha_0}{1 - \Delta \alpha} (1 + \Delta \tilde{r} - \Delta \alpha)} \tag{3.51}$$

in the leading order amplitude, and then expanding it up to $\mathcal{O}(\alpha^2)$. Note that s_w^2 is replaced by an effective expression where $\Delta \alpha$ has been resummed, while the term:

$$\Delta \tilde{r} - \Delta \alpha = -\Delta \rho + \Delta r_{rem}|_{(\alpha_0, G_\mu, M_Z)} \tag{3.52}$$

at the numerator is formally the same $\Delta \tilde{r}$ in a scheme where $\sin^2 \theta_{eff}^\ell$ is in input, but computed with the coupling values of the (α_0, G_μ, M_Z) scheme. Note that, if the `azinscheme4` is active, $\Delta \tilde{r}$ is calculated in terms of $\delta \tilde{Z}_e$ rather than δZ_e. The effective couplings can be used in the LO expressions to promote them to include the higher-order universal corrections. Of course, one has to subtract the $\mathcal{O}(\alpha)$ expansion, already present in the NLO calculation.

3.3.5 The "on-shell" running of α

We conclude the discussion on the on-shell renormalization by presenting how the running of the electromagnetic coupling constant can be taken into account in these schemes. The "on-shell running" to compute the evolution from the value of the input α to some scale q^2 reads:

$$\alpha(q^2) = \frac{\alpha_0}{1 - \frac{\alpha_0}{4\pi} \left[\frac{4}{3} \sum_f N_c^f Q_f^2 \ln \frac{q^2}{m_f^2} \right]}. \tag{3.53}$$

It has already been introduced in Eq. (2.23) in the phenomenological discussion of Chap. 2. Note that only the fermionic contribution to $\Delta \alpha$ is included:

$$\Delta \alpha(q^2) = \frac{\alpha_0}{3\pi} \sum_f N_c^f Q_f^2 \ln \frac{q^2}{m_f^2}. \tag{3.54}$$

In the code, for on-shell schemes, $\Delta \alpha$ is always computed by considering only the fermionic corrections and therefore whenever we write $\Delta \alpha(q^2)$ in the context of the implemented corrections for on-shell schemes it is understood that it is the fermionic contribution only.

3. Electroweak virtual corrections to the neutral-current Drell Yan

The treatment of hadronic contributions in the "on-shell" running

Some remarks are in order here, concerning the contributions to the running of α coming from the light quarks. We write the "on-shell" running in Eq. (3.76) up to a given scale q^2 as:

$$\alpha(q^2) = \frac{\alpha_0}{1 - \Delta\alpha(q^2)} \, . \tag{3.55}$$

The effects of the charged leptons and the top quark can be calculated in perturbation theory, by writing $\Delta\alpha$ in terms of the photon self-energy and its derivative:

$$\Delta\alpha^{\text{lept (top)}}(q^2) = -\frac{\text{Re}\Sigma_{AA}^{\text{lept (top)}}(q^2)}{q^2} + \frac{\partial\Sigma_{AA}^{\text{lept (top)}}(q^2)}{\partial q^2}\bigg|_{q^2=0} \, . \tag{3.56}$$

However, Eq. (3.56) cannot be used for light quarks, because non-perturbative QCD effects make it impossible to describe the interaction among quarks at zero momentum transfer. Provided that one works in a perturbative regime, which is the case when considering the neutral-current Drell-Yan process as simulated in the `Z_ew-BMNNPV` package, one can nonetheless introduce the light-quark masses as effective parameters in the self-energies and use the equation:

$$\Delta\alpha^{\text{had pert.}}(q^2) = -\frac{\text{Re}\Sigma_{AA}^{\text{had}}(q^2)}{q^2} + \frac{\partial\Sigma_{AA}^{\text{had}}(q^2)}{\partial q^2}\bigg|_{q^2=0} \, . \tag{3.57}$$

to compute the hadronic running of α due to the light-flavour contributions. The light-quark masses are set in input to the code, in such a way that the hadronic running of α from 0 to M_Z^2 from Eq. (3.57) matches the value obtained by using dispersion relations from experimental data on inclusive hadron production in e^+e^- annihilations ($\Delta\alpha^{\text{had fit}}$):

$$\Delta\alpha^{\text{had pert.}}(M_Z^2) = \Delta\alpha^{\text{had fit 1}}(M_Z^2) \, . \tag{3.58}$$

In this last equation, $\Delta\alpha^{\text{had fit 1}}$ represents the value obtained by the fit routine `HADR5X19.F` [120–127]. This approach is the default one in the `Z_ew-BMNNPV` code. The light-quark masses are used only in the self-energy corrections, but are zero in vertex and box contributions; in the code, in fact, QED infrared singularities coming from the light-quarks masses are treated with dimensional regularization.

Another option to compute the hadronic contribution to the running of α can be selected by activating the input flag `da_had_from_fit`. The calculation starts from:

$$\Delta\alpha^{\text{had fit 1(2)}}(q^2) = -\frac{\text{Re}\Sigma_{AA}^{\text{had}}(q^2)}{q^2} + \frac{\partial\Sigma_{AA}^{\text{had fit 1(2)}}(q^2)}{\partial q^2}\bigg|_{q^2=0} \, . \tag{3.59}$$

which can be regarded as a definition of $\frac{\partial\Sigma_{AA}^{\text{had fit 1(2)}}(q^2)}{\partial q^2}\bigg|_{q^2=0}$, at difference to what happens in Eq. (3.57), that is a definition of $\Delta\alpha^{\text{had pert.}}$. In Eq. (3.59)

3.4. Renormalization of the EW Standard Model in the $\overline{MS}$ scheme

the term $\Delta\alpha^{\mathrm{had\,fit\,1}}(q^2)$ is computed by the code with the `HADR5X19.F` routine, while $\Delta\alpha^{\mathrm{had\,fit\,2}}(q^2)$ is obtained from the `KNT v3.0.1` one [128–131]. The two options can be selected by activating the input flag `da_had_from_fit` together with the flags `fit 1` or `fit 2`, respectively. Since both these routines produce valid results only in a range $[0, q^2_{\mathrm{max\,1(2)}}]$, for $q^2 > q^2_{\mathrm{max\,1(2)}}$ the computation proceeds as:

$$
\begin{aligned}
\Delta\alpha^{\mathrm{had\,fit\,1(2)}}(q^2) &= \Delta\alpha^{\mathrm{had\,fit\,1(2)}}(q^2_{\mathrm{max\,1(2)}}) \\
&\quad + \Delta\alpha^{\mathrm{had\,pert.}}(q^2) - \Delta\alpha^{\mathrm{had\,pert.}}(q^2_{\mathrm{max\,1(2)}}).
\end{aligned}
\tag{3.60}
$$

The term $-\mathrm{Re}\Sigma^{\mathrm{had}}_{AA}(q^2)/q^2$ is computed in a perturbative way, by using the values of the masses tuned with the analogue of Eq. (3.58) at $q^2 = M_Z^2$:

$$
\Delta\alpha^{\mathrm{had\,pert.}}(M_Z^2) = \Delta\alpha^{\mathrm{had\,fit\,1(2)}}(M_Z^2),
\tag{3.61}
$$

for `fit 1` or `fit 2`, respectively. Within the calculation, one can thus exploit Eq. (3.59) to make the following replacement in the one-loop corrections to the photon propagator:

$$
\Sigma^{\mathrm{had}}_{AA}(s) - s\delta Z_A^{\mathrm{had}} \rightarrow -s\Delta\alpha^{\mathrm{had\,fit}}(q^2) + is\mathrm{Im}\Sigma^{\mathrm{had}}_{AA}(s),
\tag{3.62}
$$

and use the fact that:

$$
\delta Z_A^{\mathrm{had}} = -\frac{\partial\Sigma^{\mathrm{had}}_{AA}(q^2)}{\partial q^2}\bigg|_{q^2=0}
\tag{3.63}
$$

to get the electric charge and photon wave-function counterterms. In this way, the counterterms are formally equal to those yielded by the default option `da_had_from_fit 0`; however, since $\Delta\alpha^{\mathrm{had\,fit\,1(2)}}(s) \neq \Delta\alpha^{\mathrm{had\,pert.}}(s)$ for $s \neq M_Z^2$, the two computations for `da_had_from_fit` set to 0 and 1 are not equivalent.

3.4 Renormalization of the EW Standard Model in the $\overline{MS}$ scheme

The modified minimal subtraction ($\overline{MS}$) scheme is defined by fixing the counterterms only through the divergent parts of the radiative corrections of the bare parameters, proportional to Δ_{UV}, and by setting the finite part to zero. In addition, one has to include a term $-\ln\mu^2/\mu_{dim}^2$ in the renormalization constants. This prescription modifies the definition of the renormalization constants, but otherwise the calculation formally proceeds in the same way as in the on-shell scheme.

The modified counterterms have the effect that the renormalized parameters become functions of the renormalization scale μ, i.e. they become manifestly running. The scale μ plays the role of the renormalization point of the

theory, and as such one can arbitrarily choose its value. In most cases, μ is set equal to the energy scale of the process under study, thus making it possible to reabsorb a significant part of the radiative corrections into the definition of the running couplings and masses.

In order to make numerical predictions within the theoretical framework of the $\overline{MS}$ scheme, it becomes mandatory to find some relations between the $\overline{MS}$ renormalized parameters, that do not have a direct physical meaning, and a set of corresponding physical quantities. For example, if one takes as independent lagrangian parameters $(\alpha(\mu^2), M_W(\mu^2), M_Z(\mu^2))$, it is necessary to relate $\alpha(\mu^2)$ to the physical electromagnetic coupling and $M_{Z(W)}(\mu^2)$ to the physical boson masses by choosing a renormalization point in the μ scale.

To make another example, in the `Z_ew-BMNNPV` code, the implemented scheme is $\left(\alpha(\mu^2), \sin^2\theta_w^{\overline{MS}}(\mu^2), M_Z\right)$, where the couplings $\alpha(\mu^2)$ and $\sin^2\theta_w^{\overline{MS}}(\mu^2)$ are renormalized in the $\overline{MS}$ scheme, while M_Z is taken in the on-shell one. As input parameters, we use the numerical values of $\alpha(\mu_0^2)$ and $\sin^2\theta_w^{\overline{MS}}(\mu_0^2)$ for a given renormalization scale μ_0^2, which can set as an input to the code, together with the on-shell Z mass. The code then evolves the values of $\alpha(\mu_0^2)$ and $\sin^2\theta_w^{\overline{MS}}(\mu_0^2)$ to the ones of $\alpha(\mu^2)$ and $\sin^2\theta_w^{\overline{MS}}(\mu^2)$, with the evolution equations for $\alpha(\mu^2)$ and $\sin^2\theta_w^{\overline{MS}}(\mu^2)$ presented in the next sections. Before entering the details of the discussion, as a general observation we can note that, in the code, μ can be a dynamical renormalization scale, identified with the leptonic invariant mass at each space point, or the fixed scale in input, by default set to M_Z. The choice between dynamical or fixed scale is regulated by the flag `running_muR_sw`.

3.4.1 The running of $\alpha(\mu^2)$

We start the description of the $\left(\alpha(\mu^2), \sin^2\theta_w^{\overline{MS}}(\mu^2), M_Z\right)$ scheme by examining the running of α. As already seen in the previous section, in the Standard Model δZ_e is:

$$\delta Z_e = -\frac{1}{2}\delta Z_{AA} - \frac{s_w}{c_w}\frac{1}{2}\delta Z_{ZA} = \frac{1}{2}\frac{\partial \Sigma_T^{AA}}{\partial k^2}\bigg|_{k^2=0} - \frac{s_w}{c_w}\frac{\Sigma_T^{AZ}(0)}{M_Z^2}, \qquad (3.64)$$

where the subtraction of the term $\Sigma_T^{AZ}(0)/M_Z^2$ guarantees gauge-invariance, as it can be verified for R_ξ gauges by taking the self-energy expressions in [132]. This allows us to define $\alpha(\mu^2)$ in a gauge-invariant way, as in the following.

We specify the counterterm for the on-shell scheme:

$$\delta Z_e^{OS} = \frac{\alpha}{4\pi}\left\{\frac{2}{3}\sum_f N_f^c Q_f^2 \left[\Delta_{UV} - \ln\frac{m_f^2}{\mu_{dim}^2}\right] - \frac{7}{2}\left[\Delta_{UV} - \ln\frac{M_W^2}{\mu_{dim}^2}\right] - \frac{1}{3}\right\}, \qquad (3.65)$$

3.4. Renormalization of the EW Standard Model in the $\overline{MS}$ scheme

and in the $\overline{MS}$ one:

$$\delta Z_e^{\overline{MS}} = \frac{\alpha(\mu^2)}{4\pi} \left\{ \frac{2}{3} \sum_f N_f^c Q_f^2 \left[\Delta_{UV} - \ln \frac{\mu^2}{\mu_{dim}^2} \right] - \frac{7}{2} \left[\Delta_{UV} - \ln \frac{\mu^2}{\mu_{dim}^2} \right] \right\} .$$
(3.66)

When identifying the two scales, i.e. when the dimensional regularization parameter μ_{dim} is equal to the renormalization point μ, $\mu_{dim} = \mu$, one gets:

$$\delta Z_e^{\overline{MS}} = \frac{\alpha(\mu^2)}{4\pi} \left\{ \left[\frac{2}{3} \sum_f N_f^c Q_f^2 - \frac{7}{2} \right] \Delta_{UV} \right\} .$$
(3.67)

In the following, α_0 refers to the renormalized OS parameter, while $\alpha(\mu^2)$ to the renormalized $\overline{MS}$ one. The aim is now to compute the β function for the running coupling $e(\mu^2)$, or equivalently $\alpha(\mu^2)$, in the $\overline{MS}$ scheme. The starting point is the bare coupling:

$$e_b = \mu^\epsilon Z_e^{\overline{MS}} e ,$$
(3.68)

where it is important to note that, for simplifying the calculation, the usual choice in the literature is to set $\mu = \mu_{dim}$ and thus to use the counterterm in Eq. (3.67). By imposing that:

$$\mu \frac{de_b}{d\mu} = 0 = \epsilon \mu^\epsilon Z_e^{\overline{MS}} e + \mu \mu^\epsilon \frac{\partial Z_e^{\overline{MS}}}{\partial e} \frac{de}{d\mu} + \mu \mu^\epsilon Z_e^{\overline{MS}} \frac{de}{d\mu} ,$$
(3.69)

one finds:

$$e^2(\mu^2) = \frac{e^2(\mu_0^2)}{1 - \frac{e^2(\mu_0^2)}{16\pi^2} \left[\frac{4}{3} \sum_f N_c^f Q_f^2 - 7 \right] \ln \frac{\mu^2}{\mu_0^2}} ,$$
(3.70)

or equivalently:

$$\alpha(\mu^2) = \frac{\alpha(\mu_0^2)}{1 - \frac{\alpha(\mu_0^2)}{4\pi} \left[\frac{4}{3} \sum_f N_c^f Q_f^2 - 7 \right] \ln \frac{\mu^2}{\mu_0^2}} ,$$
(3.71)

where the fermionic and bosonic contributions are separately highlighted. However, one can also start from Eq. (3.66) and consider the electromagnetic charge as a 2-variable function $e = e(\mu, \mu_{dim})$. The calculation we are interested in is again the partial derivative w.r.t. μ, i.e. $\partial e / \partial \mu$, and the same result can be found.

Now, we have defined the renormalized $\overline{MS}$ parameter $\alpha(\mu^2)$, which has no physical meaning *per se*, but has to be related to the physical fine-structure constant $\alpha_0 \simeq 1/137$, by starting from the relation:

$$e_b = (1 + \delta Z_e^{OS}) e_0 = (1 + \delta Z_e^{\overline{MS}}) e(\mu^2) ,$$
(3.72)

47

that, by using Eq. (3.65) and (3.66), can be written as:

$$
\begin{aligned}
e_0 &= e(\mu^2)\left[1 - \delta Z_e^{OS} + \delta Z_e^{\overline{MS}}\right] && (3.73)\\
&= e(\mu^2)\left\{1 + \frac{\alpha(\mu^2)}{8\pi}\left[\frac{4}{3}\sum_f N_c^f Q_f^2 \ln\frac{m_f^2}{\mu^2} - 7\ln\frac{M_W^2}{\mu^2} - \frac{2}{3}\right]\right\}.
\end{aligned}
$$

where in the counterterms the identification $\alpha = \alpha(\mu^2)$ has been made, which is valid at NLO because the spurious terms originated by this operation are $\mathcal{O}(\alpha^2)$. The result is:

$$
e(\mu^2) = \frac{e_0}{1 - \frac{e_0^2}{32\pi^2}\left[\frac{4}{3}\sum_f N_c^f Q_f^2 \ln\frac{\mu^2}{m_f^2} - 7\ln\frac{\mu^2}{M_W^2} - \frac{2}{3}\right]}, \tag{3.74}
$$

or equivalently:

$$
\alpha_0 = \alpha(\mu^2)\left[1 - 2\delta Z_e^{OS} + 2\delta Z_e^{\overline{MS}}\right], \tag{3.75}
$$

and:

$$
\alpha(\mu^2) = \frac{\alpha_0}{1 - \frac{\alpha_0}{4\pi}\left[\frac{4}{3}\sum_f N_c^f Q_f^2 \ln\frac{\mu^2}{m_f^2} - 7\ln\frac{\mu^2}{M_W^2} - \frac{2}{3}\right]}. \tag{3.76}
$$

Another way to find this relation can be found in App. A.

3.4.2 The running of $\sin^2\theta_w^{\overline{MS}}(\mu^2)$

Different definitions of a $\overline{MS}$ weak mixing angle have been considered in the literature, particularly in connection with the determination of this parameter at low-energy experiments, by using the Møller scattering [133, 134] or neutrino-induced processes [135]. Moreover, some effort has been devoted to find a relation between an $\overline{MS}$-defined weak mixing angle and its leptonic effective counterpart, as measured at LEP [136].

We here define the $\overline{MS}$ weak mixing angle as done in [21, 77, 137], in particular proving the equivalence between the defintions in [77] and [21]. Similarly to what has been done for $\alpha(\mu^2)$, the RGE equation for $\sin^2\theta_w^{\overline{MS}}(\mu^2)$, in the following often abbreviated as $s_w^2(\mu^2)$, can be found by starting from:

$$
\mu\frac{ds_{w,B}^2}{d\mu} = 0 = \mu\frac{ds_w^2(\mu^2)}{d\mu} + \frac{d\delta s_w^2(\mu^2)}{d\mu}, \tag{3.77}
$$

and from Eq. (2.21), that we report here:

$$
\sin^2\theta_w^{\overline{MS}}(\mu^2) = \frac{e^2(\mu^2)}{g^2_{2,\overline{MS}}(\mu^2)} = \frac{4\pi\,\alpha(\mu^2)}{g^2_{2,\overline{MS}}(\mu^2)}. \tag{3.78}
$$

To define the running of $\sin^2\theta_w^{\overline{MS}}(\mu^2)$, one can consider a running $\alpha(\mu^2)$ and couple the RGE equations for these two parameters. Since the $\overline{MS}$ counterterm

3.4. Renormalization of the EW Standard Model in the $\overline{MS}$ scheme

of $\sin^2 \theta_w^{\overline{MS}}(\mu^2)$ is:

$$
\begin{aligned}
\delta \sin^2 \theta_w^{\overline{MS}}(\mu^2) &= c_w^2(\mu^2) \left[\frac{\Sigma_T^{ZZ,\,\overline{MS}}(M_Z^2)}{M_Z^2} - \frac{\Sigma_T^{W\,\overline{MS}}(M_W^2)}{M_W^2} \right] \\
&= \frac{c_w(\mu^2) s_w(\mu^2)}{4} \left[\Sigma_T^{AZ,\,\overline{MS}}(M_Z^2) + \Sigma_T^{AZ,\,\overline{MS}}(0) \right] \\
&= \frac{\alpha(\mu^2)}{4\pi} \left[\frac{11}{3} \sin^2 \theta_w^{\overline{MS}}(\mu^2) + \frac{19}{6} \right] \left(\Delta_{UV} + \ln \frac{\mu_{dim}^2}{\mu^2} \right)
\end{aligned}
\tag{3.79}
$$

where we can choose $\mu_{dim} = \mu$, the equation reads:

$$
\mu^2 \frac{ds_w^2(\mu^2)}{d\mu^2} = \frac{\alpha(\mu^2)}{4\pi} \left[\frac{11}{3} s_w^2(\mu^2) + \frac{19}{6} \right] ,
\tag{3.80}
$$

where the numerical values are obtained from the self-energy calculations:

$$
\frac{11}{3} = -7 + \frac{4}{3} \sum_f N_f^c Q_f^2
\tag{3.81}
$$

$$
\frac{19}{6} = \frac{43}{6} - \frac{2}{3} \sum_f N_f^c Q_f I_{3,\,f} .
\tag{3.82}
$$

We have separated the bosonic and fermionic parts to obtain the coefficients in the case of decoupling of the top quark and/or of the W boson more easily, as it will be seen in the next section. Now we rewrite the running of $\alpha(\mu^2)$ as:

$$
\alpha(\mu^2) = \frac{\alpha(\mu_0^2)}{1 - \frac{\alpha(\mu_0^2)}{4\pi} \frac{11}{3} \ln \frac{\mu^2}{\mu_0^2}} ,
\tag{3.83}
$$

and by defining:

$$
C = \frac{11}{3} ,
\tag{3.84}
$$

one gets:

$$
\mu^2 \frac{d\alpha(\mu^2)}{d\mu^2} = \frac{\alpha^2(\mu^2)}{4\pi} C ,
\tag{3.85}
$$

and thus:

$$
\frac{ds_w^2(\mu^2)}{\frac{11}{3} s_w^2(\mu^2) + \frac{19}{6}} = \frac{\alpha(\mu^2)}{4\pi} \frac{d\mu^2}{\mu^2} = \frac{1}{C} \frac{d\alpha(\mu^2)}{\alpha(\mu^2)} ,
\tag{3.86}
$$

where the running of $s_w^2(\mu^2)$ has been related to the one of $\alpha(\mu^2)$. By integrating this equation from μ_0^2 to μ^2, one gets:

$$
s_w^2(\mu^2) = s_w^2(\mu_0^2) \frac{\alpha(\mu^2)}{\alpha(\mu_0^2)} + \frac{19}{22} \frac{\alpha(\mu^2)}{\alpha(\mu_0^2)} - \frac{19}{22} ,
\tag{3.87}
$$

that is in agreement with the result in Eq. (12) of [77], where:

$$
\frac{\sum_i N_i^c \gamma_i Q_i I_{3,i}}{\sum_i N_i^c \gamma_i Q_i^2} = -\frac{19}{22} ,
\tag{3.88}
$$

as the reader can straightforwardly check by taking the values for γ_i provided by Table 1 of the same reference. We report here Eq. (12) of [77], since we will refer to it in the next sections:

$$s_w^2(\mu^2) = s_w^2(\mu_0^2)\frac{\alpha(\mu^2)}{\alpha(\mu_0^2)} + \frac{\sum_i N_i^c \gamma_i Q_i T_i}{\sum_i N_i^c \gamma_i Q_i^2}\left[1 - \frac{\alpha(\mu^2)}{\alpha(\mu_0^2)}\right] . \tag{3.89}$$

It is important to notice that in the sum at the denominator is on both left-handed and right-handed particles. In this way, bosons and fermions are treated in the same way in the summation. If one wants to sum on LH particles only, an extra 2 should be taken into account at the denominator when considering the fermionic contributions. By using the NLO expansion of $\alpha(\mu^2)$:

$$\alpha(\mu^2) = \alpha(\mu_0^2)\left[1 + \frac{\alpha(\mu_0^2)}{4\pi}\frac{11}{3}\ln\frac{\mu^2}{\mu_0^2}\right] , \tag{3.90}$$

one gets the analogue of Eq. (13) in [77]:

$$s_w^2(\mu^2) = s_w^2(\mu_0^2)\left[1 + \frac{\alpha(\mu_0^2)}{4\pi s_w^2(\mu_0^2)}\left(\frac{19}{6} + \frac{11}{3}s_w^2(\mu_0^2)\right)\ln\frac{\mu^2}{\mu_0^2}\right] . \tag{3.91}$$

The formulae in this subsection and in the following one are to be understood in the limit where all particles masses are smaller than the renormalization scale μ, i.e. there are no decoupling or threshold effects and no issues due to the non-perturbative hadronic contributions at low scales.

3.4.3 Inclusion of higher orders in the running

In the `Z_ew-BMNNPV` code, the RGE equations for $\alpha(\mu^2)$ and $\sin^2\theta_w^{\overline{MS}}(\mu^2)$ are implemented by taking into account not only the $\mathcal{O}(\alpha)$ corrections, but also some higher-order classes of contributions.

The running of $\alpha(\mu^2)$ is built as in Eqs. (9)–(13) of Ref. [138], i.e. by starting from:

$$\mu^2\frac{d\alpha(\mu^2)}{d\mu^2} = -\frac{\alpha^2(\mu^2)}{\pi}\left(\beta_0 + \beta_1\frac{\alpha(\mu^2)}{\pi} + \delta_1\frac{\alpha_S(\mu^2)}{\pi} + \delta_2\frac{\alpha_S^2(\mu^2)}{\pi^2} + \delta_3\frac{\alpha_S^3(\mu^2)}{\pi^3}\right) , \tag{3.92}$$

which includes the fermionic contributions to the β function up to $\mathcal{O}(\alpha)$ in QED and $\mathcal{O}(\alpha_s^3)$ in QCD, which have been calculated in [139–142]. Eq. (3.92) is valid only in a perturbative regime, and is used only for value of the renormalization scales well above $4m_b^2$. In fact, at difference to what happens for the "on-shell" running of α, in our implementation of the $\overline{MS}$ scheme the non-perturbative QCD effects are effectively included in the numerical starting-point value of $\alpha(\mu_0^2)$, which in the code is set by the user and should always be chosen at $\mu_0^2 \gg 4m_b^2$.

We can write Eq. (3.92) as done in [77]:

$$\mu^2\frac{d\alpha(\mu^2)}{d\mu^2} = \frac{\alpha^2(\mu^2)}{\pi}\left[\frac{1}{24}\sum_i K_i \gamma_i Q_i^2 + \sigma\left(\sum_q Q_q^2\right)\right] , \tag{3.93}$$

3.4. Renormalization of the EW Standard Model in the $\overline{MS}$ scheme

where the index i runs over fermions and bosons, both LH and RH particles, while the index q runs only over quarks, and we have introduced the factors:

$$
\begin{aligned}
K_i \; = \; & N_i^c \left\{ 1 + \frac{3}{4} Q_i^2 \frac{\alpha(\mu^2)}{\pi} \right. \tag{3.94} \\
& + \frac{\alpha_S(\mu^2)}{\pi} + \frac{\alpha_S^2(\mu^2)}{\pi^2} \left(\frac{125}{48} - \frac{11}{72} n_q \right) \\
& \left. + \frac{\alpha_S^3(\mu^2)}{\pi^3} \left[\frac{10487}{1728} + \frac{55}{18}\zeta(3) - \left(\frac{707}{864} + \frac{55}{54}\zeta(3) \right) n_q - \frac{77}{3888} n_q^2 \right] \right\} \\
\; = \; & N_i^c \left[1 + K_{QED}^i + K_{QCD} \right], \tag{3.95}
\end{aligned}
$$

and the QCD singlet contribution:

$$
\sigma = \frac{\alpha_s^3(\mu^2)}{\pi^3} \frac{5}{9} \left[\frac{11}{24} - \zeta(3) \right]. \tag{3.96}
$$

Symbols n_q and $\zeta(s)$ stand for the number of quark flavours and the Riemann Zeta function of s, respectively. Eq. (3.93) can be obtained from:

$$
\mu^2 \frac{d\alpha(\mu^2)}{d\mu^2} = \frac{\alpha^2(\mu^2)}{\pi} \left[\frac{1}{24} \sum_i N_i^c \gamma_i Q_i^2 \right], \tag{3.97}
$$

which is valid at $\mathcal{O}(\alpha)$, by substituting N_i^c with the modified colour factor K_i and adding the $\mathcal{O}(\alpha_S^3)$ term proportional to σ.

In analogy to what has been done at NLO, also here we relate the running of $\sin^2\theta_w^{\overline{MS}}(\mu^2)$ with the one of $\alpha(\mu^2)$, following the approach in [77, 143]. A different implementation of higher-order corrections to the RGE of a low-energy definition of $\sin^2\theta_w^{\overline{MS}}(\mu^2)$ can be found in [144], while in [145] the h.o. corrections to the relation with the on-shell weak mixing angle are investigated. Higher-order contributions to the RGE of $\sin^2\theta_w^{\overline{MS}}(\mu^2)$ can be included as in Eq. (25) by [77]:

$$
\begin{aligned}
s_w^2(\mu^2) \; = \; & s_w^2(\mu_0^2) \frac{\alpha(\mu^2)}{\alpha(\mu_0^2)} \tag{3.98} \\
& + \lambda_1 \left[1 - \frac{\alpha(\mu^2)}{\alpha(\mu_0^2)} \right] \\
& + \frac{\alpha(\mu^2)}{\pi} \left[\frac{\lambda_2}{3} \ln \frac{\mu^2}{\mu_0^2} + \frac{3\lambda_3}{4} \ln \frac{\alpha(\mu^2)}{\alpha(\mu_0^2)} + \tilde{\sigma}(\mu_0^2) - \tilde{\sigma}(\mu^2) \right],
\end{aligned}
$$

where:

$$\lambda_1 = \frac{\sum_q I_{3,q} Q_q}{2 \sum_q Q_q^2} \tag{3.99}$$

$$\lambda_2 = \frac{1}{8} \sum_{i \neq q} N_i^c \gamma_i \left(Q_i \lambda_1 - I_{3,i} Q_i \right) \tag{3.100}$$

$$\lambda_3 = \frac{\sum_i N_i^c \gamma_i \left[\lambda_1 Q_i^4 - I_{3,i} Q_i^3 \right]}{\sum_i N_i^c \gamma_i Q_i^2}, \tag{3.101}$$

$$\lambda_4 = \lambda_1 \left(\sum_q Q_q \right)^2 - \frac{1}{2} \left(\sum_q I_{3,q} \right) \left(\sum_q Q_q \right), \tag{3.102}$$

and:

$$\tilde{\sigma}(\mu^2) = \lambda_4 \frac{\alpha_s^2(\mu^2)}{\pi^2} \frac{5}{36} \frac{11 - 24\zeta(3)}{33 - 2n_q}. \tag{3.103}$$

In App. B it has been checked that the terms with coefficients λ_1 and λ_2 are already $O(\alpha)$. Thus, h.o. contributions can be included by simply adding:

$$\frac{\alpha(\mu^2)}{\pi} \left[\frac{3\lambda_3}{4} \ln \frac{\alpha(\mu^2)}{\alpha(\mu_0^2)} + \tilde{\sigma}(\mu_0^2) - \tilde{\sigma}(\mu^2) \right] \tag{3.104}$$

to the $O(\alpha)$ expression of the running in Eq. (3.89). In the Z_ew-BMNNPV code, the running can be performed also at NLO-only by activating the flag exclude-HOrun. We end this section with a phenomenological observation, by noting that in the $(\alpha(\mu^2), s_w^2(\mu^2), M_Z)$ scheme the universal higher-order effects due to fermionic corrections discussed in Sec. 3.3.2, which can be computed by the Z_ew-BMNNPV code, are already included through the running of the couplings, making it possible to reduce the impact of this kind of corrections in this scheme.

3.4.4 Decoupling of top quark and W boson

The $\overline{MS}$ scheme is useful for many reasons, the first of which is that it allows for the definition of running couplings and masses. However, it does not take into account the decoupling of heavy particles, that arises naturally in the on-shell scheme. The decoupling is based on the natural observation that two very different energy scales do not have any influence on each other.

Let us consider $m_b^2 \ll \mu^2 \ll M_W^2$ and the $\mathcal{O}(\alpha)$ running of $\alpha(\mu^2)$ to fix ideas, and suppose to vary the energy of the process s over values comparable to μ^2 and much greater than the bottom quark mass, m_b^2. All fermions, with the exception of the top quark, have a mass much smaller than μ^2, and for them we can apply the $\overline{MS}$ scheme without modifications.

On the other hand, we obtain that the top quark and the W boson contribute to the running of $\alpha(\mu^2)$ in Eq. (3.76), and to the β function of the RGE in Eq. (3.71), a feature that is quite unphysical as the low-momenta evolution

3.4. Renormalization of the EW Standard Model in the $\overline{MS}$ scheme

of the coupling constant should not be influenced by loops containing particles with $m^2 \gg \mu^2$.

To solve these issues, we can apply a different renormalization scheme for heavy particles with $m^2 \gg \mu^2$, modifying the $\overline{MS}$ scheme in the following way [146]:

$$
\delta Z_{e,\,\mathrm{dec}}^{\overline{MS}} = \frac{\alpha(\mu^2)}{8\pi} \left\{ \left[\frac{4}{3} \sum_f N_f^c Q_f^2 - 7 \right] \Delta_{UV} - \frac{4}{3} N_t Q_t^2 \ln \frac{\mu^2}{m_t^2} + 7 \ln \frac{\mu^2}{M_W^2} \right\} .
\tag{3.105}
$$

Substituting $\delta Z_{e,\,\mathrm{dec}}^{\overline{MS}}$ to $\delta Z_e^{\overline{MS}}$ we find, for the RGE Eq. 3.71 and the relation between $\alpha(\mu^2)$ and α_0 in Eq. 3.76, respectively:

$$
\alpha(\mu^2) = \frac{\alpha(\mu_0^2)}{1 - \frac{\alpha(\mu_0^2)}{4\pi} \left[\frac{4}{3} \sum_f N_c^f Q_f^2 - \frac{4}{3} N_c^t Q_t^2 \right] \ln \frac{\mu^2}{\mu_0^2}} ,
\tag{3.106}
$$

and:

$$
\alpha(\mu^2) = \frac{\alpha_0}{1 - \frac{\alpha_0}{4\pi} \left[\frac{4}{3} \sum_f N_c^f Q_f^2 \ln \frac{\mu^2}{m_f^2} - \frac{4}{3} N_c^t Q_t^2 \ln \frac{\mu^2}{m_t^2} - \frac{2}{3} \right]} .
\tag{3.107}
$$

One can see that in Eq. (3.106) there are no contributions from the heavy particles, while in Eq. (3.107) one is left with a spurious contribution $-2/3$ of bosonic origin.

This issue can be addressed by noticing that Eq. (3.71) is valid only if there is no particle threshold between μ_0^2 and μ^2, i.e. it represents the "pure" RGE running, where μ has no physical meaning. Eq. (3.76), on the other hand, takes into account the running of α from 0 to μ^2, with all particle thresholds in between, i.e. with additional physical information, that arise when one tries to connect the $\overline{MS}$ parameter $\alpha(\mu^2)$ to the physical α_0. If $\mu^2 \ll m_f^2$ for some fermion flavour f, then one can decouple fermion f and the relative terms does not enter the sum at the denominators of both Eq. (3.71) and (3.76). Since μ is an arbitrary scale, one can choose to perform such a decoupling for all $\mu^2 \leq m_f^2$, while taking into account the fermion f contribution only for $\mu^2 > m_f^2$.

Similarly, when one has also bosonic contributions, it is possible to state that Eq. (3.71) is valid when there are no particle thresholds between μ_0^2 and μ^2, while Eq. (3.76) takes into account the running from 0 to μ^2. In Eq. (3.76) we have the additional $-2/3$ term when passing the W-boson threshold, that is not taken into account in Eq. (3.71). Thus, if one wants to decouple the W boson in the electromagnetic coupling containing the extra physical information of Eq. (3.76), extra care must be paid to the fact that, when the W threshold is passed, an additional term $-2/3$ has to be taken into account. This feature represents one of the matching conditions discussed in Sec. 3.4.5: one defines a "full" theory above the threshold and an "effective" one below, and at threshold requires an observable to be the same if computed with a theory or with the

other. To decouple the W boson one has to use the following definition of the counterterm:

$$\delta Z_{e,\,\text{dec}}^{\overline{MS}} = \frac{\alpha(\mu^2)}{8\pi} \left\{ \left[\frac{4}{3} \sum_f N_f^c Q_f^2 - 7 \right] \Delta_{UV} - \frac{4}{3} N_t Q_t^2 \ln \frac{\mu^2}{m_t^2} + 7 \ln \frac{\mu^2}{M_W^2} + \frac{2}{3} \right\}.$$

(3.108)

To take into account the decoupling of the top quark and the W boson in one single formula, we can thus redefine the $\overline{MS}$ counterterm as:

$$
\begin{aligned}
\delta Z_e^{\overline{MS}} = {} & -\frac{\alpha(\mu^2)}{8\pi} \left\{ \left[\frac{4}{3} \sum_f N_f^c Q_f^2 - 7 \right] \Delta_{UV} \right. \\
& - \frac{4}{3} N_t^c Q_t^2 \ln \frac{\mu^2}{m_t^2} \, \theta(m_t^2 - \mu^2) \\
& \left. + \left(7 \ln \frac{\mu^2}{M_W^2} + \frac{2}{3} \right) \theta(M_W^2 - \mu^2) \right\},
\end{aligned}
$$

(3.109)

where the Heaviside θ-function guarantees that, for μ^2 greater than the threshold value m_t^2 (M_W^2), the only contribution of the top-quark (W-boson) loop is the one proportional to the combination $1/\epsilon$, while for $\mu^2 < m_t^2$ (M_W^2) the full top-quark (W-boson) correction is switched on.

Note that, at the considered order of the calculation, physical observables do not depend either on the decoupling prescription nor on the scale of the threshold, and therefore there is some freedom in the choice of the W threshold value: in the Z_ew-BMNNPV code, this can be set by the user via the flag MW_insw2_thr, the default option being $M_{W,\,\text{thr.}}^2 = \text{Re} M_Z^2 (1 - s_w^2(\mu_0^2))$, which is the value computed within the $\left(\alpha^{\overline{MS}}(\mu^2), \sin^2 \theta_w^{\overline{MS}}(\mu^2), M_Z \right)$ scheme. This applies also to the decoupling prescription in the running of $\sin^2 \theta_w^{\overline{MS}}(\mu^2)$, that will be addressed in Sec. 3.4.5.

In the case of the $\mathcal{O}(\alpha)$ running of $s_w^2(\mu^2)$ the practical prescription to decouple of the top quark is to substitute in Eq. (3.87):

$$\frac{11}{3} \quad \rightarrow \quad \frac{11}{3} - \frac{4}{3} N_t^c Q_t^2 = \frac{7}{3} \tag{3.110}$$

$$\frac{19}{6} \quad \rightarrow \quad \frac{19}{6} + \frac{2}{3} N_t^c Q_t I_{3,t} = \frac{23}{6} \tag{3.111}$$

$$\frac{19}{22} \quad \rightarrow \quad \frac{23}{6} \cdot \frac{3}{7} = \frac{23}{14}, \tag{3.112}$$

while for the decoupling of the W boson one has:

$$\frac{11}{3} \quad \rightarrow \quad \frac{11}{3} + 7 = \frac{32}{3} \tag{3.113}$$

$$\frac{19}{6} \quad \rightarrow \quad \frac{19}{6} - \frac{43}{6} = -4 \tag{3.114}$$

$$\frac{19}{22} \quad \rightarrow \quad -4 \cdot \frac{3}{32} = -\frac{3}{8}. \tag{3.115}$$

3.4. Renormalization of the EW Standard Model in the $\overline{MS}$ scheme

When including also higher order corrections to the running, the decoupling of particle i can be performed by removing particle-i contributions in the summation appearing in Eq. (3.93) for $\alpha(\mu^2)$ and in the coefficients λ_3 and λ_4 in Eqs. (3.101)–(3.102) for $s_w^2(\mu^2)$.

3.4.5 Threshold corrections

Eqs. (3.71) and (3.89) are valid if there is no particle threshold between the scales μ_0^2 and μ^2, with no connections to the physical value of the parameters at a particular energy scale. In this sense, the decoupling is already implemented in these equations, as the different particle contributions are switched on when passing the corresponding threshold. The particle threshold is however a physical information to be added to Eqs. (3.71) and (3.89). As pointed out in [77], to perform in the correct way the particle decoupling at given physical thresholds, some matching conditions have to be taken into account. These conditions are renormalization- and regularization-scheme dependent; they have been studied at length in the context of Effective Field Theories [147–149] and Grand Unification Theories (GUTs) [150–154]. If taken in the $\overline{MS}$ scheme with dimensional regularization, as it is done here, no $\mathcal{O}(\alpha)$ correction appear at the threshold of scalars and fermions, while we have to take into account a $\mathcal{O}(\alpha)$ shift produced by bosons in the running of $\alpha(\mu^2)$, that we already discussed in the previous section. Moreover, at fermionic thresholds $\mathcal{O}(\alpha^2)$, $\mathcal{O}(\alpha\alpha_S)$ and $\mathcal{O}(\alpha\alpha_S^2)$ terms have to be taken into account [146]. Different prescriptions for regularizing and renormalizing the theory would lead to different shifts [155, 156].

At a given fixed order in perturbation theory, e.g. at NLO in α, the threshold corrections stemming from the NLO expansion of the running are cancelled against the corresponding terms contained in the counterterms, in such a way that physical predictions are not affected by the choice of the regularization and renormalization scheme adopted [157]. This can be easily sketched taking into account for example $\alpha(\mu^2)$ and considering the NLO expansion of the running. The complete calculation can be found in App. A and allows us to conclude that the decoupling prescription and the shifts induced by threshold corrections have no effect on the physics of the process under consideration. Given that, also the position of the threshold is a matter of convention, i.e. one could in principle set the i-th threshold at values either much lower than the particle-i mass, or slightly below it, or at the physical m_i value.

To calculate the matching conditions at $\mathcal{O}(\alpha)$, we define the couplings above and below the threshold at fermion i as:

$$
\begin{array}{llll}
\alpha(m_i^2)^+ & , & s_w^2(m_i^2)^+ & \text{above threshold} \\
\alpha(m_i^2)^- & , & s_w^2(m_i^2)^- & \text{below threshold} .
\end{array} \tag{3.116}
$$

For the electromagnetic coupling constant, at the threshold of fermion f we

have:

$$
\frac{1}{\alpha(m_f^2)^+} = \frac{1}{\alpha(m_f^2)^-} - \frac{Q_f^2}{\pi} \left\{ \frac{15}{16} N_f^c Q_f^2 \frac{\alpha(m_f^2)}{\pi} \right. \tag{3.117}
$$
$$
+ \frac{(N_f^c - 1)}{2} \frac{\alpha_S(m_f^2)}{\pi} \left[\frac{13}{12} \right.
$$
$$
\left. \left. + \frac{\alpha_S(m_f^2)}{\pi} \left(\frac{655}{144}\zeta(3) - \frac{3847}{864} + \frac{361}{1296} n_q + \frac{295}{1296} \frac{\sum_{q \neq f} Q_q^2}{Q_f^2} \right) \right] \right\}
$$

and at the $W^{\pm}$ threshold:

$$
\frac{1}{\alpha(M_W^2)^+} = \frac{1}{\alpha(M_W^2)^-} + \frac{1}{6\pi} , \tag{3.118}
$$

where the term $1/(6\pi)$ stems from the additional $-2/3$ seen in the previous section. In the Z_ew-BMNNPV code, threshold corrections are implemented for the W boson at $\mathcal{O}(\alpha)$ and for top-quark including $\mathcal{O}(\alpha^2)$, $\mathcal{O}(\alpha\alpha_S)$, and $\mathcal{O}(\alpha\alpha_S^2)$ effects [138, 158].

For the weak mixing angle, we start by writing the analogue of Eq. (12) of [77]:

$$
s_w^2(m_i^2)^+ = s_w^2(\mu_0^2) \frac{\alpha(m_i^2)^+}{\alpha(\mu_0^2)} + \frac{\sum_p N_p^c \gamma_p Q_p I_{3,p}}{\sum_p N_p^c \gamma_p Q_p^2} \left[1 - \frac{\alpha(m_p^2)^+}{\alpha(\mu_0^2)} \right] , \tag{3.119}
$$

where p is an index that runs over all SM particles. Note that if p is a fermion, an extra factor 2 appears in the corresponding contribution to the sum at the denominator, namely, at fermionic thresholds, we have:

$$
s_w^2(m_i^2)^- = \frac{\alpha(m_i^2)^-}{\alpha(m_i^2)^+} s_w^2(m_i^2)^+ + \frac{Q_i I_{3,i}}{2Q_i^2} \left[1 - \frac{\alpha(m_i^2)^-}{\alpha(m_i^2)^+} \right] . \tag{3.120}
$$

To prove that this is a correct NLO expression, we have verified that, by inserting Eq. (3.119) into this last Eq. (3.120), we obtain the analogue of Eq. (3.119) for $s_w^2(m_i)^-$, namely:

$$
s_w^2(m_i^2)^- = s_w^2(\mu_0^2) \frac{\alpha(m_i^2)^-}{\alpha(\mu_0^2)} + \frac{\sum_{p \neq i} N_p^c \gamma_p Q_p I_{3,p}}{\sum_{p \neq i} N_p^c \gamma_p Q_p^2} \left[1 - \frac{\alpha(m_p^2)^-}{\alpha(\mu_0^2)} \right] , \tag{3.121}
$$

where now the sums are over all particles with the exception of particle i. Note that, to this aim, the following NLO relations have to be used:

$$
\frac{\alpha(m_i^2)^-}{\alpha(m_i^2)^+} = 1 + \frac{\alpha(\mu_0^2)}{24\pi} \left[- \sum_p N_p^c \gamma_p Q_p^2 + \sum_{p \neq i} N_p^c \gamma_p Q_p^2 \right] \ln \frac{m_p^2}{\mu_0^2} \tag{3.122}
$$
$$
= 1 - \frac{\alpha(\mu_0^2)}{24\pi} 2 N_i^c \gamma_i Q_i^2 \ln \frac{m_i^2}{\mu_0^2} ,
$$
$$
\frac{\alpha(m_i^2)^-}{\alpha(\mu_0^2)} = 1 + \frac{\alpha(\mu_0^2)}{24\pi} \sum_{p \neq i} N_p^c \gamma_p Q_p^2 \ln \frac{m_p^2}{\mu_0^2} .
$$

3.4. Renormalization of the EW Standard Model in the $\overline{MS}$ scheme

From this calculation, it is highlighted that we linked the running of $s_w^2(\mu^2)$ to the one of $\alpha(\mu^2)$ and one can notice that the discontinuities at threshold i are due only to the running of $\alpha(\mu^2)$.

Eq. (3.120) is valid also for bosons without 2 at the denominator. It can be written in the following way:

$$s_w^2(m_i^2)^+ = \frac{\alpha(m_i^2)^+}{\alpha(m_i^2)^-} s_w^2(m_i^2)^- + \frac{N_i^c \gamma_i Q_i I_{3,i}}{N_i^c \gamma_i Q_i^2} \left[1 - \frac{\alpha(m_i^2)^+}{\alpha(m_i^2)^-} \right] . \qquad (3.123)$$

For the W boson we have two contributions, one for W^+ and one for W^-, that we have to decouple, that is:

$$s_w^2(M_W^2)^+ = \frac{\alpha(M_W^2)^+}{\alpha(M_W^2)^-} s_w^2(M_W^2)^- + \frac{\sum_{i=W^+,\, W^-} N_i^c \gamma_i Q_i I_{3,i}}{\sum_{i=W^+,\, W^-} N_i^c \gamma_i Q_i^2} \left[1 - \frac{\alpha(M_W^2)^+}{\alpha(M_W^2)^-} \right] .$$
$$(3.124)$$

Since:

$$\frac{\sum_{i=W^+,\, W^-} N_i^c \gamma_i Q_i I_{3,i}}{\sum_{i=W^+,\, W^-} N_i^c \gamma_i Q_i^2} = 1 , \qquad (3.125)$$

we have:

$$s_w^2(M_W^2)^+ = 1 + \frac{\alpha(M_W^2)^+}{\alpha(M_W^2)^-} \left[s_w^2(M_W^2)^- - 1 \right] = 1 - \frac{\alpha(M_W^2)^+}{\alpha(M_W^2)^-} c_w^2(M_W^2)^- , \quad (3.126)$$

that is exactly Eq. (30) by [77]. In this relation, it is present a $\mathcal{O}(\alpha)$ discontinuity due to the term $1/(6\pi)$ arising from the running of $\alpha(\mu^2)$, as seen in Sec. 3.4.4. From a technical point of view, in the Z_ew-BMNNPV code the decoupling of the W boson and the top quark in the running of $\alpha(\mu^2)$ and $s_w^2(\mu^2)$ is performed by integrating out these particles only in the RGE equations and in the expressions of the relevant counterterms, namely $\delta Z_e^{\overline{MS}}$ and $\delta s_w^2(\mu^2)/s_w^2(\mu^2)$. However, we do not remove the W- and top-contributions from the calculation of the matrix elements, i.e. we do not completely adopt an effective field theory approach in which the heavy degrees of freedom are integrated out at low energies.

To conclude, we discuss the gauge invariance of our definition of $\sin^2 \theta_w^{\overline{MS}}(\mu^2)$, which is essentially the one in [77], complete with both fermionic and bosonic contributions and threshold corrections. In fact, gauge invariance represents an issue often associated with the definition of the $\overline{MS}$ weak mixing angle. In [133], a gauge-independent parameter $\sin^2 \hat{\theta}_w(q^2)$ is introduced on the basis of the Pinch Technique (PT) [159, 160], which consists in moving part of the corrections coming from vertex and box diagrams (the so-called *pinch parts*) into the self-energies, resulting in new gauge independent self-energies. The pinch parts can be written in terms of equal-time commutators of currents, and as such do not depend on the specific process and on the strong interaction dynamics. A generalization of the pinch technique is represented by the background-field method of quantizing the theory [161, 162].

Even if conceptually different, the definition of $\sin^2 \theta_w^{\overline{MS}}(\mu^2)$ adopted here can be proven to be mathematically identical to the one in [133] at NLO, upon the identification $\mu^2 = q^2$, and is equivalent to the definition that uses the background-field method given in [21]. Furthermore, the class of higher-order terms included in the running essentially represents corrections to the $\mathcal{O}(\alpha)$ fermionic contributions to the Z/γ propagator, and as such is gauge invariant. We can thus conclude that our definition of the $\overline{MS}$ weak mixing angle is well-posed in terms of gauge independence and can be consistently compared with experimental results.

3.5 Electroweak radiative corrections at high energy

In the high-energy region, where "high" means much larger than the electroweak scale, i.e. much larger than the W and Z masses, the W and Z bosons play the role of massless particles, the virtual exchange of which causes the appearance of large logarithms in the soft and/or collinear limit. The leading terms are the so-called Sudakov logarithms [163], that have been discussed in [159, 164–171]. At the one-loop level, the leading logarithmic contributions are double-logs of the kind $(\alpha/s_w^2) \ln^2(q^2/M_W^2)$, while the subleading ones are single-logs $(\alpha/s_w^2) \ln(q^2/M_W^2)$, where q^2 is the scale of the process under consideration, usually determined by the centre-of-mass energy $\sqrt{s}$. In the following, we will refer to the logarithmic part of these corrections with $l = \ln(q^2/M_W^2)$ and $L = \ln^2(q^2/M_W^2)$. The coefficient in front of the leading double logs is negative, giving rise to negative corrections increasing in absolute value with the energy scale. The single-log contributions, on the other hand, for many processes have positive sign, compensating in some cases the Sudakov corrections.

The origin of these terms can be understood as following. Also in QED and QCD, by virtue of the Bloch-Nordsieck [172] and Kinoshita-Lee-Nauenberg (KLN) [173, 174] theorems, double-log contributions result from the exchange of virtual photons and gluons, but are cancelled when taking into account real-emission corrections, i.e. when inclusively summing over all initial and final degenerate states, that in QED are represented by electrons dressed with soft and collinear unresolved radiation. In QCD one has to sum also over the colour index, that means taking the sum over degenerate states within the colour triplets. Moreover, the remaining single logarithms are reabsorbed into parton distribution and fragmentation functions.

In the weak sector, two issues arise: the masses of the W and Z bosons are a physical cut-off and the states within an isospin doublet constitute different experimental initial and final states, because the electroweak charges are not confined. Since real W and Z bosons are very often experimentally resolved, it is impossible to define fully inclusive cross sections, and the virtual corrections

3.5. Electroweak radiative corrections at high energy

are not cancelled, with maybe the exception of a very small fraction of unresolved vector bosons [175]. Note also that, since in this case real contributions are considered as different processes, characterised by their own cross sections, that are of course positive, this explains why the virtual corrections due to the exchange of W and Z bosons are negative.

In the so-called Sudakov regime, where all invariants associated with a certain particle reactions are large with respect to the electroweak scale, these corrections can reach also several tens of percent. On the other hand, these logarithms are connected with the external particles of the given process and are thus universal [173], allowing to derive general results at least at NLO. Different studies at one- and two-loop level exist in the literature [169–171, 176–183], to which we refer for the theoretical definition of the relevant equations. In [184–186], Sudakov logs are discussed in the context of LHC and high-energy pp colliders.

For the numerical implementation, we use mainly the code presented in [187]; the corresponding numerical results are discussed in Sec. 6.7. Alternative automations of the calculation of electroweak Sudakov logarithms can be found in [188–190].

By following in particular [178], we consider one-loop calculations, we operate within the 't Hooft-Feynman gauge and perform the renormalization as described in Sec. 3.1. This means in particular that the parameter renormalization is carried on in the on-shell scheme, while we will briefly comment on the $\overline{MS}$ scheme. A remark is in order here concerning the dimensional regularisation parameter μ_{dim}. When discussing the Sudakov corrections, one has in mind to find a good approximation for the complete NLO calculation, that is able to capture the behaviour of the cross sections in the high-energy regime. In the complete NLO calculation we know that the dependence on μ_{dim} in the evaluation of the amplitudes is cancelled by the parameter counterterms, which in a sense can be factorised on top of a leading-order structure. In the high-energy limit this cancellation results in terms of the kind $\ln(r_{kl}/M_W^2)$, where r_{kl} is a generic invariant built with the momenta of particle k and l of the tree-level process, that can be traded for s up to constant corrections that go as $\ln(r_{kl}/s)$. These $\ln(s/M_W^2)$ logarithms, that have a UV rather than IR (soft and/or collinear) origin, have however to be taken into account when describing the cross section at high energies.

Another observation is that, since the evaluation of logarithmic corrections requires the use of the eikonal and collinear limits, in which one disregards the vector-boson masses, it is essential that these mass terms appear only in numerators. In the adopted gauge, a possible issue arise for a generic process because the Feynman rules for the polarization vectors of the longitudinal gauge bosons contain inverse powers of their masses. This problem can be circumvented by invoking the Goldstone-boson equivalence theorem (further discussed in Sec. 4.1), thus substituting the longitudinal vector bosons with their associated Goldstone bosons in the amplitudes in the high-energy limit.

3. Electroweak virtual corrections to the neutral-current Drell Yan

However, this issue is absent when considering a 4-fermion process like the neutral-current Drell Yan we are interested in.

By adopting the notation used in [178], we consider a 4-fermion process mediated by a neutral current. To be precise, we take an amplitude with a quark-antiquark and a lepton-antilepton pair as external states, with the idea of applying the results to the neutral-current Drell-Yan process $q(p_1)\bar{q}(p_2) \to \ell(p_3)\bar{\ell}(p_4)$, and consider the momenta as incoming:

$$\bar{\ell}_\sigma^\kappa \ell_\sigma^\kappa q_\rho^\lambda \bar{q}_\rho^\lambda \to 0 \,, \qquad (3.127)$$

where the fermion chiralities are indicated with $\kappa, \lambda = $ R, L and the isospin indices with $\sigma, \rho = \pm$. We can write the Born amplitude in the limit of high energies as:

$$\mathcal{M}_0^{\bar{\ell}_\sigma^\kappa \ell_\sigma^\kappa q_\rho^\lambda \bar{q}_\rho^\lambda} = e^2 \left(\frac{1}{4c_w^2} Y_{\ell_\sigma^\kappa} Y_{q_\rho^\lambda} + \frac{1}{s_w^2} I_{\ell_\sigma^\kappa}^3 I_{q_\rho^\lambda}^3 \right) \frac{A_{12}}{r_{12}} \,, \qquad (3.128)$$

where we have introduced the invariant $r_{12} = (p_1 + p_2)^2 = s$, while Y and I^3 are the weak hypercharge and the third component of the weak isospin in the notation of Chap. 1, respectively. The NLO amplitude, in the logarithmic approximation which retains the leading and sub-leading logs, reads:

$$\mathcal{M}^{\bar{\ell}_\sigma^\kappa \ell_\sigma^\kappa q_\rho^\lambda \bar{q}_\rho^\lambda} = \mathcal{M}_0^{\bar{\ell}_\sigma^\kappa \ell_\sigma^\kappa q_\rho^\lambda \bar{q}_\rho^\lambda} \cdot \delta_{\bar{\ell}_\sigma^\kappa \ell_\sigma^\kappa q_\rho^\lambda \bar{q}_\rho^\lambda} \,, \qquad (3.129)$$

that is, the corrections can be factorised on top of the leading order. To study the structure of the corrections, we note that, as already stated, in general the logarithms can be written as:

$$L(|r_{kl}|, M^2) = \frac{\alpha}{4\pi} \ln^2 \frac{r_{kl}}{M^2} \,, \quad l(r_{kl}, M^2) = \frac{\alpha}{4\pi} \ln \frac{r_{kl}}{M^2} \,, \qquad (3.130)$$

but we can express them only as functions of s and M_W:

$$L(s) = \frac{\alpha}{4\pi} \ln^2 \frac{s}{M_W^2} \,, \quad l(s) = \frac{\alpha}{4\pi} \ln \frac{s}{M_W^2} \,, \qquad (3.131)$$

where, by performing this operation, the "error" we make amounts to terms of the kind $\ln(r_{kl}/s)$ or $\ln(M/M_W)$, that do not depend on the energy. Thus, one can distinguish:

- a logarithmic part, with terms proportional to $L(s)$, $l(s)\ln(r_{kl}/s)$ and to $l(s)$, that is electroweak symmetric, because we choose to set the scale to M_W for both W and Z contributions, as well as for a fictitious massive photon, that in a sense takes into account the running between the electroweak and the high-energy scale under consideration;

- an electromagnetic part, which comprehends terms of the type $\ln(M_W^2/\lambda^2)$ and $\ln(M_W^2/m_f^2)$, that account for the running between the photonic regularization mass λ or the light fermion masses and the weak scale. The leading ones of these contributions, which correspond to the emission of virtual photons, are in most cases compensated by real photonic emissions;

3.5. Electroweak radiative corrections at high energy

- a sub-leading part due to the mass difference between the W and the Z boson, that, as already stated, are of the same order of constant correction terms.

The δ factor multiplying the Born amplitude in Eq. (3.129) can be further decomposed into:

$$\delta = \delta^{LSC} + \delta^{SSC} + \delta^{C} + \delta^{R}\,, \qquad (3.132)$$

that are the leading and sub-leading soft-collinear logarithms, the collinear ones and the ones stemming from the renormalization, respectively. We now examine each of these contributions in more detail.

Soft-collinear contributions

Double-logarithmic contributions arise due to the exchange of soft-collinear gauge bosons between different external legs:
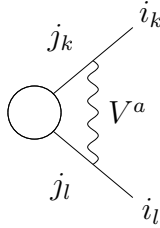
These corrections can be calculated within the eikonal approximation, which consists in neglecting the momenta of the soft-collinear gauge bosons everywhere but in the singular propagators, and correctly takes into account soft singularities. This diagram for the generic process $i_1 \ldots i_n \to 0$ can be written as:

$$\mathcal{M}^{i_1\ldots i_n} = \sum_{k=1}^{n}\sum_{l\neq k}\sum_{V^a=A,Z,W^\pm} \mathcal{I}_{j_k,i_k}^{V^a}\mathcal{I}_{j_l,i_l}^{\bar{V}^a} \cdot \mathcal{M}_0^{i_1\ldots i_k\to j_k\ldots i_l\to j_l\ldots i_n} \cdot \delta_{kl}^{V^a}\,, \qquad (3.133)$$

where $\mathcal{I}_{j_k,i_k}^{V^a}$ is the gauge group generator associated to the vertex $V^a i_k j_k$, and similarly for i_l, j_l. Note that the tree-level amplitude is the one obtained with the replacements $i_k \to j_k$ and $i_l \to j_l$, where $j_{k(l)} = i_{k(l)}$ if $V^a = A, Z$ and $j_{k(l)}$ is the $SU(2)$ transformed of $i_{k(l)}$ in case of the exchange of a W boson. The factor $\delta_{kl}^{V^a}$ corresponds to the three-point function C_0:

$$\delta_{kl}^{V^a} = -ie^2 \int \frac{d^4q}{(4\pi)^4}\frac{4p_k \cdot p_l}{(q^2 - M_{V^a}^2)\left[(p_k+q)^2 - m_k^2\right]\left[(p_l-q)^2 - m_l^2\right]}\,, \qquad (3.134)$$

which at high energies can be simplified to:

$$\delta_{kl}^{V^a} = \frac{1}{2}\left[L(s, M_{V^a}^2) + 2l(s, M_{V^a}^2)\ln\frac{|r_{kl}|}{s} + \text{constant terms}\right]\,. \qquad (3.135)$$

3. Electroweak virtual corrections to the neutral-current Drell Yan

In this expression, one can distinguish the first logarithm, that is the leading contribution (LSC in the following) and the second one, which encodes the angular dependence and gives rise to a subleading part (SSC). After summing over the A, Z, W contributions and taking into account $SU(2)_L \times U(1)_Y$ gauge invariance, one can write:

$$\mathcal{M}_{LSC}^{i_1...i_n} = \sum_{k=1}^{n} \delta_{j_k i_k}^{LSC} \mathcal{M}_0^{i_1...j_k...i_n} , \qquad (3.136)$$

where in the case of a 4-fermion process:

$$
\begin{aligned}
\delta^{LSC} &= \sum_{f_\tau^\mu = \ell_\sigma^\kappa, q_\rho^\lambda} \Bigg[C_{f_\tau^\mu}^{ew} L(s) - 2(\mathcal{I}_{f_\tau^\mu}^Z)^2 \ln \frac{M_Z^2}{M_W^2} l(s, M_Z^2) \\
&\quad + Q_{f_\tau^\mu}^2 \left(2l(s) \ln \frac{M_W^2}{\lambda^2} + L(M_W^2, \lambda^2) - L(m_{f_\tau^\mu}^2, \lambda^2) \right) \Bigg] . \quad (3.137)
\end{aligned}
$$

where C^{ew} indicates the eigenvalues of the electroweak Casimir operator, defined and tabulated in [178], and:

$$\mathcal{I}_{f_\tau^\mu}^Z = \frac{I_{f_\tau^\mu}^3 - s_w^2 Q_{f_\tau^\mu}}{s_w c_w} . \qquad (3.138)$$

The remaining SSC terms contribute to give:

$$\mathcal{M}_{SSC}^{i_1...i_n} = \sum_{k=1}^{n} \sum_{l<k} \sum_{V^a = A,Z,W^\pm} \delta_{j_k i_k, j_l i_l, V^a}^{SSC} \mathcal{M}_0^{i_1...j_k...j_l...i_n} , \qquad (3.139)$$

where δ^{SSC}, for a neutral-current annihilation process as the one we are interested in, is given in Eq. (6.11) of [178].

Single-logarithmic contributions

Single-logarithmic contributions come from two possible sources. The first one are the terms of the type $\delta Z^\phi/2$ from the wave function renormalization, which contain soft as well as collinear single logs. From a practical point of view, one can assume $M_W \sim 0$ and notice that the mass-singular infrared logs coming from $\delta Z^\phi/2$ have the same structure and the same coefficient as the UV logarithms of the form $\ln \mu^2/m_\phi^2$ in the field wave function counterterms. Thus one can extract them by setting $\mu^2 = s$ in these terms, up to suppressed terms of the kind $\ln M_W^2/m_\phi^2$. The second origin, on the other hand, is connected with the emission of virtual collinear gauge bosons from external lines, as in the diagrams of the kind:
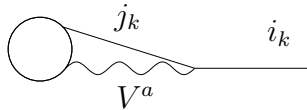
3.5. Electroweak radiative corrections at high energy

which can be evaluated in the collinear limit. It is possible to prove that single-log corrections from this type of diagrams factorise onto the tree level amplitude, by virtue of collinear Ward identities, and after subtracting with due care the contributions already included in the wave-function renormalization and in the soft-collinear corrections. The final result is:

$$\mathcal{M}_C^{i_1\dots i_n} = \sum_{k=1}^{n} \delta_{j_k i_k}^C \mathcal{M}_0^{i_1\dots j_k\dots i_n} \,, \tag{3.140}$$

where:

$$\delta^C = \delta^{\text{coll}} + \left.\frac{\delta Z^\phi}{2}\right|_{\mu^2=s} \,. \tag{3.141}$$

Contributions from the renormalization

Finally, single-logarithmic contributions of UV origin of the type $\log s/M_W^2$ may arise. We identify them with the contribution δ^R. These terms are connected to the running of couplings up to the high energy s, which are part of the parameter renormalization constants of e.g. the electromagnetic coupling or the weak mixing angle, if the on-shell renormalization scheme is adopted. As we will discuss in Chap. 6, these contributions are resummed into $\overline{MS}$ couplings and thus do not appear in the $\overline{MS}$ scheme.

3.5.1   Resummation of Sudakov logarithms

The large logarithms described in the previous section can turn to be huge as the energy is growing, becoming very relevant in the evaluation of observables at the LHC. To this aim, they should be properly resummed, at least for what concerns the double soft-collinear contributions, which are the dominant part. This can be achieved with the method in [169], which essentially presents a generalization to non-abelian theories of the Sudakov form factor of QED, based on the Renormalization Group Evolution equations. The Sudakov double-logs can thus be exponentiated:

$$\mathcal{M} = \mathcal{M}_0 \, e^{-\frac{1}{2}\sum_{i=1}^{n} W_i(s,\mu_{IR}^2)} \,, \tag{3.142}$$

where $W_i(s,\mu_{IR}^2)$ represents the probability that a soft and collinear gauge boson is exchanged between the external particle i and another external particle, and the summation is over the external legs of the process. The factor depends on μ_{IR}, which is an infrared cut-off on the transverse momenta of the emitted particles. The process amplitude can then be evolved as a function of μ_{IR}, similarly to what happens for the Renormalization Group equations [191]. In inclusive physical observables, the dependence on μ_{IR} should be cancelled, since both virtual and real corrections are taken into account within the KLN theorem. When considering also real emission, some attention should be paid to the fact that in non-abelian theories, gauge bosons carry quantum numbers and can interact with each other, thus invalidating the assumption that

3. Electroweak virtual corrections to the neutral-current Drell Yan

each emission is independent from each other. In other words, in the non-abelian case the emissions are not Poisson-distributed, but the exponentiation in Eq. (3.142) is still valid, provided that one adds an appropriate term in the exponential to take into account the emission of a virtual boson from a real one, in region where the transverse momenta of the emitted particles are much larger than μ_{IR}.

In the case of the electroweak Standard Model, one has also to deal with a spontaneously-broken gauge symmetry. In the approach of [169], one can thus solve the evolution equations in two different regions: first for $M \ll \mu_{IR} \ll \sqrt{s}$, where $M \sim M_W \sim M_Z \sim M_H \sim m_t$ is the electroweak scale, then for $\mu_{IR} \ll M$, by taking as initial condition the matching for $\mu_{IR} = M$. In the first region, one can neglect the effects due to the symmetry breaking, finding:

$$\mathcal{M} = \mathcal{M}_0 \cdot \exp\left(-\frac{e^2}{(4\pi)^2} \cdot \ln^2 \frac{s}{\mu_{IR}^2} \cdot \sum_{i=1}^{n} C_i^{ew} \right), \tag{3.143}$$

while in the second sector only photons contribute:

$$\mathcal{M} = \mathcal{M}_0 \cdot \exp\left(-\frac{e^2}{(4\pi)^2} \cdot \ln^2 \frac{s}{\mu_{IR}^2} \cdot \sum_{i=1}^{n} C_i^{ew} \right) \tag{3.144}$$
$$\cdot \exp\left[-\frac{e^2}{(4\pi)^2} \sum_{i=1}^{n} Q_i^2 \left(\ln \frac{s}{m_i M} \ln \frac{M^2}{\mu_{IR}^2} + \ln \frac{s}{m_i^2} \ln \frac{M^2}{\mu_{IR}^2} - \frac{1}{2} \ln^2 \frac{m_i^2}{M^2} \right) \right].$$

For what concerns sub-leading logarithms, resummation has not been mathematically proven, but also in this case one can use the evolutions equations, thus leading to a modification of the W_i factors to include also single logs, as shown in [179, 182]. Current results are valid up to next-to-leading- (NLL) and next-to-next-to-leading-logarithmic (N2LL) approximation [170, 192].

4

The treatment of unstable particles

his Chapter presents the long-standing issue associated with the mathematical description of unstable particles in Feynman diagrams. The problem of preventing the resonant propagator from blowing up at the pole is usually addressed by performing a Dyson summation of the self-energy corrections. When applying this method, special care has to be taken to preserve the gauge invariance. The different options to treat the resonances which are implemented in the `Z_ew-BMNNPV` code, namely the complex-mass, pole and factorization schemes, are described.

4.1 The problem of gauge invariance with unstable particles

One of the main features of the neutral-current Drell-Yan process is the presence of the Z-boson channel, characterised by an unstable boson with a lifetime that is not long enough to leave a direct trace in detectors, but that can be rather reconstructed from its decay products. As a matter of fact, many unstable particles, such as fermions, or the Higgs and gauge bosons, enter high-energy processes, making it necessary to infer their properties from the distribution of the decay products. For example, let us take a resonance P with a life-time τ_P: to measure τ_P, one can parametrise the invariant-mass distribution of the particles originated by the decay of P as a Breit–Wigner, obtain the resonance width Γ_P and then extract $\tau_P = 1/\Gamma_P$.

From a theoretical point of view, complications in standard perturbation theory stem from resonant processes. In fact, the resonance propagator $G_P(p^2)$ appearing in the Feynman diagrams of the reaction is proportional to:

$$\frac{1}{p^2 - M_P^2} \, , \tag{4.1}$$

and thus has a pole for $p^2 = M_P^2$, leading to a singularity at any fixed order in perturbation theory. To cure this behaviour, one can perform a Dyson

summation of the imaginary parts of the corrections to the particle self-energy near the pole:

$$
\begin{aligned}
G_P(p^2) \;&=\; \frac{i}{p^2 - M_P^2} \;+\; \frac{i}{p^2 - M_P^2}\, i\hat{\Sigma}_P(p^2)\, \frac{i}{p^2 - M_P^2} \\
&\quad +\; \frac{i}{p^2 - M_P^2}\, i\hat{\Sigma}_P(p^2)\, \frac{i}{p^2 - M_P^2}\, i\hat{\Sigma}_P(p^2)\, \frac{i}{p^2 - M_P^2} \;+\; \dots \\
&=\; \frac{i}{p^2 - M_P^2 + \hat{\Sigma}_P(p^2)}\;,
\end{aligned}
\tag{4.2}
$$

that can be graphically represented as:

In this way, in the complex plane the pole of the propagator for an unstable particles does not lie on the real axis, but slightly below it. Stated in other words, the way to circumvent the difficulties connected to unstable particle propagators is to use perturbation theory where the series converges, and the analytical continuation of the result in the problematic regions. One can then apply the optical theorem, that derives from the unitarity of the S-matrix (see for example Ref. [17]), to write:

$$
\begin{aligned}
i\mathrm{Im}\hat{\Sigma}_P(M_P^2) \;&=\; i\mathrm{Im}\left\{ \quad\quad\quad \right\}\bigg|_{p^2 = M_P^2} \\
&=\; \tfrac{1}{2}\sum_X \quad\quad\quad \\
&=\; \tfrac{1}{2}\sum_X \int d\Phi_X |\mathcal{M}_{P\to X}|^2 = M_P \Gamma_P\,.
\end{aligned}
$$

4.1. The problem of gauge invariance with unstable particles

The expression above theoretically relies on the so-called Cutkosky cutting rules, a generalisation of the unitarity condition on the S-matrix, which state that imaginary parts of Feynman integrals can be matched with the corresponding cut diagrams, obtained by replacing the propagators along the cut with physical on-shell intermediate states:

$$2\pi\theta(p_0)\delta(p^2 - M_P^2)\,, \tag{4.3}$$

and taking the complex conjugate (indicated with the grey rectangle near the dashed line of the cut in the illustration above) of propagators and vertices on one side of the cut [193]. Cutkosky's results are valid for stable particles; in presence of unstable states, which cannot appear as intermediate lines with real masses, a modified version of the rules exists, namely the Veltman's Largest-Time Equation, which show that cutting rules are still applicable provided that cuts on intermediate lines of unstable particles do not contribute, thus preserving unitarity [194].

We can use the fact that in the on-shell scheme $\mathrm{Re}\hat{\Sigma}(M_P^2) = 0$ to write Eq. (4.2) as:

$$G_P(p^2) = \frac{i}{p^2 - M_P^2 + iM_P\Gamma_P}\,, \tag{4.4}$$

with of course $\Gamma_P > 0$ to preserve causality in the Feynman's $+i\epsilon$ prescription. Some important consequences come from this last equation. First of all, when squaring it, one gets the shape of a Breit–Wigner resonance and, secondly, one has that the intermediate resonance P exponentially decays with the lifetime $\tau_P = 1/\Gamma_P$ [21].

As it often happens in quantum field theory, however, one finds the solution of a problem only to discover a bigger issue. In fact, the inclusion of finite-width effects via the imaginary part at the propagator denominator, obtained via a Dyson summation of self-energies, could result in a partial inclusion of perturbative orders when ones truncates the series at some loop level. On the other hand, relations ensuring gauge invariance and unitarity of the S-matrix holds order by order in perturbation theory, and could be invalidated if some perturbative orders are not completely included or are mixed together in the calculations.

We here specify that, in the Standard Model, gauge invariance means that the process amplitudes must satisfy two fundamental conditions: they must be independent from the gauge-fixing procedure employed when quantizing the gauge theory, and they must not violate the Ward identities, also called Slavnov-Taylor identities when generalised beyond QED [17]. The renormalization strategy we adopted in Chap. 3 respects this two conditions, and we are thus free to choose to work in the most convenient gauge. The same applies to the gauge-parameter independence of the definition of the running couplings in Sec. 3.4.1 and Sec. 3.4.2, as well. Following here the line of reasoning in [21], we remark that the Slavnov-Taylor identities imply some relations between the truncated Green functions with gauge-boson external lines contracted with their momenta and the ones with the corresponding would-be

Goldstone bosons. In particular, one has that, after spontaneous symmetry breaking, $U(1)_{em}$ and $SU(2)_w$ gauge invariance implies:

$$
\begin{aligned}
p^\mu T_\mu^{W^\pm}(p) &= \pm M_W T^{\phi^\pm}(p) \\
p^\mu T_\mu^Z(p) &= -i M_Z T^\chi(p) \\
p^\mu T_\mu^A(p) &= 0 \,,
\end{aligned}
\qquad (4.5)
$$

where the symbol T denotes a Green function with the vector- or Goldstone-boson legs truncated. Eqs. (4.5) descend from the symmetry of the Lagrangian under the Becchi–Rouet–Stora (BRS) transformations, from which it can be derived a set of identities for the effective action of the theory, translated to the corresponding relations among Green functions through functional derivation w.r.t. the classical fields, that are set to zero after derivation.

The first two equations state the validity of the Goldstone-boson equivalence theorem, which expresses the asymptotical proportionality between amplitudes involving high-energetic, longitudinal vector bosons and the corresponding amplitudes obtained by replacing those vector bosons with their associated would-be Goldstone fields. This relation is particularly useful when considering cross sections at high energies, as one can replace external longitudinal vector bosons with scalars, much simplifying the calculations for example in the Sudakov regime of Sec. 3.5. Moreover, it allows to have an experimental handle on the would-be Goldstone bosons and on how spontaneous symmetry breaking works, from the study of physical longitudinal vector bosons. The last equation of Eqs. (4.5), that corresponds to the Ward identities in QED, ensures the transversality of the photon field.

The violation of these relations thus can result in an unphysical behaviour of the cross sections, as it will become apparent in the following discussion. In the high-energy limit, breaking the $SU(2)_w$ gauge invariance causes the cross-section to blow up for processes like e.g. $e^+e^- \to W^+W^-$ [21, 195]. For instance, there are cases where, in an high-energy regime, an external fermion-antifermion current becomes proportional to the sum of the fermion momenta, that we denote with p. If this current is connected to a vector boson propagator, the Slavnov-Taylor identities ensure the correct behaviour of the amplitude with the energy. For W or Z bosons, here generically called with the symbol V, one can write that part of the diagram as:

$$
\frac{\text{const.}}{p^2 - M_V^2 + i M_V \Gamma_V} p^\mu T_\mu^V(p) \,, \quad \text{for } p^0 \gg M_V \,,
\qquad (4.6)
$$

and use one of the first two of Eqs. (4.5) to prevent the amplitude from behaving in an unphysical way at high energies.

Another example comes from the collinear limit in processes like $e^+e^- \to e^-\nu_e f \bar{f}$, where the angle between the incoming and outgoing electrons becomes small, or in the scattering of a light particle like the electron mediated by a photon, for vanishing photon virtuality [195–197]. In these situations, the

4.1. The problem of gauge invariance with unstable particles

$U(1)_{em}$ gauge invariance ensures that the superficial $1/p^4$ divergence due to the propagator is reduced to $1/p^2$, where p is the momentum flowing in the propagator, as the amplitude goes as:

$$\frac{\text{const.}}{p^2} p^\mu T_\mu^A(p) \quad |p^2| \to \mathcal{O}(m_e^2). \tag{4.7}$$

In single-W production in e^+e^- annihilations this fact results in large logarithmic contributions going as $\log(m_e^2/s)$, with s the squared centre-of-mass energy. Such terms can become large, leading to a dangerous amplification even of effects due to a tiny gauge violation.

The problem arising in the treatment of unstable particles is that the expression in Eq. (4.2) is not gauge invariant, because the renormalized self-energy $\hat{\Sigma}_P(p^2)$ is gauge dependent, as it can be seen in App. C in the case of the Z boson. Far from the resonance, the gauge dependence enters formally at $\mathcal{O}(\alpha^2)$, but near the peak one has that $|p^2 - M_P^2| \sim \hat{\Sigma}_P(p^2)$ and thus gauge-dependent terms are of $\mathcal{O}(\alpha)$. In [198, 199] it was argued that one can at best push the gauge dependence to $\mathcal{O}(\alpha\,\Gamma_P/M_P)$, by carefully bringing terms that contribute to the wave-function renormalization of the unstable particle into the numerator of the propagator when computing the amplitudes.

The discussion of this issue became relevant at LEP, when the treatment of unstable particles was essential. As a matter of fact, in the case of LEP1 processes, of the kind:

$$e^+e^- \to \gamma, Z \to f\bar{f}, \tag{4.8}$$

it is possible to perform a gauge-invariant separation of the correction subsets, ending up with a result which has no significant gauge dependence. Furthermore, one could argue that at the Z peak there is no dangerous large ratio of masses, the only relevant one being s/M_Z^2, and there might be hope to introduce some corrections to mitigate possible effects of gauge violation. However, the situation gets more complicated if considering LEP2, where the first techniques to deal with the gauge invariance issues associated to unstable particles were introduced: some example are the narrow-width approximation and the fermion-loop scheme [195, 196, 200–204].

In the next sections, however, we focus on modern techniques to treat the resonances. Before that, it is necessary to discuss the definitions of mass and width of unstable particles beyond the leading order.

4.1.1 Mass and width of unstable particles

The problem of defining the mass for unstable particles is intimately connected with the issue of gauge invariance encountered with the propagators, and has been extensively addressed in the literature [205–207]. In fact, when going beyond LO, one has to take into account the mass renormalization for unstable particles to identify the correct definitions of mass and width and parametrise the resonance. This is of vital importance in view of experimental determinations of these parameters. The two most common schemes used are:

- the on-shell prescription, that follows the mass renormalization for stable particles;

- the pole definition of the renormalized mass from the complex pole location $M_P^2 - i\Gamma_P M_P$.

In particular, the on-shell renormalization condition fixes the renormalized mass as the zero of the real part of the inverse propagator:

$$M_{P,B}^2 = M_{P,OS}^2 + \text{Re}\Sigma_P(M_{P,OS}^2)\,, \tag{4.9}$$

where $M_{P,B}^2$ and $M_{P,OS}^2$ are the bare and renormalized mass of particle P, respectively, and $\Sigma_P(p^2)$ is the unrenormalized transverse part of the self energy, which is not gauge invariant starting from the two-loop level [208]. The pole definition, on the other hand, stems from the relation:

$$M_{P,B}^2 = \mu_P^2 + \Sigma_P(\mu_P^2)\,, \tag{4.10}$$

which allows to identify $\mu_P^2 = M_P^2 - i\Gamma_P M_P$ with the complex location of the propagator pole. From the definition of the mass, one can derive the one for the width in one of the two prescriptions, as following.

Starting from the on-shell one, we insert Eq. (4.9) in the expression of the propagator, and expand it to find its leading resonance behaviour:

$$\frac{1}{p^2 - M_{P,OS}^2 + \Sigma_P(p^2) - \text{Re}\Sigma_P(M_{P,OS}^2)} \rightarrow$$
$$\frac{1}{(p^2 - M_{P,OS}^2)\left[1 + \text{Re}\Sigma_P'(M_{P,OS}^2)\right] + i\text{Im}\Sigma_P(p^2)}$$
$$\text{for } p^2 \rightarrow M_{P,OS}^2. \tag{4.11}$$

By comparing this expression with the traditional form at the resonance:

$$\frac{1}{p^2 - M_P + i\Gamma_P M_P}\,, \tag{4.12}$$

this yields:

$$\Gamma_{P,OS} = \frac{\text{Im}\Sigma_P(M_{P,OS}^2)}{M_{P,OS}^2\left[1 + \text{Re}\Sigma_P'(M_{P,OS}^2)\right]}\,. \tag{4.13}$$

The procedure with the pole definition is similar, the starting point being:

$$\frac{1}{p^2 - \mu_P^2 + \Sigma_P(p^2) - \Sigma_P(\mu_P^2)} \rightarrow \frac{1}{(p^2 - \mu_P^2)\left[1 + \text{Re}\Sigma_P'(\mu_P^2)\right]}$$
$$\text{for } p^2 \rightarrow \mu_P^2 \,, \tag{4.14}$$

which results in the pole mass $M_{P,pole} = M_P$ and in the pole width $\Gamma_{P,pole} = \Gamma_P$ already introduced in the definition of the pole location, $\mu_P^2 = M_P^2 - i\Gamma_P M_P$.

4.1. The problem of gauge invariance with unstable particles

Since the pole location is an intrinsic property of the S-matrix, the definitions of M_P and Γ_P are gauge independent, as discussed in [206, 207].

Note that we are using here an abuse of notation with respect to the previous section, since we label here with M_P and Γ_P the pole definitions for particle P, that will be used in the following sections for the complex mass, pole and renormalization schemes used to treat the resonances with the package `Z_ew-BMNNPV` of POWHEG-BOX-V2. When realising the running-width prescription for W and Z bosons, one should use the on-shell quantities $M_{P,OS}$ and $\Gamma_{P,OS}$. At LEP, the Tevatron and the LHC the masses and widths of the W and Z bosons have been experimentally determined by using this on-shell definition. They can be translated into pole quantities by using the relations [209]:

$$M_V = \frac{M_{V,OS}}{\sqrt{1 + \frac{\Gamma_{V,OS}^2}{M_{V,OS}^2}}}, \quad \Gamma_V = \frac{\Gamma_{V,OS}}{\sqrt{1 + \frac{\Gamma_{V,OS}^2}{M_{V,OS}^2}}}, \tag{4.15}$$

that yield:

$$M_{W,OS} - M_W \simeq 27 \, \text{MeV}, \quad M_{Z,OS} - M_Z \simeq 34 \, \text{MeV}, \tag{4.16}$$

a difference much larger than the quoted experimental uncertainties on the W and Z masses discussed in Chap. 2.

4.1.2 The complex mass scheme

The complex-mass scheme (CMS) has been first introduced in [210] for LO calculations and generalized to NLO in [211, 212]. The essential idea behind the method is a consistent identification of the mass of the generic unstable particle P, for instance the W and Z masses, with the complex pole location of the propagators. If one makes use of an input scheme including the vector-boson masses, also the derived weak mixing angle becomes complex:

$$c_w^2 = 1 - s_w^2 = \frac{\mu_W^2}{\mu_Z^2}. \tag{4.17}$$

Gauge invariance is fully respected in this scheme, since it modifies the gauge-boson masses only by an analytic continuation. However, the CMS violates unitarity, because the standard cutting relations involve complex conjugation. On the other hand, spurious unitarity-breaking terms are at (N)NLO in an (N)LO calculation, i.e. they are always at higher order without any artificial amplification, because the unitarity cancellations coming from gauge invariance are respected.

In NLO calculations, one starts by writing the real bare masses in the Lagrangian in terms of complex renormalized masses and complex counterterms. After this, the usual perturbative calculations with Feynman rules and counterterms can be carried out in the same way as in the on-shell renormalization,

the only difference being that renormalization constants are now complex, as it is described in [21, 86]. One has to take some extra care to treat the imaginary parts in the complex masses, which would correspond to higher-order contributions in the formalism for stable particles. The scheme has thus the advantage that, provided that the widths of the unstable particles have NLO accuracy, it produces NLO-accurate predictions everywhere in phase space. For this reason and the fact that it preserves gauge invariance at any order and unitarity within the required accuracy, the CMS is commonly adopted for multi-particle NLO calculations, and has been implemented in the `Z_ew-BMNNPV` code as the default option. In the past, the default of the `Z_ew-BMNNPV` package was a naif prescription to treat the resonance, which however did not guarantee gauge invariance, as it is shown in App. C.

As general remarks, since one should argue that the complex renormalization is not necessary for all unstable particles, but only for those entering the specific process to be calculated, a few points should be kept in mind:

- all initial- and final-state particles of a given process are considered to be stable, and thus have real masses;

- since when one mass is renormalized in the CMS its value enters in general all self-energies, the mass and field renormalization constants also of stable particles become complex; in this case, one has to keep the imaginary parts in all renormalization constants, to cancel all UV divergences;

- even if, for instance in neutral-current Drell Yan, only the Z boson appears as a resonance, in the CMS the complex renormalization is applied to both the W and the Z boson, to reduce the numerical impact of spurious imaginary parts from the complex weak mixing angle.

For practical purposes, it has been noted in [21] that it is possible to avoid the complications due to the evaluation of self-energies at complex squared momenta, that would require an analytic continuation of the 2-point functions to the unphysical Riemann sheet, by making an expansion of the self-energies about a real momentum, in such a way to preserve one-loop accuracy, by treating with care the case of charged or coloured particles.

Another important point concerns the width of the unstable particle P renormalized in the CMS. In fact, Γ_P enters the renormalized parameter μ_P, but is not an independent parameter of the theory, and can be calculated from the decay cross section of P or by iteratively solving the relation:

$$M_P\Gamma_P = \mathrm{Im}\Sigma_P(M_P^2 - iM_P\Gamma_P)\,. \tag{4.18}$$

This last equation would however yield a LO result if Σ_P is taken at NLO, because the imaginary part of the one-loop self-energy, obtained by employing unitarity cuts, contains only tree-level information about the width. At the same time, one needs to use Γ_P at NLO to get full NLO accuracy in the cross

4.1. The problem of gauge invariance with unstable particles

section also in the resonant region, where $|p^2 - M_P^2|$ becomes $\mathcal{O}(M_P \Gamma_P)$. Thus one should try to use a two-loop self energy to derive the width, or alternatively calculate it directly from decay amplitudes at NLO.

This fact can be understood by noticing that, in the CMS, one adds and subtracts the same imaginary part in the Lagrangian, and uses one of these terms for the imaginary part for the renormalized mass, which is resummed, and the other one in a counterterm vertex, which is kept at the numerator. Even if this addition/subtraction procedure preserves gauge invariance and unitarity cancellations in a way that is independent from the accuracy of the calculated width value, for the unitarity cut equations to be still valid at NLO one needs at least NLO decay widths [213]. In the code, we use the experimental value of the widths, given in input. The experimental determination, in fact, can be regarded as the value resulting from a calculation including all perturbative orders.

Having in mind an input scheme with a coupling $\alpha_0/\alpha(M_Z^2)/G_\mu$ and the W and Z boson masses, a final remark on the value of the electromagnetic coupling is necessary. In fact, in the CMS, the renormalized electromagnetic coupling e is complex, because the charge renormalization constant is a function of complex masses via loop corrections. Again in this case, the imaginary part of e is not among the input parameters, but can be iteratively calculated from the charge renormalization constant. The difference with respect to the width is that the imaginary part of the electromagnetic coupling is formally due to higher-order spurious terms, because the charge counterterm is defined with self-energies at zero momentum transfer, which are real if the masses are real. As a consequence, at NLO one can safely set the imaginary parts of e to zero, also in order to avoid to possibly spoil the cancellation of infrared divergences between virtual and real EW corrections.

If one uses $\alpha(M_Z^2)$ or G_μ in place of α_0 as inputs, the line of reasoning is similar. To avoid spurious $\mathcal{O}(\alpha)$ terms in the relation between α_0 and G_μ, the value of α_{G_μ} should be real, i.e. it should be calculated from the real W and Z masses. Note however that the corresponding factor Δr, which enters the charge renormalization constant in the G_μ scheme, can be calculated by using real or complex masses, because the corresponding change would be at two-loop order.

In the `Z_ew-BMNNPV` package, where the CMS is the default option for treating the resonances, the input values for M_V and Γ_V are the on-shell ones, i.e. $M_{V,OS}$ and $\Gamma_{V,OS}$, then internally converted, by means of Eq. (4.15), to the corresponding pole values, which are used throughout the rest of the code for the matrix-element evaluation.

As already stated at the beginning of the section, if M_W and M_Z are taken as input parameters, in the CMS also the weak mixing angle and its counterterm, which are calculated in terms of μ_W and μ_Z, become complex. For the schemes with $\sin^2 \theta_{eff}^\ell$ in input, on the other hand, $\sin^2 \theta_{eff}^\ell$ is a real quantity, defined through the real part of the g_V/g_A ratio. In the same way, also α_0,

$\alpha(M_Z)$, and G_μ are considered real input parameters of the code. When G_μ is among the free parameters − with the only exception of the (α_0, G_μ, M_Z) scheme −, G_μ is converted to α_{G_μ} by using the relation from the muon decay, in which also the vector-boson mass enters. In the CMS α_{G_μ} could thus become complex, but in the code its imaginary part is always eliminated by taking the real part of the mass entering the conversion equation, to reduce the impact of the corresponding spurious higher-order terms.

4.1.3 The pole scheme

The main idea at the basis of the pole scheme (PS) is the fact that the pole location of the vector boson propagator and its residue are both gauge-independent [198, 205–207, 214]. One can thus split the amplitude between the resonant part and a residue and then introduce the finite decay width only in the resonant part, in the following way [21, 86]:

$$
\begin{aligned}
\mathcal{M} &= \frac{R(p^2)}{p^2 - M_P^2} + N(p^2) = \frac{R(M_P^2)}{p^2 - M_P^2} + \frac{R(p^2) - R(M_P^2)}{p^2 - M_P^2} + N(p^2) \\
&\to \frac{\tilde{R}(\mu_P^2)}{p^2 - \mu_P^2} + \frac{R(p^2) - R(M_P^2)}{p^2 - M_P^2} + \tilde{N}(p^2) \,,
\end{aligned}
\tag{4.19}
$$

where $R(p^2)$ is the resonant part stemming from the propagator of particle P with momentum p and $N(p^2)$ is the corresponding non-resonant contribution. One thus proceed to add the term $i\Gamma_P M_P$ to the propagator denominator $p^2 - M_P^2$ in the resonant part: in this procedure, both $R(p^2)$ and $N(p^2)$ get modified into $\tilde{R}(\mu_P^2)$ and $\tilde{N}(p^2)$, respectively, in such a way that the final sum does not contain double-counted terms.

The concept of the pole scheme is interesting because it is based on the separation between a signal (the resonance) and a background (the remaining non-resonant contributions), thus making the scheme particularly suitable for the description of the resonance in terms of the pseudo observables, like total and partial decay widths, asymmetries and effective couplings, as done at LEP.

Since near the resonance $p^2 \sim M_P^2$ and the term involving Γ_P becomes dominant, the value of the width has to be at one order higher than the rest of the calculation. This scheme respects gauge invariance and treats in a uniform way the resonance and off-resonance regions, provided that enough care is paid to the separation between resonant and non-resonant contributions, in which there is some degree of arbitrariness. The implementation in the case of the neutral-current Drell-Yan process at NLO is described in [86], while it has not yet been fully implemented for processes involving multiple or charged resonances, because of extra difficulties connected with the exchange of massless particles (photons or gluons) between the resonances or initial and final states, that in these cases prevents a gauge-invariant separation between radiation emission before and after the resonance production. A similar problem is

encountered when considering higher-order corrections to the amplitude, and can be handled as described in [21, 86].

Another observation is that, since in the resonant part it is used a complex mass μ_P, one should in principle compute the matrix elements with complex momenta; however, for narrow resonances such as the W, Z or H bosons, it is possible to use real kinematical variables after performing an appropriate expansion in Γ_V / M_V.

A simplified variant of the pole scheme is the so-called pole approximation, which consists in taking into account only the resonant part of the amplitude, disregarding the non-resonant contributions: the idea is to use this approximation to get higher-order corrections near the resonance, while the remaining calculations in the off-shell regions are performed at lower accuracy. For example, one can employ the pole approximation to have NLO accuracy in the resonance region and use a LO calculation in the tails of the invariant-mass distribution, with the final result that the inclusive cross sections integrated over the resonance delivers NLO accuracy. This technique has been adopted in different contexts in the literature [198, 210, 215–225] also in comparison with the complex-mass scheme [226]

The pole scheme is present as an alternative option with respect to the CMS in the `Z_ew-BMNNPV` package and can be swicthed on with the flag `PS_scheme 1`.

4.1.4 The factorization scheme

The factorization scheme (FS) is based on the concept of factorising a resonance term on top of a gauge-invariant amplitude. At LO, this can be achieved by multiplying the amplitude with the factor:

$$f_P(p^2) = \frac{p^2 - M_P^2}{p^2 - \mu_P^2} \, , \tag{4.20}$$

from which in the resonance region it is obtained the Breit-Wigner behaviour after setting to zero the non-resonant contributions, and in the off-shell regions the only modification of the amplitude is of order $\mathcal{O}(\Gamma_P/M_P)$, i.e. it is formally at one-loop level [21, 195, 227]. At NLO some issues can be encountered if ones proceeds by simply modifying the LO amplitude with the factor given above, because of spurious terms of $\mathcal{O}(\Gamma_P/M_P)$ that spoil the one-loop accuracy. However, in some cases, like for instance the charged-current Drell-Yan process, the tree-level amplitude gets corrections with the same common resonant structure, without any additional subleading term, and the factorization scheme is applicable as described [85]. For the neutral-current Drell-Yan process, on the other hand, one has also a non-resonant diagram with the photon exchange and some additional problems arise; the FS can all the same be employed for weak corrections, as discussed in [86].

The factorization scheme can be set with the flag `FS_scheme 1`.

<div style="text-align: right; font-size: 3em;">5</div>

Photonic corrections to neutral-current Drell Yan

In this Chapter, we start to present the original numerical results of this work, by examining photonic corrections to the neutral-current Drell-Yan process. After a theoretical introduction on the issues associated to soft and collinear divergences in QED, the attention is focused on the numerical computation of NLO QED contributions due to the emission of photons: subtraction schemes, in particular the FKS one, are discussed, in order to finally introduce the POWHEG method in the case of QED and produce the results of numerical simulations performed with the `Z_ew-BMNNPV` package.

5.1 Real emission effects

As seen when discussing weak corrections in the high-energy regime, the presence of massless gauge bosons both in QED and QCD causes the appearance of infrared singularities due to the exchange of soft and/or collinear massless particles. At the electroweak scale, in particular, soft divergences are connected to the exchange of a gluon or a photon, while collinear singularities arise when a massless particle, that can be a gluon, a photon, or a light fermion in the massless limit, splits into two massless particles in loop diagrams [173]. We have furthermore already discussed that, by virtue of the Bloch-Nordsiek and Kinoshita-Lee-Nauenberg theorems, IR divergences cancel in inclusive observables when summing up the virtual corrections and the contribution from the real emission of massless particles.

We here focus on the QED effects on the relevant distributions of the neutral-current Drell-Yan process. The choice of considering only this subset of corrections can be done since they are separately gauge invariant and UV-finite by virtue of the Ward identities. We start by distinguish these corrections into their soft or collinear origins, and discuss how they are dealt

with in Monte Carlo event generators, at $\mathcal{O}(\alpha)$. In particular, the POWHEG method is briefly sketched in Chap. 5.3. In this context, it can be noted that the inclusion of QED higher-order effects due to multiple photon emissions can be performed with the resummation of leading logarithmic contributions, for instance via a Parton Shower (PS) generator; to avoid the double-counting of effects already included in the NLO computation, one should implement a matching procedure, which essentially consists in the subtraction of the $\mathcal{O}(\alpha)$ expansion of the parton shower and its replacement with the exact $\mathcal{O}(\alpha)$ matrix element. A detailed description is however beyond the scope of this work, which focuses on fixed-order calculations.

5.1.1 Soft contributions

In the soft limit, the $\mathcal{O}(\alpha)$ amplitude with the emission of a soft photon with momentum k can be related to the LO one with the Yennie-Frautschi-Suura approximation [228], in the following way:

$$|\mathcal{M}_1|^2 \sim -J_{eik}^\mu J_{eik,\,\mu}^* |\mathcal{M}_0|^2 = \sum_{n,n'} Q_n \sigma_n Q_{n'} \sigma_{n'} e^2 \frac{p_n \cdot p_{n'}}{(p_n \cdot k)(p_{n'} \cdot k)} |\mathcal{M}_0|^2 \,, \quad (5.1)$$

where the eikonal current has been introduced as:

$$J_{eik}^\mu = -\sum_n Q_n e \sigma_n \frac{p_n^\mu}{p_n \cdot k} \,. \quad (5.2)$$

In this last expression, $Q_n e$ and p_n are the charge and momentum of the particles involved in the process under consideration, and the sign factor σ_n is chosen to be $+1$ if in the process there are an incoming particle and an outgoing antiparticle (in our convention, this happens for initial-state particles), and -1 in the case of an outgoing particle and an incoming antiparticle (for the final state). After performing the integration over the photon phase-space, one gets a logarithmic singularity, which can be regularised by assuming an infinitesimal m_γ mass for the photon and obtaining a term of the kind $\ln(m_\gamma^2/s)$, or by considering dimensional regularisation. These two regularisations schemes can be related as following:

$$\ln m^2 \leftrightarrow \frac{(4\pi\mu^2)^\epsilon}{\epsilon\Gamma(1-\epsilon)} + \mathcal{O}(\epsilon) = \Delta + \ln\mu^2 + \mathcal{O}(\epsilon) \,. \quad (5.3)$$

In the literature, the most common choice for dealing with QED emissions is mass regularization. Soft singularities are cancelled when taking into account both virtual corrections and the corresponding real contribution due to the bremsstrahlung of photons, in agreement with the Bloch-Nordsiek theorem: the dependence on m_γ^2 is cancelled and one can safely restore the limit $m_\gamma \to 0$. In QCD, dimensional regularisation is generally preferred: soft-collinear singularities therefore appear as $1/\epsilon^2$ poles, while single soft or collinear ones are $1/\epsilon$ poles.

5.1. Real emission effects

5.1.2 Collinear contributions

Collinear singularities occur when photons are emitted collinear to massless fermions. In the case of light fermions, where "light" means that their masses are much smaller than the typical energy scale of the hard process, large logarithmic contributions appear. Like soft emissions, also collinear ones can happen either in the final or in the initial state, but, unlike soft emissions, in the case of hard collinear initial-state splittings, the momentum flowing into the hard scattering process is modified. One can thus introduce the QED splittings $P_{ab}(z)$ [229], which represent the probability of finding a parton with flavour a into one with flavour b, as in the figure below:
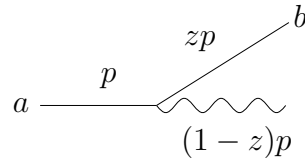
They can be specified in terms of photons and fermions:

$$P_{ff} = \left(\frac{1+z^2}{1-z}\right)_+ \qquad P_{f\gamma} = z^2 + (1-z)^2 \qquad (5.4)$$

$$P_{\gamma f} = \frac{1 + (1+z^2)}{z} \qquad P_{\gamma\gamma} = -\frac{2}{3}\delta(1-z)\,,$$

where the following + prescription has been used to regularise P_{ff}:

$$\int_0^1 dx\, f(x)_+ g(x) = \int_0^1 dx\, f(x)[g(x) - g(1)]\,, \qquad (5.5)$$

with g a generic test function. The variable z is here the fraction of the total longitudinal momentum p carried by parton b. We can for example consider the ff splitting in initial state:
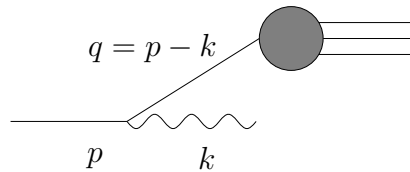
The momentum k can be written as:

$$k = (1-z)p + k_\perp + \xi n\,, \qquad (5.6)$$

where $k_\perp$ is the transverse momentum, n is a vector such as $n^2 = 0$ and $n{\cdot}p \neq 0$ and the factor ξ can be found from on-shell relations. In the collinear limit, i.e. for $p \cdot k \to 0$, the associated cross section reads:

$$\sigma_1 = \frac{\alpha}{2\pi} P_{ff}(z) \frac{dq^2}{q}\, dz\, \sigma_0(zp)\,, \qquad (5.7)$$

where σ_0 is the tree-level cross section of the hard process and depends on zp. The same formula is valid for final-state emissions, upon the replacement $\sigma_0(zp) \to \sigma_0(p)$. When considering collinear-particle exchanges in loops together with real collinear splittings, the singularities arising from the integration of Eq. (5.7) cancel according to the KLN theorem. Some issues however can arise, making it necessary to introduce the separation between initial- and final-state radiation and discuss the problems connected to photonic emissions from initial-state quarks.

5.1.3 Collinear divergences in initial and final states

The neutral-current Drell-Yan process has the property that the initial-state quark current and the final-state leptonic current, being electrically neutral, are separately gauge invariant under $U(1)_{em}$ transformations. It is thus possible to separate the QED initial-state radiation (ISR in the following) from the final-state one (FSR), and one can also define in a gauge-invariant way the initial-final interference (IFI) contribution. The total differential cross section with photonic emission at $\mathcal{O}(\alpha)$ can thus be written as:

$$d\sigma_{q\bar{q},phot.} = d\sigma_{q\bar{q},ISR} \; + \; d\sigma_{q\bar{q},IFI} \; + \; d\sigma_{q\bar{q},FSR} \; . \tag{5.8}$$

The subsets of corrections $d\sigma_{q\bar{q},ISR}$, $d\sigma_{q\bar{q},IFI}$ and $d\sigma_{q\bar{q},FSR}$ are explicitly given in [86]. The separation among the three contributions can be achieved in practice by noticing that the ISR contribution has an overall factor Q_q^2, equal to the electromagnetic charge of the initial-state quarks squared, while the FSR is proportional to Q_ℓ^2, where Q_ℓ is the electromagnetic charge of the final-state leptons, and IFI to $Q_q Q_\ell$. In a numerical code, one can thus isolate the ISR effects by switching Q_ℓ to zero, and the FSR contribution by setting $Q_q = 0$. Finally, the initial-final interference can be computed, for a given observable, by subtracting from the total photonic-emission correction the ISR and FSR terms. In the case of differential cross sections, this means to invert Eq. (5.8):

$$d\sigma_{q\bar{q},IFI} = d\sigma_{q\bar{q},phot.} \; - \; d\sigma_{q\bar{q},ISR} \; - \; d\sigma_{q\bar{q},FSR} \; . \tag{5.9}$$

Having clarified the definitions of ISR, FSR and IFI, we turn to the problem of the cancellation of collinear divergences. For FSR, if the observable under consideration is not fully inclusive, as it is always the case in presence of event-selection cuts, some finite terms of the kind $\ln(m_f^2/s)$ are left. They can become large, thus making it necessary in some cases to know at least the dominant higher-order effects. While leptonic masses constitute a physical cut-off, quarks are usually treated with dimensional regularisation. The IFI contribution, on the other hand, is process dependent and is free of collinear divergences.

Finally, the cancellation of ISR singularities is more delicate, as the kinematical mismatch between virtual and real contributions spoils the validity of the KLN theorem; one is thus left with a collinear divergent cross section,

5.1. Real emission effects

which can be factorised in a process-independent way on top of the leading order. The divergent factor can be reabsorbed into the definition of the initial-state parton densities, denoted in general by $f_q^H(x)$, which can be interpreted as the probability densities to find a parton q with longitudinal momentum fraction x inside the hadron H of momentum K. To be more precise, in the case of collinear initial-state radiation, the parton momentum xK is further reduced by a factor z, and thus the momentum entering the hard process is zxK, which differs from the xK momentum entering the hard process in the case of virtual contributions. The result is that large logarithmic contributions survive. They can however be absorbed into the PDFs, namely they can be regarded as a property of the hadron rather than of the hard scattering process.

The collinear divergences can be proven to be process independent [230], making it possible to introduce a non-physical factorisation scale μ_F to separate the hard process from long-distance collinear contributions included into the PDFs, as it is done in QCD:

$$\sigma_{H_1,H_2}(K_1, K_2) = \sum_{q_1,q_2} \int dx_1 dx_2 \, f_{q_1}^{H_1}(x_1; \mu_F) \, f_{q_2}^{H_2}(x_2; \mu_F) \, \hat{\sigma}_{q_1 q_2}(x_1 K_1, x_2 K_2; \mu_F),$$

(5.10)

Such newly-defined PDFs of course depend on μ_F and satisfy the Dokshitzer-Gribov-Lipatov-Altarelli-Parisi (DGLAP) evolution equations [229, 231, 232] with QED kernels. In the case of neutral-current Drell Yan, this fact has to be taken into account by using photon partonic density functions of the proton, which are regulated by a DGLAP QCD+QED evolution. Also the hard process acquires a dependence on μ_F in such a way that μ_F is cancelled in the calculation of physical observables. In practical cases, however, since the perturbative series is truncated at a fix order, some dependence on the choice of μ_F survives and should be included into the theoretical uncertainties associated with the calculation.

The explicit formulae for the QED splittings can be found for instance in [21] both in dimensional regularisation and using the leptonic masses as regulators. In the `Z_ew-BMNNPV` package, a hybrid scheme is adopted, in which dimensional regularisation is used for quarks and photons, while m_ℓ is used as a physical regulator for leptons.

The inclusion of initial-state collinear divergences into PDFs requires the introduction of the so-called *collinear counterterms* in the hard partonic cross section of Eq. (5.10), which cancel initial-state collinear singularities appearing in the virtual and real contributions to this equation. The hard scattering cross section of Eq. (5.10) is thus written as:

$$\hat{\sigma}_{q_1 q_2} = \hat{\sigma}_{q_1 q_2}^0 + \hat{\sigma}_{q_1 q_2}^{\text{virt}} + \hat{\sigma}_{q_1 q_2}^{\text{real}} + \hat{\sigma}_{q_1 q_2}^{\text{coll. c.t.}}, \tag{5.11}$$

namely it is the sum of the LO contributions plus the virtual and real corrections and the collinear counterterms. Note that to achieve the cancellation of initial state singularities, the coupling α in the counterterms and thus also

81

in the QED PDFs must be the same as the one used in the calculation of electroweak corrections to the matrix element.

From a phenomenological point of view, we will present in Sec. 5.4 the impact of the ISR, FSR and IFI contributions on relevant distributions: from the plots it is possible to conclude that QED FSR yields a large contribution to the invariant-mass distribution of the lepton pair, while QED ISR effects are small, because the large logarithmic contributions due to hard collinear emissions are subtracted and reabsorbed in the definition of the proton PDFs. The initial-final interference is negligible at the Z peak, but it grows in size outside the resonance.

Photon-induced processes

The inclusion of QED effects into the PDFs has the consequence that also a photon distribution function must be considered, opening the possibility of photon-induced processes. In the neutral-current Drell-Yan process one has the $q\gamma$ and $\bar{q}\gamma$ channels, which start to contribute from NLO EW, together with a leading-order channel $\gamma\gamma \to \ell^+\ell^-$, and the associated one-loop virtual corrections to $\gamma\gamma \to \ell^+\ell^-$ and real processes $\gamma\gamma \to \ell^+\ell^-\gamma$ and $\gamma q \to \ell^+\ell^- q$. We refer to [21] for a general discussion on photon-initiated processes. Note that the QED-including PDFs differ compared to the ones computed in QCD only, because the total proton momentum is now shared with an additional parton, i.e. the photon. Since the total momentum carried by the quarks is reduced, compared to the QCD-only case, also the quark-antiquark cross sections are smaller. Thus, photon-induced processes give a contribution to the total cross section that is complementary to the one of the quark-induced channels, besides having the effect of modifying the differential distributions of the final states.

However, as it can be seen for example in [86, 233] the effect of the $\gamma\gamma \to \ell^+\ell^-$ process on the cross section amounts to some % at tree-level, i.e. it is of the same size of the weak corrections to $q\bar{q} \to \ell^+\ell^-$. The one-loop electroweak corrections to $\gamma\gamma \to \ell^+\ell^-$ are negligible. Since $\gamma\gamma \to \ell^+\ell^-$ is a separate process, i.e. it is separately gauge-invariant w.r.t. $q\bar{q} \to \ell^+\ell^-$, in an experimental analysis one could think of independently simulating it and subtracting it from the $q\bar{q}$ events.

Moreover, since the numerical results presented in Sec. 5.4 are obtained by considering only leptonic final states, without additional jets, the contribution of $\gamma q \to \ell^+\ell^- q$ as well as of gluon-induced processes is absent in our simulations. The only modification that the use of QED PDFs could produce is thus related to the NLO DGLAP evolution of the quark PDFs, that is however negligible [234]. For all these reasons, the numerical results in Sec. 5.4 are presented with a set of PDFs that does not include QED corrections, given that similar results would have been obtained otherwise.

5.2 The FKS subtraction scheme

The evaluation of real emissions can be performed numerically, since in presence of phase-space cuts or for not fully-inclusive observables an analytic calculation would be prohibitive. However, the treatment of the infrared divergencies should be carried on analytically, to achieve a proper cancellation of the singularities when including also virtual corrections. This implies that one should combine in the same tool an analytical integration in phase-space regions containing the IR divergences together with a fast numerical evaluation of regular phase-space regions. It is important to notice that, by virtue of the factorization of the squared amplitude in the singular regions, as in Eqs. (5.1) and (5.7), the analytical integration can be carried out in a process-independent way. In the literature, both *slicing* and *subtraction* methods have been discussed to this aim. Here however we focus on the second approach, which can count a number of NLO variants both in QCD [235–241] and QED [242–246]: the two most used implementations are the Catani-Seymour (CS) [236, 237] and the Frixione-Kunszt-Signer (FKS) [235] subtractions, the latter employed in the POWHEG-BOX code for QCD emissions [247–249]. Since in the `Z_ew-BMNNPV` code electroweak radiation is dealt with the FKS method [101–103, 250], we will mainly focus on this one at $\mathcal{O}(\alpha)$, having in particular in mind the (unpolarized) neutral-current Drell-Yan process.

The basic idea of subtraction techniques [251, 252] is to add and subtract an auxiliary function $|\mathcal{M}_{sub}|^2$ to the original singular real-emission integrand $|\mathcal{M}_1|^2$, in such a way that, in the expression:

$$\int d\Phi_{n+1}|\mathcal{M}_1|^2 = \int d\Phi_{n+1}\left(|\mathcal{M}_1|^2 - |\mathcal{M}_{sub}|^2\right) + \int d\Phi_{n+1}|\mathcal{M}_{sub}|^2, \quad (5.12)$$

the first integral is regular and can be done numerically in all phase space, while the remaining term is evaluated analytically. Thus $|\mathcal{M}_{sub}|^2$ should be a simple function with the property of displaying the same behaviour of $|\mathcal{M}_1|^2$ in the singular regions, namely:

$$|\mathcal{M}_{sub}|^2 \sim |\mathcal{M}_1|^2 \quad \text{for} \quad k^2 \to 0, \quad p_i \cdot k \to 0, \quad p_f \cdot k \to 0, \quad (5.13)$$

where k, p_i and p_f are the momenta of the radiated photon, the initial-state and the final-state fermion, respectively. Combining the last integral of Eq. (5.12) to the virtual corrections is not trivial, since the virtual contributions are integrated over the tree-level phase space $d\Phi_n$. It is thus crucial to define a mapping:

$$d\Phi_{n+1} \to d\bar{\Phi}_n \cdot d\Phi_{rad}, \quad (5.14)$$

where $\bar{\Phi}_n$ is the phase space of the non-radiating process, which can differ from Φ_n because for instance in the case of initial-state radiation the momenta entering the hard process have to be rescaled, and Φ_{rad} is the phase space of the emitted particle, which has to be appropriately parametrised. The jacobian associated to this mapping is included into the definition of $d\Phi_{rad}$. In

the literature, $\bar{\bar{\Phi}}_n$ is called *underlying Born configuration*, and is obtained as follows:

- in the case of a soft singularity, one should eliminate the soft parton;

- in the final-state collinear region, one replaces the two collinear particles with their parent particle carrying a momentum that is equal to the sum of their momenta;

- for initial-state collinear divergences, one deletes the collinear emitted particle and assigns to the radiating parton its momentum fraction after radiation.

The mapping in Eq. (5.14) is defined in an infrared- and collinear-safe manner, and modifies the momenta of the particles in such a way that momentum conservation is preserved. We can thus write:

$$\int d\Phi_{n+1}|\mathcal{M}_1|^2 = \int d\Phi_{n+1}\left(|\mathcal{M}_1|^2 - |\mathcal{M}_{sub}|^2\right) + \int d\bar{\bar{\Phi}}_n \cdot \int d\Phi_{rad}|\mathcal{M}_{sub}|^2,$$
(5.15)

where the integration $\int d\Phi_{rad}|\mathcal{M}_{sub}|^2$ can be performed analytically and then the last term can be combined with the virtual corrections.

Singular regions in Eq. (5.13) overlap, and thus one cannot proceed to naively sum them when defining the subtraction function, because that would imply a double-counting of the singular contributions. In the FKS approach, this is handled in the following way. First of all we write the cross section for the process $q_1 q_2 \to \ell_3 \ell_4$, in the factorised form:

$$\sigma_{H_1,H_2}(K_1, K_2) = \sum_{q_1,q_2} \int dx_1 dx_2 d\, f_{q_1}^{H_1}(x_1)\, f_{q_2}^{H_2}(x_2)\, \hat{\sigma}_{q_1 q_2}(x_1 K_1, x_2 K_2),$$
(5.16)

where $\hat{\sigma}_{q_1 q_2}$ is the subtracted partonic cross section, in which the collinear initial-state emissions, already included in the parton distribution functions $f_{q_1}^{H_1}(x_1)$ and $f_{q_2}^{H_2}(x_2)$, have been cancelled by the collinear counterterms. The PDFs $f_{q_1}^{H_1}(x_1)$ and $f_{q_2}^{H_2}(x_2)$ quantify the probability of extracting a parton $q_{1(2)}$ with a longitudinal momentum fraction $x_{1(2)}$ from hadron $H_{1(2)}$. To be precise, $\hat{\sigma}_{q_1 q_2}$ can be written as:

$$\begin{aligned}
\hat{\sigma}_{q_1 q_2}(x_1 K_1, x_2 K_2) &= \int d\Phi_n\left[B(\Phi_n) + V_b(\Phi_n)\right] + \int d\Phi_{n+1} R(\Phi_{n+1}) \\
&+ \int d\Phi_{n,1}\, G_{1,b}(\Phi_{n,1}) + \int d\Phi_{n,2}\, G_{2,b}(\Phi_{n,2}),
\end{aligned}$$
(5.17)

where in the right hand side the dependence on the parton flavours q_1, q_2 is implicit. We have denoted with B the born matrix element integrated over the phase space $d\Phi_n$, where in our case $n = 4$; R is the real-emission one, which has to be integrated over $d\Phi_{n+1}$, and V_b is the virtual contribution, where the

5.2. The FKS subtraction scheme

renormalization of UV divergences has been understood, while IR singularities still survive (hence the subscript "b"). The collinear counterterms $G_{1,b}(\Phi_{n,1})$ and $G_{2,b}(\Phi_{n,2})$ account for the fact that initial-state collinear singularities are already included into the PDFs $f_{q_1}^{H_1}(x_1)$ and $f_{q_2}^{H_2}(x_2)$. To keep in mind that the counterterms contain collinear singular contributions, we have added to them the subscript "b". The divergences in V_b and $G_{1(2),b}(\Phi_{n,1(2)})$ are cancelled against the corresponding contributions in R, after integrating the latter over the radiation phase space. The counterterms are integrated over the n-particle phase spaces $d\Phi_{n,1}$ and $d\Phi_{n,2}$, which differ from $d\Phi_n$ because the momentum of the 1(2) parton entering the hard process is not $k_{1(2)} = x_{1(2)}K_{1(2)}$, but has to be rescaled to $zk_{1(2)}$, namely the substitution $x_{1(2)} \to zx_{1(2)}$ has to be made in the phase space as well as in the argument of the PDFs. In other words, $d\Phi_{n,1(2)}$ are defined as:

$$d\Phi_{n,1(2)} = d\bar{\Phi}_n \frac{dz}{z} \,. \tag{5.18}$$

We report here the final result of the subtraction procedure, which is illustrated in [248]:

$$
\begin{aligned}
\hat{\sigma}_{q_1 q_2}(x_1 K_1, x_2 K_2) &= \int d\Phi_n \left[B(\Phi_n) + V(\Phi_n) \right] + \int d\Phi_{n+1} \hat{R}(\Phi_{n+1}) \\
&\quad + \int d\Phi_{n,1} \, G_1(\Phi_{n,1}) + \int d\Phi_{n,2} \, G_2(\Phi_{n,2}) \,, \quad (5.19)
\end{aligned}
$$

where $\hat{R}(\Phi_{n+1})$ has been obtained from $R(\Phi_{n+1})$ by assuming, for every emitted particle i, a parametrisation of the singular region associated to i in terms of the variables:

$$\xi = \frac{2k_i^0}{\sqrt{s}} \,, \quad y = \cos\theta \,, \quad \phi \,, \tag{5.20}$$

which are connected to its energy k_i^0, to the angle θ between i and a reference direction and to the azimuthal angle ϕ. With this parametrisation it is possible to isolate the singular contributions in $R(\Phi_{n+1})$, integrating them on the radiation phase space and then combining them to V_b and to the collinear counterterms $G_{1(2),b}$ to get the finite quantities V and $G_{1(2)}$. The remaining term $\hat{R}(\Phi_{n+1})$ is regular and can be integrated numerically.

To proceed with the FKS subtraction, one introduces some non-negative functions to partition the $n+1$ phase space in such a way that the real contribution can be written as a sum of terms containing at most one collinear and one soft singularity associated with one particle. In particular, for every final-state particle i we can define the function S_i to describe the region where i becomes soft/collinear to some initial-state parton, and the function S_{ij} for the region where i becomes soft/collinear to some final-state particle j. We have:

$$\sum_{i=1}^{n+1} S_i + \sum_{i,j=1,\, i\neq j}^{n+1} S_{ij} = 1 \,, \tag{5.21}$$

and also the properties listed in Eqs. (2.58)–(2.61) of [248], which can be summarised by saying that, if particle m becomes soft, only the terms S_m and S_{mj} survive in the sum, if m is collinear to an initial-state parton we have only the term S_m and if m is collinear to the final-state particle j the only non-vanishing terms are S_{mj} and S_{jm}. The functions S_i and S_{ij} can be chosen to be smooth, i.e. easy to implement numerically, as described in [248]. One can thus decompose the $n+1$ phase space and project the real corrections into singular regions, as:

$$\hat{R} = \sum_{i=1}^{n+1} \hat{R}_i + \sum_{i,j=1,\,i\neq j}^{n+1} \hat{R}_{ij}\,, \quad \hat{R}_i = S_i \hat{R}\,, \quad \hat{R}_{ij} = S_{ij} \hat{R}\,, \qquad (5.22)$$

where $\hat{R}_i$ corresponds to regions where R_i is divergent because particle i becomes soft and/or collinear to an initial-state parton and $\hat{R}_{ij}$ is connected to the singularities of R_{ij} where i is soft and/or collinear to a final-state particle j. In all other regions, R_i and R_{ij} are finite. For each term in the sum, one then has to choose a parametrisation of the $n+1$ phase space in terms of an n phase space times the radiation phase space, which is described in terms of the energy of particle i (associated to soft singularities), and the angle between i and one of the initial-state partons θ_i (related to initial-state collinear singularities) for $\hat{R}_i$, and in terms of the energy of particle i and the angle betwen i and a final-state particle j, θ_{ij} (associated to final-state collinear singularities), for $\hat{R}_{ij}$. The variables used are thus:

$$\xi_i = \frac{2k_i^0}{\sqrt{s}}\,, \quad y_i = \cos\theta_i\,, \quad y_{ij} = \cos\theta_{ij}\,, \qquad (5.23)$$

with which one defines two independent functional forms for the initial-state- and final-state-emission phase spaces.

For the electroweak radiation we are interested here, the subtraction formulae are the same as in the case of the QCD fermion-fermion-gluon vertex, upon the replacements $\alpha_S \to \alpha$ and $C_F \to Q_n Q_{n'}$ where $Q_{n(n')}$ is the charge of particle $n(n')$ as in Eq. (5.1). The virtual contribution V of Eq. (5.17) is given in Eqs. (3.3)–(3.7) of [101], while the collinear counterterms $G_{1(2)}$ can be written as in Eq. (2.102) of [248] provided that one makes the relevant substitutions for the electroweak sector.

5.3 The POWHEG method

In the definition of inclusive quantities, collinear and soft divergences are cancelled by summing over degenerate final states. However, in many phenomenological or experimental cases one is interested in studying exclusive observables, rather than inclusive ones, and therefore a framework is needed to resum the large logarithms stemming from imperfect cancellations of infrared singularities. To this aim, one can employ Shower Monte Carlo (SMC) programs, which

5.3. The POWHEG method

provide fully differential information on all emitted particles. In a full simulation, one thus needs to match the fixed-order calculation, which is here at NLO, to the tower of emissions from the shower. The ideal NLO+PS matching algorithm is such that the final cross section has the following properties:

- it coincides with the NLO calculation (eventually up to NNLO terms) in the limit where the transverse momentum of the emitted particle w.r.t. the radiating one, k_T, is large;

- it reproduces correctly the value of infrared-safe observables at NLO;

- for small k_T its behaviour is like the one of standard SMC generators.

Parton showers are present in many tools in the literature: multi-purpose event generators, like Herwig [253, 254], PYTHIA [255] and Sherpa [256, 257], use QED showers to take into account photon emission radiation, while Photos [258, 259] provides a standalone QED parton shower that can be matched to any Monte Carlo program. Other examples are the Monte Carlo generators Horace [91, 93, 260, 261], KKMC-hh [99] and WINHAC/ZINHAC [94], that feature a QED resummation for specific processes, like for instance Drell-Yan processes. In the context of Higgs physics, we mention the code in [262], which includes QED corrections matched to a parton shower for Higgs+2 jets in the POWHEG framework.

There exist two main approaches to address the issue of matching NLO fixed-order calculations to a shower program. The `MC@NLO` one consists in subtracting the approximated NLO expansion of the SMC implementation from the exact NLO result [263]. However, from this subtraction negative weights could arise. The POWHEG (Positive Weight Hardest Emission Generator) method, on the other hand, guarantees that the hardest emission of radiation is generated first, in such a way that only positive-weighted events are obtained from exact NLO matrix elements [247–249]. A great advantage of this technique is that it is necessary to correct only the first emission at NLO with a modified Sudakov form factor, a procedure that can be demonstrated to be equivalent to the use of a vetoed shower [247]. In this way, all modifications act on the fixed-order computation without touching the SMC structure, that is only required to generate radiation softer than the NLO emission, i.e. with a veto on k_T. The POWHEG method can be interfaced to showers which make use of the transverse momentum of the emitted radiation as ordering variable, as well as to those featuring an angular ordering. In this last case, truncated vetoed shower should be added, to account for the large-angle and soft coherent radiation coming from the particles generated by the hardest splitting.

We report here the master formula of the POWHEG method, originally

formulated for QCD radiation, and generalised to photon emission in [101]:

$$d\hat{\sigma} = \bar{B}(\Phi_n)d\Phi_n \left[\Delta(\Phi_n, p_T^{min}) + \Delta\left(\Phi_n, k_T(\Phi_{n+1})\right) \frac{R(\Phi_{n+1})}{B(\Phi_n)} d\Phi_{rad} \right]_{\bar{\Phi}_n = \Phi_n} ,$$
(5.24)

with the Sudakov form factor:

$$\Delta(\Phi_n, p_T) = \exp\left\{ -\int d\Phi_{rad} \frac{R(\Phi_{n+1})}{B(\Phi_n)} \theta(k_T(\Phi_{n+1}) - p_T) \right\}_{\bar{\Phi}_n = \Phi_n} , \qquad (5.25)$$

which describes the probability of non emission of a particle with transverse momentum larger than p_T, and the function:

$$\bar{B}(\Phi_n) = B(\Phi_n) + V(\Phi_n) + \int d\Phi_{rad} \left[\hat{R}(\Phi_{n+1}) \right]_{\bar{\Phi}_n = \Phi_n} \qquad (5.26)$$
$$+ \int \frac{dz}{z} \left[G_1(\Phi_{n,1}) + G_2(\Phi_{n,2}) \right]_{\bar{\Phi}_n = \Phi_n} .$$

In all these equation, the $n + 1$ phase space is considered to be mapped according to Eq. (5.14) into the n phase space Φ_n times the radiation one, within a specific subtraction scheme like the FKS one. The term $\bar{B}(\Phi_n)$ is positive, since in the perturbative approach NLO corrections are smaller than the Born cross section, thus overcoming the problem of negative-weighted events. $\bar{B}(\Phi_n)$ is thus the probability with which the Born configuration is generated.

Eq. (5.24) describes how the hardest radiation is generated within the NLO computation. The first term in the squared bracket accounts for the no-emission case, i.e. describes the probability of not emitting any particle with transverse momentum above the minimum cut p_T^{min}. The second term represents the probability of emission of the hardest event, and is weighted by the factor $R(\Phi_{n+1})/B(\Phi_n)$, which is a generalisation of the Altarelli-Parisi splitting function, in the sense that it incorporates also the finite terms of the real matrix element and reduces to the Altarelli-Parisi splitting in the collinear limit. The function $k_T(\Phi_{n+1})$, which depends on the $n + 1$ phase space, in the singular limit becomes the transverse momentum of the emitted particle with respect to the radiating one, according to the mapping of Eq. (5.14); in all phase space it is assumed that $k_T(\Phi_{n+1}) > p_T^{min}$, where p_T^{min} is the minimum cut on the transverse momentum.

In the case of multiple emissions, the Sudakov form factor becomes a product of form factors defined in different singular regions arising from the partition of the real contribution. For each singular region, the suitable mapping of Eq. (5.14) has to be introduced. Moreover, particular attention has to be paid to preserve the flavour structure of the underlying Born configuration in the mapping of Eq. (5.14), where the flavour structure is defined by the flavours of the tree-level initial- and final-state particles.

Input parameter	Value	Input parameter	Value
α_0	$7.297353 \cdot 10^{-3}$	G_μ	$1.166389 \cdot 10^{-5}$
M_Z	91.1876	Γ_Z	2.4952
M_W	80.385	Γ_W	2.085
M_H	125	m_{top}	173
m_e	$0.51099907 \cdot 10^{-3}$	m_μ	0.1056583
m_τ	1.77705	m_b	4.7
m_u	0.06983	m_d	0.06984
m_s	0.15	m_c	1.2
Masses and widths are expressed in GeV			

Table 5.1: Input parameters for the simulation of QED corrections at NLO.

5.4 Numerical results

We present here numerical results relative to the fixed-order computation of the Drell-Yan amplitude of the process $q\bar{q} \to \mu^+\mu^-$, with photonic virtual and real corrections at $\mathcal{O}(\alpha)$, obtained with the Z_ew-BMNNPV package of the Monte Carlo code POWHEG-BOX-V2. Only photonic NLO corrections are switched on in the code, with LO accuracy for the weak and strong part. The code runs at $\sqrt{s} = 8$ TeV, which is a typical centre-of-mass energy for the LHC. The numerical setup for the simulation parameters is summarised in Table 5.1, while we use the default options for the treatment of the hadronic contributions to $\Delta\alpha$ and the conversion to pole masses and widths. No cuts are imposed on the final states except for the requirement of a minimum invariant mass of 50 GeV. The (α_0, M_W, M_Z) scheme is employed for the electroweak sector and the complex-mass scheme has been chosen for the treatment of the resonance. The PDF set used is the MSTW 2008 NLO one identified as MSTW2008nlo68cl [148] provided by the LHAPDF-6.2 framework [264]. The choice of a set of PDFs that does not include QED corrections has been justified in Sec. 5.1.3.

The factorisation scheme employed for the treatment of QED corrections is the $\overline{MS}$, with factorisation scale set to the leptonic invariant mass $M_{\ell\bar{\ell}}$. Different choices of the factorisation scale would have an impact on distributions, as we will comment in the following. The separation between initial- and final-state radiation is currently performed by a private version of the Z_ew-BMNNPV code and it is obtained as described in Sec. 5.1.3. The differential observables we are taking into account are the invariant-mass distribution and the forward-backward asymmetry.

To have an idea of the shape of the differential cross section, we present in Fig. 5.1 the invariant-mass distribution at LO accuracy within the (α_0, M_W, M_Z) scheme, while Fig. 5.2 shows the effect of the $\mathcal{O}(\alpha)$ photonic corrections relative to the LO, in the invariant-mass range between 50 GeV and 150 GeV. It can be seen that the FSR contribution (in red) is responsible for the most
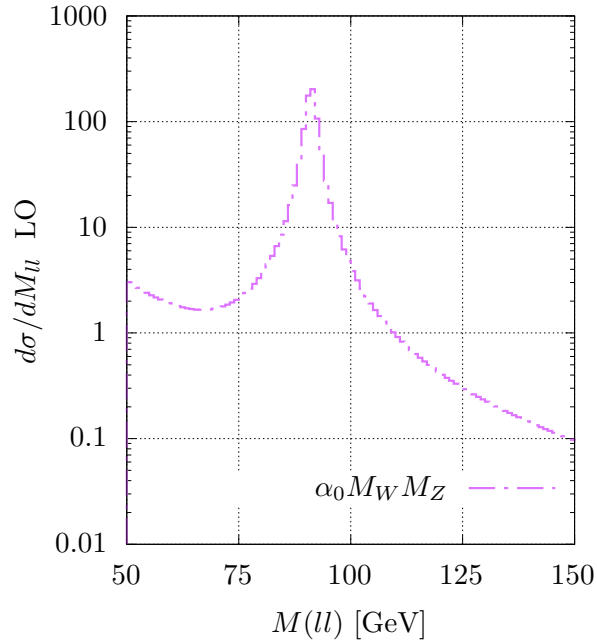
Figure 5.1: LO differential cross section as a function of the dilepton invariant mass in the (α_0, M_W, M_Z) scheme.
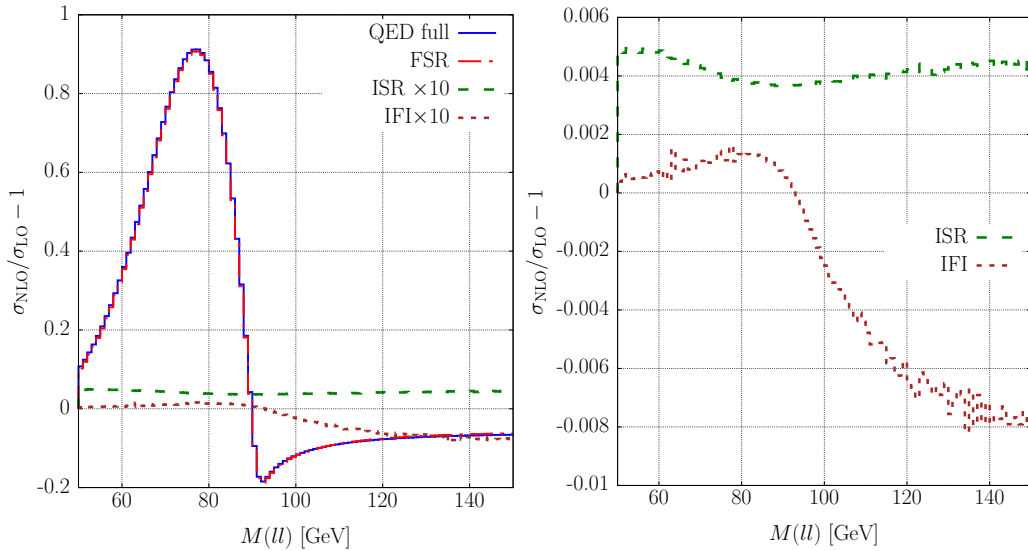

Figure 5.2: Relative correction with respect to the LO cross section as given by the $\mathcal{O}(\alpha)$ total photonic correction (labelled "QED full"), as well as the separate contributions of ISR, FSR and IFI. A zoom on ISR and IFI corrections is provided on the right.

part of the total photonic correction (in blue), varying from 15% at 50 GeV up to a maximum of 90% w.r.t. the LO around 80 GeV, then changing sign

5.4. Numerical results
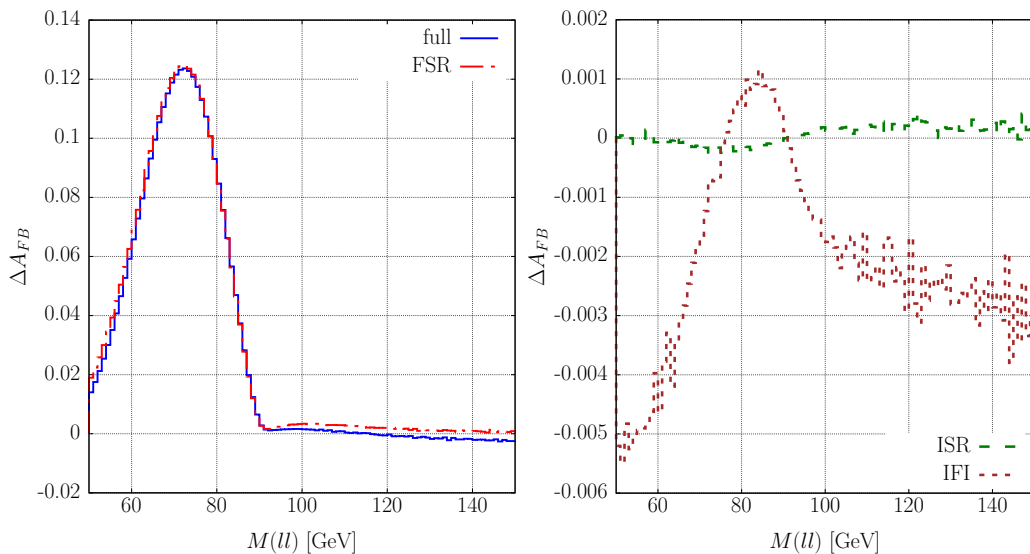
Figure 5.3: Absolute correction with respect to the LO asymmetry. In the left panel one has the $\mathcal{O}(\alpha)$ total photonic (blue) and the FSR (red) corrections, while on the right the ISR (green dashed line) and IFI (brown dotted line) contributions are showed.

to arrive to account almost 15% in absolute value. It is clear the effect of the radiative return, which shifts the bulk of events that at LO are produced at the Z peak towards lower energies. The contribution of ISR (green dashed line) is very small, as the large logarithms arising from collinear divergences are subtracted by the collinear counterterms. Also initial-final interference (brown dotted line) gives a small effect: it amounts to 1 per mille near the peak and rises in absolute value at larger invariant masses, remaining always below 1%. The zoom on the right allows to better quantify the ISR and IFI contributions.

Fig. 5.3 is the analogue of Fig. 5.2 for the forward-backward asymmetry distribution. The IFI contribution is here defined as:

$$A_{\mathrm{FB}}^{\mathrm{IFI}} = \frac{(\sigma_F - \sigma_B)^{\mathrm{NLO}} - (\sigma_F - \sigma_B)^{\mathrm{ISR}} - (\sigma_F - \sigma_B)^{\mathrm{FSR}} + 2\,(\sigma_F - \sigma_B)^{\mathrm{LO}}}{(\sigma_F + \sigma_B)^{\mathrm{NLO}} - (\sigma_F + \sigma_B)^{\mathrm{ISR}} - (\sigma_F + \sigma_B)^{\mathrm{FSR}} + 2\,(\sigma_F + \sigma_B)^{\mathrm{LO}}}\,, \tag{5.27}$$

where the "NLO" label refers to the total photonic $\mathcal{O}(\alpha)$ correction. The LO term has to be added two times to compensate for the fact that it is included in the ISR and FSR contributions, which are subtracted from the NLO.

Note that for the asymmetry we show the absolute difference between the NLO asymmetry and the leading-order one. As in the case of the cross section, the largest contribution is given by the FSR (in red on the left panel), which ranges from 2% at 50 GeV up to a maximum of more than 12% around 70 GeV and then becoming much smaller for higher invariant masses. In the left panel, the blue line represents the total NLO QED contribution, which as it can be seen is dominated by the FSR. In the right panel, the ISR effect (green dashed

Figure 5.4: Diagrammatic picture of the dynamic choice of μ_F, which is equal to the invariant mass of the dilepton system computed with the underlying-Born momenta.
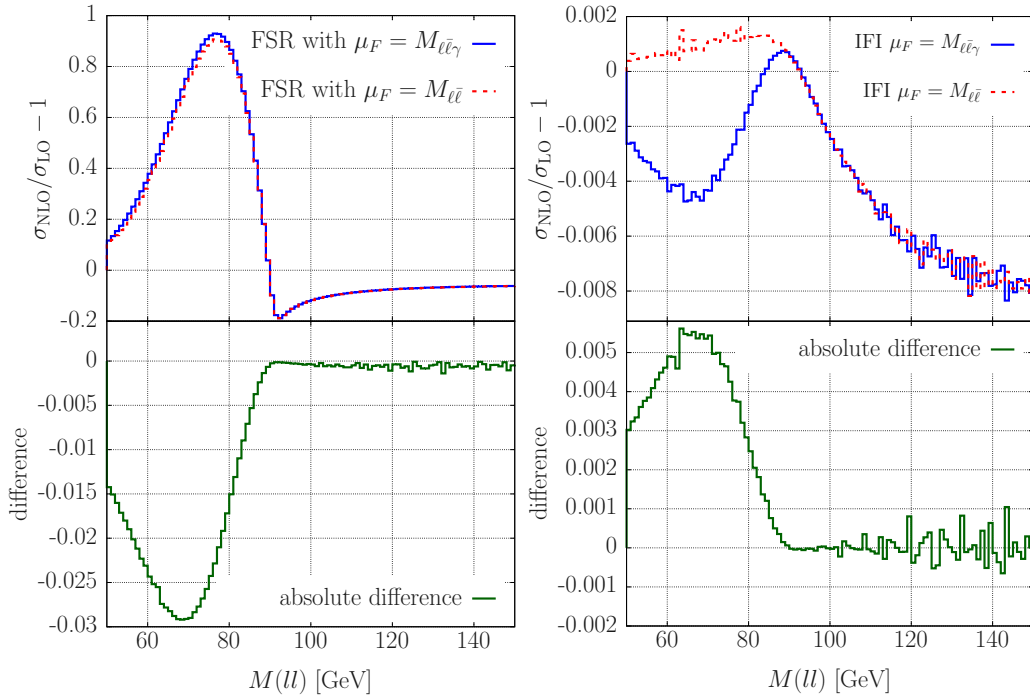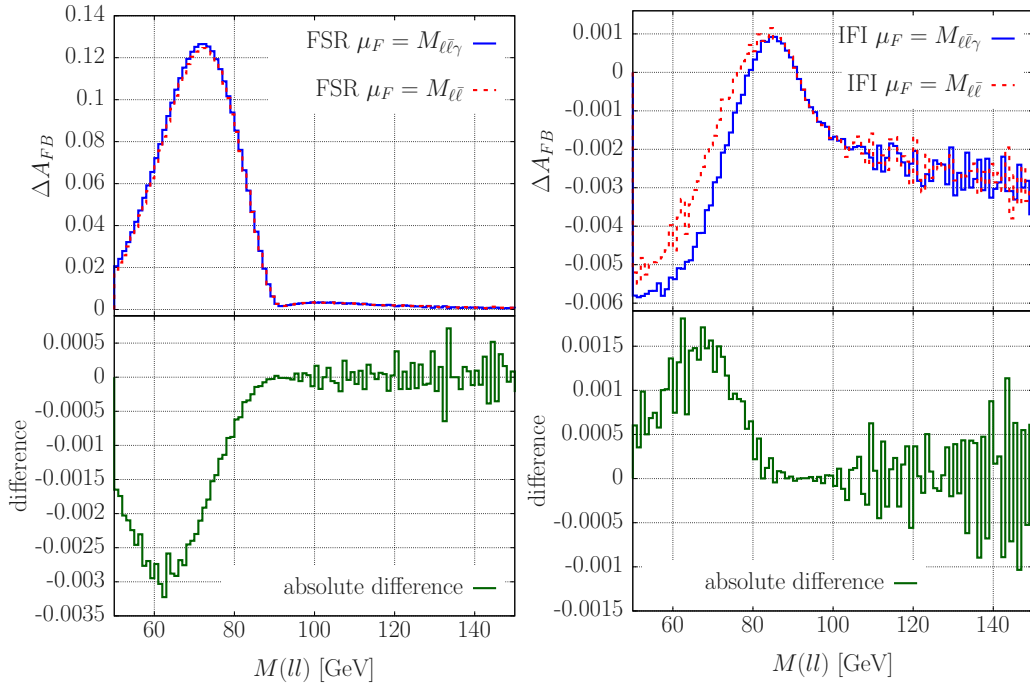

Figure 5.5: Effect of the choice $\mu_F = M_{\ell\bar{\ell}}$ with respect to the $\mu_F = M_{\ell\bar{\ell}\gamma}$ one for the FSR (left) and IFI (right) contributions to the invariant-mass distribution. The lower panels show the difference between the red and blue curves, as explained in the text.

line) is in practice negligible, while the IFI amounts to a maximum of 5 per mille in absolute value at 50 GeV, is minimum in the resonance region and then grows in size as one moves to higher invariant masses.

We now turn our attention to discuss the choice of the factorisation scale μ_F, which in the code is taken to be the same for both QED and QCD. Moreover, we set $\mu_F = \mu_R$, with μ_R the renormalisation scale. The results presented so far are obtained with $\mu_F = M_{\ell\bar{\ell}}$, where $M_{\ell\bar{\ell}}$ denotes the invariant mass of the final-state leptons taken as bare, i.e. without photon recombination. Other options are however possible: for example, one could choose to compute μ_F

5.4. Numerical results

Figure 5.6: Effect of the choice $\mu_F = M_{\ell\bar{\ell}}$ with respect to the $\mu_F = M_{\ell\bar{\ell}\gamma}$ one for the FSR (left) and IFI (right) contributions to the asymmetry distribution. The lower panels show the difference between the red and blue curves, as explained in the text.

as the leptonic invariant mass obtained with the underlying-Born momenta. This option ensures infrared safety, as $\mu_F = p^2$, where p^2 is the momentum flowing into the vector-boson propagator. In other words, this means that for initial-state radiation μ_F coincides with $M_{\ell\bar{\ell}}$, i.e. $\mu_F = M_{\ell\bar{\ell}}$, while for FSR is it equal to the invariant mass of the system $\ell\bar{\ell}\gamma$, i.e. $\mu_F = M_{\ell\bar{\ell}\gamma}$. This is sketched in the diagrams of Fig. 5.4. Thus, a different selection of μ_F leaves the correction due to ISR unchanged, but modified both FSR and IFI, and thus the total NLO photonic contribution.

Fig. 5.5 shows the effect of the choice of μ_F on the invariant mass distribution. In all plots in the following, red curves refer to the $\mathcal{O}(\alpha)$ distributions obtained with the dynamical option and blue ones to $\mu_F = M_{\ell\bar{\ell}}$ computed with bare-lepton momenta, normalised to the leading order. In the bottom panel of each figure the green line is the absolute difference, again normalised to the leading order:

$$\text{diff} = \frac{(\text{option with } \mu_F = M_{\ell\bar{\ell}}) - (\text{option with } \mu_F = M_{\ell\bar{\ell}\gamma})}{\text{LO}} . \qquad (5.28)$$

On the left of Fig. 5.5 we have the effect on the FSR distribution. To a good approximation the figure is the same for the total NLO photonic correction. We can see that choosing $\mu_F = M_{\ell\bar{\ell}\gamma}$ instead of $\mu_F = M_{\ell\bar{\ell}}$ changes the distribution

especially in the low-energy region, up to almost 3% with respect to the LO. The right panel, on the other hand, shows the effect on the IFI, which amounts to a maximum of 5 per mille of the LO for low invariant masses. In the region above the resonance, selecting one option instead of the other does not significantly modify the distributions.

In Fig. 5.6 the effect of the choice of the factorisation scale is examined for the forward-backward asymmetry distribution. Similarly to what happens for the cross section, the distributions undergo a significant modification only for low values of the invariant mass. The FSR contribution, in the left panel, is changed by at most 3 per mille in absolute value, while the effect on the IFI correction, on the right, amounts to a maximum of 1.5‰.

A remark is however in order here. The dependence of the observables on the choice of the factorisation scale is due to the fact that our computation is performed at fixed-order: in principle, μ_F is not a physical parameter and no measurable quantity would depend on it. The dependence on μ_F appearing here is mainly a QCD issue, even if it manifests itself also on QED corrections: it is due to the fact that the numerical results are taken at LO QCD, and thus no collinear counterterms are included, to compensate for the μ_F dependence of the PDFs. As such, this effect would be mitigated when including more orders in α_S.

6

Numerical results on weak corrections

W e here study the numerical impact of the weak corrections on differential observables like the invariant-mass distribution and the forward-backward asymmetry of the neutral-current Drell-Yan process at LHC energies: we examine the range from 50 to 200 GeV and the high-energy region at $1 - 3.5$ TeV.

6.1 Numerical setup and first results

We consider the process $q\bar{q} \to \mu^+\mu^-$, with $\sqrt{s} = 13$ TeV, and no cuts on final-state muons except for the invariant mass cut $M_{\ell\bar{\ell}} \geq 50$ GeV. The numerical values of the input parameters are listed in Table 6.1, while we use the default options for the treatment of higher orders, the hadronic contributions to $\Delta\alpha$ and the conversion to pole masses and widths. The scheme employed to handle the resonance, if not differently specified, is the complex mass. We remind the reader that the input values for M_V and Γ_V, with $V = Z, W$, are the on-shell ones, which are then internally converted to the corresponding pole values, used for the matrix element calculations.

Input parameter	Value	Input parameter	Value
α_0	1/137.0359909956391	G_μ	$1.1663787 \cdot 10^{-5}$
$\alpha(M_Z^2)$	1/128.93	$\sin^2 \theta_{eff}^\ell$	0.23154
M_Z	91.1876	Γ_Z	2.4952
M_W	80.385	Γ_W	2.085
M_H	125	m_{top}	173
m_e	$0.51099907 \cdot 10^{-3}$	m_μ	0.1056583
m_τ	1.77705	m_b	4.7
m_u	0.06983	m_d	0.06984
m_s	0.15	m_c	1.2
Masses and widths are expressed in GeV			

Table 6.1: Input parameters for the simulation of weak corrections at NLO.
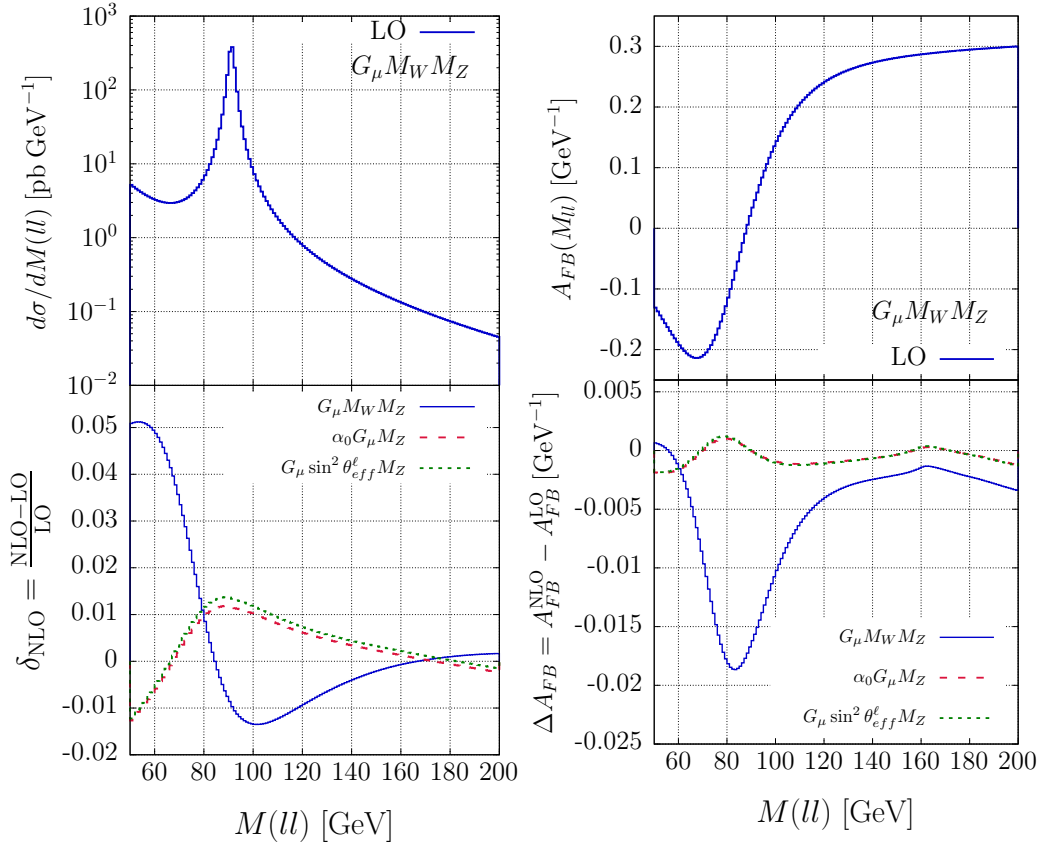
Figure 6.1: Upper panels: LO distributions of the differential cross section (left) and A_{FB} (right) as functions of $M_{\ell\bar{\ell}}$ in the (G_μ, M_W, M_Z) scheme. Lower panels: NLO corrections w.r.t. the LO for the differential cross section (left) and A_{FB} (right) in three input schemes: (G_μ, M_W, M_Z) (solid blue line), (α_0, G_μ, M_Z) (dashed red line) and $(G_\mu, \sin^2 \theta_{eff}^\ell, M_Z)$ (dotted green line).

The PDFs set used is the `NNPDF31_nlo_as_0118_luxqed` one [234, 265,

6.2. Higher order effects

266], where we set the factorization scale to the invariant mass of the dilepton system.

The upper panels of Fig. 6.1 show the leading-order distributions of the differential cross section (on the left) and A_{FB} (on the right) as functions of the leptonic invariant mass $M_{\ell\bar\ell}$ between 50 GeV and 200 GeV and with no additional kinematical cuts on the leptons. The electroweak scheme that has here been chosen as the reference is the (G_μ, M_W, M_Z) one.

In the lower panel on the left one can see the NLO relative correction to $d\sigma/dM_{\ell\bar\ell}$ w.r.t. the LO prediction, for three input schemes: (G_μ, M_W, M_Z) (solid blue line), (α_0, G_μ, M_Z) with enabled option `azinscheme4` (dashed red line) and $(G_\mu, \sin^2\theta_{eff}^\ell, M_Z)$ (dotted green line). The schemes $(G_\mu, \sin^2\theta_{eff}^\ell, M_Z)$ and (α_0, G_μ, M_Z) present corrections with similar shape and size, between -1% and about $+1\%$. The correction in the (G_μ, M_W, M_Z), on the other hand, is characterised by a different shape, with the correction varying from $+5\%$ at 50 GeV to -1% around 100 GeV. These behaviours can be explained by noticing that, in all three schemes, the NLO matrix element is written formally in the same way in terms of δZ_e and δs_w^2, the only difference being the effective expression of the counterterms and the numerical value of s_w^2. One can thus split the NLO matrix element into the one-loop amplitude of the scheme $(G_\mu, \sin^2\theta_{eff}^\ell, M_Z)$ plus a term that takes into account the fact that the LO matrix element is written as a function of a numerically different $s_w^2 \neq s_{eff}^2$, as explained in [105].

In the lower panel on the right it is presented the NLO correction to the asymmetry, defined as the absolute difference w.r.t. the LO. As in the case of the cross section, the NLO corrections in the schemes $(G_\mu, \sin^2\theta_{eff}^\ell, M_Z)$ (dotted green line) and (α_0, G_μ, M_Z) (dashed red line) display similar shapes and sizes: as pointed out in [53], the corrections to the asymmetry are rather small, counting up to 0.002. In the (G_μ, M_W, M_Z) scheme, on the other hand, the corrections are larger, reaching a maximum (in absolute value) of -0.018 at about 80 GeV.

6.2   Higher order effects

We proceed here to show the effects of including the higher-order universal corrections on the cross section and asymmetry distributions.

Fig. 6.2 shows the impact of higher orders on the invariant-mass distribution on the left and on the forward-backward asymmetry on the right, in the three renormalization schemes (G_μ, M_W, M_Z), (α_0, G_μ, M_Z) with `azinscheme4` on and $(G_\mu, \sin^2\theta_{eff}^\ell, M_Z)$. The higher-order corrections in these plots are obtained by including $\Delta\rho$ as in Eq. (3.19). The usual convention of displaying the relative corrections, normalised to the LO, for the cross section and the absolute correction for $A_{FB}(M_{\ell\bar\ell})$, is adopted. For the cross section, when the effective leptonic weak mixing angle is in input, as expected, one gets the smallest correction, of the order of -2 per mille, while in the (α_0, G_μ, M_Z) the effect is zero
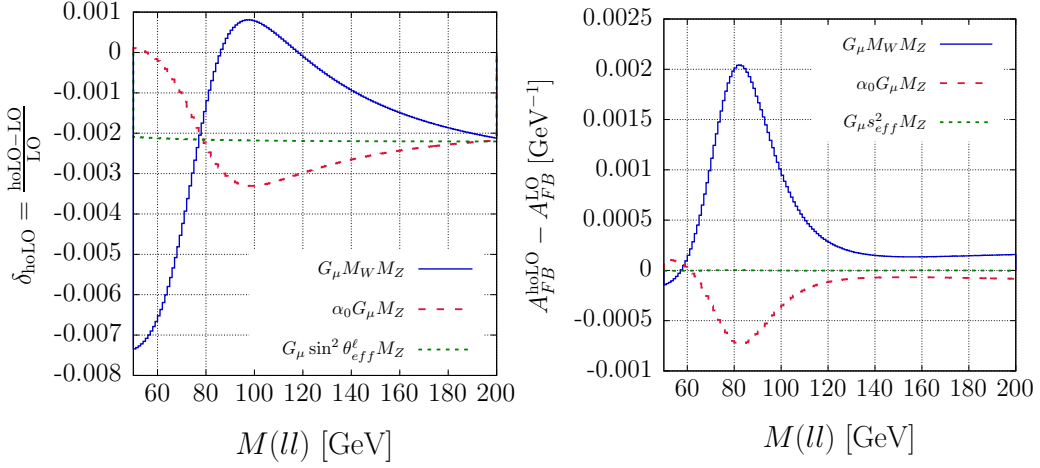
Figure 6.2: Higher-order correction to the differential cross section (left) and forward-backward asymmetry (right) distributions as a function of the leptonic invariant mass, for three different choices of renormalization scheme as indicated.
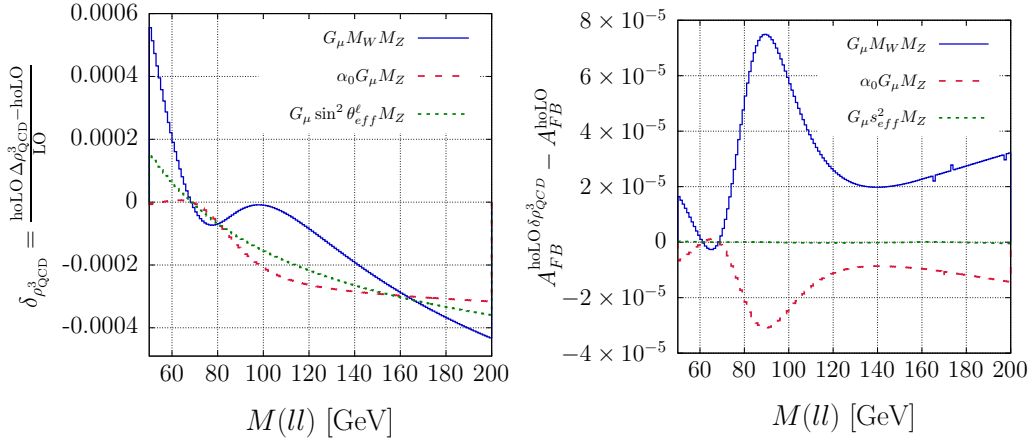

Figure 6.3: Impact of the three-loop QCD contribution to $\Delta\rho$ on the cross section distribution (left) and on the asymmetry (right), for the three renormalization schemes indicated by the labels.

at low invariant masses, then reaching a maximum of $-3‰$ around the Z peak: this can be understood by considering the extra shift, w.r.t. the one-loop one, in the value of s_w^2 induced by the h.o. contributions, which only enters in the Z-exchange amplitude. In the (G_μ, M_W, M_Z) scheme, the contribution is large for low invariant masses, reaching more than 0.7% in absolute value, and then decreases at higher scales, hitting a minimum around the resonance region and then remaining of the order of 0.2%: on top of the shift in s_w^2, in this scheme there is an additional overall factor $2(\Delta\rho - \Delta\rho|_{1-loop})c_w/s_w + \Delta\rho^2 c_w^2/s_w^2$ coming from the relation between α and G_μ, which affects also the photon-exchange

6.3. Input scheme comparison

diagram, dominant at lower energies [105]. For the asymmetry, the overall factors cancel; the (G_μ, M_W, M_Z) and (α_0, G_μ, M_Z) schemes show a specular behaviour, due to the shift in the value of s_w^2, which is larger in the former case. In the $(G_\mu, \sin^2\theta_{eff}^\ell, M_Z)$ scheme, on the other hand, the correction is negligible.

Fig. 6.3 presents the effect of switching on only the three-loop QCD correction to $\Delta\rho$, $\delta_{QCD}^{(3)}$ in Eq. 3.19, presented as a relative (absolute) difference between the invariant-mass cross section (asymmetry) distribution obtained with and without $\delta_{QCD}^{(3)}$, normalised to the LO predictions. On the left, we can see that the largest correction to the cross section occur in the (G_μ, M_W, M_Z) scheme in the low invariant-mass region, with a value of 0.05%, then reaching the -0.01% level in the Z resonance region and decreasing to about -0.04% at large energies. This is due to the fact that the $\Delta\rho$-dependence in this scheme stems from both δs_w^2 and the overall factor $c_w^2/s_w^2\Delta\rho$ from the $\alpha - G_\mu$ relation: the latter one is the dominant effect for low invariant masses. In the (α_0, G_μ, M_Z) scheme the contribution is limited to the range $[-0.03\%, 0]$: it comes from the linear $\Delta\rho$ correction to the coupling in Z-exchange diagram, and as such is negligible when the photon contribution dominates, at low energy. Finally, the $(G_\mu, \sin^2\theta_{eff}^\ell, M_Z)$ scheme presents a correction which varies between 0.015% and -0.04%, due to the overall factor $6x_t(\Delta\rho^{(1)} + x_t\Delta\rho^{(2)}) \times \alpha_S^2/\pi^2 \times \delta_{QCD}^{(3)}$ stemming from the $\alpha - G_\mu$ relation, which is three times smaller than the corresponding contribution in the G_μ scheme. The dependence on the invariant mass can be related to the residual scale dependence of the QCD correction.

In the right part of Fig. 6.3, one can observe that in the case of the asymmetry distribution all overall effects cancel, leading to very small corrections in all schemes. In particular, for the $(G_\mu, \sin^2\theta_{eff}^\ell, M_Z)$ scheme the impact is vanishing, because $\Delta\rho$ cancels almost completely between numerator and denominator.

6.3 Input scheme comparison

The study of the corrections within different schemes is completed by Fig. 6.4, where the cross section (relative differences, on the left) and asymmetry (absolute differences, on the right) distributions are compared to the reference predictions in the $(\alpha(M_Z^2), s_{eff}^2, M_Z)$ scheme, for different levels of perturbative accuracy: the LO in the upper panels, the NLO in the middle and the NLO with additional universal higher-order corrections, labelled NLO+HO, at the bottom. In these lower panels, also the predictions obtained with the $\overline{MS}$ scheme $(\alpha(\mu), s_w^2(\mu), M_Z)$, introduced in Sec. 3.4, are shown (dash-dotted black line). For the schemes with α_0 in input, the higher orders are realised by including the correction due to $\Delta\alpha(M_Z)$, computed at a fixed scale set to the Z mass, instead of the scale-dependent factor $\Delta\alpha(s)$.

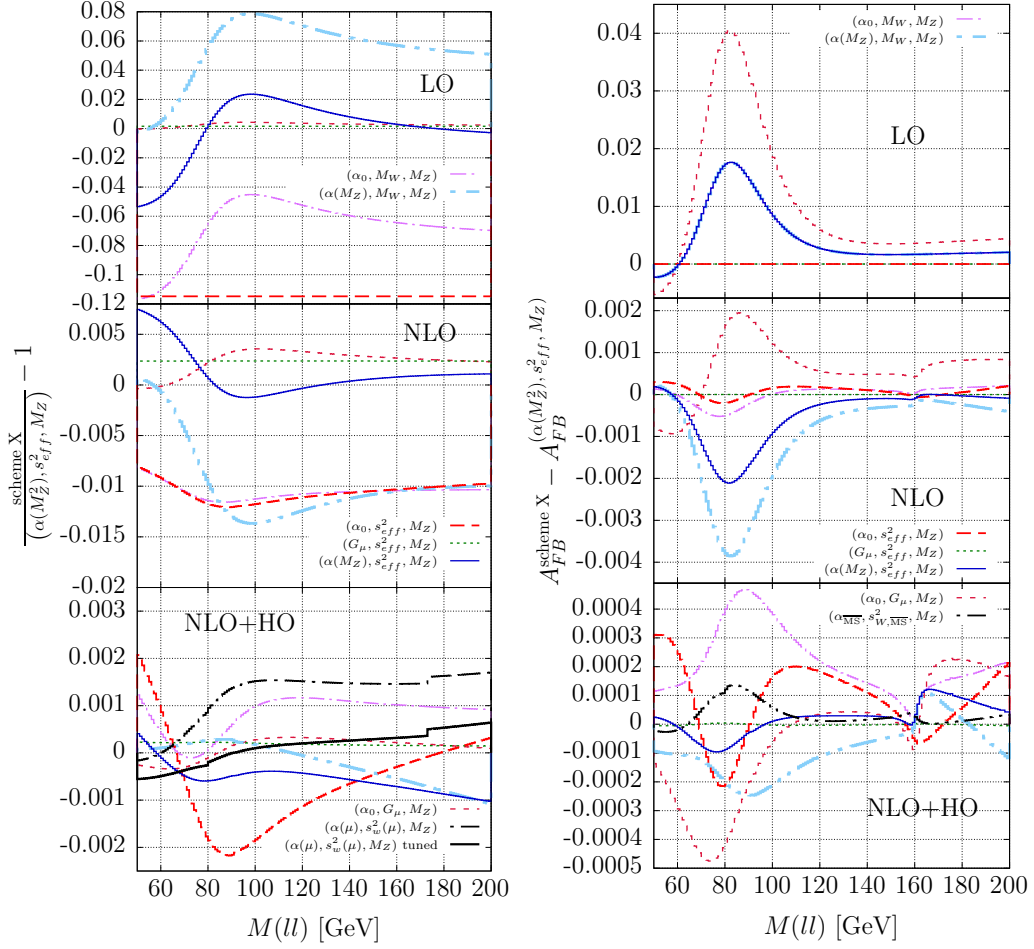The first general observation is that the convergence of the perturbative

Figure 6.4: Invariant-mass distribution ratio and asymmetry difference in different schemes, w.r.t. the $(\alpha(M_Z^2), s_{eff}^2, M_Z)$ one. In the h.o. it is used $\Delta\alpha(M_Z)$.

series is apparent, as the differences among the schemes tend to come closer together, starting from several per cents at LO, counting less then 2% at NLO and ending at few 0.1% at NLO+HO for the cross section; for the asymmetry, the absolute differences amount to a maximum of approximately 0.02 at LO and few 0.001 at NLO, reducing to few 10^{-4} when including the higher-order fermionic corrections. The difference among the predictions obtained with different input and renormalization schemes can be understood by splitting the corrections into a non-enhanced part − formally equal to the one in the reference $(\alpha(M_Z^2), s_{eff}^2, M_Z)$, but with a different numerical value for α and the weak mixing angle − plus the shift in s_w^2 described in Sec. 6.1, plus the overall effect due to the running of α or to the corrections to the $\alpha - G_\mu$ relation if α_0 or G_μ are in input, respectively. The size of these contributions is fully illustrated and justified in [105], by referring to the explicit form of the corrections within each scheme presented in Chap. 3.

6.3. Input scheme comparison
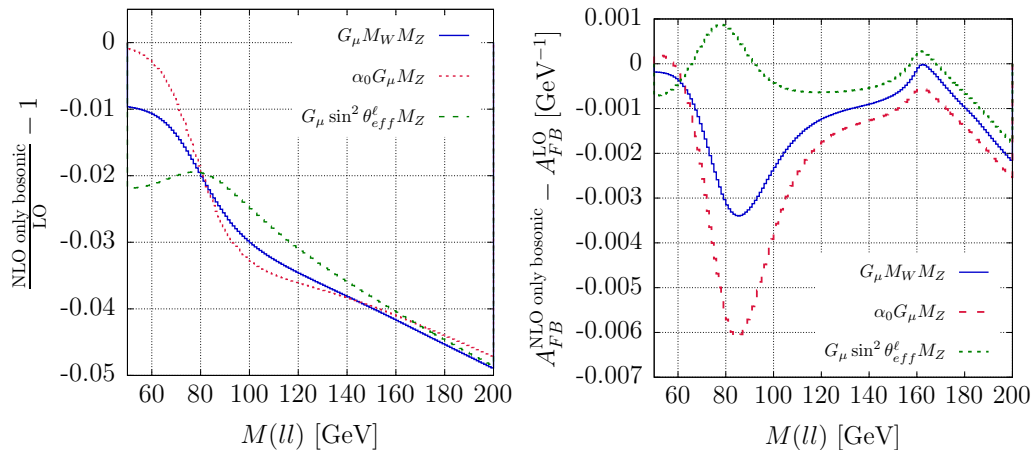
Figure 6.5: Relative corrections to the invariant-mass distribution (left) and absolute corrections to the forward-backward asymmetry (right) obtained by considering only NLO bosonic contributions.

To have an idea of the NNLO missing corrections which are not included in the lower panels of Fig. 6.4, one can look at the size of the NLO bosonic corrections in the different schemes, displayed in Fig. 6.5 for the three representative schemes of Sec. 6.1. On the left panel, it is shown the relative effect of NLO bosonic contributions w.r.t. to the LO for the invariant-mass distribution, where one can see that the bosonic corrections are in general negative and quite large, reaching up to 5% at 200 GeV. On the right we have the absolute difference for the asymmetry distribution: here one has an almost specular trend for the schemes with M_W in input with respect to the ones with $\sin^2 \theta_{eff}^\ell$ as free parameter, with corrections which amount to few 10^{-3}. The largest effect from NLO bosonic contributions is visible in the (α_0, G_μ, M_Z) scheme, where it reaches a maximum of $6 \cdot 10^{-3}$ near 83 GeV.

The bosonic corrections at NLO are quite large in all schemes, and, by comparing the middle panels of Fig. 6.5 with Fig. 6.4, one could infer that there are important cancellations between the fermionic and bosonic part of the NLO contributions. This can partially explain why the differences among schemes are still significant at the NLO+HO level: in fact, one could expect that a rough estimate of the bosonic contribution to the full NNLO calculation is obtained by squaring the NLO bosonic corrections, which will contribute to reduce the spread among different schemes up of several 10^{-4} in the case of the cross section and of some 10^{-5} for the asymmetry. One can conclude that the leading fermionic corrections at higher orders constitute only a partial approximation of the complete NNLO calculation.

6.3.1 Comparison with LEP results

The comparison among the different schemes here presented deserves some more words: in fact, the differences at NLO+HO are quite large, in ostensible contrast to results in the literature, especially connected with the high-precision predictions for the LEP1 experiment [28, 50, 200]. In this section, we will reproduce the calculations performed for LEP, by using our language and including only the universal higher-order corrections, available at and outside the resonance. Note that this prescription differs from the calculations and related codes used in [28], which included also sub-leading two-loop effects at the peak [111–113]. As of today, the predictions at the Z resonance have been updated to include the full NNLO corrections [267].

First of all, we decide to adopt the pole scheme for the treatment of the resonance, to avoid spurious contaminations from terms of the kind Γ_V/M_V, and consider the calculation of the $Z\ell\bar{\ell}$ width, in a similar fancy to what is done in Table 4 of [28]. We do not aim at reproducing the exact LEP numbers, as we stick to the parameter values of Table 6.1, where e.g. the Higgs and top masses are the measured ones. The goal here is to reproduce the level of agreement among different schemes as declared in [28], which amounts to 10^{-4} on the $Z\ell\bar{\ell}$ width, as a check of the internal consistency of our code.

Since the calculations in [28] made use of the input data α_0, G_μ and M_Z, we follow this prescription as well: in particular, α_0 is used to compute $\alpha(M_Z^2)$, which is the overall coupling of the weak corrections. In our code, this is equivalent to consider three input schemes: $(\alpha(M_Z^2), G_\mu, M_Z)$ — i.e. the usual (α_0, G_μ, M_Z) with `azinscheme4` on, already used in the previous sections and here relabelled in analogy with the other schemes —, $(\alpha(M_Z^2), M_W|_{G_\mu}, M_Z)$, with the value of $M_W|_{G_\mu}$ computed by using the values of α_0, G_μ and M_Z, and $(\alpha(M_Z^2), \sin^2\theta_{eff}^\ell|_{G_\mu}, M_Z)$, where $\sin^2\theta_{eff}^\ell|_{G_\mu}$ is extracted from α_0, G_μ and M_Z. An important remark is in order here: the code usually computes the values of derived quantities with tree-level relations, while here we want to do something different, i.e. to compute the derived parameters with the accuracy corresponding to the one of the predictions, to reduce as much as possible the introduction of spurious terms, formally not under control. The three schemes $(\alpha(M_Z^2), G_\mu, M_Z)$, $(\alpha(M_Z^2), M_W|_{G_\mu}, M_Z)$ and $(\alpha(M_Z^2), \sin^2\theta_{eff}^\ell|_{G_\mu}, M_Z)$ thus differ for the form of the corrections and the renormalization conditions, as discussed in Chap. 3, but they all take as input quantities α_0, G_μ and M_Z.

The relevant formulae for the calculation of the $Zf\bar{f}$ width at LO, NLO and when including also the universal higher-order corrections can be found in App. D. The derived parameters are computed in an iterative way with the

6.3. Input scheme comparison

following equations:

$$
M_W|_{G_\mu} = \frac{M_Z^2}{2}\left(1 + \sqrt{1 - \frac{\sqrt{8}\pi}{G_\mu M_Z^2}\,\alpha(M_Z^2)\,\frac{1 + \Delta r^{(1)} - \Delta\alpha + \frac{c_W^2}{s_W^2}\Delta\rho^{(1,X)}}{1 + \frac{c_W^2}{s_W^2}\Delta\rho^{(X)}}}\right)
$$

$$
s_{eff}^2|_{G_\mu} = \frac{1}{2} - \sqrt{\frac{1}{4} - \frac{\pi}{\sqrt{2}G_\mu M_Z^2}\,\alpha(M_Z^2)\left(1 + \Delta\tilde{r}^{(1)} - \Delta\alpha + \Delta\rho^{(1)} - \Delta\rho\right)},
$$

$$(6.1)$$

where $\Delta r^{(1)}$ is the one-loop Δr computed in the scheme with M_W in input, while $\Delta\tilde{r}^{(1)}$ is the one with s_{eff}^2 as free parameter. The term $\alpha(M_Z^2)$ is calculated as:

$$
\alpha(M_Z^2) = \frac{\alpha_0}{1 - \Delta\alpha}. \tag{6.2}
$$

The factor $\Delta\rho^{(1)}$ is the one-loop contribution to $\Delta\rho$, which in turn includes both one- and two-loop (plus eventually higher orders in QCD) terms, while $\Delta\rho^{(1,X)}$ is defined as:

$$
\Delta\rho^{(1,X)} = \frac{\Sigma_T^{ZZ}(M_Z)}{M_Z^2} - \frac{\Sigma_T^{W}(M_W)}{M_W^2}\Bigg|_{fin,\,\mu_{dim}=M_Z}, \tag{6.3}
$$

that is, it is the difference between the self-energies without the UV poles and with μ_{dim} set to M_Z; finally, $\Delta\rho^{(X)}$ is analogous to $\Delta\rho$, but the one-loop contribution is given by $\Delta\rho^{(1,X)}$ instead of $\Delta\rho^{(1)}$. Note that in $\Delta\rho^{(X)}$ the overall coupling is G_μ.

To implement the higher-order corrections, we use an Improved Born Approximation, with the couplings given by $\alpha(M_Z^2)$ and an effective $\tilde{s}_w^2$ computed for the different schemes as described in the following. The key observation here is that one can always define an effective weak mixing angle, as an observable at NLO accuracy, as:

$$
\tilde{s}_{w,\,\mathrm{LO}}^2 = \frac{1}{2}\frac{-g_R}{g_L - g_R}
$$

$$
\tilde{s}_{w,\,\mathrm{NLO}}^2 = \frac{1}{2}\frac{-g_R}{g_L - g_R} + \frac{1}{2}\frac{g_L g_R}{(g_L - g_R)^2}\mathrm{Re}\left(\frac{\delta g_L}{g_L} - \frac{\delta g_R}{g_R}\right). \tag{6.4}
$$

$(\alpha(M_Z^2), \sin^2\theta_{eff}^\ell|_{G_\mu}, M_Z)$ scheme

The input couplings in this scheme are already the effective ones, with $\tilde{s}_w^2 = \sin^2\theta_{eff}^\ell|_{G_\mu}$. It does not receive corrections when going from NLO to NLO+HO.

$(\alpha(M_Z^2), G_\mu, M_Z)$ scheme

In this scheme, it can be demonstrated that the NLO counterterm of s_w^2, i.e. $\delta s_w^2/s_w^2$, can be written as the one for the effective weak mixing angle $\delta s_{eff}^2/s_{eff}^2$,

	$(\alpha(M_Z^2), M_W\vert_{G_\mu}, M_Z)$	$(\alpha(M_Z^2), s_{eff}^2\vert_{G_\mu}, M_Z)$	$(\alpha(M_Z^2), G_\mu, M_Z)$
$\tilde{s}_{w,\,\mathrm{NLO+HO}}^2$	0.2316749	0.2315919	0.2315965
Γ_e LO	$8.58920545 \cdot 10^{-2}$	$8.3203418 \cdot 10^{-2}$	$8.3315838 \cdot 10^{-2}$
Γ_e NLO+HO	$8.3697741 \cdot 10^{-2}$	$8.3717562 \cdot 10^{-2}$	$8.3717744 \cdot 10^{-2}$

Table 6.2: Results for the $Z\ell\bar{\ell}$ width at LO and NLO+HO in the three schemes described in the text. In the first line, we report also the value for the effective coupling $\tilde{s}_{w,\,\mathrm{NLO+HO}}^2$ used to compute the NLO+HO.

plus a term $\Delta\tilde{r}$ formally equivalent to the one with s_{eff}^2 in input, but computed with the numerical value of s_w^2 obtained in the $(\alpha(M_Z^2), G_\mu, M_Z)$. At NLO thus we can introduce an effective coupling as:

$$\tilde{s}_{w,\,\mathrm{NLO}}^2 = s_w^2 + \frac{s_w^2 c_w^2}{c_w^2 - s_w^2}\Delta\tilde{r}\,, \tag{6.5}$$

and at NLO+HO one can resum the $\Delta\tilde{r}$ term:

$$\tilde{s}_{w,\,\mathrm{NLO+HO}}^2 = \frac{1}{2} - \sqrt{\frac{1}{4} - \frac{\pi\alpha}{\sqrt{2}G_\mu M_Z^2}(1 + \Delta\tilde{r})}\,. \tag{6.6}$$

Note that Eq. (6.5) is the one-loop expansion of Eq. (6.6).

$(\alpha(M_Z^2), M_W, M_Z)$ scheme

At NLO is valid the second of Eqs. (6.4), while at NLO+HO one can write:

$$\begin{aligned}
\tilde{s}_{w,\,\mathrm{NLO+HO}}^2 &= s_w^2\left(1 + \frac{c_w^2}{s_w^2}\Delta\rho^{(X)}\right) \tag{6.7}\\
&\cdot \left[1 - \frac{c_w^2}{s_w^2}\Delta\rho^{(1,X)} + \frac{1}{s_w^2}\frac{1}{2}\frac{g_L g_R}{(g_L - g_R)^2}\mathrm{Re}\left(\frac{\delta g_L}{g_L} - \frac{\delta g_R}{g_R}\right)\right]\,.
\end{aligned}$$

Note that the terms in the second parenthesis should be computed with the same coupling used as the overall of the NLO weak corrections in the code.

We thus substitute these effective couplings into the Born width, and subtract the one-loop contribution, which is already computed by the code following the equations of App. D. By using the numerical setup of Sec. 6.1 and by switching on the 2-loop mixed and the 3-loop QCD contributions to $\Delta\rho$, we obtain the results of Table 6.2.

It can be seen that the overall agreement among the values of the $Z\ell\bar{\ell}$ width when including the universal higher-order corrections is at the level of 10^{-4}, even better if we consider only the schemes $(\alpha(M_Z^2), s_{eff}^2\vert_{G_\mu}, M_Z)$ and $(\alpha(M_Z^2), G_\mu, M_Z)$, where the equivalence between the $\delta s_w^2/s_w^2$ counterterms can be proven analytically also for terms formally beyond accuracy. We
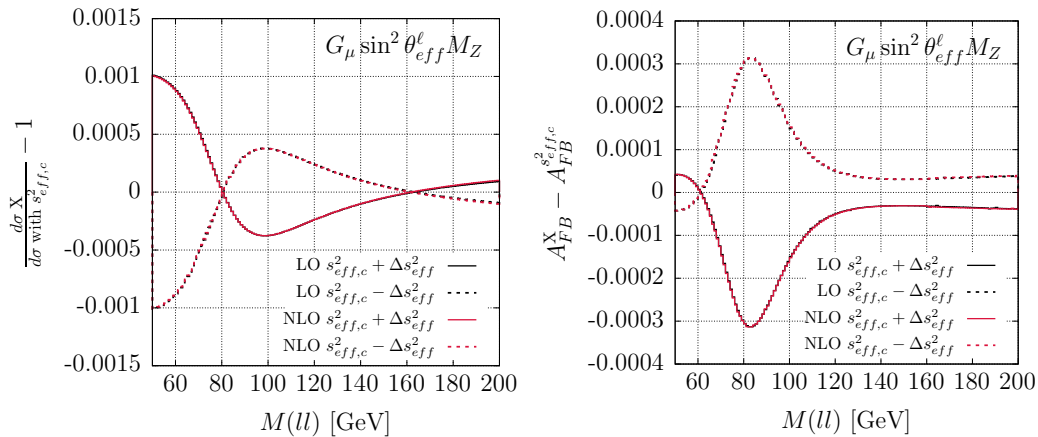
Figure 6.6: Effects of varying the input parameter $\sin^2 \theta^\ell_{eff} = 0.23154 \pm 0.00016$ in the $(G_\mu, \sin^2 \theta^\ell_{eff}, M_Z)$ scheme from the central value to the upper and lower ones, at LO and NLO. On the left it is shown the relative difference between the invariant-mass distribution obtained with the upper/lower value of $\sin^2 \theta^\ell_{eff}$ and the one with the central value $\sin^2 \theta^\ell_{eff,c} = 0.23154$, on the right the absolute difference between the asymmetry distribution obtained with the upper/lower value of $\sin^2 \theta^\ell_{eff}$ and the one with the central value.

remark that, at difference to what was available at LEP, we did not include the full NNLO corrections to the width, leaving it to future work. It would be indeed interesting to compare our findings with existing tools that provide exact NNLO accuracy for the form factors and the leptonic width at the Z peak [100, 267].

6.4 Parametric uncertainties

An important feature that has to be taken into account in the choice of an input scheme is the experimental accuracy at which the relevant parameters are known. In this Section, we study the parametric uncertainties due to the current experimental errors on two important inputs, M_W and $\sin^2 \theta^\ell_{eff}$, which enter the computations in the schemes (G_μ, M_W, M_Z) and $(G_\mu, \sin^2 \theta^\ell_{eff}, M_Z)$, respectively. We decide to treat the (α_0, G_μ, M_Z) scheme as it was not affected by parametric uncertainties, given the excellent accuracy with which α_0, G_μ and M_Z are known. As in the previous sections, we consider these effects on the cross section and the asymmetry distributions, as functions of the leptonic invariant mass.

Figure 6.6 shows the impact due to a variation of $\sin^2 \theta^\ell_{eff}$ within the LEP range 0.23154 ± 0.00016 [50] in the $(G_\mu, \sin^2 \theta^\ell_{eff}, M_Z)$ scheme at LO and NLO accuracy (black and red lines, respectively). On the left side, it is plotted the
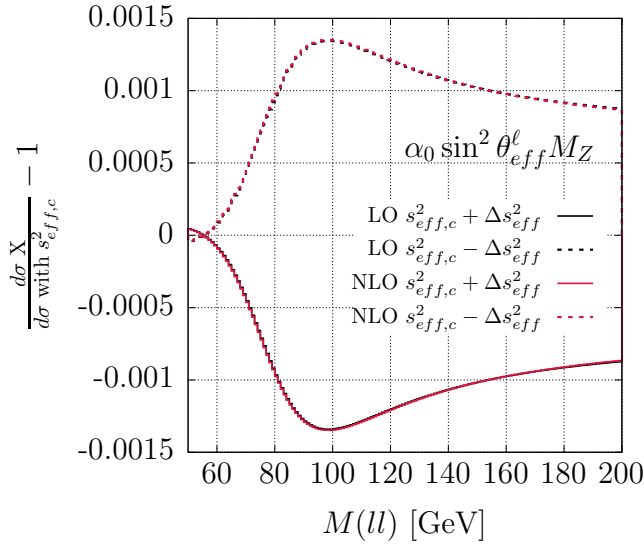
105

Figure 6.7: Effects induced on the dilepton invariant-mass distribution by a variation of the input parameter $\sin^2 \theta_{eff}^\ell = 0.23154 \pm 0.00016$ in the $(\alpha_0, \sin^2 \theta_{eff}^\ell, M_Z)$ scheme from the central value to the upper and lower ones, at LO and NLO. Same notation and conventions of the left panel of Fig. 6.6.

relative difference on the cross section distribution, i.e. the quantity:

$$\delta^\pm = \frac{d\sigma}{dM_{\mu^+\mu^-}^{s^2_{eff,c} \pm \Delta s^2_{eff}}} \bigg/ \frac{d\sigma}{dM_{\mu^+\mu^-}^{s^2_{eff,c}}} - 1 \,, \tag{6.8}$$

where $s^2_{eff,c}$ refers to the central value of $\sin^2 \theta_{eff}^\ell$, namely 0.23154, while $\Delta s^2_{eff} = 0.00016$. In the $(G_\mu, \sin^2 \theta_{eff}^\ell, M_Z)$ scheme, the renormalisation conditions are imposed in such a way that the radiative corrections do not affect $\sin^2 \theta_{eff}^\ell$: as a consequence, varying $\sin^2 \theta_{eff}^\ell$ produces the same effect at LO and at NLO EW. The differential cross section as a function of the invariant mass depends on $\sin^2 \theta_{eff}^\ell$ not only through the g_V/g_A factor arising from the $Z f \overline{f}$ vertices, but also via the overall coupling[1]:

$$\alpha_{G_\mu} = \frac{\sqrt{2}}{\pi} G_\mu \sin^2 \theta_{eff}^\ell \left(1 - \sin^2 \theta_{eff}^\ell\right) M_Z^2 \,. \tag{6.9}$$

This dependence of the overall α on the value of the input $\sin^2 \theta_{eff}^\ell$ explains the enhancement in the low-mass region on the left panel of Fig. 6.6, as one can better understand by comparing this plot with Fig. 6.7, which is obtained in the $(\alpha_0, \sin^2 \theta_{eff}^\ell, M_Z)$ scheme, where the overall coupling is α_0, i.e. it is independent from $\sin^2 \theta_{eff}^\ell$. In light of these observations, it is better to consider a normalized differential cross-section distribution if one aims to study

---

[1]In the complex-mass scheme, the real part of M_Z^2 should be taken.
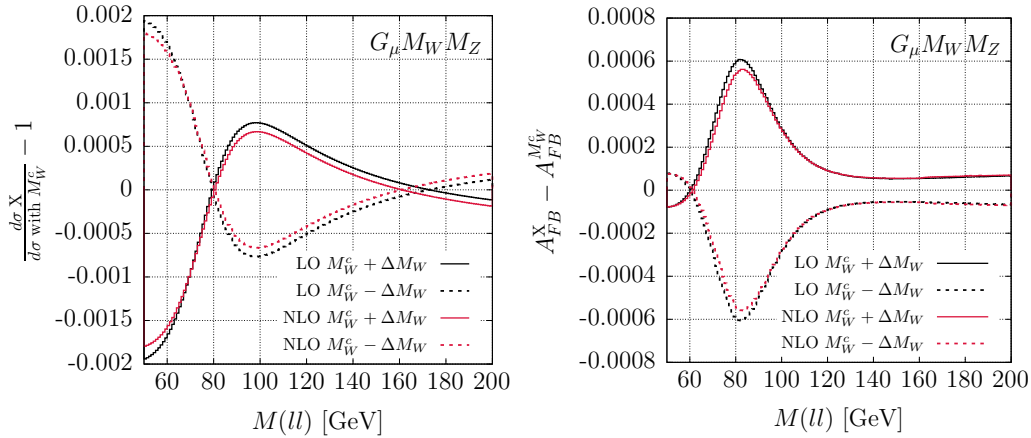
6.4. Parametric uncertainties

Figure 6.8: Effects of varying the input parameter $M_W = 80.385 \pm 0.015$ GeV in the (G_μ, M_W, M_Z) scheme from the central value to the upper and lower ones, at LO and NLO. On the left it is shown the relative difference between the invariant-mass distribution obtained with the upper/lower value of M_W and the one with the central value $M_W^c = 80.385$ GeV. One the right one has the absolute difference between the asymmetry distribution obtained with the upper/lower value of M_W and the one with the central value.

the sensitivity of this observable to the leptonic effective weak mixing angle, which is considered as a measure of the $Zf\overline{f}$ coupling through the g_V/g_A ratio.

On the right side of Fig. 6.6 we show the effects of varying $\sin^2 \theta_{eff}^\ell$ on the asymmetry distribution. In particular, it is plotted the absolute difference:

$$\Delta^\pm = \frac{dA_{FB}}{dM_{\mu^+\mu^-}^{s_{eff,c}^2 \pm \Delta s_{eff}^2}} - \frac{dA_{FB}}{dM_{\mu^+\mu^-}^{s_{eff,c}^2}} . \tag{6.10}$$

As in the case of the cross section, the dependence on $\sin^2 \theta_{eff}^\ell$ is basically the same at LO and at NLO, amounting to $\pm 6 \cdot 10^{-4}$ near the Z peak and vanishing away from the resonance region. One can notice that, since A_{FB} is defined through a ratio of differential cross sections, the overall spurious dependence on $\sin^2 \theta_{eff}^\ell$ cancels and with this plot one can quantify the "true" sensitivity of this observable to the effective leptonic weak mixing angle.

Figure 6.8 shows the impact of the parametric uncertainty due to the value of the W-boson mass within the (G_μ, M_W, M_Z) scheme. In particular, on the right is it plotted the same quantity of Eq. (6.8) and on the left the one in Eq. (6.10), but with the central W-mass value $M_W^c = 80.385$ GeV in place of $s_{eff,c}^2$ and the variation $\Delta M_W = \pm 15$ MeV instead of Δs_{eff}^2 [2]. The behaviour of the cross section and asymmetry distributions in Fig. 6.8 is very similar to

---

[2] This was the 1σ error of Ref. [268]. As seen in Chap. 2, the current PDG error on the M_W world average is 12 MeV [30], excluding the latest CDF measurement. However, for our illustration purposes taking $\Delta M_W = \pm 15$ MeV is enough.
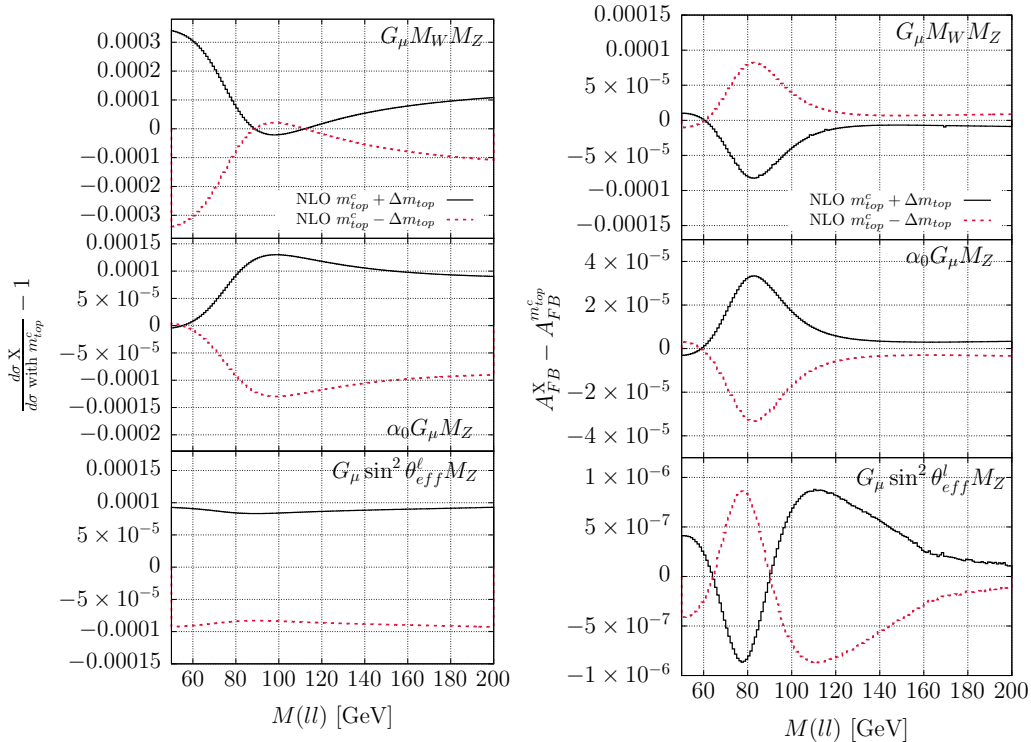
Figure 6.9: Effects of varying the top-quark mass $m_{top} = 173.0 \pm 0.4$ GeV in the three considered schemes. The top-quark mass enters only the NLO corrections. On the left, it is shown the relative difference between the invariant-mass distribution obtained with the upper/lower value of m_{top} and the one with the central value $m_{top}^c = 173.0$ GeV. On the right there is the absolute difference of the asymmetry distributions obtained in the same m_{top} range.

the corresponding one in Fig. 6.6, as it can be understood at LO by considering the relation:

$$\delta \sin^2 \theta_{eff}^\ell = -2 \left(\frac{M_W}{M_Z^2} \right) \delta M_W \,, \tag{6.11}$$

which links the variation of M_W to the one of $\sin^2 \theta_{eff}^\ell$. From Eq. (6.11) it can be calculated that, for example, varying the W mass of 15 MeV is equivalent to a shift of -0.0003 in $\sin^2 \theta_{eff}^\ell$, a quantity that is approximately twice the Δs_{eff}^2 considered in Fig. 6.6. The same pattern is present also at NLO, even if beyond the leading order the relation between the shifts of $\sin^2 \theta_{eff}^\ell$ and M_W is more complicated: in fact, in Fig. 6.8 the NLO curves do not overlap with the LO ones, at difference from what happens in Fig. 6.6.

On the left panel of Fig. 6.8 we can observe again a spurious enhancement of the sensitivity in the low invariant-mass region due to the dependence of α on the W mass:

$$\alpha_{G_\mu} = \frac{\sqrt{2}}{\pi} G_\mu M_W^2 \left(1 - \frac{M_W^2}{M_Z^2} \right) \,, \tag{6.12}$$
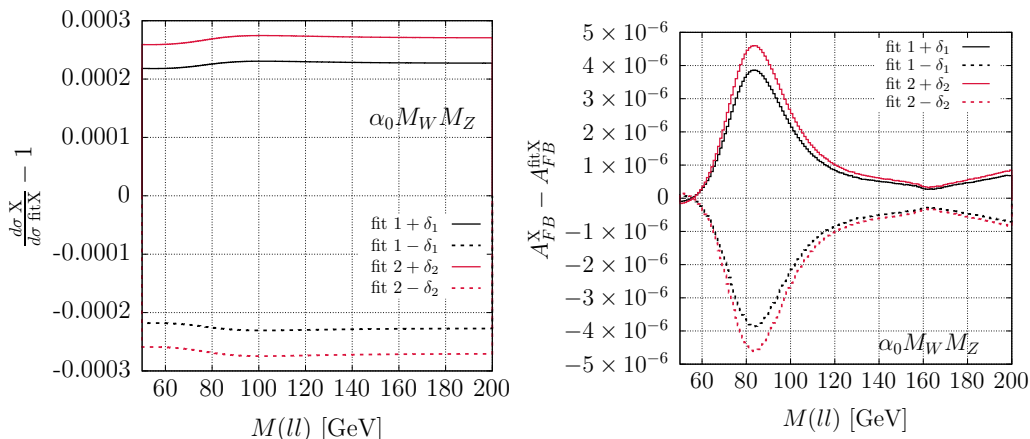
Figure 6.10: Change in the cross section as a function of the invariant mass (left) and in the asymmetry distribution (right) if one takes the central value for $\triangle\alpha^{\mathrm{had\,fit}}$ (that here coincides with zero) plus its error $\delta\triangle\alpha^{\mathrm{had\,fit}}$, here labelled δ_1 for results obtained with the flag `fit=1`, and δ_2 for results with the flag `fit=2`. The input scheme used here is (α_0, M_W, M_Z).

where if the complex-mass scheme is employed one should take the real part of the masses.

To conclude the section, we show the sensitivity of the two considered observables on the top-quark mass, which enters the loop corrections in all three schemes (G_μ, M_W, M_Z), $\left(G_\mu, \sin^2\theta_{eff}^\ell, M_Z\right)$ and (α_0, G_μ, M_Z). We take into account a variation of 400 MeV from the central value $m_{top}^c = 173$ GeV, which corresponds to the error quoted in [269], recently improved to $m_{top} = 172.69 \pm 0.30$ GeV in [30]. The results are presented only at NLO accuracy, because the top mass has an impact only through radiative corrections. For the differential cross section, the dependence on the variation of the top mass is of the order of 0.01% for all schemes. On the other hand, within the $\left(G_\mu, \sin^2\theta_{eff}^\ell, M_Z\right)$ scheme the asymmetry distribution is not affected by m_{top} in a relevant way [53], while in the other two schemes the sensitivity of the asymmetry to the top mass remains below the 0.01% level.

6.5 Treatment of $\triangle\alpha^{\mathrm{had}}$

We here present results connected to the treatment of the hadronic running of the electromagnetic coupling constant described in Sec. 3.4.1, in its improved and most recent version. Since the effects of the hadronic running of α are not visible in schemes that do not have α_0 as input, because the terms that depend logarithmically on the light-quark masses vanish, we choose to work within the (α_0, M_W, M_Z) scheme.

On the left side of Fig. 6.10 one can see the dependence of the differential cross section on the error associated with the two options of computing
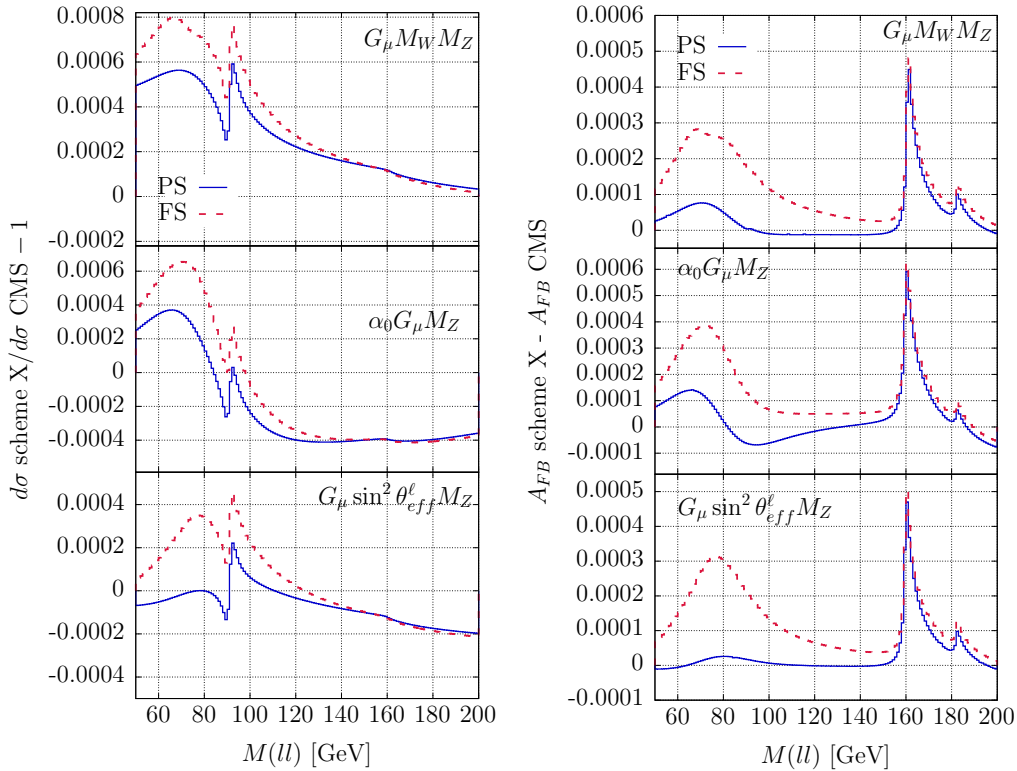
Figure 6.11: Difference of the pole/factorization scheme with respect to the default complex-mass scheme in the distribution of the differential cross section (left) and in the forward-backward asymmetry distribution (right), at NLO. The difference PS-CMS is shown by the solid blue curve, while the FS-CMS one by the dashed red one. Every panel corresponds to a different choice of the renormalization scheme. Upper panel: (G_μ, M_W, M_Z); middle panel: (α_0, G_μ, M_Z); lower panel: $(G_\mu, \sin^2\theta^\ell_{eff}, M_Z)$.

$\Delta\alpha^{\mathrm{had,\,fit}}$, namely the routine `HADR5X19.F` [120–127], denoted with the label "fit 1", and the `KNT v3.0.1` one [128–131], labelled "fit 2". For the cross section, we show the relative difference between the distribution obtained by shifting the central value of $\Delta\alpha^{\mathrm{had}}$ of $\pm\delta\Delta\alpha^{\mathrm{had}}$, with respect to the one with $\Delta\alpha^{\mathrm{had}}$ fixed to its nominal value. The impact is of $\pm0.022\%$ for `HADR5X19.F` and $\pm0.027\%$ for `KNT v3.0.1`. On the right, we show the absolute difference in the asymmetry distribution, obtained within the same range of variation of $\Delta\alpha^{\mathrm{had}}$: in this case, the effect is negligible, below the 10^{-5} level.

6.6   Treatment of the Z width

We compare the different options implemented in the code for the treatment of the Z resonance described in Chap. 4: the default is the complex-mass scheme (CMS), but one can switch on the pole scheme (PS) or the factorisation scheme

6.7. High energy regime

(FS) and see the impact of this choice on the differential distributions.

Fig. 6.11 shows, on the left, the relative difference between the pole (or factorization) scheme, represented by the blue (or red) line, with respect to the default CMS, for the differential cross-section distribution. We take into account the usual three different schemes, all with G_μ as an input: (G_μ, M_W, M_Z), (α_0, G_μ, M_Z) and $(G_\mu, \sin^2\theta^\ell_{eff}, M_Z)$. In all schemes it is possible to observe an oscillation of few 0.01% of amplitude in the resonance region. This has already been pointed out in [86], separately for initial state characterised by the $u\bar{u}$ or $d\bar{d}$ channels. Another general consideration is that in all schemes the shape of the differences is comparable, with the pole scheme that is closer than the FS to the CMS . Quantitatively, the largest difference appears in the (G_μ, M_W, M_Z) and the (α_0, G_μ, M_Z) schemes with the FS, in the energy region around 70 GeV. It is here not recognisable the structure at the WW threshold visible in Fig. 6 of Ref. [86], as here the contributions from up- and down-quark channels partially cancel.

In the right panel of Fig. 6.11, it is shown the absolute difference between the PS (FS) and the CMS, in the A_{FB} distribution. The difference in the asymmetry presents a smooth behaviour around the Z peak, and overall it is of the order of few 0.01%. In the case of the asymmetry distribution, the WW threshold produces a clear enhancement, of the order of 0.05% in all three schemes.

6.7 High energy regime

The results so far presented, which refer to the physics at the Z resonance, can be completed by an analysis of the NLO EW corrections in the high-energy regime in different renormalization schemes. Such a study could be relevant in view of the upcoming physics programme at future high-energy colliders.

We start the discussion by observing that, if considering only the valence quarks within the proton, one can write the DY LO amplitude as $M_u\, u(x, \mu_F) + M_d\, d(x, \mu_F)$, and the NLO one as $\delta_u\, M_u\, u(x, \mu_F) + \delta_d\, M_d\, d(x, \mu_F)$, where $M_{u(d)}$ is the leading-order hard scattering amplitude and $\delta_{u(d)}$ is the relative one-loop correction with only the up(down) contribution in the initial state, while $u(d)(x, \mu_F)$ is the corresponding PDF. It follows that, in all plots shown in this chapter, the ratio NLO/LO is sensitive to the relative PDF weight $u/(u+d)$ and $d/(u+d)$. In the high-mass regime, it can happen to reach the kinematical limit of the PDFs, with the consequence that the ratio between up- and down-quark contributions gets modified, ending up in unphysical behaviours when plotting NLO/LO ratios. For this reason, we here plot distributions in the down-quark channel only, having checked that results with up quarks are similar.

On the left side of Fig. 6.12 it is presented the comparison among all different renormalization schemes, at LO (upper panel), one-loop (central panel) and NLO+HO (lower panel): as already done for Fig. 6.4, we plot the relative difference w.r.t the reference $(\alpha(M_Z^2), s^2_{eff}, M_Z)$ scheme, in the energy range
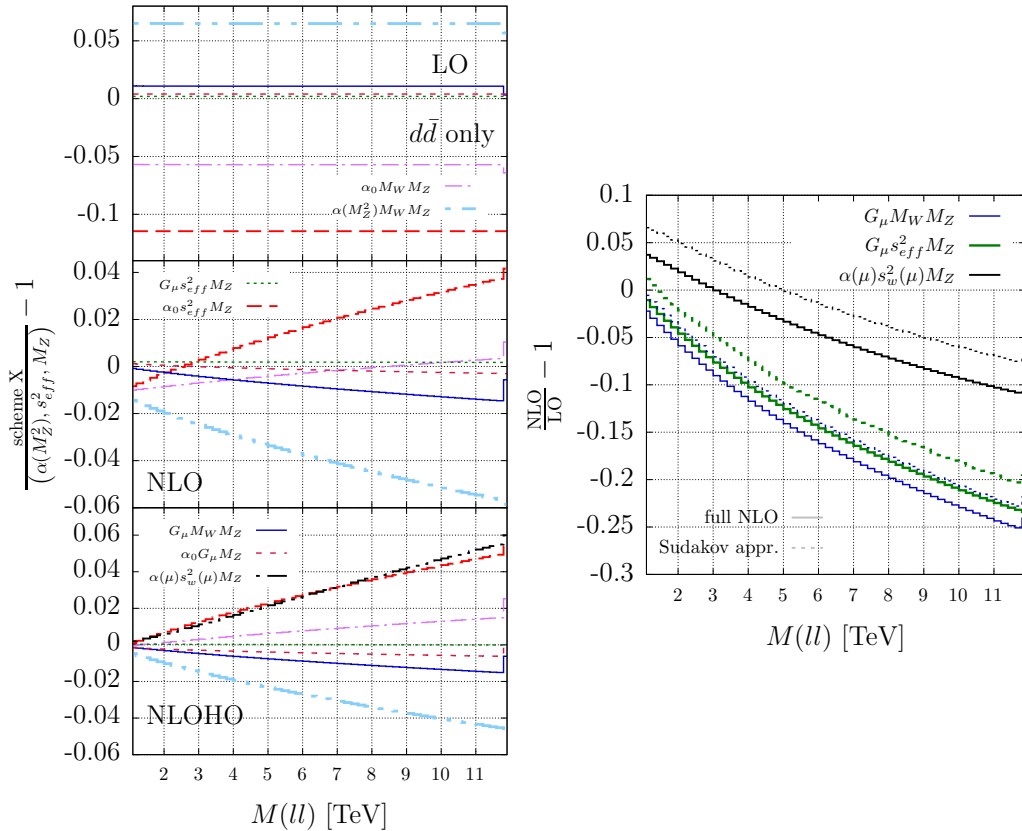
Figure 6.12: Left: comparison among different renormalization schemes, at LO (upper panel) and including NLO weak corrections (lower panel), in the energy range between 1 TeV and 12 TeV. Right: comparison between the Sudakov approximation described in the text (dotted lines) and the full NLO calculation (solid lines), for three different schemes. In both plots, results refer to the down-quark channel in the initial state.

between 1 TeV and 12 TeV. A first observation is that, since in the high-energy regime the invariant-mass dependence of the LO amplitude can be factorised as an overall $1/M_{\ell\bar{\ell}}^2$ up to an error of the size of the terms M_Z^2/s, the ratio between different schemes does not depend on the invariant mass. In fact, the shift w.r.t $(\alpha(M_Z^2), s_{eff}^2, M_Z)$ is due mainly to the ratio of the numerical values of the overall couplings, plus a tiny shape effect − not visible on the scale of the plot − due to the different value of $\sin^2\theta_{eff}^\ell$ in the schemes where M_W is in input.

At LO the maximum difference exceeds 10%, remaining large also at NLO, where it can reach up to $6 - 7\%$ and increases with the invariant mass. The inclusion of higher-order corrections improves the agreement among different schemes in the 1-TeV region, but it does not modify the NLO behaviour of the curves for larger energy values. In fact, at one-loop, some of the corrections connected to the coupling running are included in an effective way in the

6.7. High energy regime

countertems, thus reducing the scheme dependence in the part of the amplitude proportional to the LO structure. On the other hand, the difference due to the remaining corrections gets enhanced with the energy due to the effect of Sudakov logarithms, which are multiplied by a scheme-dependent factor and, being bosonic corrections, are not reabsorbed by including h.o. contributions.

In the Sudakov regime, it is interesting to find a recipe to approximate the full NLO calculation, for instance by taking into account the leading double and single logs as described in Sec. 3.5: the idea is then to resum the dominant contributions from large logs to all orders. However, for all schemes except the $\overline{MS}$ one, to get a good proxy of the full NLO it is necessary to consider also some additional logarithmic contributions of the form $\log M_{\ell\bar{\ell}}^2/M_W^2$, connected with the one-loop expansion of the running of couplings from the electroweak scale to the high $M_{\ell\bar{\ell}}$ of the process, which can be numerically relevant. Moreover, since the NLO correction is the result of a severe cancellation between fermionic and bosonic contributions, but the Sudakov logarithms are only bosonic, it is necessary to add also the fermionic leading corrections associated to $\Delta\alpha$ for schemes with α_0 in input and to $\Delta\rho$ if G_μ is among the free parameters. The final recipe to get a good approximated NLO behaviour is thus to sum the Sudakov logs + the logarithms of UV origin + the leading fermionic corrections.

Some words should be spent on the $\overline{MS}$ scheme on its own. In fact, the running couplings already incorporate the resummation of logarithms coming from the coupling renormalization and part of the fermionic contributions, making it not feasible to consistently separate fermionic and bosonic corrections. Thus, the described recipe to approximate the NLO does not apply to the $\overline{MS}$ scheme, where the UV logs and fermionic contributions are already included.

The right panel of Fig. 6.12 shows the comparison between the complete NLO correction (solid lines) and the approximation obtained with the described prescription (dotted lines), in the case of the (G_μ, M_W, M_Z) scheme (in blue), the $(G_\mu, \sin^2\theta_{eff}^\ell, M_Z)$ one (in green), and the $\overline{MS}$ one (in black). The difference between the full NLO and its approximation amounts to a few percent in all schemes, and remains almost constant throughout the considered invariant-mass range. Given these results, to quantify the uncertainty stemming from missing higher-order bosonic corrections, one could take the square of the Sudakov double and single logs. Alternatively, given that for the neutral-current Drell Yan the Sudakov logs coincide with the full bosonic one-loop correction with good approximation, we could take the exponentiation of double and single logs, under the assumption that they factorise on top of the complete amplitude.

7

Direct determination of the weak mixing angle at high energy

As already stated, the neutral-current Drell-Yan production is particularly suitable for the extraction of the weak mixing angle at hadronic machines. Measurements of this process at high energies can be used to test the energy scale dependence, i.e. the running, of the parameter in regions where New Physics effects can become important. Of course, such a determination requires the implementation of at least the full NLO EW radiative corrections, using a $\overline{MS}$ renormalization scheme featuring the electroweak mixing angle as input parameter, as the one discussed in Sec. 3.4.

In this chapter we present some results on the sensitivity to the weak mixing angle of the neutral-current Drell-Yan process in the Run-3 and High-Luminosity phases of the LHC, obtained with the package `Z_ew-BMNNPV` of POWHEG-BOX. In the upcoming years, a great production of neutral-current Drell-Yan events at high energy is expected at the LHC, by means of proton-proton collisions at a center-of-mass energy of $\sqrt{s} = 13.6$ TeV. A preliminary study of the feasibility to probe the weak mixing angle with such dataset thus appears crucial. Moreover, as already pointed out when discussing existent determinations of the $\overline{MS}$ weak mixing angle in Sec. 2.2.3, the running of this parameter at time-like scales above the Z-boson mass has never been probed experimentally, and would constitute a complementary point of view to low-energy studies, allowing a far from trivial test of the internal consistency of the Standard Model.

7.1 The weak mixing angle at high energy

Exploring the weak mixing angle in the high energy regime is particularly interesting: in fact, according to the renormalization group equation, which regulates the evolution of $\sin^2 \theta_W^{\overline{MS}}(\mu)$ as predicted within the Standard Model, the running of the parameter acquires a steep positive slope [77] at scales above the

7. Direct determination of the weak mixing angle at high energy

W-boson mass, where the contribution of the W-boson opens up. In addition, a high energy determination of the weak mixing angle could indirectly probe new physics particles, as long as they carry electroweak quantum numbers. Such new states would in fact enter the running of the electroweak gauge couplings, and thus such analyses would not require to know their particular decay modes [79–81]. In the literature, a conspicuous number of studies exists on the potential of LHC and future hadronic machines to constrain New Physics models by analysing the running couplings with Drell-Yan processes [270–273].

In this work, we adopt a pure Standard Model approach, that is independent of any particular New Physics parametrization. Furthermore, the study presented here aims at going beyond the approximation on which existing analyses are based, namely the use of leading-order electroweak matrix elements, where the running couplings include only the leading logarithmic contributions to the beta functions. In fact, the `Z_ew-BMNNPV` package offers the possibility to directly probe the running of $\sin^2\theta_w^{\overline{MS}}(\mu)$ by means of a full NLO electroweak calculation, with the hybrid $\overline{MS}$ renormalization scheme described in Sec. 3.4, where the Lagrangian parameters e and $\sin^2\theta_w$ are renormalized in the $\overline{MS}$ scheme and the Z-boson mass in the on-shell scheme.

As final remark, note that our approach is configured as complementary to model-independent searches performed via Effective Field Theories, as explored in Refs. [274–276] and references therein. The EFT techniques are effective at describing New Physics effects where a separation of scales can be applied, i.e. the observed deviations are due to states with a mass much greater than the scale of the process under consideration. A pure Standard Model approach, on the other hand, can be employed also in proximity of the mass thresholds of these new states.

7.2 Code settings

Traditionally, the extraction of the weak mixing angle at the Z peak is performed through measurements of the forward-backward asymmetry A_{FB}. At the energies here considered, of the order of 1 TeV, however, it has been found that the absolute differential cross section is more sensitive to $\sin^2\theta_w^{\overline{MS}}(\mu)$ and thus could constitute a more appropriate choice for its determination. A possible way to see this is to evaluate the logarithmic derivative w.r.t. $\sin^2\theta_w$, i.e. the relative variation under the change of $\sin^2\theta_w$, of the cross section and of A_{FB}, for $M_{\ell\bar{\ell}}$ values much greater than M_Z [273]. At 1 TeV, keeping the effect of finite M_Z, the logarithmic derivative multiplied by $\sin^2\theta_w$ has been evaluated with POWHEG-BOX and found to be:

$$s_w^2 \, \frac{1}{d\sigma/dM_{\ell\bar{\ell}}} \, \frac{\partial(d\sigma/dM_{\ell\bar{\ell}})}{\partial s_w^2} \simeq 0.9 \quad \text{w.r.t.} \quad s_w^2 \, \frac{1}{A_{FB}} \, \frac{\partial A_{FB}}{\partial s_w^2} \simeq 0.3 \,. \tag{7.1}$$

Motivated by this fact, we start by considering neutral-current Drell-Yan production at $\sqrt{s} = 13.6$ TeV in two scenarios: the first one assumes an

7.2. Code settings

integrated luminosity of 300 fb^{-1}, as expected at the end of the LHC Run 3, while the second one takes into account a number of events given by 3000 fb^{-1} of luminosity and corresponds to the HL-LHC phase [277]. The observable chosen for this sensitivity study is the triple differential cross section, as a function of the invariant mass $M_{\ell\bar{\ell}}$, of the rapidity $y_{\ell\bar{\ell}}$ of the leptonic pair, and of the cosine of the angle between the incoming and outgoing fermions in the Collins-Soper reference frame, θ. Since it can be sampled separately in the forward and backward directions, the triple differential cross section has the advantage of encoding the information coming from both the absolute cross-sections and the forward-backward asymmetry, and thus combines the sensitivity to $\sin^2\theta_w$ of both these classes of observables. At LO this triple differential cross section can be expressed as:

$$\frac{d^3\sigma}{dM_{\ell\bar{\ell}}dy_{\ell\bar{\ell}}\mathrm{d}\cos\theta} = \frac{\pi\alpha^2}{3M_{\ell\bar{\ell}}s}\Bigg((1+\cos^2\theta)\sum_q S_q[f_q(x_1,Q^2)f_{\bar{q}}(x_2,Q^2)$$

$$+ f_q(x_2,Q^2)f_{\bar{q}}(x_1,Q^2)] + \cos\theta\sum_q A_q\mathrm{sign}(y_{\ell\bar{\ell}}) \qquad (7.2)$$

$$\cdot [f_q(x_1,Q^2)f_{\bar{q}}(x_2,Q^2) - f_q(x_2,Q^2)f_{\bar{q}}(x_1,Q^2)]\Bigg),$$

where we have denoted with $M_{\ell\bar{\ell}} = \hat{s} = x_1x_2s$ the partonic centre-of-mass energy and with s the hadronic one. The functions $f_{q(\bar{q})}(x,Q^2)$, with $Q^2 = M_{\ell\bar{\ell}}^2$, are the PDFs associated to the extraction of a parton $q(\bar{q})$ with momentum fraction x from the protons. In particular, the two momentum fractions x_1 and x_2 are related to the invariant mass $M_{\ell\bar{\ell}}$ and rapidity $y_{\ell\bar{\ell}}$ as:

$$x_{1,2} = \frac{M_{\ell\bar{\ell}}}{\sqrt{s}}e^{\pm y_{\ell\bar{\ell}}} . \qquad (7.3)$$

In Eq. (7.2), two coupling combinations appear, one that is symmetric (S) and one anti-symmetric (A) [278]. They are given by:

$$\begin{aligned}S_q &= e_\ell^2 e_q^2 + P_{\gamma Z}\cdot e_\ell v_\ell e_q v_q + P_{ZZ}\cdot(v_\ell^2+a_\ell^2)(v_q^2+a_q^2)\\ A_q &= P_{\gamma Z}\cdot 2e_\ell a_\ell e_q a_q + P_{ZZ}\cdot 8v_\ell a_\ell v_q a_q\,,\end{aligned} \qquad (7.4)$$

where e_i is the electric charge, expressed in units of the positron charge, and v_i (a_i) is the vector (axial-vector) coupling. The propagator factors can be explicitly written as:

$$\begin{aligned}P_{\gamma Z}(M_{\ell\bar{\ell}}) &= \frac{2M_{\ell\bar{\ell}}^2(M_{\ell\bar{\ell}}^2 - M_Z^2)}{\sin^2\theta_w\cos^2\theta_w[(M_{\ell\bar{\ell}}^2 - M_Z^2)^2 + \Gamma_Z^2 M_Z^2]}\,,\\ P_{ZZ}(M_{\ell\bar{\ell}}) &= \frac{M_{\ell\bar{\ell}}^4}{\sin^4\theta_w\cos^4\theta_w[(M_{\ell\bar{\ell}}^2 - M_Z^2)^2 + \Gamma_Z^2 M_Z^2]}\,.\end{aligned} \qquad (7.5)$$

The bin choice for the evaluation of the triple differential cross section is the following: six bins in $M_{\ell\bar{\ell}}$ with boundaries 116, 150, 200, 300, 500, 1500,

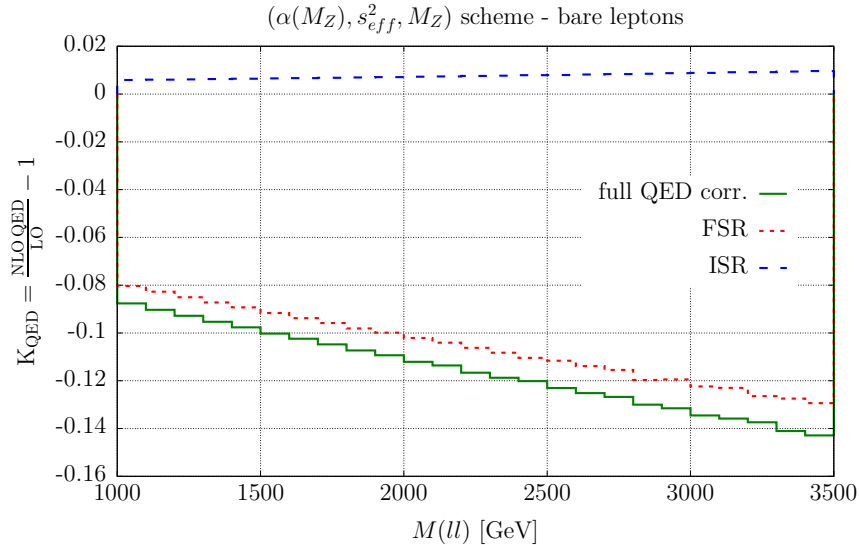## 7. Direct determination of the weak mixing angle at high energy

Figure 7.1: Effects of QED radiation due to ISR (blue stripes), FSR (dotted red line) and the total contribution (solid green line) on the dilepton invariant mass distribution, in the case of bare leptons and for the scheme $(\alpha_0, \sin^2\theta_{eff}^\ell, M_Z)$. The results are presented as relative corrections $K_{\text{QED}} = \text{NLO QED}/\text{LO} - 1$.

5000 GeV, six bins in $|y_{\ell\bar\ell}|$ with boundaries 0.0, 0.4, 0.8, 1.2, 1.6, 2.0, 2.5, and two bins in $\cos\theta$ for the forward and backward directions, for a total of 72 bins.

Concerning selection criteria, the final leptons of the process $pp \to \gamma/Z \to \ell^+\ell^-$ are defined at Born level, i.e. with recombination of final-state photon emission, and are selected by using the usual cuts employed in ATLAS and CMS measurements (one example can be found in [279]): the leading (subleading) lepton must have a transverse momentum $p_T^\ell > 40(30)$ GeV and an absolute pseudorapidity $|\eta_\ell| < 2.5$.

We then proceed with the generation of Monte Carlo predictions, that are simulated at NLO plus parton shower in QCD, including NLO virtual weak corrections but no photonic corrections, a choice made possible by the fact that the two sets of corrections are separately gauge invariant, as discussed in Chap. 5. In each $M_{\ell\bar\ell}$ bin, 10^9 events are produced at parton level with POWHEG-BOX-V2, and then interfaced to PYTHIA8.307 [255], to add the effects due to emission of QCD radiation via parton showering, the underlying event, the hadronization process and the photonic radiation from quarks, i.e. only initial-state QED radiation. FSR and IFI effects are not taken into account in this study. As already discussed in Chap. 5 and as it can be seen in Fig. 7.1, the largest contribution to the total QED radiation comes from QED FSR. In the plot, the correction is presented as a K-factor:

$$K_{\text{QED}} = \frac{\text{NLO QED}}{\text{LO}} - 1\,, \tag{7.6}$$
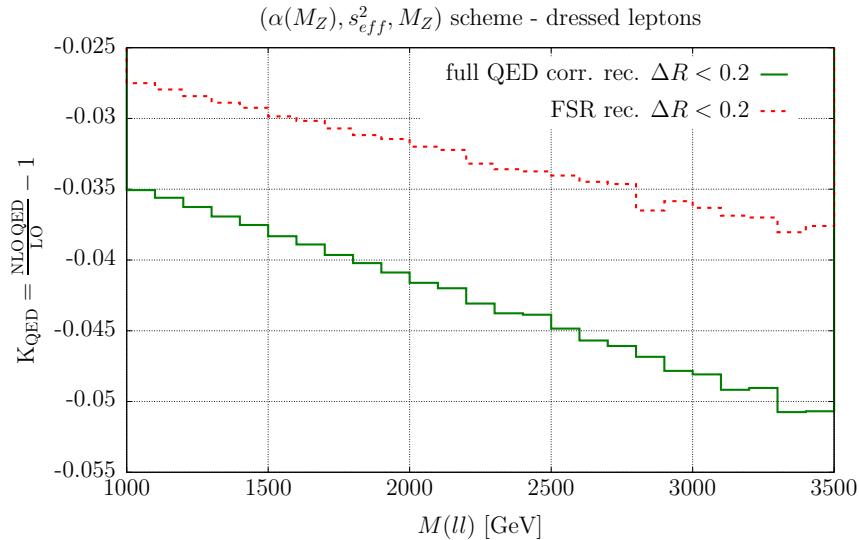
7.2. Code settings

Figure 7.2: Effects of QED radiation due to FSR (dotted red line) and the total contribution (solid green line) on the dilepton invariant mass distribution, in the case of dressed leptons and for the scheme $(\alpha_0, \sin^2\theta^\ell_{eff}, M_Z)$. The results are presented as relative corrections $\mathrm{K_{QED}} = \mathrm{NLO\,QED}/\mathrm{LO} - 1$. Photons emitted within a cone defined by $\Delta R \leq 0.2$ have been recombined with the nearest lepton.

where "NLO QED" stands here for the one-loop contribution when considering only the impact of photonic corrections, without QCD and weak contributions. For high invariant masses, one can see that the effect due to FSR is negative and ranges from 8% at 1 TeV to 13% at 3.5 TeV. The figure refers to the neutral-current Drell-Yan process simulated with POWHEG-BOX-V2 where the leptons are not taken at Born-level (they are "bare", not "dressed") and the adopted renormalization scheme features $(\alpha_0, \sin^2\theta^\ell_{eff}, M_Z)$ as input parameters. Results produced with this scheme are not very different from those expected with the hybrid $\overline{MS}$ scheme $(\alpha(\mu), \sin^2\theta_w^{\overline{MS}}(\mu), M_Z)$. In the present analysis, QED final-state radiation is however negligible, due to the fact that we chose to work with Born-level leptons, meaning that the photonic radiation lying within the cone denoted by:

$$\Delta R = \sqrt{\Delta\eta^2 + \Delta\phi^2} \leq 0.2 \qquad (7.7)$$

has been recombined to the nearest lepton. In this last equation, $\Delta\eta = \eta_1 - \eta_2$ is the difference of the pseudorapidity of particle 1 and particle 2, while $\Delta\phi = \phi_1 - \phi_2$ is the difference in the azimuthal angle ϕ.

In Fig. 7.2 it is shown the correction due to FSR and the total contribution (FSR+ISR+IFI) on the dilepton invariant mass distribution, in the case of dressed leptons and for the scheme $(\alpha_0, \sin^2\theta^\ell_{eff}, M_Z)$. By comparing Fig. 7.2 with Fig. 7.1, one can see the effect of recombination: the FSR correction for dressed leptons amounts to some percent, staying well under 4% in the range

7. Direct determination of the weak mixing angle at high energy

$M_{\ell\ell}^{\text{lo}}$ [GeV]	$M_{\ell\ell}^{\text{hi}}$ [GeV]	$\hat{M}_{\ell\bar{\ell}}$ [GeV]	$(\alpha(\hat{M}_{\ell\bar{\ell}}))^{-1}$	$\sin^2\theta_w^{\overline{\text{MS}}}(\hat{M}_{\ell\bar{\ell}})$
66	116	M_Z	127.951	0.23122
116	150	133	127.838	0.23323
150	200	175	127.752	0.23468
200	300	250	127.544	0.23648
300	500	400	127.269	0.23885
500	1500	1000	126.735	0.24350
1500	5000	3250	126.047	0.24954

Table 7.1: The input parameters of the $(\alpha(\mu), \sin^2\theta_w^{\overline{MS}}(\mu), M_Z)$ scheme. In each mass bin, the first three columns indicate the lower and upper bin edges and the respective centre of the bin. The last two columns show the values of $(\alpha(\mu))^{-1}$ and $\sin^2\theta_w^{\overline{MS}}(\mu)$ at $\mu = \hat{M}_{\ell\bar{\ell}}$ as predicted by the Standard Model running.

$1-3.5$ TeV. Accordingly, the total correction ranges from 3.5% at 1 TeV to a maximum of approximately 5% at 3.5 TeV. It should be noted that there is a spurious effect due to ISR contributing to the total correction: in fact, the code tries to recombine all photons, without distinguishing between photons coming from FSR or from ISR, so it may happen that some initial-state radiation, by chance lying in the $\Delta R \leq 0.2$ cone, is occasionally mis-recombined to a final-state lepton; this has as a consequence a spurious enhancement of the correction due to ISR when switching on the recombination.

As it can be seen from Fig. 7.1, the remaining contributions of QED radiation from quarks and initial-final interference are small, reaching at most 1%. It has been checked that the ISR+IFI correction has a flat behaviour with dilepton invariant masses and stays within 1% between 1.5 TeV and 5 TeV. Since QED radiation from quarks is included in the analysis, one can conservatively estimate the uncertainty associated with this choice by squaring the magnitude of the corresponding contribution, which is therefore negligible for the present study.

Within the $(\alpha(\mu), \sin^2\theta_w^{\overline{MS}}(\mu), M_Z)$ scheme for the electroweak renormalization, the input parameters for the nominal template are set to their $\overline{MS}$ values at M_Z, and evolved to their value in each bin according to the renormalization group equation. The running of the couplings is computed by switching on the decoupling of the W boson and the top quark for $\mu < M_W$ and $\mu < m_{\text{top}}$, respectively, but not the $\mathcal{O}(\alpha)$ threshold correction for $\mu = M_W$, that is set to zero. The values of the parameters used in each bin are reported in Table 7.1. In the table and in the following, $\hat{M}_{\ell\bar{\ell}}$ denotes the central point of the bin. For each $M_{\ell\bar{\ell}}$ bin, three templates are generated: in the nominal one, the initial condition for the running of $\sin^2\theta_w^{\overline{MS}}(\mu)$ is set to the expected Standard Model value at the starting scale $\mu = \hat{M}_{\ell\bar{\ell}}$, while in the other two templates $\sin^2\theta_w^{\overline{MS}}(\mu)$ is varied from the nominal value of ± 0.01. The Standard Model running of $\alpha(\mu)$ is always assumed.

As final remark on the electroweak settings, the complex-mass scheme is used for the gauge-invariant handling of the unstable Z-boson propagator.

For what concerns the treatment of QCD corrections, the factorisation and renormalization scales are set in the code to $\mu_R = \mu_F = M_{\ell\bar{\ell}}$ and convoluted with the `NPDF31_nnlo_as_0118_hessian` [280] PDF set.

Finally, to obtain a realistic measurement scenario, parameterized lepton efficiencies and resolutions are employed to get a simplified description of the detector response. The leptonic identification and reconstruction efficiencies and energy-smearing functions are taken from ATLAS analyses during LHC Run 2 [281–283] and evaluated using RIVET [284].

7.3 Uncertainty estimation

The sensitivity study described here is completed with a quantification of experimental and theoretical uncertainties. While statistical uncertainties in the pseudo-data are simply extracted from the reconstructed-level number of events in each bin, systematics require a more careful evaluation. Starting from existing ATLAS measurement of high-mass Drell-Yan cross sections at $\sqrt{s} = 8$ TeV [285], systematic uncertainties in the lepton reconstruction and efficiencies have been extrapolated to the working conditions of Run 3 and HL-LHC, by applying a reduction of a factor of two and four, respectively. In the fit, these kind of uncertainties have been conservatively propagated to the different bins by taking them as uncorrelated in $M_{\ell\bar{\ell}}$, $|y_{\ell\bar{\ell}}|$ and $\cos\theta$. The luminosity is considered to be determined with an error of 1.5% for Run 3 and 1% for HL-LHC [277].

Theoretical uncertainties due to the knowledge of PDFs within the chosen set `NNPDF31_nnlo_as_0118_hessian` are evaluated by eigenvector propagation, while the error associated with the variation of scales and of the Bjorken variable is estimated by using interpolating grids generated with `Madgraph_aMC@NLO` and `aMCfast` [286, 287].

Another source of uncertainties is represented by missing higher-order terms in perturbative calculations of the cross sections, that within a sensitivity study can be estimated by making use of reasonable approximations. The state-of-art on neutral-current Drell-Yan production calculations consists in the inclusion of corrections up to N3LO in QCD [288] with exact NNLO mixed QCD-EW corrections [289–291] and up to NLO plus leading higher-order contributions in the electroweak coupling constant. For what concerns QCD corrections, missing NNLO and N3LO corrections can be quantified by examining the impact of seven-point scale variations of the renormalization and factorization scales, μ_R and μ_F, at both NNLO and N3LO, with the code `n3loxs` [292]. The study has been performed under the assumption that results not to depend on $|y_{\ell\bar{\ell}}|$ and $\cos\theta$, but only on the invariant mass of the di-lepton system. Furthermore, it does not include the effects of fiducial lepton selections, that can be neglected at high $M_{\ell\bar{\ell}}$. In the first four invariant mass bins, one finds similar

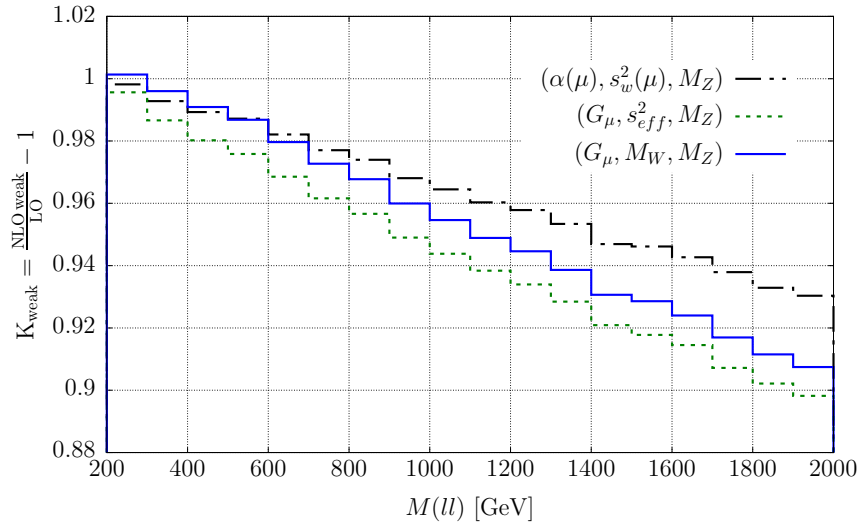## 7. Direct determination of the weak mixing angle at high energy

Figure 7.3: Effect of the pure weak corrections in the range between 200 GeV and 2 TeV, shown as the factor $K_{\text{weak}} = \text{NLO pure weak}/\text{LO} - 1$. It is clear the negative logarithmic growth due to Sudakov logs in all schemes shown: $\left(\alpha(\mu), \sin^2\theta_w^{\overline{MS}}(\mu), M_Z\right)$ (black strips), $\left(G_\mu, \sin^2\theta_{eff}^\ell, M_Z\right)$ (dotted green line) and (G_μ, M_W, M_Z) (solid blue line).

scale variations at NNLO and N3LO, while in the last two bins, NNLO scale variations are larger with respect to N3LO ones; nonetheless, the corrections to the cross section amount to $2-3\%$ at maximum, a value that is negligible when compared to the leading uncertainties in those bins, primarily due to PDF variations, which account for approximately 20% of the total error, and statistical uncertainties, that contribute up to 80% of the total error in the last bin. In the fit, also this class of uncertainty is propagated by assuming uncorrelation in $M_{\ell\bar{\ell}}$, $|y_{\ell\bar{\ell}}|$ and $\cos\theta$.

The pure weak radiative corrections amount to few 0.1% around the Z peak, but grow to $\mathcal{O}(10\%)$ at the few TeV scale because of the presence of Sudakov logarithms of the form $\alpha \log^2(M_{\ell\bar{\ell}}/M_V)$, where M_V is the mass of the gauge vector bosons, W or Z. An example of this behaviour can be seen in Fig. 7.3, where the correction due to pure weak contributions is shown as the factor:

$$K_{\text{weak}} = \frac{\text{NLO pure weak}}{\text{LO}} - 1\,, \tag{7.8}$$

in the range between 200 GeV and 2 TeV, for the three different schemes $\left(\alpha(\mu), \sin^2\theta_w^{\overline{MS}}(\mu), M_Z\right)$, $\left(G_\mu, \sin^2\theta_{eff}^\ell, M_Z\right)$ and (G_μ, M_W, M_Z). As one could expect, in the $\left(\alpha(\mu), \sin^2\theta_w^{\overline{MS}}(\mu), M_Z\right)$ scheme the effect is smaller when compared with the other two, due to the fact that part of the correction is reabsorbed in the running couplings. Fig. 7.4 shows a similar plot, but in the range $3.5-7$ TeV and for the two schemes (G_μ, M_W, M_Z) and $\left(\alpha(\mu), \sin^2\theta_w^{\overline{MS}}(\mu), M_Z\right)$, the latter with the two options "running turned on" or "running turned off".

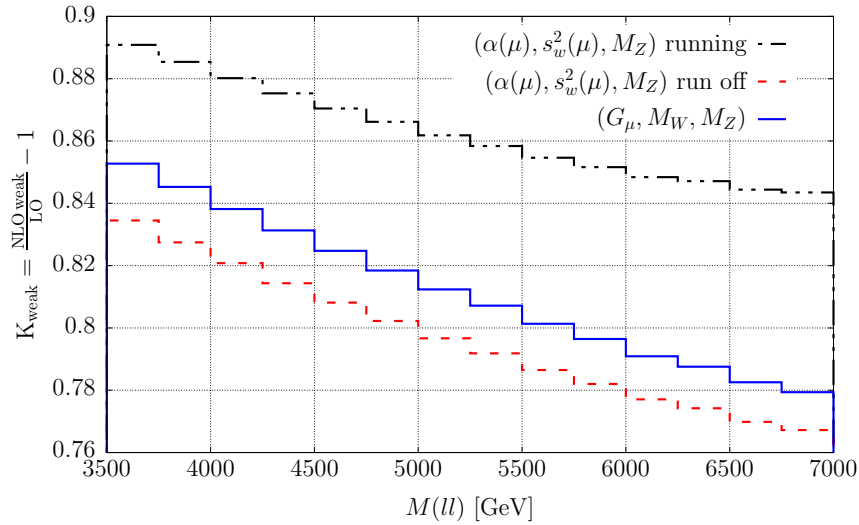## 7.3. Uncertainty estimation

Figure 7.4: Effect of the pure weak corrections in a pure Sudakov regime range between 3.5 TeV and 7 TeV, shown as the factor $K_{\text{weak}} = \text{NLO pure weak}/\text{LO} - 1$, for the $\left(\alpha(\mu), \sin^2 \theta_w^{\overline{MS}}(\mu), M_Z \right)$ scheme with running on (black strips) and off (red dashed line) and for (G_μ, M_W, M_Z) (solid blue line).

When the running is switched off, the couplings are set to their value at $\mu = M_Z$ and do not change with energy: in this case results in the $\overline{MS}$ scheme are very similar to ones in the $\left(\alpha(M_Z^2), \sin^2 \theta_{eff}^\ell, M_Z \right)$ scheme. In the $\overline{MS}$ scheme, the weak corrections amount to approximately 11% at 3.5 TeV up to 16% at 7 TeV. In the higher-mass region of the plot, it is visible a spurious effect due to the fact that the simulation is run with a centre-of-mass energy of 20 TeV and near 7 TeV one starts to reach the kinematical limit of the PDFs, where the Bjorken variable x acquires large values, causing an unphysical bending in the curves, still not clearly visible here, but more pronounced for higher invariant masses.

To treat electroweak corrections in the high energy regime with the due care, one should include in the code the resummation of large Sudakov logarithms, as proposed, for instance, in Ref. [293]. However, since this would fall outside the purpose of this analysis, we restrict our simulations to NLO fixed-order contributions. To quantify the uncertainty associated to missing electroweak higher-order contributions, we proceed in two ways. The first approach consists in a rough estimate, that can be obtained by squaring the size of the NLO weak correction: this leads to an uncertainty at the per cent level in the last $M_{\ell\bar{\ell}}$ bin. The second method is given by a two-point variation of the $\overline{MS}$ renormalization scale, which by default is fixed to $M_{\ell\bar{\ell}}$, of a factor of two, $\mu = M_{\ell\bar{\ell}}/2$ and $\mu = 2M_{\ell\bar{\ell}}$. When shifting the scale, the cross sections change by about $\mathcal{O}(\%)$ variations at LO accuracy and 0.1% at NLO. In both cases, considering that the statistical and PDF uncertainties in the last invariant-mass bin are at the level of 10%, one can conclude that the uncer-

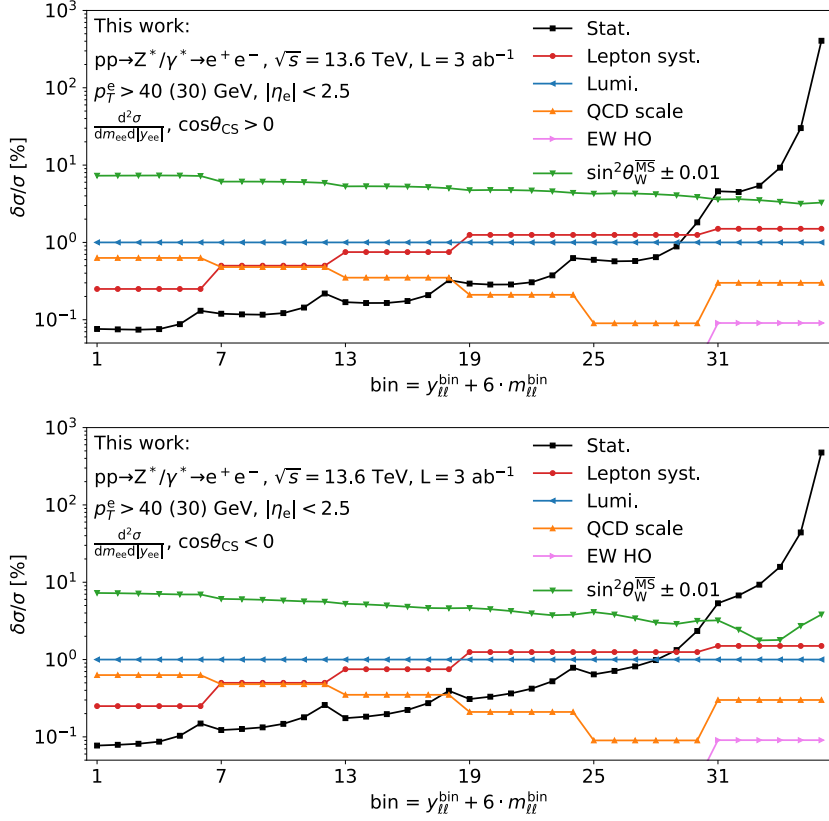# 7. Direct determination of the weak mixing angle at high energy

Figure 7.5: Relative contribution of the different sources of uncertainty to the triple differential cross section $\mathrm{d}\sigma/\mathrm{d}|y_{\ell\bar{\ell}}|\mathrm{d}M_{\ell\bar{\ell}}$ in the forward (up) and backward (bottom) directions, for the electron channel in the HL-LHC scenario. Variations of $\sin^2\theta_w^{\overline{MS}}(\mu)$ by a factor ± 0.01 are also shown.

tainty stemming from the inclusion of weak corrections would not change the sensitivity estimate discussed in the study.

Finally, the subtraction of background processes represents another source of uncertainty. In fact, it is customary in realistic analyses to regard for instance the emission of real W or Z bosons as a background, and subsequently subtract its contribution from data. Diboson production is however typically subdominant with respect to other backgrounds arising from top quark production processes with leptonic decays, so that both classes of processes should be properly treated as background. The assessment of uncertainties due to such backgrounds is usually derived from control regions by using empirical data, and as such its relevance would be diminished by increasing statistics. From existing high-mass Drell-Yan measurements [294], one can note that these uncertainties can be neglected if compared to other error sources.

The content of this section is summarised in Fig. 7.5, that illustrates the contributions of different uncertainty sources, as well as the variation of $\sin^2\theta_w^{\overline{MS}}(\mu)$ by ± 0.01 of the templates, for the triple-differential cross section

7.3. Uncertainty estimation

$\hat{M}_{\ell\bar{\ell}}$ [GeV]	$\sin^2\theta_W^{\overline{MS}}(\hat{M}_{\ell\bar{\ell}})$	Run 3		HL-LHC	
		$\delta\sin^2\theta_W^{\overline{MS}}(\hat{M}_{\ell\bar{\ell}})$	[%]	$\delta\sin^2\theta_W^{\overline{MS}}(\hat{M}_{\ell\bar{\ell}})$	[%]
133	0.23323	0.00216	0.9	0.00159	0.7
175	0.23468	0.00271	1.2	0.00202	0.9
250	0.23648	0.00339	1.4	0.00260	1.1
400	0.23885	0.00434	1.8	0.00345	1.4
1000	0.24350	0.00569	2.3	0.00468	1.9
3250	0.24954	0.01640	6.6	0.00870	3.5

Table 7.2: The Standard Model predicted value of the electroweak mixing angle in the $\overline{MS}$ renormalisation scheme in each invariant-mass bin, $\sin^2\theta_W^{\overline{MS}}(\hat{M}_{\ell\bar{\ell}})$, and the expected sensitivity $\delta\sin^2\theta_W^{\overline{MS}}(\hat{M}_{\ell\bar{\ell}})$ shown as absolute and in %, for the Run 3 and HL-LHC scenarios.
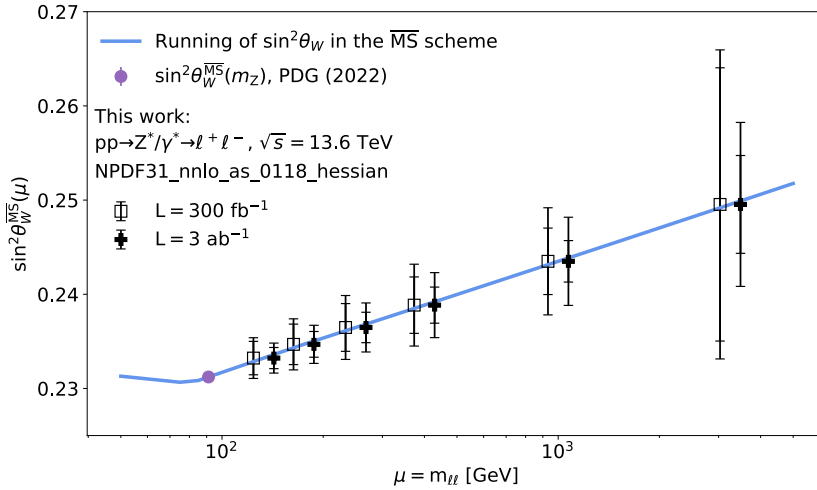
Figure 7.6: The scale dependence of the electroweak mixing angle as predicted by the SM RGE (blue line), compared to the combined experimental measurement at $\mu = M_Z$ (violet point) from hadronic and leptonic colliders. Our results are shown for LHC Run 3 (black crosses) and HL-LHC (black squares), shifted to the left and right with respect to the centre of the bin, respectively, for the sake of clarity. The outer error bars represent the total expected uncertainty on $\sin^2\theta_w^{\overline{MS}}(\mu)$, while the inner error bars include only statistical and experimental uncertainties (excluding PDFs, QCD and electroweak higher-order uncertainties).

in the electron channel and for the HL-LHC scenario. Considering the muon channel would yield similar results.

$\hat{M}_{\ell\bar{\ell}}$ [GeV]	$\delta \sin^2 \theta_W^{\overline{\mathrm{MS}}}(\hat{M}_{\ell\bar{\ell}})$ [%]				
	NNPDF31	NNPDF40	MSHT20	CT18A	ABMP16
133	0.5	0.3	0.6	0.9	0.5
175	0.6	0.4	0.8	1.0	0.6
250	0.8	0.5	0.9	1.2	0.7
400	1.2	0.6	1.2	1.5	0.8
1000	1.6	0.8	1.6	1.8	1.0
3250	2.7	1.6	2.5	2.8	1.3

Table 7.3: The contribution of the PDF uncertainty, coming from the use of different sets, to $\delta \sin^2 \theta_W^{\overline{\mathrm{MS}}}(\hat{M}_{\ell\bar{\ell}})$ in the HL-LHC scenario.

7.4 Results from the fit

To assess the sensitivity to the running weak mixing angle, the uncertainty $\delta \sin^2 \theta_w^{\overline{MS}}(\mu)$ on the expected value of the parameter is fitted in each bin, assuming a Standard Model running for $\alpha(\mu)$. To be more precise, the fit of the triple-differential cross section to the pseudo-data is performed in such a way that independent parameters for $\delta \sin^2 \theta_w^{\overline{MS}}(\mu)$ for each $M_{\ell\bar{\ell}}$ bin are determined simultaneously, by minimising a χ^2 function with the xFitter analysis tool [295]. When evaluating the χ^2, the cross section in each bin is considered to be linearly dependent on $\sin^2 \theta_w^{\overline{MS}}(\mu)$, an assumption that is valid within the range of variations considered. We include the statistical and experimental systematic uncertainties, and the theoretical uncertainties from PDFs and missing higher orders, in the χ^2 definition, as nuisance parameters that can be constrained in the fit.

The results on $\delta \sin^2 \theta_w^{\overline{MS}}(\mu)$ are presented in Table 7.2, in both absolute and relative form, and are illustrated in Fig. 7.6. The sensitivity on $\sin^2 \theta_w^{\overline{MS}}(\mu)$ ranges from about 1% to 7% under LHC Run 3 working conditions, and from 1% up to 3% for the HL-LHC. In this last case, a significant improvement can be expected in these figures, because at the HL-LHC larger datasets will make it possible to reduce experimental uncertainties.

As expected, the uncertainty on $\delta \sin^2 \theta_w^{\overline{MS}}(\mu)$ is dominated by the error from the PDFs in the kinematic range of high Bjorken x, that is probed in the high mass Drell-Yan production [278]. Given this, the fit has been repeated with different PDF sets, CT18ANNLO [296], MSHT20nnlo_as0118 [297], ABMP16_5_nnlo [298], and NNPDF40_nnlo_as_01180_hessian [299], to quantify the dependence of the results on the choice of the particular set. Table 7.3 shows the relative contribution coming from different PDF sets to $\delta \sin^2 \theta_w^{\overline{MS}}(\mu)$ for the HL-LHC working conditions. The PDF uncertainty heavily depends on the chosen set, varying by up to 50% in the last $M_{\ell\bar{\ell}}$ bin. Similar results are obtained if one considers in this study also PDF sets including the photon contribution.

The results shown here allow one to conclude that measurements of Drell-

7.4. Results from the fit

Yan production would make it possible to achieve a sensitivity on $\sin^2\theta_w^{\overline{MS}}(\mu)$ of the order of some per cent in the LHC Run 3 and at the per-cent level at the High Luminosity phase of the LHC. Even if this study, that has been performed by considering only the triple-differential cross section, has lead to promising results, in the future it would be necessary a more refined analysis that takes into account also other observables.

Conclusions and future prospects

This thesis work is framed within the global effort of pushing particle physics to the next frontier: the programme envisaged at the LHC and the HL-LHC in the next years foresees to explore the electroweak and Higgs sectors with a level of precision never reached before. This will open the possibility for high-precision determinations of fundamental parameters of the Standard Model, as the W-boson mass and the weak mixing angle, allowing for important consistency checks of the theory.

Since at hadronic colliders such measurements are obtained through a template-fit method, it is necessary to have a simulation setup which allows to perform the direct determination of these parameters with high accuracy: this implies being able to take into account as many orders as possible in perturbation theory, as well as having under control the theoretical uncertainties of both intrinsic and parametric origin. In this work, we have analysed the theoretical ingredients which have to be considered for a precision determination of the weak mixing angle, both in its effective definition valid at the Z peak and at higher energies, and implemented them in a novel version of the package `Z_ew-BMNNPV`, which is devoted to the simulation of the neutral-current Drell-Yan process in the POWHEG-BOX-V2 code.

After a general introduction on the Lagrangian of the Standard Model and on the current status of precision determinations of the W mass and the weak mixing angle, the focus has been on the renormalization procedure in the electroweak sector of the Standard Model, and in particular on the choice of the input parameters when defining the renormalization scheme. The use of a scheme including the parameter to be measured in input is essential to perform its determination in a consistent way at every perturbative order. Different sets of electroweak input parameters and input data have been discussed in a critical way, in both on-shell and $\overline{MS}$ schemes. In particular, a novel scheme, featuring the $\overline{MS}$ weak mixing angle and electromagnetic coupling and the on-shell Z-boson mass as inputs, has been developed. Such a scheme opens the

possibility of a high-energy test of the Standard Model, in the region above 1 TeV: the sensitivity to the weak mixing angle of future time-like datasets collected during Run 3 and HL-LHC has been explored here for the first time.

The critical comparison among different schemes at the best possible accuracy, which can be regarded as a conservative measure of the theoretical uncertainty associated to the choice of the scheme, has been completed by connecting our findings to the ones obtained at LEP: with an appropriate tuning of the parameters and a careful treatment of the corrections which are formally beyond the considered perturbative order, in fact, the difference among schemes can be considerably reduced and brought back to the precision level claimed at LEP, at least for the $Z\ell\bar{\ell}$ width.

In addition, other aspects have to be taken into account when considering electroweak corrections to the NCDY: in this work, three different options for handling the Z resonance in a gauge invariant way, which already existed in the literature, have been implemented in the Monte Carlo and their effects on differential distributions have been compared. Furthermore, we discussed new implemented options for taking into account the hadronic contribution to the running of the electromagnetic coupling. On top of this, we have explored the size of pure QED corrections as well as the possibility of building a Sudakov approximation of the NLO contribution when going to high energies: this latter aspect is important if one aims at resumming the large-logarithm effects at all orders.

To discuss all these results, a realistic simulation of the neutral-current Drell-Yan process $pp \to \mu^+\mu^-$ has been studied, focusing on the differential cross section and forward-backward asymmetry as functions of the lepton-pair invariant mass, making it possible to evaluate the effects of the discussed radiative corrections on these observables. As such, this work can be a precious contribution for the data analysis connected to the precise determination of the weak mixing angle at the Z peak or above.

From the point of view of theory and numerical development, the present code could be interfaced to existing tools in the literature which assure exact NNLO accuracy at the Z peak, thus obtaining an event generator able to provide NNLO predictions at the resonance, while retaining the current accuracy, which comprises NLO+universal higher-order contributions, in the non-resonant region.

Finally, a phenomenological expansion of this work will consist in a study of the sensitivity not only to the $\overline{MS}$ weak mixing angle, but also to the running electromagnetic coupling, by performing a two-variable fit in future LHC scenarios. In fact, the possible outcomes of the direct determination of the running weak mixing angle and electromagnetic coupling could be compared with the evolution of these parameters from low to the highest energies as predicted by the Renormalization Group Evolution equation, providing a fundamental test of the Standard Model.

The running of α

A.1 The $\Delta\alpha$ correction term

The results for the calculation of $\Delta\alpha(k^2)$ are here presented, for a generic k^2 momentum transfer, in the OS scheme, by taking into account the full fermionic+bosonic correction to the process $q\bar{q} \to\to \ell^-\ell^+$. The starting point is the relation:

$$\Delta\alpha(k^2) = -\mathrm{Re}\left[\frac{\Sigma_T^{AA}(k^2)}{k^2} + 2\frac{s_w}{c_w}\frac{\Sigma^{AZ}(0)}{M_Z^2} + 2\delta Z_e^{OS}\right] , \qquad \text{(A.1)}$$

from which, by making use of Eq. (3.65), one finds:

- $0 < k^2 < 4m_i^2$ for all m_i appearing in the expression

$$
\begin{aligned}
\Delta\alpha(k^2) = & \ \frac{\alpha}{4\pi}\left\{\frac{4}{3}\sum_f N_f Q_f^2\left[-\frac{5}{3} - 4\frac{m_f^2}{k^2}\right.\right. && \text{(A.2)}\\
& + \left.\left(4\frac{m_f^4}{k^4} + \frac{m_f^2}{k^2} - \frac{1}{2}\right)\frac{4}{\sqrt{\frac{4m_f^2}{k^2}-1}}\arctan\left(\frac{1}{\sqrt{\frac{4m_f^2}{k^2}-1}}\right)\right]\\
& + \frac{16}{3} + 8\frac{M_W^2}{k^2}\\
& - \left.\left(8\frac{M_W^4}{k^4} + 4\frac{M_W^2}{k^2} - \frac{3}{2}\right)\frac{4}{\sqrt{\frac{4M_W^2}{k^2}-1}}\arctan\left(\frac{1}{\sqrt{\frac{4M_W^2}{k^2}-1}}\right)\right\}
\end{aligned}
$$

- $k^2 < 0$ or $k^2 > 4m_i^2$ for all m_i appearing in the expression

$$
\Delta\alpha(k^2) = \frac{\alpha}{4\pi}\left\{ \frac{4}{3}\sum_f N_f Q_f^2 \left[-\frac{5}{3} - 4\frac{m_f^2}{k^2} \right. \right.
\tag{A.3}
$$

$$
+ \left(4\frac{m_f^4}{k^4} + \frac{m_f^2}{k^2} - \frac{1}{2} \right) \frac{2}{\sqrt{1-\frac{4m_f^2}{k^2}}} \ln\left| \frac{1-\sqrt{1-\frac{4m_f^2}{k^2}}}{1+\sqrt{1-\frac{4m_f^2}{k^2}}} \right| \right]
$$

$$
+ \frac{16}{3} + 8\frac{M_W^2}{k^2}
$$

$$
- \left(8\frac{M_W^4}{k^4} + 4\frac{M_W^2}{k^2} - \frac{3}{2} \right) \frac{2}{\sqrt{\frac{4M_W^2}{k^2}-1}} \ln\left| \frac{1-\sqrt{1-\frac{4M_W^2}{k^2}}}{1+\sqrt{1-\frac{4M_W^2}{k^2}}} \right| \right\}.
$$

In the $\overline{MS}$ scheme, one can write, by using the definition of the QED counterterm in Eq. (3.67):

$$
\Delta\alpha(k^2,\mu^2) = -\mathrm{Re}\left[\frac{\Sigma_T^{AA}(k^2)}{k^2} + 2\frac{s_w}{c_w}\frac{\Sigma^{AZ}(0)}{M_Z^2} + 2\delta Z_e^{\overline{MS}} \right],
\tag{A.4}
$$

and thus:

- $0 < k^2 < 4m_i^2$ for all m_i appearing in the expression

$$
\Delta\alpha(k^2,\mu^2) = \frac{\alpha(\mu)}{4\pi}\left\{ \frac{4}{3}\sum_f N_f Q_f^2 \left[-\frac{5}{3} + \ln\frac{m_f^2}{\mu^2} - 4\frac{m_f^2}{k^2} \right. \right.
\tag{A.5}
$$

$$
+ \left(4\frac{m_f^4}{k^4} + \frac{m_f^2}{k^2} - \frac{1}{2} \right) \frac{4}{\sqrt{\frac{4m_f^2}{k^2}-1}} \arctan\left(\frac{1}{\sqrt{\frac{4m_f^2}{k^2}-1}} \right) \right]
$$

$$
+ \frac{16}{3} - 7\ln\frac{M_W^2}{\mu^2} + 8\frac{M_W^2}{k^2}
$$

$$
- \left(8\frac{M_W^4}{k^4} + 4\frac{M_W^2}{k^2} - \frac{3}{2} \right)
$$

$$
\cdot \frac{4}{\sqrt{\frac{4M_W^2}{k^2}-1}} \arctan\left(\frac{1}{\sqrt{\frac{4M_W^2}{k^2}-1}} \right) \right\}
$$

A.1. The $\Delta\alpha$ correction term

- $k^2 < 0$ or $k^2 > 4m_i^2$ for all m_i appearing in the expression

$$\Delta\alpha(k^2, \mu^2) = \frac{\alpha(\mu)}{4\pi}\left\{\frac{4}{3}\sum_f N_f Q_f^2\left[-\frac{5}{3} + \ln\frac{m_f^2}{\mu^2} - 4\frac{m_f^2}{k^2}\right.\right.$$

$$+ \left(4\frac{m_f^4}{k^4} + \frac{m_f^2}{k^2} - \frac{1}{2}\right)\frac{2}{\sqrt{1 - \frac{4m_f^2}{k^2}}}\left.\ln\left|\frac{1 - \sqrt{1 - \frac{4m_f^2}{k^2}}}{1 + \sqrt{1 - \frac{4m_f^2}{k^2}}}\right|\right]$$

$$+ \frac{16}{3} - 7\ln\frac{M_W^2}{\mu^2} + 8\frac{M_W^2}{k^2}$$

$$\left. - \left(8\frac{M_W^4}{k^4} + 4\frac{M_W^2}{k^2} - \frac{3}{2}\right)\frac{2}{\sqrt{\frac{4M_W^2}{k^2} - 1}}\ln\left|\frac{1 - \sqrt{1 - \frac{4M_W^2}{k^2}}}{1 + \sqrt{1 - \frac{4M_W^2}{k^2}}}\right|\right\}. \tag{A.6}$$

The limit for $k^2 \to 0$ is:

$$\Delta\alpha(0, \mu^2) = -\frac{\alpha(\mu)}{4\pi}\left\{\frac{4}{3}\sum_f N_f Q_f^2 \ln\frac{\mu^2}{m_f^2} - 7\ln\frac{\mu^2}{M_W^2}\right\}. \tag{A.7}$$

A.1.1 The relation between α and $\alpha(\mu)$

We consider the $ee\gamma$ vertex one-loop function, with on-shell electron lines, in the limit of vanishing photon momentum, i.e. $k^2 \to 0$. In this limit, the general relation defining the three-point renormalized Green function in the $\overline{MS}$ scheme is:

$$\Gamma_{\mu,R}^{(1,2)}(k^2, p_1^2, p_2^2) = ie_R\gamma_\mu\left[1 + \delta Z_e - \frac{1}{2}\frac{\Sigma_T^{AA}(k^2)}{k^2}\right] = ie_R\gamma_\mu\left[1 + \frac{1}{2}\Delta\alpha(k^2, \mu^2)\right], \tag{A.8}$$

where the last equality makes use of the definition of $\Delta\alpha(k^2, \mu^2)$ of the previous section. In the $\overline{MS}$ scheme, and in the limit $k^2 \to 0$, this can be rewritten as:

$$\Gamma_{\mu,R}^{(1,2)}(0, p^2, -p^2) = ie(\mu)\gamma_\mu\left[1 + \frac{1}{2}\Delta\alpha(0, \mu^2)\right]. \tag{A.9}$$

One thus obtains that the physical electric charge e is defined through the following relation:

$$e = e(\mu)\left[1 + \frac{1}{2}\Delta\alpha(0, \mu^2)\right] \tag{A.10}$$

In terms of α, by making use of Eq. (A.7), this can be expressed as:

$$\alpha = \alpha(\mu)\left[1 + \Delta\alpha(0, \mu^2)\right] = \alpha(\mu)\left[1 - \frac{\alpha(\mu)}{4\pi}\left\{\frac{4}{3}\sum_f N_f Q_f^2 \ln\frac{\mu^2}{m_f^2} - 7\ln\frac{\mu^2}{M_W^2}\right\}\right], \tag{A.11}$$

that coincide with the result (18) by S. Sakakibara [300] in the limit of QED in which only electrons contribute to $\Delta\alpha$. We perturbatively invert this equation, by writing:

$$
\begin{aligned}
\alpha &= \alpha(\mu) - \frac{\alpha^2(\mu)}{4\pi}\left\{\frac{4}{3}\sum_f N_f Q_f^2 \ln\frac{\mu^2}{m_f^2} - 7\ln\frac{\mu^2}{M_W^2}\right\} \\
&= \alpha(\mu) - \frac{\alpha(\mu)\,\alpha}{4\pi}\left\{\frac{4}{3}\sum_f N_f Q_f^2 \ln\frac{\mu^2}{m_f^2} - 7\ln\frac{\mu^2}{M_W^2}\right\} \\
&= \alpha(\mu)\left[1 - \frac{\alpha}{4\pi}\left\{\frac{4}{3}\sum_f N_f Q_f^2 \ln\frac{\mu^2}{m_f^2} - 7\ln\frac{\mu^2}{M_W^2}\right\}\right],
\end{aligned}
\tag{A.12}
$$

and thus:

$$
\alpha(\mu) = \frac{\alpha}{1 - \frac{\alpha}{4\pi}\left\{\frac{4}{3}\sum_f N_f Q_f^2 \ln\frac{\mu^2}{m_f^2} - 7\ln\frac{\mu^2}{M_W^2}\right\}}.
\tag{A.13}
$$

From the RG function, in the $\overline{MS}$ scheme, we find:

$$
\alpha(\mu) = \frac{\alpha(\mu_0)}{1 - \frac{\alpha(\mu_0)}{4\pi}\left[\frac{4}{3}\sum_f N_c^f Q_f^2 - 7\right]\ln\frac{\mu^2}{\mu_0^2}},
\tag{A.14}
$$

For μ^* such that $\Delta\alpha(0,\mu^*) = 0$, we have $\alpha(\mu) = \alpha$:

$$
\mu^* = \prod_f m_f^{4N_f Q_f^2/11}\, M_W^{-21/11} \simeq 2\cdot 10^{-5}\ \text{GeV}\,.
\tag{A.15}
$$

In the RGE the same result can be found by choosing the renormalization point $\mu_0 = \mu^*$, that is $\alpha(\mu_0) = \alpha$.

A.1.2   Check: the decoupling prescription does not modify the total amplitude

We consider at first the hybrid $\overline{MS}$ scheme with independent parameters $\alpha(\mu)$, M_W, M_Z and the complex-mass scheme to treat the resonance. The notation and the Feynman rules are taken from [107]. The amplitude of the Drell-Yan process $q\bar{q} \to \ell\bar{\ell}$, considering the weak NLO correction, reads:

$$
\begin{aligned}
\mathcal{M}^{\pm\pm} = \mathcal{A}^{\pm\pm}\Bigg\{ &-e^2(\mu)\frac{Q_q Q_\ell}{k^2}\left[F_{qq\gamma,\ weak}^{\pm}(k^2) + F_{\ell\ell\gamma,\ weak}^{\pm}(k^2)\right.&(\text{A.16})\\
&\left. +2\delta Z_e^{\overline{MS}} + \delta Z_{qq}^{\pm} + \delta Z_{\ell\ell}^{\pm} - \frac{\Sigma_T^{AA}(k^2)}{k^2}\right]\\
&-e^2(\mu)\frac{g_q^{\pm}g_\ell^{\pm}}{k^2 - \mu_Z^2}\left[F_{qqZ,\ weak}^{\pm}(k^2) + F_{\ell\ell Z,\ weak}^{\pm}(k^2) + \frac{\delta g_q^{\pm}}{g_q^{\pm}} + \frac{\delta g_\ell^{\pm}}{g_\ell^{\pm}}\right.\\
&\left.\left. +\delta Z_{qq}^{\pm} + \delta Z_{\ell\ell}^{\pm} - \frac{\Sigma_T^{ZZ}(k^2) - \delta M_Z^2}{k^2 - \mu_Z^2} + \frac{Q_\ell g_q^{\pm} + Q_q g_\ell^{\pm}}{g_q^{\pm}g_\ell^{\pm}}\frac{\Sigma_T^{AZ}(k^2)}{k^2}\right]\right\}\,,
\end{aligned}
$$

A.1. The $\Delta\alpha$ correction term

where:

$$A^{\pm\pm} = \bar{v}(\bar{q})\gamma^\mu \omega_\pm u(q)\bar{u}(\mu^-)\gamma^\nu \omega_\pm v(\mu^+)g_{\mu\nu}, \tag{A.17}$$

and:

$$\frac{\delta g_f^+}{g_f^+} = \delta Z_e^{\overline{MS}} + \frac{1}{c_w^2}\frac{\delta s_w}{s_w} \tag{A.18}$$

$$\frac{\delta g_f^-}{g_f^-} = \delta Z_e^{\overline{MS}} + \frac{s_w^2}{c_w^2}\frac{\delta s_w}{s_w} - \frac{I_3^f + s_w^2 Q_f}{I_3^f - s_w^2 Q_f}\frac{\delta s_w}{s_w}. \tag{A.19}$$

It is easy to see that, if one makes the change $\delta Z_e^{\overline{MS}} \to \delta Z_e^{\overline{DS}}$ with $\delta Z_e^{\overline{DS}}$ as in Eq. (3.108) to perform the decoupling of the top quark and the W boson, this amounts to write at one-loop order:

$$
\begin{aligned}
\alpha(\mu) &= \alpha[1 + \Delta\alpha(0,\mu^2)] \tag{A.20}\\
&\to \alpha\left\{1 + \Delta\alpha(0,\mu^2) - \frac{\alpha}{4\pi}\left[\frac{4}{3}N_c^t Q_t^2 \ln\frac{\mu^2}{m_f^2} - 7\ln\frac{\mu^2}{M_W^2} - \frac{2}{3}\right]\right\}\\
&= \alpha\left\{1 - \frac{\alpha}{4\pi}\left[\frac{4}{3}\sum_f N_c^f Q_f^2 \ln\frac{\mu^2}{m_f^2} - 7\ln\frac{\mu^2}{M_W^2} - \frac{2}{3}\right]\right.\\
&\quad\left. - \frac{\alpha}{4\pi}\left[\frac{4}{3}N_c^t Q_t^2 \ln\frac{\mu^2}{m_t^2} - 7\ln\frac{\mu^2}{M_W^2} - \frac{2}{3}\right]\right\},
\end{aligned}
$$

and:

$$2\,\delta Z_e^{\overline{MS}} \to 2\,\delta Z_e^{\overline{MS}} + \frac{\alpha}{4\pi}\left[\frac{4}{3}N_c^t Q_t^2 \ln\frac{\mu^2}{m_f^2} - 7\ln\frac{\mu^2}{M_W^2} - \frac{2}{3}\right]. \tag{A.21}$$

The correction in Eq. (A.16) is proportional to:

$$
\alpha(\mu) \left\{ 2\, \delta Z_e^{\overline{MS}} + \text{other terms} \right\} \rightarrow \alpha \left\{ 1 + \right.
$$

$$
- \frac{\alpha}{4\pi} \left[\frac{4}{3} \sum_f N_c^f Q_f^2 \ln \frac{\mu^2}{m_f^2} - 7 \ln \frac{\mu^2}{M_W^2} - \frac{2}{3} \right]
$$

$$
- \frac{\alpha}{4\pi} \left[\frac{4}{3} N_c^t Q_t^2 \ln \frac{\mu^2}{m_f^2} - 7 \ln \frac{\mu^2}{M_W^2} - \frac{2}{3} \right]
$$

$$
+ 2\, \delta Z_e^{\overline{MS}}
$$

$$
+ \frac{\alpha}{4\pi} \left[\frac{4}{3} N_c^t Q_t^2 \ln \frac{\mu^2}{m_f^2} - 7 \ln \frac{\mu^2}{M_W^2} - \frac{2}{3} \right]
$$

$$
\left. + \text{other terms} \right\}
$$

$$
= \alpha \left\{ 1 + \right.
$$

$$
- \frac{\alpha}{4\pi} \left[\frac{4}{3} \sum_f N_c^f Q_f^2 \ln \frac{\mu^2}{m_f^2} - 7 \ln \frac{\mu^2}{M_W^2} - \frac{2}{3} \right]
$$

$$
\left. + 2\, \delta Z_e^{\overline{MS}} + \text{other terms} \right\}
$$

$$
= \alpha(\mu) \left\{ 2\, \delta Z_e^{\overline{MS}} + \text{other terms} \right\}, \qquad \text{(A.22)}
$$

where the equalities are valid at NLO.

B

The running of $s_w^2(\mu)$

In this appendix we explicitly derive the relevant formulae for the implementation of higher-order contributions to the RGE of $\sin^2 \theta_w^{\overline{MS}}(\mu)$, as performed in [77]. We start from Eq. (18) by [77], which can be obtained from the $\mathcal{O}(\alpha)$ running:

$$\mu^2 \frac{ds_w^2(\mu^2)}{d\mu^2} = \frac{\alpha(\mu^2)}{\pi} \left[\frac{1}{24} \sum_i N_i^c \gamma_i \left(Q_i^2 s_w^2(\mu^2) - I_{3,i} Q_i \right) \right] , \qquad \text{(B.1)}$$

by modifying the colour factors to K_i and adding the $\mathcal{O}(\alpha_S^3)$ contributions due to σ:

$$
\begin{aligned}
\mu^2 \frac{ds_w^2(\mu^2)}{d\mu^2} &= \frac{\alpha(\mu^2)}{\pi} \left[\frac{1}{24} \sum_i K_i \gamma_i \left(Q_i^2 s_w^2(\mu^2) - I_{3,i} Q_i \right) \right. \\
&\left. + \sigma s_w^2(\mu^2) \left(\sum_q Q_q \right)^2 - \frac{\sigma}{2} \left(\sum_q I_{3,q} \right) \left(\sum_q Q_q \right) \right]
\end{aligned}
\qquad \text{(B.2)}
$$

By making use of the running of $\alpha(\mu)$ in Eq. (3.93) one gets:

$$\mu^2 \frac{d}{d\mu^2} \left(\frac{s_w^2(\mu)}{\alpha(\mu)} \right) = -\frac{1}{24\pi} \sum_i K_i \gamma_i I_{3,i} Q_i - \frac{\sigma}{2\pi} \left(\sum_q I_{3,q} \right) \left(\sum_q Q_q \right) , \quad \text{(B.3)}$$

By using the definition of λ_1 in Eq. (3.99), we can write:

$$\mu^2 \frac{d}{d\mu^2} \left(\frac{\lambda_1}{\alpha(\mu)} \right) = -\mu^2 \lambda_1 \frac{1}{\alpha^2(\mu)} \frac{d\alpha(\mu)}{d\mu^2} = -\frac{\lambda_1}{\pi} \left[\frac{1}{24} \sum_i K_i \gamma_i Q_i^2 + \sigma \left(\sum_q Q_q \right)^2 \right] .$$

$$\text{(B.4)}$$

Subtracting this equation from Eq. (B.3) one gets:

$$\mu^2 \frac{d}{d\mu^2}\left(\frac{s_w^2(\mu)}{\alpha(\mu)} - \frac{\lambda_1}{\alpha(\mu)}\right) = -\frac{1}{24\pi}\sum_i K_i\gamma_i(I_{3,i}Q_i - \lambda_1 Q_i^2) \tag{B.5}$$

$$-\frac{\sigma}{2\pi}\left(\sum_q I_{3,q}\right)\left(\sum_q Q_q\right) + \lambda_1 \frac{\sigma}{\pi}\left(\sum_q Q_q\right)^2.$$

Now, we write $K_i = K_i^{QED} + K^{QCD}$ and:

$$\sum_i K_i\gamma_i(T_iQ_i - \lambda_1 Q_i^2) = \sum_{l=lept.,bos.}(1 + K_l^{QED})\gamma_l(I_{3,l}Q_l - \lambda_1 Q_l^2) \tag{B.6}$$

$$+ \sum_q K^{QCD}\gamma_q\left(I_{3,q}Q_q - \frac{\sum_q I_{3,q}Q_q}{2\sum_{q=LH}Q_q^2}Q_q^2\right).$$

By exploiting the fact that γ_q and K_q are the same for every quark, the last term can be written as:

$$K^{QCD}\gamma_q \sum_{q=LH,RH}\left(I_{3,q}Q_q - \frac{\sum_{q=LH,RH}I_{3,q}Q_q}{\sum_{q=LH,RH}Q_q^2}Q_q^2\right) = 0, \tag{B.7}$$

where we eliminated the factor 2 at the denominator and performed the sum on both LH and RH particles. Thus:

$$\sum_i K_i\gamma_i(I_{3,i}Q_i - \lambda_1 Q_i^2) = \sum_{b=bos.}N_b^c\gamma_b(I_{3,b}Q_b - \lambda_1 Q_b^2)$$

$$+ \sum_{l=lept.}(I_{3,l}Q_l - \lambda_1 Q_l^2)\frac{3}{4}\frac{\alpha}{\pi}Q_l^2 N_l^c\gamma_l. \tag{B.8}$$

From Eq. (19) by [77], we can also write:

$$\frac{\alpha}{\pi} = \frac{1}{\alpha}\left(\mu^2\frac{d\alpha}{d\mu^2}\right)\frac{1}{\frac{1}{24}\sum_i K_i\gamma_i Q_i^2 + \sigma\left(\sum_q Q_q\right)^2}, \tag{B.9}$$

where:

$$\mu^2\frac{1}{\alpha}\frac{d\alpha}{d\mu^2} = \mu^2\frac{d}{d\mu^2}\ln\alpha, \tag{B.10}$$

and, expanding at $O(\alpha)$:

$$\frac{1}{\frac{1}{24}\sum_i K_i\gamma_i Q_i^2 + \sigma\left(\sum_q Q_q\right)^2} \simeq \frac{1}{\frac{1}{24}\sum_i N_i^c\gamma_i Q_i^2} \tag{B.11}$$

$$\cdot \left[1 - \frac{K_{QED}^i + K_{QCD} + \sigma\left(\sum_q Q_q\right)^2}{\sum_i N_i^c\gamma_i Q_i^2}\right].$$

Putting everything together we can write:

$$\mu^2 \frac{d}{d\mu^2} \left(\frac{s_w^2 - \lambda_1}{\alpha} + \frac{3}{4\pi} \frac{\sum_{l=lept.}(I_{3,l}Q_l^3 - \lambda_1 Q_l^4)N_l^c \gamma_l}{\sum_i N_i^c \gamma_i Q_i^2} \ln \alpha \right) =$$

$$- \frac{1}{24\pi} \sum_i N_i^c \gamma_i (I_{3,i}Q_i - \lambda_1 Q_i^2)$$

$$+ \frac{\sigma}{\pi} \left[\lambda_1 \left(\sum_q Q_q^2 \right)^2 - \frac{1}{2} \left(\sum_q I_{3,q} \right) \left(\sum_q Q_q \right) \right]. \qquad (B.12)$$

By using the definitions of $\lambda_1, \lambda_2, \lambda_3, \lambda_4$ in Eqs. (3.99)–(3.102), the last equation becomes:

$$\mu^2 \frac{d}{d\mu^2} \left(\frac{s_w^2 - \lambda_1}{\alpha} - \frac{3}{4\pi} \lambda_3 \ln \alpha \right) = \frac{\lambda_2}{3\pi} + \frac{\sigma}{\pi} \lambda_4. \qquad (B.13)$$

Now we observe that:

$$\sigma \sim \alpha_s^3 = \alpha_s^2 \alpha_s = \frac{-\beta(\alpha_s)}{b_0} \alpha_s = -\mu^2 \frac{d\alpha_s}{d\mu^2} \frac{1}{b_0} \alpha_s = -\frac{1}{b_0} \frac{1}{2} \mu^2 \frac{d}{d\mu^2} \alpha_s^2, \qquad (B.14)$$

with:

$$b_0 = \frac{1}{12\pi}(35 - 2n_q). \qquad (B.15)$$

Thus we have:

$$\begin{aligned}
\frac{\sigma}{\pi} \lambda_4 &= \alpha_s \frac{1}{\pi} \lambda_4 \frac{\alpha_s^3}{\pi^3} \frac{5}{9} \left(\frac{11}{24} - \zeta(3) \right) && (B.16) \\
&= \lambda_4 \frac{1}{\pi^3} \frac{5}{9} \left(\frac{11}{24} - \zeta(3) \right) \left(-\mu^2 \frac{d}{d\mu^2} \alpha_s^2 \right) \frac{6}{33 - 2n_q} \\
&= -\frac{\lambda_4}{\pi^3} \left(\mu^2 \frac{d}{d\mu^2} \alpha_s^2 \right) \frac{5}{36} \frac{11 - 24\zeta(3)}{33 - 2n_q} \\
&= -\mu^2 \frac{d}{d\mu^2} \left[\frac{\lambda_4}{\pi} \frac{\alpha_s^2}{\pi^2} \frac{5}{36} \frac{11 - 24\zeta(3)}{33 - 2n_q} \right] = -\mu^2 \frac{d}{d\mu^2} \tilde{\sigma}(\mu).
\end{aligned}$$

We can now write:

$$\mu^2 \frac{d}{d\mu^2} \left(\frac{s_w^2 - \lambda_1}{\alpha} - \frac{3}{4\pi} \lambda_3 \ln \alpha + \frac{\tilde{\sigma}}{\pi} \right) = \frac{\lambda_2}{3\pi}, \qquad (B.17)$$

that is Eq. (23) by [77]. We conclude that terms with coefficients λ_1 and λ_2 are already $O(\alpha)$ and h.o. contributions can be included by simply adding terms in λ_3 and λ_4.

C

The treatment of the resonance in the `Z_ew-BMNNPV` code

In this appendix we address some issues connected with the resonance treatment within the `Z_ew-BMNNPV` package of POWHEG-BOX-V2, which have led to change the old default prescription to the complex-mass one, and to the implementation of other gauge independent variants like the pole and the factorization scheme. The main result of the calculation here presented is that the difference between the old prescription (denoted as CLA scheme) and the pole scheme is gauge dependent in the R_ξ-gauge class in the case of the neutral current Drell-Yan process at NLO EW.

In the following, renormalized vertex and self-energies are denoted with a caret, to distinguish them from bare ones. We start by writing the neutral

current Drell-Yan amplitude at NLO EW with the old prescription:

$$
\begin{aligned}
\mathcal{M}_{\mathrm{CLA}}^{\pm\pm} \;=\; & -Q_q Q_\ell\, e^2 A_{spinor}^{\pm\pm} \frac{1}{k^2} \left[1 + \Delta\alpha(k^2) - \frac{i\mathrm{Im}\Sigma_T^{AA}(k^2)}{k^2} \right. \\[4pt]
& -\frac{1}{2}\left(\frac{g_q^\pm}{Q_q} + \frac{g_\ell^\pm}{Q_\ell} \right) \delta Z_{ZA} + \delta Z_q^\pm + \delta Z_\ell^\pm \\[4pt]
& \left. + \hat{F}_{qqV,\,\mathrm{phot}}(k^2) + \hat{F}_{\ell\ell V,\,\mathrm{phot}}(k^2) + F_{qq\gamma,\,\mathrm{weak}}^\pm(k^2) + F_{\ell\ell\gamma,\,\mathrm{weak}}^\pm(k^2) \right] \\[6pt]
& - e^2 (g_q^\pm)(g_\ell^\pm) A_{spinor}^{\pm\pm} \frac{1}{k^2 - M_Z^2 + i\Gamma_z M_Z} \left[1 + \Delta\alpha(k^2) + \frac{\mathrm{Re}\Sigma_T^{AA}(k^2)}{k^2} \right. \\[4pt]
& + \left(\frac{\delta g_q^\pm}{g_q^\pm} - \delta Z_e \right) + \left(\frac{\delta g_\ell^\pm}{g_\ell^\pm} - \delta Z_e \right) + \delta Z_q^\pm + \delta Z_\ell^\pm \\[4pt]
& + \frac{Q_\ell}{g_\ell^\pm} \frac{\Sigma_T^{AZ}(k^2)}{k^2} + \frac{Q_q}{g_q^\pm} \frac{\Sigma_T^{AZ}(k^2)}{k^2} + \frac{1}{2}\left(\frac{g_q^\pm}{Q_q} + \frac{g_\ell^\pm}{Q_\ell} \right) \delta Z_{ZA} \\[4pt]
& - \frac{\Sigma_T^{ZZ}(k^2) - \Sigma_T^{ZZ}(M_Z^2)}{k^2 - M_Z^2} \\[4pt]
& \left. + \hat{F}_{qqV,\,\mathrm{phot}}(k^2) + \hat{F}_{\ell\ell V,\,\mathrm{phot}}(k^2) + F_{qqZ,\,\mathrm{weak}}^\pm(k^2) + F_{\ell\ell Z,\,\mathrm{weak}}^\pm(k^2) \right] \\[4pt]
& + A_{spinor}^{\pm\pm} \left[f_{q\bar q}^{\gamma\gamma,\,\pm\pm}(s,t) + f_{q\bar q}^{Z\gamma\,\pm\pm}(s,t) + f_{q\bar q}^{ZZ,\,\pm\pm}(s,t) + f_{q\bar q}^{WW,\,\pm\pm}(s,t) \right] \,,
\end{aligned}
\tag{C.1}
$$

with $s = k^2$ and:

$$
A_{spinor}^{\pm\pm} = \bar{v}(p_2)\gamma^\mu \omega_\pm u(p_1)\bar{u}(p_3)\gamma^\nu \omega_\pm v(p_4)(-i)g_{\mu\nu}\,.
\tag{C.2}
$$

In the pole scheme, introduced in [86], we have:

$$
\begin{aligned}
\mathcal{M}_{\mathrm{PS}}^{\pm\pm} \;=\; & A_{spinor}^{\pm\pm} \left[f_{q\bar q}^{\mathrm{LO},\,\pm\pm}(s) + f_{q\bar q,\,\mathrm{phot}}^{\mathrm{vert},\,\pm\pm}(s) + f_{q\bar q,\,\mathrm{phot}}^{\mathrm{box},\,\pm\pm}(s,t) \right. \tag{C.3} \\[4pt]
& \left. + f_{q\bar q,\,\mathrm{weak}}^{\mathrm{vert},\,\pm\pm}(s) + f_{q\bar q,\,\mathrm{weak}}^{\mathrm{self},\,\pm\pm}(s) + f_{q\bar q,\,\mathrm{weak}}^{\mathrm{box},\,\pm\pm}(s,t) \right] . \tag{C.4}
\end{aligned}
$$

with the leading order term:

$$
f_{q\bar q}^{\mathrm{LO},\,\pm\pm}(s = k^2) = -e^2 \left[\frac{Q_q Q_\ell}{k^2} + \frac{g_q^\pm\, g_\ell^\pm}{k^2 - M_Z^2 + i\Gamma_z M_Z} \right] ,
\tag{C.5}
$$

which of course is the same as in Eq. (C.1). In the same way, also the box contributions are the same in our scheme and the one in [86], namely:

$$
\begin{aligned}
f_{q\bar q,\,\mathrm{phot}}^{\mathrm{box},\,\pm\pm}(s,t) &= f_{q\bar q}^{\gamma\gamma,\,\pm\pm}(s,t) + f_{q\bar q}^{Z\gamma\,\pm\pm}(s,t)\,, \\[4pt]
f_{q\bar q,\,\mathrm{weak}}^{\mathrm{box},\,\pm\pm}(s,t) &= f_{q\bar q}^{ZZ,\,\pm\pm}(s,t) + f_{q\bar q}^{WW,\,\pm\pm}(s,t)\,,
\end{aligned}
\tag{C.6}
$$

since the box diagrams are non resonant and do not receive any modification in the pole scheme. Pure QED vertex corrections given by the factor:

$$
\begin{aligned}
f_{q\bar q,\,\mathrm{phot}}^{\mathrm{vert},\,\pm\pm}(s) \;=\; & -e^2 \left[\hat{F}_{qqV,\,\mathrm{phot}}(k^2) + \hat{F}_{\ell\ell V,\,\mathrm{phot}}(k^2) \right] \tag{C.7} \\[4pt]
& \left[\frac{Q_q Q_\ell}{k^2} + (g_q^\pm)(g_\ell^\pm)\frac{1}{k^2 - M_Z^2 + i\Gamma_z M_Z} \right] ,
\end{aligned}
$$

are as well the same in both schemes. We can thus safely focus on the pure weak part of the vertex and self-energy corrections. We can split the calculation into different pieces and compare them one at the time with the corresponding one in the pole scheme. For a better comparison with the expressions in [86], we write the relevant part of the amplitude in Eq. (C.1) in terms of renormalized vertex and self-energies:

$$
\begin{aligned}
\mathcal{M}_{\mathrm{CLA}}^{\pm\pm} &= -Q_q Q_\ell\, e^2 A_{spinor}^{\pm\pm} \frac{1}{k^2} \left[1 - \frac{\hat{\Sigma}_T^{AA}(k^2)}{k^2} \right. \\
&\quad \left. + \hat{F}_{qq\gamma,\,\mathrm{weak}}^{\pm}(k^2) + \hat{F}_{\ell\ell\gamma,\,\mathrm{weak}}^{\pm}(k^2) \right] \\
&\quad - e^2 A_{spinor}^{\pm\pm} \frac{Q_q g_\ell^{\pm} + Q_\ell g_q^{\pm}}{k^2 - M_Z^2 + i\Gamma_Z M_Z} \frac{\hat{\Sigma}_T^{AZ}(k^2)}{k^2} \\
&\quad - e^2 (g_q^{\pm})(g_\ell^{\pm}) A_{spinor}^{\pm\pm} \frac{1}{k^2 - M_Z^2 + i\Gamma_z M_Z} \left[1 - \frac{\hat{\Sigma}_T^{ZZ}(k^2)}{k^2 - M_Z^2} \right. \\
&\quad \left. + \hat{F}_{qqZ,\,\mathrm{weak}}^{\pm}(k^2) + \hat{F}_{\ell\ell Z,\,\mathrm{weak}}^{\pm}(k^2) \right] \,.
\end{aligned}
\tag{C.8}
$$

In [86], the vertex and self-energy correction factors are written as:

$$
\begin{aligned}
f_{q\bar{q},\mathrm{weak}}^{\mathrm{vert},\,\pm\pm}(s) &= -e^2 \frac{Q_q Q_\ell}{k^2} \left[\hat{F}_{qq\gamma,\,\mathrm{weak}}^{\pm}(k^2) + \hat{F}_{\ell\ell\gamma,\,\mathrm{weak}}^{\pm}(k^2) \right] \\
&\quad - e^2\, g_q^{\pm} g_\ell^{\pm} \left[\frac{\hat{F}_{qqZ,\,\mathrm{weak}}^{\pm}(M_Z^2) + \hat{F}_{\ell\ell Z,\,\mathrm{weak}}^{\pm}(M_Z^2)}{k^2 - M_Z^2 + i\Gamma_Z M_Z} \right. \\
&\quad + \frac{\hat{F}_{qqZ,\,\mathrm{weak}}^{\pm}(k^2) - \hat{F}_{qqZ,\,\mathrm{weak}}^{\pm}(M_Z^2)}{k^2 - M_Z^2} \\
&\quad \left. + \frac{\hat{F}_{\ell\ell Z,\,\mathrm{weak}}^{\pm}(k^2) - \hat{F}_{\ell\ell Z,\,\mathrm{weak}}^{\pm}(M_Z^2)}{k^2 - M_Z^2} \right] \,,
\end{aligned}
\tag{C.9}
$$

$$
\begin{aligned}
f_{q\bar{q},\mathrm{weak}}^{\mathrm{self},\,\pm\pm}(s) &= -e^2 \frac{Q_q Q_\ell}{k^2} \hat{\Sigma}_T^{AA}(k^2) \\
&\quad + e^2 g_q^{\pm} g_\ell^{\pm} \left\{ \frac{-\hat{\Sigma}_T^{\prime\,ZZ}(M_Z^2)}{k^2 - M_Z^2 + i\Gamma_Z M_Z} \right. \\
&\quad \left. + \frac{\hat{\Sigma}_T^{ZZ}(k^2) - \hat{\Sigma}_T^{ZZ}(M_Z^2) - (k^2 - M_Z^2)\hat{\Sigma}_T^{\prime\,ZZ}(M_Z^2)}{(k^2 - M_Z^2)^2} \right\} \\
&\quad + (Q_\ell g_q^{\pm} + Q_q g_\ell^{\pm}) \left\{ \frac{1}{k^2 - M_Z^2 + i\Gamma_Z M_Z} \frac{\hat{\Sigma}_T^{AZ}(M_Z^2)}{M_Z^2} \right. \\
&\quad \left. + \frac{1}{k^2 - M_Z^2} \left(\frac{\hat{\Sigma}_T^{AZ}(k^2)}{k^2} - \frac{\hat{\Sigma}_T^{AZ}(M_Z^2)}{M_Z^2} \right) \right\} \,.
\end{aligned}
\tag{C.10}
$$

C. The treatment of the resonance in the `Z_ew-BMNNPV` code

C.0.1 Photon-exchange contribution

The first term we consider is the γ-exchange contribution. In our prescription it reads:

$$
\begin{aligned}
\mathcal{M}_{\gamma,\mathrm{CLA}}^{\pm\pm} &= -Q_q Q_\ell\, e^2 A_{spinor}^{\pm\pm} \frac{1}{k^2} \left[\Delta\alpha(k^2) - \frac{i\mathrm{Im}\Sigma_T^{AA}(k^2)}{k^2} \right. && \text{(C.11)} \\
&\quad \left. + \left(\frac{g_q^\pm}{Q_q} + \frac{g_\ell^\pm}{Q_\ell} \right) \delta Z_{ZA} + F_{qqV,\,\mathrm{weak}}^\pm(k^2) + F_{\ell\ell V,\,\mathrm{weak}}^\pm(k^2) + \delta Z_q^\pm + \delta Z_\ell^\pm \right] \\
&= -Q_q Q_\ell\, e^2 A_{spinor}^{\pm\pm} \frac{1}{k^2} \left[2\delta Z_e + \delta Z_{AA} - \frac{\Sigma_T^{AA}(k^2)}{k^2} - \delta Z_{AA} \right. \\
&\quad \left. + \left(\frac{g_q^\pm}{Q_q} + \frac{g_\ell^\pm}{Q_\ell} \right) \delta Z_{ZA} + F_{qqV,\,\mathrm{weak}}^\pm(k^2) + F_{\ell\ell V,\,\mathrm{weak}}^\pm(k^2) + \delta Z_q^\pm + \delta Z_\ell^\pm \right] .
\end{aligned}
$$

We can furthermore split this contribution into vertex and self-energy terms, to make contact with what is done in [86].

Vertex contribution to photon exchange

The vertex correction to the γ exchange diagrams reads:

$$
-Q_q Q_\ell\, e^2 A_{spinor}^{\pm\pm} \frac{1}{k^2} \left[2\delta Z_e + \delta Z_{AA} - \frac{1}{2} \left(\frac{g_q^\pm}{Q_q} + \frac{g_\ell^\pm}{Q_\ell} \right) \delta Z_{ZA} \right. \tag{C.12}
$$

$$
\left. + F_{qqV,\,\mathrm{weak}}^\pm(k^2) + F_{\ell\ell V,\,\mathrm{weak}}^\pm(k^2) + \delta Z_q^\pm + \delta Z_\ell^\pm \right] , \tag{C.13}
$$

and is of course the same as in [86], namely:

$$
f_{q\bar{q},\mathrm{weak}}^{\mathrm{vert},\,\pm\pm}(s)\big|_\gamma = \hat{F}_{qq\gamma,\,\mathrm{weak}}^\pm(k^2) + \hat{F}_{\ell\ell\gamma,\,\mathrm{weak}}^\pm(k^2) , \tag{C.14}
$$

with:

$$
\begin{aligned}
\hat{F}_{qq\gamma,\,\mathrm{weak}}^\pm(k^2) &= F_{qq\gamma,\,\mathrm{weak}}^\pm(k^2) + \delta Z_e + \frac{1}{2}\delta Z_{AA} + \delta Z_q^\pm - \frac{1}{2}\frac{g_q^\pm}{Q_q}\delta Z_{ZA} , \\
\hat{F}_{\ell\ell\gamma,\,\mathrm{weak}}^\pm(k^2) &= F_{\ell\ell\gamma,\,\mathrm{weak}}^\pm(k^2) + \delta Z_e + \frac{1}{2}\delta Z_{AA} + \delta Z_\ell^\pm - \frac{1}{2}\frac{g_\ell^\pm}{Q_\ell}\delta Z_{ZA} ,
\end{aligned}
$$

since the photon contribution is non resonant.

Self-energy contribution to photon exchange

The self-energy correction to the γ exchange diagrams is:

$$
-\frac{\Sigma_T^{AA}(k^2)}{k^2} - \delta Z_{AA} \tag{C.15}
$$

which, being non resonant, is the same as in Eq. (C.9), with:

$$
\frac{\hat{\Sigma}_T^{AA}(k^2)}{k^2} = \frac{\Sigma_T^{AA}(k^2)}{k^2} + \delta Z_{AA} , \tag{C.16}
$$

which is of course the same for both prescriptions.

C.1   Calculation for $k^2 \neq M_Z^2$

C.1.1   Interference contribution

The mixed $Z - \gamma$ and $\gamma - Z$ contribution from Eq. (C.8) reads:

$$\mathcal{M}_{\text{interf,CLA}}^{\pm\pm} = -e^2 A_{spinor}^{\pm\pm} \frac{Q_q g_\ell^\pm + Q_\ell g_q^\pm}{k^2 - M_Z^2 + i\Gamma_Z M_Z} \frac{\hat{\Sigma}_T^{AZ}(k^2)}{k^2}, \tag{C.17}$$

which comes only from the renormalized self-energy diagrams:

$$\hat{\Sigma}_T^{AZ}(k^2) = \Sigma_T^{AZ}(k^2) + \frac{1}{2}k^2 \delta Z_{AZ} + \frac{1}{2}(k^2 - M_Z^2)\delta Z_{ZA}. \tag{C.18}$$

At NLO, for $k^2 \neq M_Z^2$ (that is, away from the Z peak) we can manipulate the expression in Eq. (C.17) in the following way:

$$
\begin{aligned}
\frac{1}{k^2 - M_Z^2 + i\Gamma_Z M_Z} \frac{\hat{\Sigma}_T^{AZ}(k^2)}{k^2} &= \frac{1}{k^2 - M_Z^2 + i\Gamma_Z M_Z} \\
&\quad \cdot \left[\frac{\hat{\Sigma}_T^{AZ}(k^2)}{k^2} - \frac{\hat{\Sigma}_T^{AZ}(M_Z^2)}{M_Z^2} + \frac{\hat{\Sigma}_T^{AZ}(M_Z^2)}{M_Z^2} \right] \\
&= \frac{1}{k^2 - M_Z^2} \left(1 - \frac{i\text{Im}\hat{\Sigma}_T^{ZZ}(M_Z^2)}{k^2 - M_Z^2} \right) \\
&\quad \cdot \left[\frac{\hat{\Sigma}_T^{AZ}(k^2)}{k^2} - \frac{\hat{\Sigma}_T^{AZ}(M_Z^2)}{M_Z^2} \right] \\
&\quad + \frac{1}{k^2 - M_Z^2 + i\Gamma_Z M_Z} \frac{\hat{\Sigma}_T^{AZ}(M_Z^2)}{M_Z^2} \\
&= \frac{1}{k^2 - M_Z^2} \left[\frac{\hat{\Sigma}_T^{AZ}(k^2)}{k^2} - \frac{\hat{\Sigma}_T^{AZ}(M_Z^2)}{M_Z^2} \right] \\
&\quad + \frac{1}{k^2 - M_Z^2 + i\Gamma_Z M_Z} \frac{\hat{\Sigma}_T^{AZ}(M_Z^2)}{M_Z^2} \\
&\quad - \frac{i\text{Im}\hat{\Sigma}_T^{ZZ}(M_Z^2)}{k^2 - M_Z^2} \left[\frac{\hat{\Sigma}_T^{AZ}(k^2)}{k^2} - \frac{\hat{\Sigma}_T^{AZ}(M_Z^2)}{M_Z^2} \right],
\end{aligned}
\tag{C.19}
$$

in which, by inspecting Eq. (C.9), one can see that the first two lines are exactly what one would get in the pole scheme, and the difference is:

$$\text{diff}_{\text{interf,k}^2 \neq \text{M}_Z^2} = -\frac{i\text{Im}\hat{\Sigma}_T^{ZZ}(M_Z^2)}{k^2 - M_Z^2} \left[\frac{\hat{\Sigma}_T^{AZ}(k^2)}{k^2} - \frac{\hat{\Sigma}_T^{AZ}(M_Z^2)}{M_Z^2} \right]. \tag{C.20}$$

In the calculation we have used the fact that $\text{Im}\hat{\Sigma}_T^{ZZ}(M_Z^2) = \Gamma_Z M_Z$, which is a gauge-invariant quantity at NLO, since it can be expressed in terms of

145

physical quantities. Note also that $\mathrm{Re}\hat{\Sigma}^{ZZ}_T(M^2_Z) = 0$ and that $\hat{\Sigma}^{ZZ}_T(M^2_Z)$ and its derivative evaluated at the Z on-shell mass are gauge invariant. A proof of this can be achieved by taking the bare self-energy expressions listed in Eqs. (5.407)-(5.418) of [301], and deriving the gauge-dependencies for renormalized self energies, with an important remark: we have adopted the so-called Parameter Renormalized Tadpole Scheme employed e.g. in [107, 302] and therefore, in our self-energies, tadpoles do not explicitly appear, at difference from what is done in Eqs. (5.407)-(5.418) of [301]. In particular we can write:

$$\Sigma^{ZZ}_T(k^2)|_\xi = \Sigma^{ZZ}_T(k^2)|_{\xi=1} + \Sigma^{ZZ}_{add}(k^2) \tag{C.21}$$

$$\Sigma^{ZZ}_{add}(k^2) = -\frac{k^2 - M^2_Z}{6}\Phi_{ZZ}(-k^2, \xi)\,, \tag{C.22}$$

where $\Phi_{ZZ}(-k^2, \xi)$ is given in Eq. (5.410) of [301].

C.1.2 Z-exchange contribution

The Z-exchange contribution reads:

$$
\begin{aligned}
\mathcal{M}^{\pm\pm}_Z &= -e^2(g^\pm_q)(g^\pm_\ell)A^{\pm\pm}_{spinor}\frac{1}{k^2 - M^2_Z + i\Gamma_Z M_Z}\left[1 - \frac{\hat{\Sigma}^{ZZ}_T(k^2)}{k^2 - M^2_Z}\right.\\
&\left. + \hat{F}_{qqV,\,\mathrm{phot}}(k^2) + \hat{F}_{\ell\ell V,\,\mathrm{phot}}(k^2) + \hat{F}^\pm_{qqZ,\,\mathrm{weak}}(k^2) + \hat{F}^\pm_{\ell\ell Z,\,\mathrm{weak}}(k^2)\right]\,.
\end{aligned}
$$

Self-energy contribution to Z exchange

In analogy to what has been done for the interference term, the self-energy contribution can be written as:

$$
\begin{aligned}
-\frac{1}{k^2 - M^2_Z + i\Gamma_Z M_Z}\frac{\hat{\Sigma}^{ZZ}_T(k^2)}{k^2 - M^2_Z} &= \frac{1}{k^2 - M^2_Z + i\Gamma_Z M_Z} \tag{C.23}\\
&\cdot\frac{\hat{\Sigma}^{ZZ}_T(k^2) \pm \hat{\Sigma}^{ZZ}_T(M^2_Z)}{k^2 - M^2_Z} \pm \hat{\Sigma}'^{ZZ}_T(M^2_Z)\\
&= -\frac{\hat{\Sigma}^{ZZ}_T(k^2) - \hat{\Sigma}^{ZZ}_T(M^2_Z)}{k^2 - M^2_Z} - \hat{\Sigma}'^{ZZ}_T(M^2_Z)\\
&\cdot\left(1 - \frac{i\mathrm{Im}\hat{\Sigma}^{ZZ}_T(M^2_Z)}{k^2 - M^2_Z}\right)\\
&-\frac{\hat{\Sigma}^{ZZ}_T(M^2_Z) + (k^2 - M^2_Z)\hat{\Sigma}'^{ZZ}_T(M^2_Z)}{(k^2 - M^2_Z)(k^2 - M^2_Z + i\Gamma_Z M_Z)}
\end{aligned}
$$

The difference with Eq. (C.9) amounts to:

$$\mathrm{diff}_{\mathrm{self\,Z,k^2\neq M^2_Z}} = \frac{i\mathrm{Im}\hat{\Sigma}^{ZZ}_T(M^2_Z)}{k^2 - M^2_Z}\frac{\hat{\Sigma}^{ZZ}_T(k^2) - (k^2 - M^2_Z)\hat{\Sigma}'^{ZZ}_T(M^2_Z)}{(k^2 - M^2_Z)^2}\,, \tag{C.24}$$

which is gauge invariant, as seen in the previous section.

C.1. Calculation for $k^2 \neq M_Z^2$

Vertex contribution to Z exchange

The weak vertex part reads:

$$\frac{1}{k^2 - M_Z^2 + i\Gamma_Z M_Z}\left[\hat{F}^{\pm}_{qqZ,\,\text{weak}}(k^2) + \hat{F}^{\pm}_{\ell\ell Z,\,\text{weak}}(k^2)\right] =$$

$$\frac{1}{k^2 - M_Z^2 + i\Gamma_Z M_Z}\left[\hat{F}^{\pm}_{qqZ,\,\text{weak}}(k^2) + \hat{F}^{\pm}_{\ell\ell Z,\,\text{weak}}(k^2)\right.$$

$$\left.\pm\ \hat{F}^{\pm}_{qqZ,\,\text{weak}}(M_Z^2) \pm \hat{F}^{\pm}_{\ell\ell Z,\,\text{weak}}(M_Z^2)\right] =$$

$$\frac{\hat{F}^{\pm}_{qqZ,\,\text{weak}}(k^2) + \hat{F}^{\pm}_{\ell\ell Z,\,\text{weak}}(k^2) - \hat{F}^{\pm}_{qqZ,\,\text{weak}}(M_Z^2) - \hat{F}^{\pm}_{\ell\ell Z,\,\text{weak}}(M_Z^2)}{k^2 - M_Z^2}$$

$$\cdot\left(1 - \frac{i\text{Im}\hat{\Sigma}^{ZZ}_T(M_Z^2)}{k^2 - M_Z^2}\right)$$

$$+\left[\hat{F}^{\pm}_{qqZ,\,\text{weak}}(M_Z^2) + \hat{F}^{\pm}_{\ell\ell Z,\,\text{weak}}(M_Z^2)\right]\frac{1}{k^2 - M_Z^2 + i\Gamma_Z M_Z}.$$

The difference with respect to Eq. (C.9) is the term:

$$\text{diff}_{\text{vert Z},k^2\neq M_Z^2} = -\frac{i\text{Im}\hat{\Sigma}^{ZZ}_T(M_Z^2)}{k^2 - M_Z^2} \tag{C.25}$$

$$\frac{\hat{F}^{\pm}_{qqZ,\,\text{weak}}(k^2) + \hat{F}^{\pm}_{\ell\ell Z,\,\text{weak}}(k^2) - \hat{F}^{\pm}_{qqZ,\,\text{weak}}(M_Z^2) - \hat{F}^{\pm}_{\ell\ell Z,\,\text{weak}}(M_Z^2)}{k^2 - M_Z^2}.$$

Finally we have the pure QED corrections:

$$\frac{1}{k^2 - M_Z^2 + i\Gamma_Z M_Z}\left[\hat{F}_{qqV,\,\text{phot}}(k^2) + \hat{F}_{\ell\ell V,\,\text{phot}}(k^2)\right], \tag{C.26}$$

which are treated in the same way in our prescription and in the pole scheme, and thus do not represent an issue.

The total difference between our old prescription and the pole scheme, omitting the common factor $A^{\pm\pm}_{spinor}$, thus is:

$$\text{CLA}\ -\ \text{PS} = e^2\frac{i\text{Im}\hat{\Sigma}^{ZZ}_T(M_Z^2)}{k^2 - M_Z^2} \tag{C.27}$$

$$\cdot\left\{g^{\pm}_q g^{\pm}_\ell\left[-\frac{\hat{\Sigma}^{ZZ}_T(k^2) - (k^2 - M_Z^2)\hat{\Sigma}'^{ZZ}_T(M_Z^2)}{(k^2 - M_Z^2)^2}\right.\right.$$

$$\left.+\frac{\hat{F}^{\pm}_{qqZ,\,\text{weak}}(k^2) + \hat{F}^{\pm}_{\ell\ell Z,\,\text{weak}}(k^2) - \hat{F}^{\pm}_{qqZ,\,\text{weak}}(M_Z^2) - \hat{F}^{\pm}_{\ell\ell Z,\,\text{weak}}(M_Z^2)}{k^2 - M_Z^2}\right]$$

$$+ (Q_\ell g^{\pm}_q + Q_q g^{\pm}_\ell)\left[\frac{\hat{\Sigma}^{AZ}_T(k^2)}{k^2} - \frac{\hat{\Sigma}^{AZ}_T(M_Z^2)}{M_Z^2}\right]\left.\right\},$$

which is equal to the combination left untouched by the modification of the pole scheme in [86], except for a term $\hat{\Sigma}_T^{ZZ}(M_Z^2)/(k^2 - M_Z^2)$, which is nonetheless gauge invariant. Since the combination left untouched in the the pole scheme is gauge invariant by construction, we can conclude that also Eq. (C.27) is so.

Thus, the difference between the CLA prescription and the PS scheme away from the Z-boson resonance is gauge invariant. One has however to evaluate the same difference in the limit $k^2 \to M_Z^2$.

C.2 Calculation for $k^2 = M_Z^2$

C.2.1 Interference contribution

We list here the limits in the PS and CLA schemes for the interference contribution at $k^2 = M_Z^2$. In the pole scheme we have:

$$
\begin{aligned}
\mathcal{M}_{\text{interf, PS}}^{\pm\pm} &= -e^2 A_{spinor}^{\pm\pm} \frac{Q_q g_\ell^\pm + Q_\ell g_q^\pm}{M_Z^2} \\
&\quad \cdot \left[\frac{\hat{\Sigma}_T^{AZ}(M_Z^2)}{i\Gamma_Z M_Z} - \frac{\hat{\Sigma}_T^{AZ}(M_Z^2)}{M_Z^2} + \hat{\Sigma}_T'^{AZ}(M_Z^2) \right],
\end{aligned}
\tag{C.28}
$$

while in the CLA scheme:

$$
\mathcal{M}_{\text{interf, CLA}}^{\pm\pm} = -e^2 A_{spinor}^{\pm\pm} \frac{Q_q g_\ell^\pm + Q_\ell g_q^\pm}{i\Gamma_Z M_Z} \frac{\hat{\Sigma}_T^{AZ}(M_Z^2)}{M_Z^2}.
\tag{C.29}
$$

The difference CLA-PS is thus:

$$
\text{diff}_{\text{interf Z,k}^2=\text{M}_Z^2} = -e^2 A_{spinor}^{\pm\pm} \frac{Q_q g_\ell^\pm + Q_\ell g_q^\pm}{M_Z^2} \left(\frac{\hat{\Sigma}_T^{AZ}(M_Z^2)}{M_Z^2} - \hat{\Sigma}_T'^{AZ}(M_Z^2) \right).
\tag{C.30}
$$

C.2.2 Z-exchange contribution

Self-energy contribution to Z exchange

The self-energy contribution to the Z exchange for $k^2 = M_Z^2$ in the PS is:

$$
\mathcal{M}_{\text{self Z,PS}}^{\pm\pm} = -e^2 (g_q^\pm)(g_\ell^\pm) A_{spinor}^{\pm\pm} \left[-\frac{\hat{\Sigma}_T'^{ZZ}(M_Z^2)}{i\Gamma_Z M_Z} - \frac{\hat{\Sigma}_T''^{ZZ}(M_Z^2)}{2} \right],
\tag{C.31}
$$

while in our prescription is:

$$
\mathcal{M}_{\text{self Z,CLA}}^{\pm\pm} = -e^2 (g_q^\pm)(g_\ell^\pm) A_{spinor}^{\pm\pm} \left[-\frac{i\text{Im}\Sigma_T'^{ZZ}(M_Z^2)}{i\Gamma_Z M_Z} \right],
\tag{C.32}
$$

C.2. Calculation for $k^2 = M_Z^2$

where $\Sigma_T^{\prime ZZ}(M_Z^2)$ is the bare self-energy. The difference thus amounts to:

$$\text{diff}_{\text{self Z},k^2=M_Z^2} = -e^2 A_{spinor}^{\pm\pm}(g_q^\pm)(g_\ell^\pm) \tag{C.33}$$
$$\cdot \left[-\frac{i\text{Im}\Sigma_T^{\prime ZZ}(M_Z^2)}{i\Gamma_Z M_Z} + \frac{\hat{\Sigma}_T^{\prime ZZ}(M_Z^2)}{i\Gamma_Z M_Z} + \frac{\hat{\Sigma}_T^{\prime\prime ZZ}(M_Z^2)}{2} \right] .$$

Vertex contribution to Z exchange

The weak vertex part reads:

$$\mathcal{M}_{\text{vert Z,PS}}^{\pm\pm} = -e^2(g_q^\pm)(g_\ell^\pm)A_{spinor}^{\pm\pm} \left[\frac{\hat{F}_{qqZ,\,\text{weak}}^\pm(M_Z^2) + \hat{F}_{\ell\ell Z,\,\text{weak}}^\pm(M_Z^2)}{i\Gamma_Z M_Z} \right.$$
$$\left. + \hat{F}_{qqZ,\,\text{weak}}^{\prime\,\pm}(M_Z^2) + \hat{F}_{\ell\ell Z,\,\text{weak}}^{\prime\,\pm}(M_Z^2) \right] , \tag{C.34}$$

while in our prescription one has:

$$\mathcal{M}_{\text{vert Z,CLA}}^{\pm\pm} = -e^2(g_q^\pm)(g_\ell^\pm)A_{spinor}^{\pm\pm} \frac{\hat{F}_{qqZ,\,\text{weak}}^\pm(M_Z^2) + \hat{F}_{\ell\ell Z,\,\text{weak}}^\pm(M_Z^2)}{i\Gamma_Z M_Z} . \tag{C.35}$$

The difference CLA-PS for the vertex part is thus:

$$\text{diff}_{\text{vert Z},k^2=M_Z^2} = -e^2(g_q^\pm)(g_\ell^\pm)A_{spinor}^{\pm\pm} \left[-\hat{F}_{qqZ,\,\text{weak}}^{\prime\,\pm}(M_Z^2) - \hat{F}_{\ell\ell Z,\,\text{weak}}^{\prime\,\pm}(M_Z^2) \right] \tag{C.36}$$

The total difference at the Z resonance is given by:

$$\text{CLA} - \text{PS} = e^2 \left\{ g_q^\pm g_\ell^\pm \left(\hat{F}_{qqZ,\,\text{weak}}^{\prime\,\pm}(M_Z^2) + \hat{F}_{\ell\ell Z,\,\text{weak}}^{\prime\,\pm}(M_Z^2) \right) \right. \tag{C.37}$$
$$+ \frac{Q_q g_\ell^\pm + Q_\ell g_q^\pm}{M_Z^2} \left(-\frac{\hat{\Sigma}_T^{AZ}(M_Z^2)}{M_Z^2} + \hat{\Sigma}_T^{\prime AZ}(M_Z^2) \right)$$
$$\left. + g_q^\pm g_\ell^\pm \left[\frac{i\text{Im}\Sigma_T^{\prime ZZ}(M_Z^2)}{i\Gamma_Z M_Z} - \frac{\hat{\Sigma}_T^{\prime ZZ}(M_Z^2)}{i\Gamma_Z M_Z} - \frac{\hat{\Sigma}_T^{\prime\prime ZZ}(M_Z^2)}{2} \right] \right\} .$$

To evaluate the gauge invariance of this equation, we note that the derivative w.r.t. k^2 evaluated in $k^2 = M_Z^2$ of the gauge invariant combination already introduced in the previous section, namely:

$$g_q^\pm g_\ell^\pm \left[-\frac{\hat{\Sigma}_T^{ZZ}(k^2) - (k^2 - M_Z^2)\hat{\Sigma}_T^{\prime ZZ}(M_Z^2)}{(k^2 - M_Z^2)^2} \right.$$
$$\left. + \frac{\hat{F}_{qqZ,\,\text{weak}}^\pm(k^2) + \hat{F}_{\ell\ell Z,\,\text{weak}}^\pm(k^2) - \hat{F}_{qqZ,\,\text{weak}}^\pm(M_Z^2) - \hat{F}_{\ell\ell Z,\,\text{weak}}^\pm(M_Z^2)}{k^2 - M_Z^2} \right]$$
$$+ (Q_\ell g_q^\pm + Q_q g_\ell^\pm) \left[\frac{\hat{\Sigma}_T^{AZ}(k^2)}{k^2} - \frac{\hat{\Sigma}_T^{AZ}(M_Z^2)}{M_Z^2} \right] \tag{C.38}$$

C. The treatment of the resonance in the `Z_ew-BMNNPV` code

is:

$$g_q^{\pm} g_\ell^{\pm} \left(\hat{F}_{qqZ,\,\text{weak}}^{'\,\pm}(M_Z^2) + \hat{F}_{\ell\ell Z,\,\text{weak}}^{'\,\pm}(M_Z^2) \right) \tag{C.39}$$

$$+ \frac{Q_q g_\ell^{\pm} + Q_\ell g_q^{\pm}}{M_Z^2} \left(-\frac{\hat{\Sigma}_T^{AZ}(M_Z^2)}{M_Z^2} + \hat{\Sigma}_T^{'\,AZ}(M_Z^2) \right)$$

$$- g_q^{\pm} g_\ell^{\pm} \frac{\hat{\Sigma}_T^{''\,ZZ}(M_Z^2)}{2} \,.$$

This is still a gauge invariant quantity, as it can be proven in the R_ξ gauge class by considering the Schwarz theorem applied to the derivatives $\partial^2/(\partial\xi\partial k^2)$ and $\partial^2/(\partial k^2\partial\xi)$, where ξ is the gauge parameter. This last equation coincides with Eq. (C.37), the only difference being the term:

$$e^2 g_q^{\pm} g_\ell^{\pm} \left[\frac{i\text{Im}\Sigma_T^{'\,ZZ}(M_Z^2)}{i\Gamma_Z M_Z} - \frac{\hat{\Sigma}_T^{'\,ZZ}(M_Z^2)}{i\Gamma_Z M_Z} \right] , \tag{C.40}$$

of which we have now to evaluate the gauge invariance. While $\hat{\Sigma}_T^{'\,ZZ}(M_Z^2)$ is gauge invariant, its unrenormalized conterpart $\Sigma_T^{'\,ZZ}(M_Z^2)$ is not. As tadpole do not depend on the momentum, we can directly use the expressions in [301] for the derivatives of self-energies. The ξ-dependent part of the combination in Eq. (C.40) thus can be written as:

$$e^2 g_q^{\pm} g_\ell^{\pm} \frac{1}{6} \frac{1}{i\Gamma_Z M_Z} \text{Im}\Phi_{ZZ}(-M_Z^2, \xi) , \tag{C.41}$$

which is not zero, finally proving that the CLA scheme is gauge dependent.

The $Zf\bar{f}$ width

The LO expression for the Z boson decay width into $f\bar{f}$ $\Gamma(Z \to f\bar{f})$ is:

$$\Gamma(Z \to f\bar{f})_{\text{LO}} = 4\Gamma^0 N_f^c 2s_w^2 c_w^2 \left[g_{R,f}^2 + g_{L,f}^2 \right], \tag{D.1}$$

where:

$$g_{R,f} = -\frac{s_w}{c_w} Q_f, \qquad g_{L,f} = \frac{I_3^f - s_w^2 Q_f}{s_w \, c_w}, \tag{D.2}$$

N_f^c is the colour number and

$$\Gamma^0 = \frac{G_\mu M_Z^3}{24\sqrt{2}\pi}. \tag{D.3}$$

At NLO this can be written as:

$$\Gamma(Z \to f\bar{f})_{\text{NLO}} = 4\Gamma^0 2s_w^2 c_w^2 \left[g_{R,f}^2 + g_{L,f}^2 + 2\,g_{R,f}^2 \frac{\delta g_{R,f}}{g_{R,f}} + 2\,g_{L,f}^2 \frac{\delta g_{L,f}}{g_{L,f}} \right], \tag{D.4}$$

where $2\,\delta g_{R,f}/g_{R,f}$ and $2\,\delta g_{L,f}/g_{L,f}$ are the vertex form factors (multiplied by 2).

In the following we report the equations for the implementation of the leading fermionic contributions at higher orders in the different input schemes.

G_μ scheme

We first consider the (G_μ, M_W, M_Z) scheme. In this scheme one has to write Eq. (D.1) as:

$$\begin{aligned}
\Gamma(Z \to f\bar{f})_{G_\mu} &= N_f^c \frac{\sqrt{2}G_\mu M_Z^3}{6\pi} \left[2s_w^4 Q_f^2 + I_{3,f}^2 - 2I_{3,f}\, s_w^2 Q_f \right] \\
&= \frac{\alpha_{G_\mu} M_Z}{6s_w^2 c_w^2} \left[2s_w^4 Q_f^2 + I_{3,f}^2 - 2I_{3,f}\, s_w^2 Q_f \right], \tag{D.5}
\end{aligned}$$

where we have substituted the expression for Γ^0 in the G_μ scheme, and the formulae of $g_{R/L,e}$. Note that:

$$\alpha_{G_\mu} = \frac{\sqrt{2}G_\mu M_Z^2 s_w^2 c_w^2}{\pi}.$$

(D.6)

According to [86, 107], the recipe for universal h.o. contributions in the G_μ scheme consists in the following substitution:

$$s_w^2 \rightarrow \bar{s}_{eff}^2 = s_w^2 + c_w^2 \Delta\rho,$$

$$c_w^2 \rightarrow \bar{c}_{eff}^2 = c_w^2(1 - \Delta\rho),$$

$$\alpha_{G_\mu} \rightarrow \alpha_{G_\mu}\left[1 + \frac{c_w^2}{s_w^2}\Delta\rho\right].$$

(D.7)

We then need to subtract the terms at one-loop in $\Delta\rho$ and $\Delta\alpha$, with $\Delta\rho^{1-\text{loop}}$ computed with the coupling of the scheme considered. We finally obtain:

$$
\begin{aligned}
\Gamma(Z \rightarrow f\bar{f})_{G_\mu,\text{ho}} &= \frac{\alpha_{G_\mu}M_Z}{6s_w^2 c_w^2}N_f^c\left\{2Q_f^2 s_w^4 + I_{3,f}^2 - 2I_{3,f}Q_f s_w^2\right. \\
&+ \left(\Delta\rho - \Delta\rho^{1-\text{loop}}\right)\left[4Q_f^2 s_w^2 c_w^2 - 2I_{3,f}Q_f + 2Q_f^2 s_w^4 + I_{3,f}^2\right] \\
&+ \left.(\Delta\rho)^2\left[I_{3,f}^2 - 2I_{3,f}Q_f + 2Q_f^2\right]\right\}
\end{aligned}
$$

(D.8)

$(G_\mu, \sin^2\theta_{eff}^\ell, M_Z)$ scheme

Also in this scheme we start from:

$$\Gamma(Z \rightarrow f\bar{f})_{G_\mu,s_{eff}^2} = \frac{\alpha_{G_\mu}M_Z}{6s_{eff}^2 c_{eff}^2}N_f^c\left[2s_{eff}^4 Q_f^2 + I_{3,f}^2 - 2I_{3,f}\, s_{eff}^2 Q_f\right],$$

(D.9)

but, differently from the G_μ scheme, we apply only the substitution:

$$\alpha_{G_\mu} \rightarrow \alpha_{G_\mu}\left[1 + \Delta\rho\right],$$

(D.10)

because $\sin^2\theta_{eff}^\ell$ is in input and does not get any correction. We thus find:

$$
\begin{aligned}
\Gamma(Z \rightarrow f\bar{f})_{G_\mu,s_{eff}^2,\text{ho}} &= \frac{\alpha_{G_\mu}M_Z}{6s_{eff}^2 c_{eff}^2}N_f^c\left[2s_{eff}^4 Q_f^2 + I_{3,f}^2 - 2I_{3,f}\, s_{eff}^2 Q_f\right] \\
&\cdot \left[1 + \left(\Delta\rho - \Delta\rho^{1-\text{loop}}\right)\right].
\end{aligned}
$$

(D.11)

α_0 scheme

In the (α_0, M_W, M_Z) scheme, Eq. (D.1) reads:

$$\Gamma(Z \rightarrow f\bar{f})_{\alpha_0} = \frac{\alpha_0 M_Z}{6s_w^2 c_w^2}N_f^c\left[2s_w^4 Q_f^2 + I_{3,f}^2 - 2I_{3,f}\, s_w^2 Q_f\right].$$

(D.12)

One makes the following substitutions:

$$s_w^2 \;\to\; \bar{s}_w^2 = s_w^2 + c_w^2 \Delta\rho\,, \tag{D.13}$$
$$c_w^2 \;\to\; \bar{c}_w^2 = c_w^2 (1 - \Delta\rho)\,,$$
$$\alpha_0 \;\to\; \frac{\alpha_0}{1 - \Delta\alpha}\,.$$

where $\Delta\alpha$ is the fermionic contribution to $\Delta\alpha$. We thus obtain:

$$
\begin{aligned}
\Gamma(Z \to f\bar{f})_{\alpha_0} \;=\;& \frac{\alpha_0}{1 - \Delta\alpha} \frac{M_Z}{6 s_w^2 c_w^2} N_f^c \frac{1}{1 + \frac{c_w^2}{s_w^2}\Delta\rho} \frac{1}{1 - \Delta\rho} \\
& \cdot \left[2Q_f^2 \left(s_w^2 + c_w^2 \Delta\rho\right)^2 + I_{3,f}^2 - 2 I_{3,f} Q_f \left(s_w^2 + c_w^2 \Delta\rho\right) \right]\,,
\end{aligned}
\tag{D.14}
$$

where we note that the terms in the parenthesis are the same as in the G_μ scheme. By expanding this expression at $\mathcal{O}\left((\Delta\alpha)^2\right)$ and $\mathcal{O}\left((\Delta\rho)^2\right)$ and subtracting the 1-loop contribution, we get:

$$
\begin{aligned}
\Gamma(Z \to f\bar{f})_{\alpha_0,\,\mathrm{ho}} \;=\;& \frac{\alpha_0 M_Z}{6 s_w^2 c_w^2} N_f^c \left\{ 2Q_f^2 s_w^4 + I_{3,f}^2 - 2 I_{3,f} Q_f s_w^2 \right. \\
& + \left(\Delta\rho - \Delta\rho^{1-\mathrm{loop}}\right)\left[2Q_f^2 s_w^2 - 2 I_{3,f} Q_f s_w^2 + 2 I_{3,f}^2 - \frac{I_{3,f}^2}{s_w^2} \right] \\
& + \Delta\alpha\,\Delta\rho \left[2Q_f^2 s_w^2 - 2 I_{3,f} Q_f s_w^2 + 2 I_{3,f}^2 - \frac{I_{3,f}^2}{s_w^2} \right] \\
& + (\Delta\alpha)^2 \left[2Q_f^2 s_w^4 + I_{3,f}^2 - 2 I_{3,f} Q_f s_w^2 \right] \\
& \left. + (\Delta\rho)^2 \left[2Q_f^2 s_w^2 - 2 I_{3,f} Q_f s_w^2 + 3 I_{3,f}^2 - 3\frac{I_{3,f}^2}{s_w^2} + \frac{I_{3,f}^2}{s_w^4} \right] \right\}\,.
\end{aligned}
\tag{D.15}
$$

Note that, since in the code we are not including the 2-loop contribution to $\Delta\alpha$, there is no term linear in $\Delta\alpha$ because this kind of corrections are already included in the NLO calculation.

$(\alpha_0, \sin^2\theta_{eff}^\ell, M_Z)$ scheme

In the $(\alpha_0, \sin^2\theta_{eff}^\ell, M_Z)$ scheme, we start from:

$$\Gamma(Z \to f\bar{f})_{\alpha_0,\,s_{eff}^2} = \frac{\alpha_0 M_Z}{6 s_{eff}^2 c_{eff}^2} N_f^c \left[2s_{eff}^4 Q_f^2 + I_{3,f}^2 - 2 I_{3,f}\, s_{eff}^2 Q_f \right]\,, \tag{D.16}$$

and make the only substitution:

$$\alpha_0 \;\to\; \frac{\alpha_0}{1 - \Delta\alpha}\,. \tag{D.17}$$

After subtracting the 1-loop contribution $\Delta\alpha$ we thus obtain:

$$
\begin{aligned}
\Gamma(Z \to f\bar{f})_{\alpha_0,\,s_{eff}^2} \;=\;& \frac{\alpha_0 M_Z}{6 s_{eff}^2 c_{eff}^2} N_f^c \left[1 + (\Delta\alpha)^2 \right] \\
& \cdot \left[2s_{eff}^4 Q_f^2 + I_{3,f}^2 - 2 I_{3,f}\, s_{eff}^2 Q_f \right]\,.
\end{aligned}
\tag{D.18}
$$

153

$(\alpha(M_Z), M_W, M_Z)$ scheme

In the $(\alpha(M_Z), M_W, M_Z)$ scheme, Eq. (D.1) reads:

$$\Gamma(Z \to f\bar{f})_{\alpha(M_Z)} = \frac{\alpha(M_Z)M_Z}{6s_w^2 c_w^2} N_f^c \left[2s_w^4 Q_f^2 + I_{3,f}^2 - 2I_{3,f}\, s_w^2 Q_f \right]. \quad \text{(D.19)}$$

One has to make only the following substitutions:

$$
\begin{aligned}
s_w^2 &\to \bar{s}_{eff}^2 = s_w^2 + c_w^2 \Delta\rho, \\
c_w^2 &\to \bar{c}_{eff}^2 = c_w^2(1 - \Delta\rho).
\end{aligned}
\quad \text{(D.20)}
$$

After subtracting the 1-loop contribution we obtain:

$$
\begin{aligned}
\Gamma(Z \to f\bar{f})_{\alpha(M_Z)} =\ & \frac{\alpha(M_Z)M_Z}{6s_w^2 c_w^2} N_f^c \left\{ 2Q_f^2 s_w^4 + I_{3,f}^2 - 2I_{3,f}Q_f s_w^2 \right. \quad \text{(D.21)} \\
+\ & \left(\Delta\rho - \Delta\rho^{1-\text{loop}}\right) \left[2Q_f^2 s_w^2 - 2I_{3,f}Q_f s_w^2 + 2I_{3,f}^2 - \frac{I_{3,f}^2}{s_w^2} \right] \\
+\ & \left(\Delta\rho\right)^2 \left. \left[2Q_f^2 s_w^2 - 2I_{3,f}Q_f s_w^2 + 3I_{3,f}^2 - 3\frac{I_{3,f}^2}{s_w^2} + \frac{I_{3,f}^2}{s_w^4} \right] \right\}.
\end{aligned}
$$

$\left(\alpha(M_Z), \sin^2\theta_{eff}^\ell, M_Z\right)$ scheme

In this scheme $\Gamma(Z \to f\bar{f})$ does not take leading higher order corrections.

(α_0, G_μ, M_Z) scheme

In the (α_0, G_μ, M_Z) scheme, one has:

$$\Gamma(Z \to f\bar{f})_{\alpha_0 G_\mu} = \frac{\alpha_0 M_Z}{6s_w^2 c_w^2} N_f^c \left[2s_w^4 Q_f^2 + I_{3,f}^2 - 2I_{3,f}\, s_w^2 Q_f \right]. \quad \text{(D.22)}$$

The substitutions to be made are the ones discussed in Sec. 6.3.1:

$$
\begin{aligned}
s_w^2 &\to \frac{1}{2} - \sqrt{\frac{1}{4} - \frac{\pi\alpha}{\sqrt{2}G_\mu M_Z^2}(1 + \Delta\tilde{r} - \Delta\alpha)}, \quad \text{(D.23)} \\
\alpha_0 &\to \frac{\alpha_0}{1 - \Delta\alpha}.
\end{aligned}
$$

The result after the subtraction of the NLO contribution is:

$$
\begin{aligned}
\Gamma(Z \to f\bar{f})_{\alpha_0 G_\mu, \text{ho}} =\ & \frac{\alpha_0 M_Z}{6s_w^2 c_w^2} N_f^c \left\{ 2Q_f^2 s_w^4 + I_{3,f}^2 - 2I_{3,f}Q_f s_w^2 \right. \quad \text{(D.24)} \\
+\ & \left(\Delta\rho - \Delta\tilde{r}_{rem} - \Delta\rho^{1-\text{loop}}\right) \\
& \cdot \left[I_{3,f}^2 + c_1 Q_f^2 - c_1 Q_f I_{3,f} \right] \\
+\ & \left(\Delta\tilde{r} \cdot \Delta\alpha\right) \frac{4s_w^2 c_w^2}{(c_w^2 - s_w^2)^3} \left[Q_f^2 - Q_f I_{3,f} \right] \\
+\ & \left. \left(\Delta\rho - \Delta\tilde{r}_{rem}\right)^2 \left[I_{3,f}^2 + c_2 Q_f^2 - c_2 Q_f I_{3,f} \right], \right.
\end{aligned}
$$

with:

$$c_1 = \frac{6s_w^2 c_w^2(1 - 2s_w^2 c_w^2) + (c_w^2 - s_w^2)(1 - 4s_w^2 c_w^2) - 1}{(c_w^2 - s_w^2)^3},$$

$$c_2 = \frac{2s_w^2 + 6s_w^2 c_w^2(c_w^2 - s_w^2)(1 - s_w^2 c_w^2) - 8s_w^2 c_w^2(1 - 2s_w^2 c_w^2)}{(c_w^2 - s_w^2)^4}.$$

(D.25)

Aknowledgements

List of publications

1. Amoroso, S., Chiesa, M., Del Pio, C. L., Lipka, E., Piccinini, F., Vazzoler, F., Vicini, A., *Probing the weak mixing angle at high energies at the LHC and HL-LHC*, Phys. Lett. B 844 (2023) 138103

2. Budassi, E., Carloni Calame, C. M., Del Pio, C. L., Piccinini, F., *Single π^0 production in μe scattering at MUonE*, Phys. Lett. B 829 (2022) 137138

3. Budassi, E., Carloni Calame, C. M., Chiesa, M., Del Pio, C. L., Hasan, S. M., Montagna, G., Nicrosini, O., Piccinini, F., *NNLO virtual and real leptonic corrections to muon-electron scattering*, JHEP11 (2021) 098

4. Chiesa, M., Del Pio, C. L., Piccinini, F., *On electroweak corrections to neutral current Drell-Yan with the POWHEG BOX*, arXiv:2402.14659v1 [hep-ph]

5. Electroweak Working Group Report, *Determination of the weak mixing angle from the Neutral-Current Drell-Yan process at hadron collider*, in preparation

6. Del Pio, C. L., *et al.*, *Probing the weak mixing angle at high energy*, Proceedings of DIS2023 - XXX International Workshop on Deep-Inelastic Scattering and related subjects — SLAC eCONF service

7. Vazzoler, F., Amoroso, S., Lipka, E., Del Pio, C. L., Chiesa, M., Piccinini, F., Vicini, A., *Probing the Weak Mixing Angle at high energies at the LHC*, Proceedings of 41st International Conference on High Energy physics — PoS(ICHEP2022) **414** 890

8. Del Pio, C. L., Budassi, E., *Neutral pion production in muon-electron scattering at MUonE*, Proceedings of 41st International Conference on High Energy physics — PoS(ICHEP2022) **414** 1035

9. Budassi, E., Del Pio, C. L., *High precision calculations for the MUonE experiment*, Proceedings of 41st International Conference on High Energy physics — PoS(ICHEP2022) **414** 796

Bibliography

[1] G. W. Bennett *et al.*, "Final report of the E821 muon anomalous magnetic moment measurement at BNL," *Physical Review D* **73** no. 7, (Apr, 2006) .

[2] B. Abi *et al.*, "Measurement of the Positive Muon Anomalous Magnetic Moment to 0.46 ppm," *Physical Review Letters* **126** no. 14, (Apr, 2021) .

[3] T. Aoyama, N. Asmussen, *et al.*, "The anomalous magnetic moment of the muon in the Standard Model," *Physics Reports* **887** (Dec, 2020) 1–166.

[4] The Muon $g-2$ Collaboration Collaboration, D. P. Aguillard *et al.*, "Measurement of the Positive Muon Anomalous Magnetic Moment to 0.20 ppm," *Phys. Rev. Lett.* **131** (Oct, 2023) 161802.

[5] S. L. Glashow, "Partial-symmetries of weak interactions," *Nuclear Physics* **22** no. 4, (1961) 579–588.

[6] S. Weinberg, "A Model of Leptons," *Phys. Rev. Lett.* **19** (Nov, 1967) 1264–1266.

[7] A. Salam, "Weak and electromagnetic interactions," *Elementary Particle Theory* (Oct, 1968) 367–377.

[8] S. L. Glashow, J. Iliopoulos, and L. Maiani, "Weak Interactions with Lepton-Hadron Symmetry," *Phys. Rev. D* **2** (Oct, 1970) 1285–1292.

[9] P. M. Zerwas and H. A. Kastrup, "QCD — 20 Years Later." Jun, 1993.

[10] R. K. Ellis, W. J. Stirling, and B. R. Webber, *QCD and collider physics*, vol. 8. Cambridge University Press, Feb, 2011.

[11] F. Halzen and A. D. Martin, *Quarks and Leptons*. John Wiley & Sons, Jan, 1984.

[12] T. Muta, *Foundations of Quantum Chromodynamics*. World Scientific, 1998.

[13] P. W. Higgs, "Broken symmetries and the masses of gauge bosons," *Phys. Rev. Lett.* **13** (Oct, 1964) 508–509.

[14] F. Englert and R. Brout, "Broken symmetry and the mass of gauge

vector mesons," *Phys. Rev. Lett.* **13** (Aug, 1964) 321–323.

[15] T. W. B. Kibble, "Symmetry breaking in non-abelian gauge theories," *Phys. Rev.* **155** (Mar, 1967) 1554–1561.

[16] G. 't Hooft, "Renormalizable Lagrangians for massive Yang-Mills fields," *Nucl. Phys. B* **35** no. 1, (1971) 167–188.

[17] M. Böhm, A. Denner, and H. Joos, *Gauge Theories of the Strong and Electroweak Interaction.* Vieweg+Teubner Verlag, 2001.

[18] F. Mandl and G. P. Shaw, *Quantum Field Theory.* Wiley, May, 2010.

[19] M. E. Peskin, *An Introduction To Quantum Field Theory.* CRC Press, May, 2018.

[20] C. M. Becchi and G. Ridolfi, *An Introduction to Relativistic Processes and the Standard Model of Electroweak Interactions.* Springer, Sept, 2016.

[21] A. Denner and S. Dittmaier, "Electroweak radiative corrections for collider physics," *Physics Reports* **864** (Jun, 2020) 1–163.

[22] E. S. Abers and B. W. Lee, "Gauge theories," *Physics Reports* **9** no. 1, (Nov, 1973) 1–2.

[23] L. Faddeev and V. Popov, "Feynman diagrams for the Yang-Mills field," *Phys. Lett. B* **25** no. 1, (1967) 29–30.

[24] CMD3 Collaboration, "Measurement of the $e^+e^- \to \pi^+\pi^-$ cross section from threshold to 1.2 GeV with the CMD-3 detector." 2023. `arXiv:2302.08834 [hep-ex]`.

[25] CDF Collaboration, T. Aaltonen *et al.*, "High-precision measurement of the W boson mass with the CDF II detector," *Science* **376** no. 6589, (2022) 170–176.

[26] G. Arnison *et al.*, "Experimental observation of isolated large transverse energy electrons with associated missing energy at $\sqrt{s} = 540$ GeV," *Phys. Lett. B* **122** no. 1, (Feb, 1983) 103–116.

[27] M. Banner *et al.*, "Observation of single isolated electrons of high transverse momentum in events with missing transverse energy at the CERN pp collider," *Phys. Lett. B* **122** no. 5-6, (Mar, 1983) 476–485.

[28] D. Y. Bardin *et al.*, "Electroweak Working Group Report." 1997. `arXiv:hep-ph/9709229 [hep-ph]`.

[29] G. Montagna, O. Nicrosini, and F. Piccinini, "Precision physics at LEP," *La Rivista del Nuovo Cimento* **21** no. 9, (Sep, 1998) 1–162.

[30] Particle Data Group Collaboration, R. L. Workman *et al.*, "Review of Particle Physics," *PTEP* **2022** (2022) 083C01.

[31] D0 Collaboration Collaboration, S. Abachi *et al.*, "Observation of the top quark," *Phys. Rev. Lett.* **74** (Apr, 1995) 2632–2637.

[32] CDF Collaboration Collaboration, F. Abe *et al.*, "Observation of Top Quark Production in $\overline{p}p$ Collisions with the Collider Detector at Fermilab," *Phys. Rev. Lett.* **74** (Apr, 1995) 2626–2631.

[33] S. Chatrchyan *et al.*, "Observation of a new boson at a mass of 125 GeV with the CMS experiment at the LHC," *Phys. Lett. B* **716** no. 1,

(2012) 30–61.

[34] G. Aad *et al.*, "Observation of a new particle in the search for the Standard Model Higgs boson with the ATLAS detector at the LHC," *Phys. Lett. B* **716** no. 1, (2012) 1–29.

[35] O. S. Brüning, P. Collier, P. Lebrun, S. Myers, R. Ostojic, J. Poole, and P. Proudlock, *LHC Design Report*. CERN Yellow Reports: Monographs. CERN, Geneva, 2004.

[36] "CERN Yellow Reports: Monographs, Vol. 10 (2020): High-Luminosity Large Hadron Collider (HL-LHC): Technical design report,".

[37] H. Flächer, M. Goebel, J. Haller, A. Hoecker, K. Mönig, and J. Stelzer, "Revisiting the global electroweak fit of the Standard Model and beyond with Gfitter," *EPJC* **60** no. 4, (Mar, 2009) 543–583.

[38] J. Haller, A. Hoecker, R. Kogler, K. Mönig, T. Peiffer, and J. Stelzer, "Update of the global electroweak fit and constraints on two-Higgs-doublet models," *EPJC* **78** no. 8, (Aug, 2018) .

[39] J. Erler, "Global Fits to Electroweak Data Using GAPP." 2000. `arXiv:hep-ph/0005084 [hep-ph]`.

[40] A. Sirlin, "Radiative corrections in the $SU(2)_L \times U(1)$ theory: A simple renormalization framework," *Phys. Rev. D* **22** (Aug, 1980) 971–981.

[41] G. Passarino and M. Veltman, "One-loop corrections for e^+e^- annihilation into $\mu^+\mu^-$ in the Weinberg model," *Nuclear Physics B* **160** no. 1, (Nov, 1979) 151–207.

[42] K. Aoki *et al.*, "Electroweak Theory - Framework of On-Shell Renormalization and Study of Higher Order Effects," *Progress of Theoretical Physics Supplement* **73** (1982) 1–226.

[43] G. Degrassi, P. Gambino, and P. P. Giardino, "The $M_W - M_Z$ interdependence in the Standard Model: a new scrutiny," *JHEP* **2015** no. 5, (May, 2015) .

[44] ALEPH, DELPHI, L3, OPAL, LEP Electroweak Working Group Collaboration, J. Alcaraz *et al.*, "A Combination of Preliminary Electroweak Measurements and Constraints on the Standard Model," tech. rep., CERN, Geneva, 2005. 2005 SUMMER CONFERENCES.

[45] ATLAS Collaboration, "Improved W boson Mass Measurement using 7 TeV Proton-Proton Collisions with the ATLAS Detector," tech. rep., CERN, Geneva, 2023.

[46] T. Aaltonen *et al.*, "Combination of CDF and D0 W-Boson mass measurements," *Phys. Rev. D* **88** no. 5, (Sep, 2013) .

[47] M. Aaboud *et al.*, "Measurement of the W-boson mass in pp collisions at $\sqrt{7}$ TeV with the ATLAS detector," *EPJC* **78** no. 2, (Feb, 2018) .

[48] R. Aaij *et al.*, "Measurement of forward $W \to e\nu$ production in pp collisions at $\sqrt{s} = 8$ TeV," *JHEP* **2016** no. 10, (Oct, 2016) .

[49] S. Amoroso, N. Andari, *et al.*, "Compatibility and combination of world W-boson mass measurements." 2023. `arXiv:2308.09417 [hep-ex]`.

[50] The ALEPH Collaboration, the DELPHI Collaboration, the L3

Collaboration, the OPAL Collaboration, the SLD Collaboration, the LEP Electroweak Working Group, the SLD electroweak, heavy flavour groups Collaboration, "Precision electroweak measurements on the Z resonance," *Physics Reports* **427** no. 5-6, (May, 2006) 257–454.

[51] D. Kennedy, B. Lynn, C.-C. Im, and R. Stuart, "Electroweak cross sections and asymmetries at the Z_0," *Nucl. Phys. B* **321** no. 1, (Jul, 1989) 83–107.

[52] J. C. Collins and D. E. Soper, "Angular distribution of dileptons in high-energy hadron collisions," *Phys. Rev. D* **16** (Oct, 1977) 2219–2225.

[53] M. Chiesa, F. Piccinini, and A. Vicini, "Direct determination of $\sin^2\vartheta_{\text{eff}}^\ell$ at hadron colliders," *Phys. Rev. D* **100** (Oct, 2019) 071302.

[54] V. M. Abazov *et al.*, "Measurement of the Effective Weak Mixing Angle in $p\bar{p} \to Z/\gamma^* \to e^+e^-$ events ," *Physical Review Lett.* **115** no. 4, (Jul, 2015) .

[55] CDF Collaboration, T. Aaltonen *et al.*, "Measurement of $\sin^2\theta_{\text{eff}}^{\text{lept}}$ using e^+e^- pairs from γ^*/Z bosons produced in $p\bar{p}$ collisions at a center-of-momentum energy of 1.96 TeV," *Phys. Rev. D* **93** (Jun, 2016) 112016.

[56] J. Erler and M. Schott, "Electroweak precision tests of the Standard Model after the discovery of the Higgs boson," *Progress in Particle and Nuclear Physics* **106** (May, 2019) 68–119.

[57] ATLAS Collaboration, "Measurement of the effective leptonic weak mixing angle using electron and muon pairs from Z-boson decay in the ATLAS experiment at $\sqrt{s} = 8$ TeV," tech. rep., CERN, Geneva, 2018.

[58] CMS Collaboration, A. M. Sirunyan *et al.*, "Measurement of the weak mixing angle using the forward-backward asymmetry of Drell-Yan events in pp collisions at 8 TeV," *EPJC* **78** no. 9, (Sep, 2018) .

[59] LHCb Collaboration, R. Aaij *et al.*, "Measurement of the forward-backward asymmetry in $Z/\gamma^* \to \mu^+\mu^-$ decays and determination of the effective weak mixing angle," *JHEP* **11** (2015) 190.

[60] C. S. Wood, S. C. Bennett, D. Cho, B. P. Masterson, J. L. Roberts, C. E. Tanner, and C. E. Wieman, "Measurement of Parity Nonconservation and an Anapole Moment in Cesium," *Science* **275** no. 5307, (Mar, 1997) 1759–1763.

[61] Guéna, J. and Lintz, M. and Bouchiat, M. A., "Measurement of the parity violating $6S-7S$ transition amplitude in cesium achieved within 2×10^{-13} atomic-unit accuracy by stimulated-emission detection," *Phys. Rev. A* **71** (Apr, 2005) 042108.

[62] J. Ginges and V. Flambaum, "Violations of fundamental symmetries in atoms and tests of unification theories of elementary particles," *Physics Reports* **397** no. 2, (Jul, 2004) 63–154.

[63] D. Antypas, A. M. Fabricant, J. E. Stalnaker, K. Tsigutkin, V. V. Flambaum, and D. Budker, "Isotopic variation of parity violation in atomic ytterbium: Description of the measurement method and analysis

of systematic effects," *Physical Review A* **100** no. 1, (Jul, 2019) .

[64] E. Beise, M. Pitt, and D. Spayde, "The SAMPLE experiment and weak nucleon structure," *Progress in Particle and Nuclear Physics* **54** no. 1, (Mar, 2005) 289–350.

[65] C. Prescott *et al.*, "Further measurements of parity non-conservation in inelastic electron scattering," *Phys. Lett. B* **84** no. 4, (Jul, 1979) 524–528.

[66] The PVDIS Collaboration, D. Wang *et al.*, "Measurement of parity-violating asymmetry in electron-deuteron inelastic scattering," *Phys. Rev. C* **91** (Apr, 2015) 045506.

[67] Jefferson Lab Qweak Collaboration, D. Androić *et al.*, "Precision measurement of the weak charge of the proton," *Nature* **557** no. 7704, (May, 2018) 207–211.

[68] SLAC E158 Collaboration, P. L. Anthony *et al.*, "Precision Measurement of the Weak Mixing Angle in Möller Scattering," *Phys. Rev. Lett.* **95** (Aug, 2005) 081601.

[69] Y. X. Zhao, A. Deshpande, J. Huang, K. S. Kumar, and S. Riordan, "Neutral-current weak interactions at an EIC," *The European Physical Journal A* **53** no. 3, (Mar, 2017) .

[70] A. Blondel *et al.*, "Electroweak parameters from a high statistics neutrino nucleon scattering experiment," *Zeitschrift für Physik C Particles and Fields* **45** no. 3, (Sep, 1990) 361–379.

[71] J. V. Allaby *et al.*, "A precise determination of the electroweak mixing angle from semileptonic neutrino scattering," *Zeitschrift für Physik C Particles and Fields* **36** no. 4, (Dec, 1987) 611–628.

[72] K. McFarland *et al.*, "A precision measurement of electroweak parameters in neutrino-nucleon scattering," *EPJC* **1** no. 3, (Feb, 1998) 509–513.

[73] G. P. Zeller *et al.*, "Precise Determination of Electroweak Parameters in Neutrino-Nucleon Scattering," *Phys. Rev. Lett.* **88** (Feb, 2002) 091802.

[74] R. M. Abraham, S. Foroughi-Abari, F. Kling, and Y.-D. Tsai, "Neutrino Electromagnetic Properties and the Weak Mixing Angle at the LHC Forward Physics Facility." 2023. `arXiv:2301.10254 [hep-ph]`.

[75] ZEUS Collaboration, H. Abramowicz *et al.*, "Combined QCD and electroweak analysis of HERA data," *Phys. Rev. D* **93** (May, 2016) 092002.

[76] H1 Collaboration, V. Andreev *et al.*, "Determination of electroweak parameters in polarised deep-inelastic scattering at HERA," *EPJC* **78** no. 9, (Sep, 2018) .

[77] J. Erler and M. J. Ramsey-Musolf, "Weak mixing angle at low energies," *Phys. Rev. D* **72** (Oct, 2005) 073003.

[78] S. Amoroso *et al.*, "Probing the weak mixing angle at high energies at the LHC and HL-LHC," *Phys. Lett. B* **844** (2023) 138103.

[79] H. Georgi, H. R. Quinn, and S. Weinberg, "Hierarchy of Interactions in

Unified Gauge Theories," *Phys. Rev. Lett.* **33** (Aug, 1974) 451–454.

[80] W. J. Marciano, "Weak mixing angle and grand unified gauge theories," *Phys. Rev. D* **20** (Jul, 1979) 274–288.

[81] M. B. Einhorn and D. R. T. Jones, "The weak mixing angle and unification mass in supersymmetric $SU(5)$," *Nuclear Physics* **196** (1982) 475–488.

[82] T. Aoyama, T. Kinoshita, and M. Nio, "Theory of the anomalous magnetic moment of the electron," *Atoms* **7** no. 1, (Feb, 2019) 28.

[83] Working Group on Radiative Corrections, Monte Carlo Generators for Low Energies Collaboration, S. Actis *et al.*, "Quest for precision in hadronic cross sections at low energy: Monte Carlo tools vs. experimental data," *Eur. Phys. J. C* **66** (2010) 585–686, `arXiv:0912.0749 [hep-ph]`.

[84] S. Bethke, "The 2009 world average of α_S," *EPJC* **64** no. 4, (Oct, 2009) 689–703.

[85] S. Dittmaier and M. Krämer, "Electroweak radiative corrections to W-boson production at hadron colliders," *Phys. Rev. D* **65** no. 7, (Mar, 2002) .

[86] S. Dittmaier and M. Huber, "Radiative corrections to the neutral-current Drell-Yan process in the Standard Model and its minimal supersymmetric extension," *JHEP* **2010** no. 1, (Jan, 2010) .

[87] U. Baur, S. Keller, and D. Wackeroth, "Electroweak radiative corrections to W boson production in hadronic collisions," *Phys. Rev. D* **59** (1999) 013002.

[88] U. Baur, S. Keller, and W. K. Sakumoto, "Qed radiative corrections to z-boson production and the forward-backward asymmetry at hadron colliders," *Phys. Rev. D* **57** no. 1, (Jan, 1998) 199–215.

[89] U. Baur, O. Brein, W. Hollik, C. Schappacher, and D. Wackeroth, "Electroweak radiative corrections to neutral current Drell-Yan processes at hadron colliders," *Phys. Rev. D* **65** (2002) 033007.

[90] U. Baur and D. Wackeroth, "Electroweak radiative corrections to $p\bar{p} \to W^{\pm} \to \ell^{\pm}\nu$ beyond the pole approximation," *Phys. Rev. D* **70** (2004) 073015.

[91] C. M. C. Calame, G. Montagna, O. Nicrosini, and A. Vicini, "Precision electroweak calculation of the charged current Drell-Yan process," *JHEP* **2006** no. 12, (Dec, 2006) 016–016.

[92] C. M. C. Calame, G. Montagna, O. Nicrosini, and A. Vicini, "Precision electroweak calculation of the production of a high transverse-momentum lepton pair at hadron colliders," *JHEP* **2007** no. 10, (Nov, 2007) 109–109.

[93] C. M. C. Calame *et al.*, "Precision measurement of the W-boson mass: Theoretical contributions and uncertainties," *Phys. Rev. D* **96** no. 9, (Nov, 2017) .

[94] W. Placzek and S. Jadach, "Multiphoton radiation in leptonic W-boson

decays," *EPJC* **29** no. 3, (Jul, 2003) 325–339.

[95] W. Płaczek, S. Jadach, and M. Krasny, "Drell-Yan Processes with WINHAC," *Acta Physica Polonica B* **44** no. 11, (2013) 2171.

[96] A. Arbuzov *et al.*, "One-loop corrections to the Drell–Yan process in SANC: the charged current case," *EPJC* **46** no. 2, (Mar, 2006) 407–412.

[97] A. Arbuzov *et al.*, "One-loop corrections to the Drell–Yan process in SANC: (II) The neutral current case," *EPJC* **54** no. 3, (Feb, 2008) 451–460.

[98] D. Bardin *et al.*, "SANC integrator in the progress: QCD and EW contributions," *JETP Letters* **96** no. 5, (Nov, 2012) 285–289.

[99] S. Jadach, B. F. L. Ward, Z. A. Was, and S. A. Yost, "KK MC-hh: Resumed exact EW corrections in a hadronic MC event generator," *Phys. Rev. D* **94** no. 7, (Oct, 2016) .

[100] A. Arbuzov *et al.*, "Computer package DIZET v. 6.45," *Comp. Phys. Comm.* **291** (Oct, 2023) 108846.

[101] L. Barzè, G. Montagna, P. Nason, O. Nicrosini, and F. Piccinini, "Implementation of electroweak corrections in the POWHEG BOX: single W production," *JHEP* **2012** no. 4, (Apr, 2012) .

[102] L. Barzè, G. Montagna, P. Nason, O. Nicrosini, F. Piccinini, and A. Vicini, "Neutral-current Drell-Yan with combined QCD and electroweak corrections in the POWHEG BOX," *EPJC* **73** no. 6, (Jun, 2013) .

[103] C. Bernaciak and D. Wackeroth, "Combining next-to-leading order QCD and electroweak radiative corrections to W-boson production at hadron colliders in the POWHEG framework," *Phys. Rev. D* **85** (May, 2012) 093003.

[104] S. Alioli *et al.*, "Precision studies of observables in $pp \rightarrow W \rightarrow l\nu_l$ and $pp \rightarrow \gamma, Z \rightarrow l^+l^-$ processes at the LHC," *EPJC* **77** no. 5, (May, 2017) .

[105] M. Chiesa, C. L. D. Pio, and F. Piccinini, "On electroweak corrections to neutral current Drell-Yan with the POWHEG BOX." 2024. `arXiv:2402.14659 [hep-ph]`.

[106] M. Böhm, W. Hollik, and H. Spiesberger, "Electroweak parameters and leptonic processes," *Zeitschrift für Physik C Particles and Fields* **27** no. 4, (Dec, 1985) 523–534.

[107] A. Denner, "Techniques for the Calculation of Electroweak Radiative Corrections at the One-Loop Level and Results for W-physics at LEP 200," *Fortschritte der Physik/Progress of Physics* **41** no. 4, (1993) 307–420.

[108] C. L. Del Pio, "Electroweak Radiative Corrections to the Drell-Yan processes at the LHC." 2020.

[109] M. Consoli, W. Hollik, and F. Jegerlehner, "The effect of the top quark on the $M_W - M_Z$ interdependence and possible decoupling of heavy fermions from low energy physics," *Phys. Lett. B* **227** no. 1, (Aug, 1989) 167–170.

[110] K.-P. O. Diener, S. Dittmaier, and W. Hollik, "Electroweak higher-order effects and theoretical uncertainties in deep-inelastic neutrino scattering," *Phys. Rev. D* **72** no. 9, (Nov, 2005) .

[111] M. Veltman, "Limit on mass differences in the Weinberg model," *Nucl. Phys. B* **123** no. 1, (May, 1977) 89–99.

[112] J. Fleischer, O. Tarasov, and F. Jegerlehner, "Two-loop heavy top corrections to the ρ parameter. A simple formula valid for arbitrary Higgs mass," *Phys. Lett. B* **319** no. 1-3, (Dec, 1993) 249–256.

[113] J. Fleischer, O. V. Tarasov, and F. Jegerlehner, "Two-loop large top mass corrections to electroweak parameters: analytic results valid for arbitrary Higgs mass," *Phys. Rev. D* **51** no. 7, (1995) 3820–3837.

[114] A. Djouadi and C. Verzegnassi, "Virtual very heavy top effects in LEP/SLC precision measurements," *Phys. Lett. B* **195** no. 2, (Sep, 1987) 265–271.

[115] A. Djouadi, " $\mathcal{O}(\alpha\alpha_S)$ Vacuum Polarization Functions of the Standard Model Gauge Bosons," *Nuovo Cim. A* **100** (1988) 357.

[116] B. A. Kniehl, "Two-loop corrections to the vacuum polarizations in perturbative QCD," *Nucl. Phys. B* **347** no. 1-2, (Dec, 1990) 86–104.

[117] L. Avdeev, J. Fleischer, S. Mikhailov, and O. Tarasov, "O $(\alpha\,\alpha_S^2)$ correction to the electroweak ρ parameter," *Phys. Lett. B* **336** no. 3-4, (Sep, 1994) 560–566.

[118] M. Faisst, J. Kühn, T. Seidensticker, and O. Veretin, "Three loop top quark contributions to the ρ parameter," *Nucl. Phys. B* **665** (Aug, 2003) 649–662.

[119] K. G. Chetyrkin, M. Faisst, J. H. Kühn, P. Maierhöfer, and C. Sturm, "Four-Loop QCD Corrections to ρ Parameter," *Physical Review Lett.* **97** no. 10, (Sep, 2006) .

[120] F. Jegerlehner, "Hadronic contributions to electroweak parameter shifts," *Zeitschrift für Physik C Particles and Fields* **32** no. 2, (Jun, 1986) 195–207.

[121] H. Burkhardt, F. Jegerlehner, G. Penso, and C. Verzegnassi, "Uncertainties in the hadronic contribution to the QED vacuum polarization," *Zeitschrift für Physik C Particles and Fields* **43** no. 3, (Sep, 1989) 497–501.

[122] S. Eidelman and F. Jegerlehner, "Hadronic contributions to $(g-2)$ of the leptons and to the effective fine structure constant $\alpha(M_Z^2)$," *Zeitschrift für Physik C Particles and Fields* **67** no. 4, (Dec, 1995) 585–601.

[123] F. Jegerlehner, "The role of $\sigma(e^+e^- \to \text{hadrons})$ in precision tests of the Standard Model," *Nucl. Phys. B - Proceedings Supplements* **131** (Apr, 2004) 213–222.

[124] F. Jegerlehner, "Precision measurements of σ_{hadronic} for $\alpha_{eff}(E)$ at ILC energies and $(g-2)_\mu$," *Nucl. Phys. B - Proceedings Supplements* **162** (Dec, 2006) 22–32.

[125] F. Jegerlehner, "The running fine structure constant via the Adler function," *Nucl. Phys. B - Proceedings Supplements* **181-182** (Sep, 2008) 135–140.

[126] F. Jegerlehner, "Electroweak effective couplings for future precision experiments," *Il Nuovo Cimento C* no. Online First, (Dec, 2011) 31–40.

[127] F. Jegerlehner, "$\alpha_{\mathrm{QED, eff}}(s)$ for precision physics at the FCC-ee/ILC," *CERN Yellow Reports: Monographs* **Vol. 3** no. 2020, (May, 2020) 8–11 January 2019.

[128] K. Hagiwara, A. D. Martin, D. Nomura, and T. Teubner, "Predictions for $g - 2$ of the muon and $\alpha_{QED}(m_z^2)$," *Phys. Rev. D* **69** no. 9, (May, 2004) .

[129] K. Hagiwara, A. Martin, D. Nomura, and T. Teubner, "Improved predictions for $g - 2$ of the muon and $\alpha_{QED}(m_z^2)$," *Phys. Lett. B* **649** no. 2-3, (May, 2007) 173–179.

[130] K. Hagiwara, R. Liao, A. D. Martin, D. Nomura, and T. Teubner, "$(g - 2)_\mu$ and $\alpha(m_z^2)$ re-evaluated using new precise data," *Journal of Physics G: Nuclear and Particle Physics* **38** no. 8, (Jun, 2011) 085003.

[131] A. Keshavarzi, D. Nomura, and T. Teubner, "Muon $g - 2$ and $\alpha(m_z^2)$: a new data-based analysis," *Phys. Rev. D* **97** no. 11, (Jun, 2018) .

[132] G. Degrassi and A. Sirlin, "Gauge dependence of basic electroweak corrections of the Standard Model," *Nucl. Phys. B* **383** no. 1-2, (Sep, 1992) 73–92.

[133] A. Ferroglia, G. Ossola, and A. Sirlin, "The electroweak form factor $\hat{\kappa}(q^2)$ and the running of $\sin^2 \hat{\theta}_w$," *EPJC* **34** no. 2, (May, 2004) 165–171.

[134] A. Czarnecki and W. J. Marciano, "Polarized Møller scattering asymmetriesS," *International Journal of Modern Physics A* **15** no. 16, (Jun, 2000) 2365–2375.

[135] W. J. Marciano and A. Sirlin, "Radiative corrections to neutrino-induced neutral-current phenomena in the $SU(2)_L \times U(1)$ theory," *Phys. Rev. D* **22** no. 11, (Dec, 1980) 2695–2717.
W. J. Marciano and A. Sirlin, "Erratum: Radiative corrections to neutrino-induced neutral-current phenomena in the $SU(2)_L \times U(1)$ theory," *Phys. Rev. D* **31** (Jan, 1985) 213–213.

[136] P. Gambino and A. Sirlin, "Relation between $sin^2\theta_W(m_Z)$ and $sin^2\theta_{\mathrm{eff}}^{\mathrm{lept}}$," *Phys. Rev. D* **49** (Feb, 1994) R1160–R1162.

[137] W. J. Marciano, "Quantitative Tests of the Standard Model of Electroweak Interactions," *Annual Review of Nuclear and Particle Science* **41** no. 1, (Dec, 1991) 469–509.

[138] J. Erler, "Calculation of the QED coupling $\hat{\alpha}(M_Z)$ in the modified minimal-subtraction scheme," *Phys. Rev. D* **59** (Feb, 1999) 054008.

[139] S. Gorishny, A. Kataev, and S. Larin, "Next-next-to-leading QCD correction to $\sigma_{tot}(e^+e^- \rightarrow$ hadrons): Analytical calculation and estimation of the parameter," *Phys. Lett. B* **212** no. 2, (Sep, 1988) 238–244.

[140] L. R. Surguladze and M. A. Samuel, "Total hadronic cross section in e^+e^- annihilation at the four-loop level of perturbative QCD," *Phys. Rev. Lett.* **66** (Feb, 1991) 560–563.
L. R. Surguladze and M. A. Samuel, "Erratum: Total hadronic cross section in e^+e^- annihilation at the four-loop level of perturbative QCD [Phys. Rev. Lett. 66, 560 (1991)]," *Phys. Rev. Lett.* **66** (May, 1991) 2416–2416.

[141] S. Larin, T. van Ritbergen, and J. Vermaseren, "The large quark mass expansion of $\lambda(z^0) \to$ hadrons) and $\lambda(\tau^- \to \nu_\tau +$ hadrons) in the order α_s^3," *Nucl. Phys. B* **438** no. 1-2, (Mar, 1995) 278–304.

[142] K. Chetyrkin, "Quark mass anomalous dimension to $\mathcal{O}(\alpha_s^4)$," *Phys. Lett. B* **404** no. 1-2, (Jul, 1997) 161–165.

[143] J. Erler and R. Ferro-Hernández, "Weak mixing angle in the Thomson limit," *JHEP* **2018** no. 3, (Mar, 2018) .

[144] G. Degrassi, P. Gambino, and A. Sirlin, "Precise calculation of M_W, $\sin^2\hat{\theta}(M_Z)$, and $sin^2\theta_{eff}^{lept}$," *Phys. Lett. B* **394** no. 1-2, (Feb, 1997) 188–194.

[145] A. Sirlin, "Considerations concerning the renormalization of the electroweak sector of the Standard Model," *Nucl. Phys. B* **332** no. 1, (Feb, 1990) 20–38.

[146] S. Fanchiotti, B. Kniehl, and A. Sirlin, "Incorporation of QCD effects in basic corrections of the electroweak theory," *Phys. Rev. D* **48** no. 1, (Jul, 1993) 307–331.

[147] S. Weinberg, "Effective gauge theories," *Phys. Lett. B* **91** no. 1, (Mar, 1980) 51–55.

[148] A. D. Martin, W. J. Stirling, R. S. Thorne, and G. Watt, "Parton distributions for the LHC," *EPJC* **63** no. 2, (Jul, 2009) 189–285.

[149] K. Chetyrkin, "Decoupling relations to $\mathcal{O}(\alpha_S^3)$ and their connection to low-energy theorems," *Nucl. Phys. B* **510** no. 1-2, (Jan, 1998) 61–87.

[150] J. Ellis, M. K. Gaillard, D. Nanopoulos, and S. Rudaz, "Uncertainties in the proton lifetime," *Nucl. Phys. B* **176** no. 1, (Dec, 1980) 61–99.

[151] C. Llewellyn Smith, G. Ross, and J. Wheater, "Low-energy predictions from grand unified theories," *Nucl. Phys. B* **177** no. 2, (Jan, 1981) 263–281.

[152] W. J. Marciano and A. Sirlin, "Precise $SU(5)$ Predictions for $\sin^2\theta_W^{exp}$, m_W, and m_Z," *Phys. Rev. Lett.* **46** (Jan, 1981) 163–166.

[153] L. Hall, "Grand unification of effective gauge theories," *Nucl. Phys. B* **178** no. 1, (Feb, 1981) 75–124.

[154] P. Binétruy and T. Schücker, "Gauge and renormalization scheme dependence in GUTS," *Nucl. Phys. B* **178** no. 2, (Feb, 1981) 293–306.
P. Binétruy and T. Schücker, "The use of dimensional renormalization schemes in unified theories," *Nucl. Phys. B* **178** no. 2, (Feb, 1981) 307–330.

[155] P. Langacker and N. Polonsky, "Uncertainties in coupling constant

unification," *Phys. Rev. D* **47** no. 9, (May, 1993) 4028–4045.

[156] I. Antoniadis, C. Kounnas, and C. Roiesnel, "Symmetry-breaking effects in grand unified theories," *Nucl. Phys. B* **198** no. 2, (May, 1982) 317–364.

[157] V. Bertone *et al.*, "Improving methods and predictions at high-energy e^+e^- colliders within collinear factorisation." 2022. `arXiv:2207.03265 [hep-ph]`.

[158] K. Chetyrkin, J. Kühn, and M. Steinhauser, "Three-loop heavy-quark vacuum polarization," *Nucl. Phys. B - Proceedings Supplements* **51** no. 3, (Dec, 1996) 66–70.

[159] G. Degrassi and A. Sirlin, "Gauge-invariant self-energies and vertex parts of the Standard Model in the pinch technique framework," *Phys. Rev. D* **46** (Oct, 1992) 3104–3116.

[160] D. Binosi and J. Papavassiliou, "Pinch technique: Theory and applications," *Physics Reports* **479** no. 1-6, (Aug, 2009) 1–152.

[161] A. Denner, G. Weiglein, and S. Dittmaier, "Gauge invariance of Green functions: background-field method versus pinch technique," *Phys. Lett. B* **333** no. 3-4, (Aug, 1994) 420–426.

[162] A. Denner, G. Weiglein, and S. Dittmaier, "Application of the background-field method to the electroweak Standard Model," *Nucl. Phys. B* **440** no. 1-2, (Apr, 1995) 95–128.

[163] V. V. Sudakov, "Vertex parts at very high-energies in quantum electrodynamics," *Sov. Phys. JETP* **3** (1956) 65–71.

[164] M. Kuroda, G. Moultaka, and D. Schildknecht, "Direct one-loop renormalization of $SU(2)_L \times U(1)_Y$ four-fermion processes and running coupling constants," *Nucl. Phys. B* **350** no. 1-2, (Feb, 1991) 25–72.

[165] W. Beenakker, A. Denner, S. Dittmaier, R. Mertig, and T. Sack, "High-energy approximation for on-shell W-pair production," *Nucl. Phys. B* **410** no. 2, (Dec, 1993) 245–279.

[166] A. Denner, S. Dittmaier, and R. Schuster, "Radiative corrections to $\gamma\gamma \to W^+W^-$ in the Electroweak Standard Model," *Nucl. Phys. B* **452** no. 1-2, (Oct, 1995) 80–108.

[167] A. Denner, S. Dittmaier, and T. Hahn, "Radiative corrections to $ZZ \to ZZ$ in the Electroweak Standard Model," *Phys. Rev. D* **56** no. 1, (Jul, 1997) 117–134.

[168] M. Beccaria, G. Montagna, F. Piccinini, F. M. Renard, and C. Verzegnassi, "Rising bosonic electroweak virtual effects at high energy e^+e^- colliders," *Phys. Rev. D* **58** no. 9, (Oct, 1998) .

[169] V. S. Fadin, L. N. Lipatov, A. D. Martin, and M. Melles, "Resummation of double logarithms in electroweak high energy processes," *Phys. Rev. D* **61** no. 9, (Mar, 2000) .

[170] J. Kühn, A. Penin, and V. Smirnov, "Summing up subleading Sudakov logarithms," *EPJC* **17** no. 1, (Oct, 2000) 97–105.

[171] P. Ciafaloni and D. Comelli, "Electroweak Sudakov form factors and

nonfactorizable soft QED effects at NLC energies," *Phys. Lett. B* **476** no. 1-2, (Mar, 2000) 49–57.

[172] F. Bloch and A. Nordsieck, "Note on the Radiation Field of the Electron," *Phys. Rev.* **52** (Jul, 1937) 54–59.

[173] T. Kinoshita, "Mass Singularities of Feynman Amplitudes," *Journal of Mathematical Physics* **3** no. 4, (Jul, 1962) 650–677.

[174] T. D. Lee and M. Nauenberg, "Degenerate systems and mass singularities," *Phys. Rev.* **133** (Mar, 1964) B1549–B1562.

[175] U. Baur, "Weak boson emission in hadron collider processes," *Phys. Rev. D* **75** (Jan, 2007) 013005.

[176] M. Ciafaloni, P. Ciafaloni, and D. Comelli, "Bloch-Nordsieck Violating Electroweak Corrections to Inclusive TeV Scale Hard Processes," *Phys. Rev. Lett.* **84** (May, 2000) 4810–4813.

[177] M. Hori, H. Kawamura, and J. Kodaira, "Electroweak Sudakov at two loop level," *Phys. Lett. B* **491** no. 3-4, (Oct, 2000) 275–279.

[178] A. Denner and S. Pozzorini, "One-loop leading logarithms in electroweak radiative corrections," *EPJC* **18** no. 3, (Jan, 2001) 461–480.
A. Denner and S. Pozzorini, "One-loop leading logarithms in electroweak radiative corrections," *EPJC* **21** no. 1, (Jun, 2001) 63–79.

[179] M. Melles, "Resummation of angular dependent corrections in spontaneously broken gauge theories," *EPJC* **24** no. 2, (Jun, 2002) 193–204.
M. Melles, "Electroweak radiative corrections in high energy processes," *Physics Reports* **375** no. 4, (Feb, 2003) 219–326.

[180] W. Beenakker and A. Werthenbach, "Electroweak two-loop Sudakov logarithms for on-shell fermions and bosons," *Nucl. Phys. B* **630** no. 1-2, (May, 2002) 3–54.

[181] A. Denner, M. Melles, and S. Pozzorini, "Two-loop electroweak angular-dependent logarithms at high energies," *Nucl. Phys. B* **662** no. 1-2, (Jul, 2003) 299–333.

[182] B. Jantzen, J. H. Kühn, A. A. Penin, and V. A. Smirnov, "Two-loop high-energy electroweak logarithmic corrections in a spontaneously broken $SU(2)$ gauge model," *Phys. Rev. D* **72** (Sep, 2005) 051301.
B. Jantzen, J. H. Kühn, A. A. Penin, and V. A. Smirnov, "Erratum: Two-loop high-energy electroweak logarithmic corrections in a spontaneously broken $SU(2)$ gauge model [Phys. Rev. D 72, 051301 (2005)]," *Phys. Rev. D* **74** (Jul, 2006) 019901.

[183] A. Denner, B. Jantzen, and S. Pozzorini, "Two-loop electroweak next-to-leading logarithmic corrections to massless fermionic processes," *Nucl. Phys. B* **761** no. 1-2, (Jan, 2007) 1–62.

[184] A. V. Manohar, B. Shotwell, C. W. Bauer, and S. Turczyk, "Non-cancellation of electroweak logarithms in high-energy scattering," *Phys. Lett. B* **740** (Jan, 2015) 179–187.

[185] C. W. Bauer and N. Ferland, "Resummation of electroweak Sudakov

logarithms for real radiation," *JHEP* **2016** no. 9, (Sep, 2016) .

[186] C. W. Bauer, N. Ferland, and B. R. Webber, "Combining initial-state resummation with fixed-order calculations of electroweak corrections," *JHEP* **2018** no. 4, (Apr, 2018) .

[187] M. Chiesa, G. Montagna, L. Barzè, M. Moretti, O. Nicrosini, F. Piccinini, and F. Tramontano, "Electroweak Sudakov Corrections to New Physics Searches at the LHC," *Phys. Rev. Lett.* **111** no. 12, (2013) 121801.

[188] E. Bothmann and D. Napoletano, "Automated evaluation of electroweak Sudakov logarithms in SHERPA," *EPJ C* **80** no. 11, (Nov, 2020) .

[189] D. Pagani and M. Zaro, "One-loop electroweak Sudakov logarithms: a revisitation and automation," *JHEP* **2022** no. 2, (Feb, 2022) .

[190] D. Pagani, T. Vitos, and M. Zaro, "Improving NLO QCD event generators with high-energy EW corrections." 2023. `arXiv:2309.00452 [hep-ph]`.

[191] R. Kirschner and L. N. Lipatov, "Double-logarithmic asymptotics of quark scattering amplitudes with flavor exchange," *Phys. Rev. D* **26** (Sep, 1982) 1202–1205.

[192] J. Kühn, S. Moch, A. Penin, and V. Smirnov, "Next-to-next-to-leading logarithms in four-fermion electroweak processes at high energy," *Nucl. Phys. B* **616** no. 1-2, (Nov, 2001) 286–306.

[193] R. E. Cutkosky, "Singularities and Discontinuities of Feynman Amplitudes," *Journal of Mathematical Physics* **1** no. 5, (Sep, 1960) 429–433.

[194] M. Veltman, "Unitarity and causality in a renormalizable field theory with unstable particles," *Physica* **29** no. 3, (Mar, 1963) 186–207.

[195] E. N. Argyres *et al.*, "Stable calculations for unstable particles: restoring gauge invariance," *Phys. Lett. B* **358** no. 3-4, (Sep, 1995) 339–346.

[196] G. Passarino, "Single-W production and Fermion-Loop scheme: numerical results," *Nucl. Phys. B* **578** no. 1-2, (Jul, 2000) 3–26.

[197] Y. Kurihara, D. Perret-Gallix, and Y. Shimizu, "$e^+e^- \to e^-\nu_e ud$ from LEP to linear collider energies," *Phys. Lett. B* **349** (1994) 367–374.

[198] R. G. Stuart, "Gauge invariance, analyticity and physical observables at the Z_0 resonance," *Phys. Lett. B* **262** no. 1, (Jun, 1991) 113–119.

[199] R. G. Stuart, "General renormalization of the gauge-invariant perturbation expansion near the Z_0 resonance," *Phys. Lett. B* **272** no. 3-4, (Dec, 1991) 353–358.

[200] *Z Physics at LEP1: CERN, Geneva, Switzerland 20 - 21 Feb, 8 - 9 May and 4 - 5 Sep 1989. Workshop on Z Physics at LEP1*. CERN, Geneva, 1989. Coordinated and supervised by G. Altarelli.

[201] W. Beenakker *et al.*, "The fermion-loop scheme for finite-width effects in e^+e^--annihilation into four fermions," *Nucl. Phys. B* **500** no. 1-3,

(Sep, 1997) 255–298.

[202] C. G. Papadopoulos, "On the determination of the trilinear boson couplings in at LEPII," *Phys. Lett. B* **352** no. 1-2, (Jun, 1995) 144–154.

[203] *Physics at LEP2: CERN, Geneva, Switzerland 2 - 3 Nov 1995. Workshop on Physics at LEP2.* CERN, Geneva, 1996. Composed by 3 sessions.

[204] M. L. Nekrasov, "W-pair production in modified perturbation theory," *Modern Phys. Lett. A* **26** no. 24, (Aug, 2011) 1807–1816.

[205] A. Sirlin, "Observations concerning mass renormalization in the electroweak theory," *Phys. Lett. B* **267** no. 2, (Sep, 1991) 240–242.

[206] P. Gambino and P. A. Grassi, "Nielsen identities of the SM and the definition of mass," *Phys. Rev. D* **62** no. 7, (Aug, 2000) .

[207] P. A. Grassi, B. A. Kniehl, and A. Sirlin, "Width and partial widths of unstable particles in the light of the Nielsen identities," *Phys. Rev. D* **65** no. 8, (Mar, 2002) .

[208] A. Sirlin, "Theoretical considerations concerning the z^0 mass," *Phys. Rev. Lett.* **67** (Oct, 1991) 2127–2130.

[209] D. Bardin, A. Leike, T. Riemann, and M. Sachwitz, "Energy-dependent width effects in e^+e^--annihilation near the Z-boson pole," *Phys. Lett. B* **206** no. 3, (May, 1988) 539–542.

[210] A. Denner, S. Dittmaier, M. Roth, and D. Wackeroth, "Predictions for all processes $e^+e^- \to 4$ fermions $+\gamma$," *Nucl. Phys. B* **560** no. 1-3, (Nov, 1999) 33–65.

[211] A. Denner, S. Dittmaier, M. Roth, and L. Wieders, "Electroweak corrections to charged-current fermion processes: Technical details and further results," *Nucl. Phys. B* **724** no. 1-2, (Sep, 2005) 247–294.

[212] A. Denner and S. Dittmaier, "The complex-mass scheme for perturbative calculations with unstable particles," *Nucl. Phys. B - Proceedings Supplements* **160** (Oct, 2006) 22–26.

[213] A. Denner and J.-N. Lang, "The complex-mass scheme and unitarity in perturbative quantum field theory," *EPJC* **75** no. 8, (Aug, 2015) .

[214] R. G. Stuart, "Structure of the Z^0 resonance and the physical properties of the Z^0 boson," *Phys. Rev. Lett.* **70** (May, 1993) 3193–3196.

[215] A. Aeppli, F. Cuypers, and G. Jan van Oldenborgh, "$\mathcal{O}(\Gamma)$ corrections to W pair production in e^+e^- and γ collisions," *Physics Letters B* **314** no. 3–4, (Sep, 1993) 413–420.

[216] A. Aeppli, G. J. Oldenborgh, and D. Wyler, "Unstable particles in one loop calculations," *Nucl. Phys. B* **428** no. 1-2, (Oct, 1994) 126–146.

[217] K. Melnikov and O. Yakovlev, "Final state interaction in the production of heavy unstable particles," *Nucl. Phys. B* **471** no. 1-2, (Jul, 1996) 90–120.

[218] W. Beenakker, A. Chapovsky, and F. Berends, "Non-factorizable corrections to W-pair production: Methods and analytic results," *Nucl. Phys. B* **508** no. 1-2, (Dec, 1997) 17–63.

[219] A. Denner, S. Dittmaier, and M. Roth, "Non-factorizable photonic corrections to $e^+e^- \to WW \to 4$ fermions," *Nucl. Phys. B* **519** no. 1-2, (May, 1998) 39–84.

[220] A. Denner, S. Dittmaier, M. Roth, and D. Wackeroth, "Electroweak radiative corrections to $e^+e^- \to WW \to 4$ fermions in double-pole approximation - the RacoonWW approach," *Nucl. Phys. B* **587** no. 1-3, (Oct, 2000) 67–117.

[221] A. Denner, S. Dittmaier, M. Roth, and D. Wackeroth, "$\mathcal{O}(\alpha)$ corrections to $e^+e^- \to WW \to 4$ fermions+γ: first numerical results from RacoonWW," *Physics Letters B* **475** no. 1-2, (Feb, 2000) 127–134.

[222] V. S. Fadin, V. A. Khoze, and A. D. Martin, "Interference radiative phenomena in the production of heavy unstable particles," *Phys. Rev. D* **49** (Mar, 1994) 2247–2256.

[223] W. Beenakker, F. Berends, and A. Chapovsky, "Radiative corrections to pair production of unstable particles: Results for $e^+e^- \to 4$ fermions," *Nucl. Phys. B* **548** no. 1-3, (May, 1999) 3–59.

[224] S. Dittmaier, A. Huss, and C. Schwinn, "Mixed QCD-electroweak $\mathcal{O}(\alpha_S\alpha)$ corrections to Drell-Yan processes in the resonance region: Pole approximation and non-factorizable corrections," *Nucl. Phys. B* **885** (Aug, 2014) 318–372.

[225] M. Billoni, S. Dittmaier, B. Jäger, and C. Speckner, "Next-to-leading order electroweak corrections to $pp \to W^+W^- \to 4$ leptons at the LHC in double-pole approximation," *JHEP* **12** (2013) 043.

[226] B. Biedermann, M. Billoni, A. Denner, S. Dittmaier, L. Hofer, B. Jäger, and L. Salfelder, "Next-to-leading-order electroweak corrections to $pp \to W^+W^- \to 4$ leptons at the LHC," *JHEP* **06** (2016) 065.

[227] Y. Kurihara, D. Perret-Gallix, and Y. Shimizu, "ee → eu from LEP to linear collider energies," *Phys. Lett. B* **349** no. 3, (Apr, 1995) 367–374.

[228] D. Yennie, S. Frautschi, and H. Suura, "The infrared divergence phenomena and high-energy processes," *Annals of Physics* **13** no. 3, (Jun, 1961) 379–452.

[229] G. Altarelli and G. Parisi, "Asymptotic freedom in parton language," *Nucl. Phys. B* **126** no. 2, (Aug, 1977) 298–318.

[230] J. Collins, "Foundations of Perturbative QCD." Apr, 2011.

[231] V. Gribov and L. Lipatov, "Deep inelastic electron scattering in perturbation theory," *Phys. Lett. B* **37** no. 1, (Nov, 1971) 78–80.

[232] Y. L. Dokshitzer, "Calculation of the Structure Functions for Deep Inelastic Scattering and e^+e^- Annihilation by Perturbation Theory in Quantum Chromodynamics.," *Sov. Phys. JETP* **46** (1977) 641–653.

[233] A. Denner and S. Dittmaier, "Production of light fermion-antifermion pairs in $\gamma\gamma$ collisions," *EPJC* **9** no. 3, (Jul, 1999) 425–435.

[234] V. Bertone, S. Carrazza, N. Hartland, and J. Rojo, "Illuminating the photon content of the proton within a global PDF analysis," *SciPost Physics* **5** no. 1, (Jul, 2018) .

[235] S. Frixione, Z. Kunszt, and A. Signer, "Three-jet cross sections to next-to-leading order," *Nucl. Phys. B* **467** no. 3, (May, 1996) 399–442.

[236] S. Catani and M. Seymour, "The dipole formalism for the calculation of QCD jet cross sections at next-to-leading order," *Phys. Lett. B* **378** no. 1-4, (Jun, 1996) 287–301.

[237] S. Catani and M. Seymour, "A general algorithm for calculating jet cross sections in NLO QCD," *Nucl. Phys. B* **485** no. 1-2, (Feb, 1997) 291–419.

[238] S. Catani, S. Dittmaier, M. H. Seymour, and Z. Trócsányi, "The dipole formalism for next-to-leading order QCD calculations with massive partons," *Nucl. Phys. B* **627** no. 1-2, (Apr, 2002) 189–265.

[239] R. Ellis, D. Ross, and A. Terrano, "The perturbative calculation of jet structure in e^+e^- annihilation," *Nucl. Phys. B* **178** no. 3, (Feb, 1981) 421–456.

[240] L. Phaf and S. Weinzierl, "Dipole formalism with heavy fermions," *JHEP* **2001** no. 04, (Apr, 2001) 006–006.

[241] R. Frederix, S. Frixione, F. Maltoni, and T. Stelzer, "Automation of next-to-leading order computations in QCD: the FKS subtraction," *JHEP* **2009** no. 10, (Oct, 2009) 003–003.

[242] S. Dittmaier, "A general approach to photon radiation off fermions," *Nucl. Phys. B* **565** no. 1-2, (Jan, 2000) 69–122.

[243] R. Frederix *et al.*, "The automation of next-to-leading order electroweak calculations," *JHEP* **2018** no. 7, (Jul, 2018) .

[244] S. Dittmaier, A. Kabelschacht, and T. Kasprzik, "Polarized QED splittings of massive fermions and dipole subtraction for non-collinear-safe observables," *Nucl. Phys. B* **800** no. 1-2, (Sep, 2008) 146–189.

[245] L. Basso, S. Dittmaier, A. Huss, and L. Oggero, "Techniques for the treatment of IR divergences in decay processes at NLO and application to the top-quark decay," *EPJC* **76** no. 2, (Jan, 2016) .

[246] M. Schönherr, "An automated subtraction of NLO EW infrared divergences," *EPJC* **78** no. 2, (Feb, 2018) .

[247] P. Nason, "A New method for combining NLO QCD with shower Monte Carlo algorithms," *JHEP* **11** (2004) 040.

[248] S. Frixione, P. Nason, and C. Oleari, "Matching NLO QCD computations with Parton Shower simulations: the POWHEG method," *JHEP* **11** (2007) 070.

[249] S. Alioli, P. Nason, C. Oleari, and E. Re, "A general framework for implementing NLO calculations in shower Monte Carlo programs: the POWHEG BOX," *JHEP* **06** (2010) 043.

[250] A. Mück and L. Oymanns, "Resonace-improved parton-shower matching for the Drell-Yan process including electroweak corrections," *JHEP* **2017** no. 5, (May, 2017) .

[251] S. D. Ellis, Z. Kunszt, and D. E. Soper, "One-Jet Inclusive Cross

Section at Order α_s^3: Gluons Only," *Phys. Rev. Lett.* **62** (Feb, 1989) 726–729.

[252] Z. Kunszt and D. E. Soper, "Calculation of jet cross sections in hadron collisions at order α_s^3," *Phys. Rev. D* **46** (Jul, 1992) 192–221.

[253] M. H. Seymour, "Photon radiation in final state parton showering," *Zeitschrift für Physik C Particles and Fields* **56** no. 1, (Mar, 1992) 161–170.

[254] K. Hamilton and P. Richardson, "Simulation of QED radiation in particle decays using the YFS formalism," *JHEP* **2006** no. 07, (Jul, 2006) 010–010.

[255] C. Bierlich *et al.*, "A comprehensive guide to the physics and usage of PYTHIA 8.3." 2022. `arXiv:2203.11601 [hep-ph]`.
T. Sjöstrand *et al.*, "An introduction to PYTHIA 8.2" *Comput. Phys. Commun.* **191** (2015) 159–177.

[256] M. Schönherr and F. Krauss, "Soft photon radiation in particle decays in SHERPA," *JHEP* **2008** no. 12, (Dec, 2008) 018–018.

[257] S. Höche, S. Schumann, and F. Siegert, "Hard photon production and matrix-element parton-shower merging," *Phys. Rev. D* **81** no. 3, (Feb, 2010) .

[258] E. Barberio, B. van Eijk, and Z. Was, "PHOTOS - a universal Monte Carlo for QED radiative corrections in decays," *Comp. Phys. Comm.* **66** no. 1, (Jul, 1991) 115–128.
E. Barberio and Z. Was, "PHOTOS - a universal Monte Carlo for QED radiative corrections: version 2.0" *Comp. Phys. Comm.* **79** no. 2, (Apr, 1994) 291–308.

[259] P. Golonka and Z. Was, "PHOTOS Monte Carlo: a precision tool for QED correctionsin Z and W decays," *EPJC* **45** no. 1, (Jan, 2006) 97–107.

[260] C. C. Calame, G. Montagna, O. Nicrosini, and M. Treccani, "Higher-order QED corrections to W-boson mass determination at hadron colliders," *Phys. Rev. D* **69** no. 3, (Feb, 2004) .

[261] C. M. C. Calame, G. Montagna, O. Nicrosini, and M. Treccani, "Multiple photon corrections to the neutral-current Drell-Yan process," *JHEP* **2005** no. 05, (May, 2005) 019–019.

[262] B. Jäger and J. Scheller, "Electroweak corrections and shower effects to Higgs production in association with two jets at the LHC," *Journal of High Energy Physics* **2022** no. 9, (Sep, 2022) .

[263] S. Frixione and B. R. Webber, "Matching NLO QCD computations and parton shower simulations," *JHEP* **2002** no. 06, (Jun, 2002) 029–029.

[264] A. Buckley, J. Ferrando, S. Lloyd, K. Nordström, B. Page, M. Rüfenacht, M. Schönherr, and G. Watt, "LHAPDF6: parton density access in the LHC precision era," *EPJC* **75** no. 3, (Mar, 2015) .

[265] A. Manohar, P. Nason, G. P. Salam, and G. Zanderighi, "How Bright is the Proton? A Precise Determination of the Photon Parton

Distribution Function," *Phys. Rev. Lett.* **117** (Dec, 2016) 242002.

[266] L. Buonocore, P. Nason, F. Tramontano, and G. Zanderighi, "Leptons in the proton," *JHEP* **2020** no. 8, (Aug, 2020) .

[267] L. Chen and A. Freitas, "GRIFFIN: A C++ library for electroweak radiative corrections in fermion scattering and decay processes," `arXiv:2211.16272 [hep-ph]`.

[268] Particle Data Group Collaboration, C. Patrignani *et al.*, "Review of Particle Physics," *Chin. Phys. C* **40** no. 10, (2016) 100001.

[269] Particle Data Group Collaboration, M. Tanabashi *et al.*, "Review of Particle Physics," *Phys. Rev. D* **98** no. 3, (2018) 030001.

[270] D. Rainwater and T. M. P. Tait, "Testing Grand Unification at the (S)LHC," *Phys. Rev. D* **75** (2007) 115014.

[271] D. S. M. Alves, J. Galloway, J. T. Ruderman, and J. R. Walsh, "Running Electroweak Couplings as a Probe of New Physics," *JHEP* **02** (2015) 007.

[272] M. Farina, G. Panico, D. Pappadopulo, J. T. Ruderman, R. Torre, and A. Wulzer, "Energy helps accuracy: electroweak precision tests at hadron colliders," *Phys. Lett. B* **772** (2017) 210–215.

[273] C. Gross, O. Lebedev, and J. M. No, "Drell–Yan constraints on new electroweak states: LHC as a $pp \to l^+l^-$ precision machine," *Mod. Phys. Lett. A* **32** no. 16, (2017) 1750094.

[274] L. Di Luzio, R. Gröber, and G. Panico, "Probing new electroweak states via precision measurements at the LHC and future colliders," *JHEP* **2019** no. 1, (Jan, 2019) .

[275] R. Torre, L. Ricci, and A. Wulzer, "On the $W\&Y$ interpretation of high-energy Drell-Yan measurements," *JHEP* **2021** no. 2, (Feb, 2021) .

[276] S. Alioli, R. Boughezal, E. Mereghetti, and F. Petriello, "Novel angular dependence in Drell-Yan lepton production via dimension-8 operators," *Phys. Lett. B* **809** (2020) 135703.

[277] A. Dainese *et al.*, "Report on the Physics at the HL-LHC, and Perspectives for the HE-LHC," tech. rep., Geneva, Switzerland, 2019.

[278] R. D. Ball *et al.*, "Parton distributions and new physics searches: the Drell–Yan forward–backward asymmetry as a case study," *Eur. Phys. J. C* **82** no. 12, (2022) 1160.

[279] CMS Collaboration, CMS Collaboration, "Measurement of the weak mixing angle using the forward-backward asymmetry of Drell-Yan events in pp collisions at 8 TeV," *Eur. Phys. J. C* **78** no. 9, (2018) 701.

[280] NNPDF Collaboration, R. D. Ball *et al.*, "Parton distributions from high-precision collider data," *Eur. Phys. J. C* **77** no. 10, (2017) 663.

[281] ATLAS Collaboration, "Electron reconstruction and identification in the ATLAS experiment using the 2015 and 2016 LHC proton-proton collision data at $\sqrt{s} = 13$ TeV," *Eur. Phys. J. C* **79** no. 8, (2019) 639.

[282] ATLAS Collaboration, "Muon reconstruction performance in early $\sqrt{s}$ = 13 TeV data,".

[283] ATLAS Collaboration, "Studies of the muon momentum calibration and performance of the ATLAS detector with pp collisions at $\sqrt{s}$=13 TeV," `arXiv:2212.07338 [hep-ex]`.

[284] A. Buckely, J. Butterworth, D. Grellscheid, H. Hoeth, L. Lonnblad, J. Monk, H. Schulz, and F. Siegert, "Rivet user manual," *Comp. Phys. Comm.* **184** (2013) 2803–2819.

[285] ATLAS Collaboration, "Measurement of the double-differential high-mass Drell-Yan cross section in pp collisions at $\sqrt{s} = 8$ TeV with the ATLAS detector," *JHEP* **08** (2016) 009.

[286] V. Bertone *et al.*, "aMCfast: automation of fast NLO computations for PDF fits," *JHEP* **08** (2014) 166.

[287] J. Alwall *et al.*, "The automated computation of tree-level and next-to-leading order differential cross sections, and their matching to parton shower simulations," *JHEP* **07** (2014) 079.

[288] C. Duhr and B. Mistlberger, "Lepton-pair production at hadron colliders at N³LO in QCD," *JHEP* **03** (2022) 116.

[289] R. Bonciani, F. Buccioni, N. Rana, and A. Vicini, "Next-to-Next-to-Leading Order Mixed QCD-Electroweak Corrections to on-Shell Z Production," *Phys. Rev. Lett.* **125** no. 23, (2020) 232004.

[290] R. Bonciani *et al.*, "Mixed Strong-Electroweak Corrections to the Drell-Yan Process," *Phys. Rev. Lett.* **128** no. 1, (2022) 012002.

[291] F. Buccioni *et al.*, "Mixed QCD-electroweak corrections to dilepton production at the LHC in the high invariant mass region," *JHEP* **06** (2022) 022.

[292] J. Baglio, C. Duhr, B. Mistlberger, and R. Szafron, "Inclusive production cross sections at N³LO," *JHEP* **12** (2022) 066.

[293] C. W. Bauer, N. Ferland, and B. R. Webber, "Combining initial-state resummation with fixed-order calculations of electroweak corrections," *JHEP* **04** (2018) 125.

[294] CMS Collaboration, A. M. Sirunyan *et al.*, "Measurements of differential Z boson production cross sections in proton-proton collisions at $\sqrt{s} = 13$ TeV," *JHEP* **2019** no. 12, (Dec, 2019) .

[295] S. Alekhin *et al.*, "HERAFitter," *Eur. Phys. J. C* **75** no. 7, (2015) 304.

[296] T.-J. Hou *et al.*, "New CTEQ global analysis of quantum chromodynamics with high-precision data from the LHC," *Phys. Rev. D* **103** no. 1, (2021) 014013.

[297] S. Bailey, T. Cridge, L. A. Harland-Lang, A. D. Martin, and R. S. Thorne, "Parton distributions from LHC, HERA, Tevatron and fixed target data: MSHT20 PDFs," *Eur. Phys. J. C* **81** no. 4, (2021) 341.

[298] S. Alekhin, J. Blümlein, S. Moch, and R. Placakyte, "Parton distribution functions, α_s, and heavy-quark masses for LHC Run II," *Phys. Rev. D* **96** no. 1, (2017) 014011.

[299] NNPDF Collaboration, R. D. Ball *et al.*, "The path to proton structure at 1% accuracy," *Eur. Phys. J. C* **82** no. 5, (2022) 428.

[300] S. Sakakibara, "The use of the minimal subtraction scheme in electroweak theories," *Zeitschrift für Physik C Particles and Fields* **11** no. 1, (Mar, 1981) 43–49.

[301] D. Bardin and G. Passarino, *The Standard Model in the Making.* Oxford University Press, 1999.

[302] M. Bohm, H. Spiesberger, and W. Hollik, "On the One Loop Renormalization of the Electroweak Standard Model and Its Application to Leptonic Processes," *Fortsch. Phys.* **34** (1986) 687–751.

[303] A. Denner, "Techniques for the calculation of electroweak radiative corrections at the one-loop level and results for W-physics at LEP200." 2007. arXiv:0709.1075 [hep-ph].